D E D I C A T I O N

This thesis is dedicated to the
memory of my father.

ELECTRON SPIN RESONANCE STUDIES OF SOME MAGNETIC ALLOYS

Thesis submitted for the Degree of Doctor of Philosophy of the University of London

by

RICHARD HAMILTON TAYLOR

Physics Department
Imperial College of Science and Technology
London SW7

October 1972

ABSTRACT

A study has been made of the X-band esr behaviour of a number of dilute alloys and intermetallic compounds containing s-state ions between 300K and 1.7K.

A large negative g-shift has been observed in the most dilute alloys of Gd in Pd (to 1.77); the g-shift reducing at higher concentrations of Gd as the Pd d-band is filled. A positive g-shift has been observed in the Pd-Mn (to 2.15) and $LaAl_2$-Gd systems. The sign of the g-shifts has been related to theory. The temperature dependence of the g-value and linewidth in Pd-Gd and Pd-Mn alloys has been interpreted in terms of the effect of the increase in demagnetising fields in the particles of the sample at the onset of ferromagnetic order. The esr measurements in Pd-Mn show a form consistent with an increasing magnetisation in a field of 3KGauss at concentrations above 3at% Mn, in contrast to the results of static susceptibility measurements.

Comparison of the present results with previous data suggests that in these dilute alloys there may be a frequency dependent contribution to the residual linewidth.

The g-value and temperature dependence of the linewidth has been measured for a number of compounds. Characteristic forms of behaviour have been distinguished for ferromagnets (including $GdAl_2$, $GdPt_2$, $GdCu_6$, $EuPd_2$, EuPd and Pd_2MnSn) and antiferromagnets (including $GdAg_3$, $GdCu_2$, GdB_6, GdB_4, $GdZn_{12}$, Gd_2Zn_{17} and "$GdCu_4$"). In the last five antiferromagnets an increase in linewidth at temperatures far above the Neel point has been observed and tentatively interpreted in terms of an extended regime of short-range order. For a number of the compounds, ordering temperatures have been predicted from the esr results.

The compound $GdPd_3$ showed anomalous behaviour possibly characteristic of metamagnetism. Compounds of Mn in Zn showed completely anomalous esr behaviour.

ACKNOWLEDGEMENTS

I would first like to thank sincerely Prof. B. R. Coles for his continual advice, help and interest throughout the course of this work, which was carried out under his supervision. I am also grateful to Dr. D. Griffiths for teaching me how to use the present apparatus and for his advice on many aspects of experimental technique.

Many other members of the Metal Physics Group, both past and present, have been of great help to me. Much of the work in this thesis has been carried out in conjunction with other members of the research group, who have made other measurements on the same alloys. I would specially like to thank Dr. H. E. N. Stone for his considerable metallurgical advice and assistance, Dr. I. R. Harris of the University of Birmingham for supplying me with a number of alloys and Drs. A. M. Stewart, N. Rivier and A. P. Murani for valuable discussions.

Finally, I would like to thank Chris Meyer for typing the thesis and my wife for not only putting up with me whilst the thesis was being written, but also for teaching me (I hope) the rudiments of punctuation.

The work was carried out under an SRC Studentship.

CONTENTS

		Page No.
ABSTRACT		2
ACKNOWLEDGEMENTS		4
CONTENTS		5
GENERAL INTRODUCTION		9
CHAPTER 1 -	THEORY OF THE ISOLATED IMPURITY ATOM IN A METAL	11
1.1	Formation of a Moment	12
1.2	Conduction Electron - Local Moment Exchange	20
1.3	Divergence of Perturbation Theory - The Kondo Effect	31
CHAPTER 2 -	INTERACTIONS BETWEEN MOMENTS AND MAGNETIC ORDERING	34
2.1	Interactions Between Moments via the Conduction Electrons	34
2.2	Interactions Between Neighbouring Magnetic Atoms - Local Environment Effects	38
2.3	Interactions in Disordered Systems	43
2.4	Magnetic Ordering	47
CHAPTER 3 -	PREVIOUS WORK AND REVIEW OF MAGNETIC ORDERING IN INTERMETALLIC COMPOUNDS AND SOLID SOLUTION ALLOYS	55
3.1	Intermetallic Compounds	55
	(a) Rare Earths	55
	(b) Transition Metals	66
3.2	Solid Solution Alloys	71
	(a) Bound State in Exchange Enhanced Transition Metal	72
	(b) Virtual Bound State with Good (3d) Moment in Enhanced Transition Metal	74
	(c) Virtual Bound State with Good (3d) Moment in a Simple Metal	79
	(d) Some Other Interesting Systems	81

CHAPTER 4 -	THEORY OF ELECTRON SPIN RESONANCE	84
4.1	Basic Theory	84
4.2	Longitudinal Relaxation	84
4.3	The Bloch Model	87
4.4	The Spin Hamiltonian	91
4.5	The g-shift and Linewidth of Ions in Metals	94
	(a) First Order and Second Order g-shift	94
	(b) Indirect g-shift	96
	(c) Hasegawa's Treamtnet - the esr Bottleneck	96
	(d) Extensions of Hasegawa's Work	101
4.6	Hyperfine Splitting	102
4.7	Residual Linewidth	103
4.8	Ferromagnetic and Antiferromagnetic Resonance	106
	(a) Ferromagnetic Resonance	106
	(b) Antiferromagnetic Resonance	108
	(c) Theories and Measurements just above the Critical Temperature	109
CHAPTER 5 -	EXPERIMENTAL REVIEW OF ESR OF IONS IN METALS	112
5.1	Rare Earth s-state Ions	112
	(a) Pure Rare Earths	112
	(b) Rare Earth Intermetallic Compounds	113
	(c) Intermetallic Compound Hosts with Rare Earth Impurities	116
	(d) Rare Earths in Pd and Pd Binary Alloys	122
	(e) Gd in Y, Lu, Sc and La	125
	(f) Rare Earth Ions in Other Hosts	127
5.2	Transition Metal s-state Ions	129
	(a) Mn in Cu, Ag and Au	129
	(b) Mn in Pd	135
	(c) Mn in Zn, Mg and Al	136
	(d) Other Transition Metals	137
5.3	Non s-state Resonances	137
5.4	Transmission Electron Spin Resonance	142
CHAPTER 6 -	METALLURGY	145
6.1	General Alloying Theory	145
	(a) Size Factor	145
	(b) Electron Concentration	146
	(c) Electrochemical Factor	146
6.2	Purity of Materials	147
6.3	Furnaces	148

CHAPTER 6 - (Continued)

6.4 Metallurgical Examination of Samples 148
(a) Metallographic Examination 148
(b) Hardness 149
(c) "Wet" Analysis 149
(d) Electron Microprobe Analysis 149
(e) X-Ray Analysis 149

6.5 The Intermetallic Compounds 149
(a) Ag-Gd 149
(b) Al-Gd 150
(c) Au-Mn 153
(d) B-Gd, Tb, Er 154
(e) Cu-Gd 156
(f) In-Gd 160
(g) Pd-Eu 161
(h) Pd-Gd, Er, Yb 161
(i) Pt-Gd 162
(j) Zn-Gd, Er 165
(k) Zn-Mn 166
(l) Pd_2MnSn 167

6.6 Dilute Solid Solutions 168
(a) Pd-Gd and Pd-Ni-Gd 168
(b) Pd-Mn 169
(c) Zn-Mn 170
(d) Rh-Mn 171

CHAPTER 7 - APPARATUS AND EXPERIMENTAL METHOD 172

7.1 The ESR Spectrometer 172

7.2 Thermometry 175

7.3 Measurement of Magnetic Field 177

7.4 The Resonant Cavity 178

7.5 Sensitivity 182

7.6 Possible Improvements in Sensitivity 187

7.7 Preparation of Specimens 190

7.8 Experimental Procedure 191

7.9 Shape of Lines - Corrections 195

CHAPTER 8 - RESULTS AND THEIR INTERPRETATION 198

8.1 Gd in Dilute Solid Solutions 198
(a) Pd-Gd 198
(b) Pd-Ni-Gd 203
(c) $LaAl_2$-Gd 204

8.2 Solid Solution Alloys Containing Mn 210
(a) Pd-Mn 210
(b) Other Solid Solution Alloys Containing Mn 216

CHAPTER 8 - (Continued)

8.3	Intermetallic Compounds - Results and Discussion	227
	(a) Ag_3Gd	227
	(b) $GdAl_2$	228
	(c) GdB_6 and GdB_4	230
	(d) Cu_2Gd, "Cu_4Gd" and Cu_6Gd	233
	(e) $GdIn_3$	235
	(f) Pd_2Eu and PdEu	235
	(g) Pd_3Gd, Yb	236
	(h) The Pt-Gd Compounds	239
	(i) $Zn_{12}Gd$ and $Zn_{17}Gd_2$	241
	(j) Au_3Mn	243
	(k) Pd_2MnSn	243
	(l) $Zn_{13}Mn$ and "$Zn_{10}Mn$"	244
8.4	Intermetallic Compounds - Conclusions	265
REFERENCES		267
APPENDIX 1 -	Search for a Ce Resonance	281
APPENDIX 2 -	Summary of Magnetic and Structural Data on Intermetallic Compounds	284
APPENDIX 3 -	The Korringa Relation and Relaxation Times	296
APPENDIX 4 -	Directory of ESR of Ions in Metals	298
APPENDIX 5 -	Correction Curves for ESR Lines	305

GENERAL INTRODUCTION

The magnetic behaviour of alloys presents many interesting experimental and theoretical problems and it is often said that a study of the magnetic properties of alloy systems may give an insight into the origins of magnetism in pure transition metals.

In this thesis both dilute solid solutions, in which the magnetic ions are well localised, and intermetallic compounds where the ions are periodic in the lattice, are studied by the technique of electron spin resonance (esr). This technique has been extensively used in the past for studying the interaction between a localised moment and the conduction electrons and for identifying the crystal field split ground state of non-s-state ions. In the present work, although a few attempts have been made to observe resonances from Er and Yb in a number of intermetallic compounds and from the Ce^{3+} ion in a number of hosts, the greater part of it has been concerned with identifying the characteristic behaviour of Gd, Eu^{2+} and Mn ions with the onset of magnetic order.

In the first two chapters an outline is given of the general theory of the formation of moments, the interaction of magnetic ions with the conduction electrons and the various forms of interaction between the local moments which lead to a magnetically ordered state at low temperatures. In chapter 3, a brief survey of the behaviour of a number of alloys is reviewed, with particular reference to the systems studied in this thesis.

Chapters 4 and 5 are devoted to electron spin resonance. In the first, the general theory of esr is presented and then applied to the more complicated situation where the behaviour of the magnetic ion is modified by the role of the conduction electrons - the well-known phenomenom of bottlenecking. In chapter 5, a comprehensive survey is presented of previous esr measurements of ions in metals.

In chapter 6, the preparation of the alloys used for the measurements in this work is described and the metallurgy of a number of systems such as Cu-Gd and Pt-Gd, which have been of particular interest, are discussed in some detail. The penultimate chapter contains a description of the spectrometer, a brief discussion of sensitivity in esr spectrometers and a number of suggestions for improvements to the present apparatus.

Finally, the results on the alloys are presented and discussed systematically and a number of suggestions made for future extensions of the present study.

CHAPTER 1

THEORY OF THE ISOLATED IMPURITY ATOM IN A METAL

In this chapter various models will be outlined which attempt to explain how a magnetic moment may be formed on a single solute atom dissolved in a metallic host. The interaction of the magnetic impurity with the conduction electrons of the matrix will then be discussed.

When a magnetic atom is dissolved in a metal, two situations may occur. If the energy of the orbitals responsible for magnetism lie well below the range of energies of the conduction band, the local moment maintains its free ion character - interacting little with the conduction electrons - and the magnetic moment of the ground state is given by Hund's rules (1.1). This configuration is generally expected to occur for the rare earths and is known as a real bound state. Band structure calculations (1.2) on Gd, for example, show that the 4f state responsible for the magnetism is about 005 eV wide and 11 eV below the conduction band.

The 3d transition metals and some rare-earths in certain hosts, such as Ce in Y (1.3), Eu in Au (1.4), Yb in Au-Ag (1.5) and Pr in ZrB_{12} (1.6), have magnetic orbitals which lie within the range of conduction band energies and here the idea of the bound state breaks down. Matthias et al (1.7) dissolved Fe in second row transition metals and their alloys and found large variations in magnetic moment and, indeed, no moment at all in some cases.

Reviews of the problem of moment formation have been given by Anderson (1.8) and Heeger (1.9).

1.1 Formation of a Moment

Friedel (1.10) began the theoretical interpretation of the complex forms of behaviour illustrated above, by introducing the concept of the Virtual Bound State. He considered the scattering of conduction electrons by a spherically symmetric potential V(r), representing the impurity atom, and analysed the free electron wave functions in terms of spherical harmonics and their associated phase shifts η_l. An expression was first obtained for the screening charge, $\Delta\rho$, per unit K, inside a sphere of radius R. At large R:

$$\Delta\rho = \frac{1}{2\pi^2 r^3} \sum (2l+1) \int_0^{K_F} \sin\eta_l \sin(2Kr + \eta_l - l\pi)\, 2rdK \qquad \ldots\ldots\ldots\ldots\ldots\ldots \quad 1.1$$

Integration up to K_F for the total charge locally displaced by the impurity potential, and considerations of charge neutrality in the matrix give the Friedel sum rule:

$$Z = \frac{2}{\pi} \sum_l (2l+1)\, \eta_l (E_F) \qquad \ldots\ldots\ldots\ldots\ldots\ldots\ldots\ldots \quad 1.2$$

where Z is the excess impurity charge.

If an impurity potential is initially strong enough to accept an lth bound state, but is then progressively reduced in strength, the energy of the lth state increases in energy and merges into the continuum of extended states. Here it resonates with the lth component and broadens in energy to form a virtual bound state. When the initial bound state lies close to the Fermi surface, it has a large scattering cross-section and makes a large contribution to properties which depend on the density of states at the Fermi surface. Friedel was able, using this concept, to account for the peak in the residual resistivity of transition metal impurities in Al, on moving across the transition series.

Friedel also considered the circumstances under which a virtual bound state would split into two halves under the influence of exchange correlation. He obtained the condition

$$p \Delta E > w \qquad \ldots\ldots\ldots\ldots\ldots\ldots\ldots \quad 1.3$$

for this to occur; where p is the number of electrons or holes in the d-state, ΔE is the exchange energy per electron and w the width of the virtual state defined from the phase shift against energy relation of the state.

Blandin and Friedel (1.11) justified this result in a more detailed calculation and showed that it predicts quite well the distribution of magnetised states in simple metal - transition metal alloys. A split virtual state leads to two separate peaks in the residual resistivity as each half crosses the Fermi level.

The ideas of Friedel were quantified and developed by Anderson (1.2) into what is now generally known as the Friedel-Anderson theory. Anderson considered the case of an orbitally non-degenerate d-impurity in a simple metal using a self-consistent Hartree-Fock treatment. The Hamiltonian contains four terms:

$$H = H_{ok} + H_{od} + U n_{d\downarrow} n_{d\uparrow} + H_{kd} \qquad \ldots\ldots\ldots\ldots\ldots\ldots \quad 1.4$$

The first two terms, H_{ok} and H_{od} are the unperturbed Hamiltonians of the free electron system. The third term, $U n_{d\downarrow} n_{d\uparrow}$ represents the term for the repulsive energy amongst the d-electrons of opposite spin, where U is the direct Coulomb energy between electrons and is defined by

$$U = \int |\phi_d(r_1)|^2 \frac{e^2}{r_{12}} |\phi_d(r_2)|^2 d\tau_1 d\tau_2 \qquad \ldots\ldots\ldots\ldots\ldots\ldots \quad 1.5$$

and $n_{d\downarrow}$, $n_{d\uparrow}$ are the number operators for electrons with spin down and spin up in the localised level. This term tends to favour the occupation of the state by electrons of a particular spin and gives a tendency towards magnetism. If an electron with spin up occupies the singly degenerate d-state with energy E below the Fermi level, the energy of a d-electron with spin down will be E + U. If this energy lies above the Fermi level, it will be empty and the impurity will be magnetic.

The last term in the Hamiltonian represents the interaction between the d-electrons and the conduction electrons. This is known as the admixture term and leads to broadening of the impurity state. It may be thought of as a hopping process where the band electrons hop on to the impurity and stay there for a time τ before hopping off - the broadening is then $h/\tau = \Delta$. This mixing term tends to favour the transfer on to the impurity of an electron of opposite spin to the one already there and competes with the coulomb term. The energy of the spin-up state is raised to $E + U\delta n$ and the spin-down state is lowered in energy to $E + U - U\delta n$, where δn is the number of electrons transferred from the up to the down state. These ideas are shown in fig. (1.1)

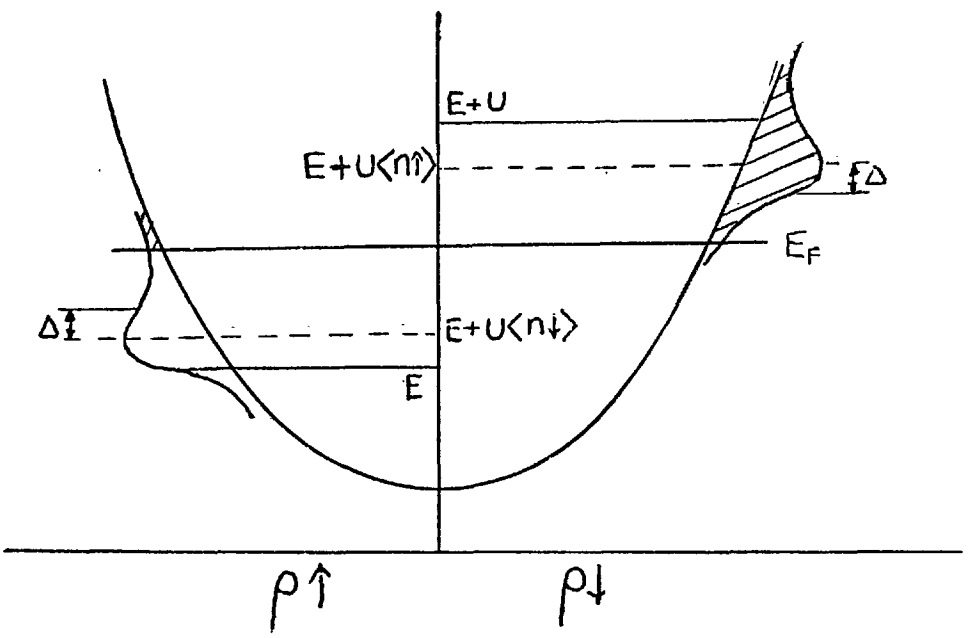


Fig. 1.1

Using a Green's function technique, Anderson obtained a solution for the density of the d-states:

$$\rho_{d\sigma}(E) = \frac{1}{\pi} \frac{\Delta}{(E - E_\sigma)^2 + \Delta^2} \quad \ldots\ldots\ldots\ldots \quad 1.6$$

which is of Lorentzian form; the width Δ is given by:

$$= \pi \langle V_{kd}^2 \rangle \rho(E_F) \quad \ldots\ldots\ldots\ldots\ldots\ldots \quad 1.7$$

where $\langle V_{kd}^2 \rangle$ is the matrix element associated with the s - d interaction between localised and band states. E_σ is the centre of the extended state of spin σ at $E + n_\sigma U$. In order to determine the number of d-electrons of a given spin, σ, (1.6) is integrated up to E_F and for self consistency the two equations

$$\langle n_d\uparrow \rangle = \frac{1}{\pi} \cot^{-1} \left(\frac{E - E_F + U\langle n_d\downarrow \rangle}{\Delta} \right)$$

$$\langle n_d\downarrow \rangle = \frac{1}{\pi} \cot^{-1} \left(\frac{E - E_F + U\langle n_d\uparrow \rangle}{\Delta} \right) \quad \ldots\ldots\ldots \quad 1.8$$

must be solved simultaneously. Anderson introduces two dimensionless parameters

$$y = \frac{U}{\Delta}$$

$$x = \frac{(E_F - E)}{U} \quad \ldots\ldots\ldots\ldots\ldots\ldots \quad 1.9$$

and plotting these against each other (fig. (1.2)), magnetism is found to be possible within the shaded area.

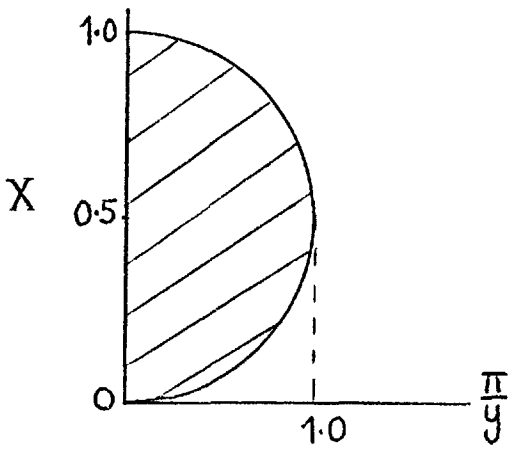


Fig. 1.2

Conditions are most favourable for the existence of magnetism when $x = \frac{1}{2}$, i.e, when the levels are symmetrically placed about the Fermi level. When $x = \frac{1}{2}$ the condition for magnetism is that

$$\Delta < \frac{U}{\pi} \qquad \ldots\ldots\ldots\ldots\ldots\ldots \quad 1.10$$

This is similar to equation 1.3 in Friedel's analysis.

For the iron group $U \sim 10$ eV, $\rho(E) \sim 0.2$ eV^{-1}, $\langle V^2 \rangle \sim 1$ eV and thus

$$\frac{\pi\Delta}{U} \sim 0.2$$

magnetism is thus likely.

Anderson (in an appendix) extended the physically rather unreal single added orbital model presented here, to the more realistic case of a degenerate d-level. The Hamiltonian takes the same general form as 1.4 above, but allowance is made for the repulsion of electrons with parallel spins but different orbits, and the reduction of this repulsion by the effects of an atomic exchange integral:

$$J = \int \phi_1^*(1)\phi_2^*(2)\frac{e^2}{r_{12}}\phi_1(2)\phi_2(1)d\tau_1 d\tau_2 \ldots\ldots \quad 1.11$$

which is $\sim 1 - 2$ eV.

Yosida et al (1.13) and Klein and Heeger (1.14) showed that the new Hamiltonian may be solved to obtain a condition

$$\frac{U + 4J}{\pi\Delta} \geqslant 1 \qquad \ldots\ldots\ldots\ldots\ldots\ldots \quad 1.12$$

for the existence of magnetism at the most favourable position of the virtual state with respect to the Fermi level. The condition implies that the effect of a degenerate d-level is to increase the likelihood of a magnetic state forming.

In the same analysis, the condition for quenching of the orbital angular momentum is found by Yosida et al to be

$$\frac{U - J}{\pi\Delta} < 1 \quad \ldots\ldots\ldots\ldots\ldots\ldots \quad 1.13$$

The Anderson model and it's extension to the non-degenerate case assume that any crystal field splitting is less than the virtual level width, and the effects of spin - orbit, orbit - orbit and d - d interactions in the host are neglected.

From the conditions above, Yosida et al estimated a value of $U + 4J \sim 5 - 7$ eV, i.e., $U \sim 3 - 4$ eV for d impurities in simple metals. This reduction of the value for U from the higher value quoted above assumed by Anderson, is attributed to screening of the Coulomb integral by conduction electrons. It clearly implies a tendency away from moment formation.

Wolff (1.15) and Clogston (1.16) treat the conduction electron impurity system as a scattering problem where the impurity is represented by a potential which scatters electrons from states of a single band. The wave function is expanded in terms of Wannier functions derived from a single band, i.e.,

$$\psi = N^{-\frac{1}{2}} \sum_{R_i} U_m (R_i)\, a_m (r - R_i) \quad \ldots\ldots\ldots\ldots\ldots \quad 1.14$$

It is assumed that V has no matrix elements between Wannier functions from different bands and that there is no matrix element of the potential for Wannier functions centred on neighbouring atoms, i.e.,

$$\langle a_n (r - R_i) \mid V \mid a_{n'} (r - R_J) \rangle =$$

$$V_{nn} \delta_{nn'} \delta (R_i - R_o) \delta (R_J - R_o) \quad \ldots\ldots\ldots\ldots\ldots \quad 1.15$$

where R_o is the impurity site.

Wolff finds that the amplitude of the Wannier function centred on the impurity site is given by

$$U_m(R_o) = \frac{e^{iK.R_o}}{1 - V_{mm}F_m(E)} + i\pi V_{mm}\rho_m(E) \quad \ldots\ldots\ldots\ldots \quad 1.16$$

where V_{mm} is the matrix element of V between states within the band and $\rho_m(E)$ is the density of states of the band. $F_m(E)$ depends on $\rho_m(E)$ as shown in fig. (1.3)

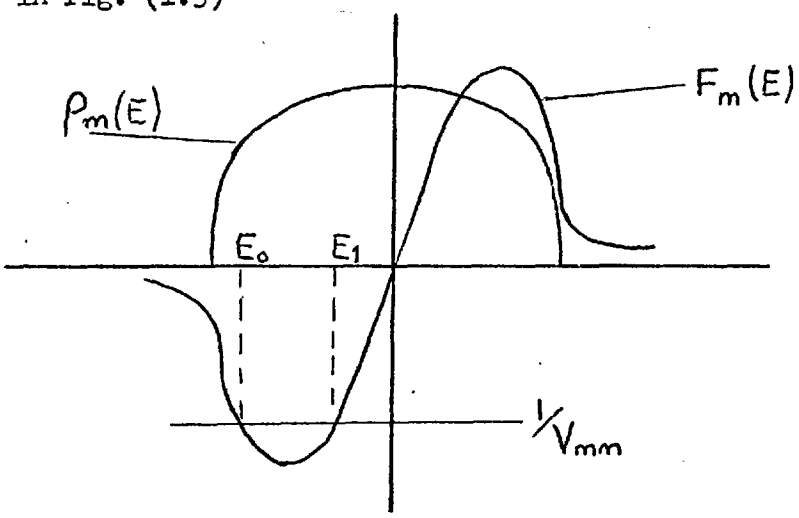


Fig. 1.3

The amplitude of $|U_m(R_o)|^2$ is a maximum when $\left[1 - V_{mm}F_m(E)\right] = 0$. If the energy E_o lies within the band, $U_m(R_o)$ has a resonance maximum and Clogston shows that a virtual state has been created at E_o. If the energy of E_o lies below the bottom of the band (i.e., for increasing V) $\rho_m(E)$ is zero, $U_m(R_o)$ is infinite and a bound state is obtained.

If a small spin dependent potential (of the same form as Anderson's) is added to V, giving potentials for up and down spin $V + \Delta V\uparrow$ and $V + \Delta V\downarrow$, two simultaneous equations are obtained for $U\uparrow(R_o)$ and $U\downarrow(R_o)$ and these are used to calculate the Hartree-Fock field of the impurity. Expressions for $\Delta V\uparrow$ and $\Delta V\downarrow$ are obtained and solved graphically for small $\Delta V/V$. It is shown that the criterion for

magnetism is of the form:

$$\left| \frac{U}{\pi^2 V^4 \rho(E)\, F'} \right| > \frac{\Delta^2 + (E_F - E_o)^2}{\Delta^2} \qquad \ldots\ldots\ldots\ldots \quad 1.17$$

where U is the Coulomb integral between different spins and $F' = \frac{dF(E)}{dE}$.

The Wolff-Clogston model is best suited to problems involving transition metals dissolved in other transition metals (e.g., Fe in Mo) where the impurity state can be regarded as a superposition of band states. Rivier (1.17) has shown that the Anderson and Wolff-Clogston models are essentially the same.

Both of these models use a Hartree-Fock approximation to treat the problem, assuming that the repulsive potential of a spin-up electron in a given orbital is proportional to the average number of spin-down electrons in the same orbit. This assumption is equivalent (1.9) to saying that the lifetime $(\frac{\hbar}{\Delta})$ of an electron on the impurity site is shorter than the time required to 'obtain information' on the occupation of the other spin states $(\frac{\hbar}{U})$

$$\text{i.e., that} \quad \frac{U}{\Delta} < 1$$

This suggests that the Hartree-Fock approximation is only valid in the non-magnetic limit.

Electron correlation effects, which take into account the possibility that the spin-down electron 'recedes' from the orbit as the spin-up electron jumps into it, have been considered by Schrieffer and Mattis (1.18) for the case where the number of electrons (or holes) occupying the virtual level is less than 0.3. In this limit, for non-degenerate orbitals, they predict that the effective Coulomb interaction $\bar{U}$ will be such that even for infinite U, the virtual state may not be magnetised.

A further difficulty with these simple models is that an unphysically sharp boundary is predicted between the magnetic and non-magnetic states. The important concept of localised spin fluctuations overcomes this problem (1.17, 1.19). Starting from the extreme non-magnetic virtual bound state in the Friedel-Anderson model (i.e., $U \ll \pi\Delta$), at finite temperatures the populations of spin-up and spin-down electrons will fluctuate $\sim KT$ in energy about the Fermi level. As the magnetic limit is approached (i.e., $U \longrightarrow \pi\Delta$), correlations increase the fluctuation amplitudes and lifetimes, i.e., the localised spin fluctuation lifetime, τ_{LSF}. The observation of a magnetic state requires the time of the experimental 'probe' to be short compared with τ_{LSF}.

Caplin and Rizzuto (1.20) have measured the low temperature impurity resistance of dilute AlMn and AlCr alloys, which are non-magnetic in the Friedel-Anderson sense, and correlated these measurements with the high temperature enhanced Pauli susceptibility using the spin fluctuation concept.

1.2 Conduction Electron - Local Moment Exchange

The interaction between localised moments and the conduction electrons may be written in the form (1.21)

$$H_{EX} = -2J\underline{S}.\underline{s} \quad \ldots\ldots\ldots\ldots\ldots\ldots\ldots \quad 1.18$$

where $\underline{S}$ is the spin of the local moment and $\underline{s}$ is the spin of the conduction electron, provided that the impurity is well localised and that the direct interaction between impurity atoms is small.

If the conduction electron wavefunctions are represented by plane waves and the interaction potential is Coulombic, the exchange integral in 1.18 may be written

$$J(\underline{K},\underline{K}') = \frac{1}{V}\int \psi^{*}_{LOC}(\underline{r}_i)\, e^{i\underline{K}.\underline{r}_2} \frac{e^2}{r_{12}} \psi_{LOC}(\underline{r}_2)\, e^{-i\underline{K}'.\underline{r}_1} d\underline{r}_1 d\underline{r}_2 \quad \ldots\ldots\ldots\ldots \quad 1.19$$

A number of further approximations are usually made. The full range of the Coulomb potential will be reduced by screening effects, and thus the potential is often taken as a delta function and in this case, $J(\underline{K},\underline{K}')$ depends only on the magnitude of $(\underline{K} - \underline{K}') = \underline{q}$. In the interpretation of experimental results, it is often further assumed that $J(\underline{q})$ may be taken as a constant. Kaplan and Lyons (1.22) have shown that anisotropic terms may also be important.

In rare-earth ions, the total angular momentum $\underline{J}$ is a good quantum number and de Gennes (1.23) suggested that the effects of orbital angular momentum may be included in 1.18 by replacing $\underline{S}$ by its projection on $\underline{J}$, i.e., by $(g - 1)\underline{J}$, where g is the Lande factor. Liu (1.24) has shown this approximation to be valid if

(i) the conduction electrons are s-like so that their wave functions are spherically symmetric and

(ii) that the wavelength of the conduction electron is large compared with the size of the 4f shell. Since the radius of the 4f shell ~ 0.4Å and a free electron estimate of the conduction electron wavelength is ~ 0.7Å, it may be seen that this condition is not well obeyed.

Zener (1.25) suggested from a first order perturbation calculation of the energy of the system, that the energy of the conduction electrons with spin parallel to the local moment is lowered with respect to those of spin antiparallel, thus depopulating the latter across the Fermi surface. The result is a uniform polarisation of the conduction band.

Yosida (1.26), following a similar treatment by Ruderman and Kittel (1.27) for the conduction electron - nuclear spin system, showed that if the first order perturbation of the conduction electron wavefunction is included, the spin polarisation oscillates with rapidly decreasing amplitude as a function of distance from the impurity. Yosida obtained an expression for the spin density of up and down spins at $\underline{r}$ from an impurity of spin up

$$\rho_{\pm}(r) = \rho_o \left\{ 1 \pm \frac{3}{8E_F N} \int_o^{\infty} J(q) f(q) S^z \chi \left[e^{i\underline{q}\underline{r}} + e^{-i\underline{q}\underline{r}} \right] dq \right\} \quad \ldots\ldots\ldots\ldots\ldots \quad 1.20$$

using the J(q) and free electron approximations, where $2\rho_o$ is the mean conduction electron density, N the number of lattice sites and f(q) the susceptibility function is given by

$$f(q) = 1 + \frac{4K_F^2 - q^2}{4K_F q} \ln \left| \frac{2K_F + q}{2K_F - q} \right| \quad \ldots\ldots\ldots\ldots\ldots \quad 1.21$$

This quantity, sometimes known as the Lindhardt function, is related to the susceptibility $\chi(q)$ by

$$\chi(q) = \chi_{PAULI} \; f(q) \quad \ldots\ldots\ldots\ldots\ldots \quad 1.22$$

for a free electron gas, where

$$\chi_{PAULI} = 2\mu_B^2 \rho(E_F) \quad \ldots\ldots\ldots\ldots\ldots \quad 1.23$$

The form of $\chi(q)$ for a free electron gas is shown in fig. (1.4)

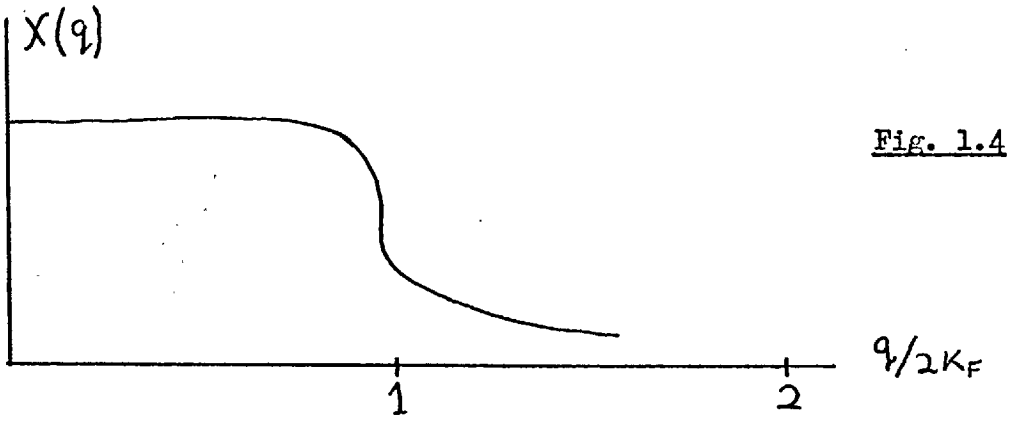


Fig. 1.4

The susceptibility function for a general matrix is given by Wolff (1.28) for a single band as

$$\chi(q) = -2\mu_B^2 \sum_{\underline{k}} \frac{f(\underline{K} + \underline{q}) - f(\underline{K})}{E(\underline{K} + \underline{q}) - E(\underline{K})} \quad \ldots\ldots\ldots\ldots \quad 1.24$$

Where $f(\underline{K})$ and $E(\underline{K})$ are the occupation number and band energy of the state $\underline{K}$, 1.24 may peak at $q \neq 0$.

Returning to the analysis of Yosida, if the further approximation that $J(q) = J$ is made, integration of 1.20 gives

$$\rho_{\pm}(\underline{r}) = \rho_o \left[1 \mp \frac{18\pi n}{E_F N} J S^z F(2K_F r)\right] \quad \ldots\ldots\ldots\ldots \quad 1.25$$

where 2n is the total number of conduction electrons. The function F(x) is given by

$$F(x) = \frac{x \cos x - \sin x}{x^4} \quad \ldots\ldots\ldots\ldots\ldots\ldots\ldots \quad 1.26$$

and the result is known as the RKKY (Ruderman, Kittel, Kasuya, Yosida) polarisation.

In the equation 1.25, $\rho_{\pm}(r) \longrightarrow \infty$ as $r \rightarrow 0$. This singularity is in contradiction to the observed densities at the local moment nucleus ρ_o, which are normally about an order of magnitude greater than the spin density at nearest neighbours, ρ_{NN}, (1.29). If better approximations for J(q) are used, the singularity is removed. Since f(q) decreases abruptly near $q = 2K_F$ Yosida considered the approximation

$$\begin{aligned} J(q)\, f(q) &= 2J \quad \text{for } q < 2K_F \\ &= 0 \quad \text{for } q > 2K_F \end{aligned} \quad \ldots\ldots\ldots\ldots\ldots\ldots \quad 1.27$$

in order to give a heavier weighting to low q components. One then obtains:

$$\rho^{\pm}(r) = \rho_o \left[1 \mp \frac{36}{E_F} J S^z F(2K_F r)\, 2K_F r\right] \quad \ldots\ldots\ldots\ldots \quad 1.28$$

which has a finite value at r = 0. Overhauser (1.30) approximated the exchange integral by the atomic form factor:

$$J_{FF}(q) = \int e^{i\underline{q}\underline{r}} \left| \Psi_{LOC}(\underline{r}) \right|^2 d\underline{r} \quad \ldots\ldots\ldots\ldots\ldots \quad 1.29$$

and this is estimated to give $\rho_{RKKY}/\rho_0 \sim 10^3$.

The analysis above assumes that the conduction electrons have an infinite mean free path. De Gennes (1.31) attempted to take this into account by introducing an exponential decay which is written as $\exp(-R/\lambda)$, where λ is the conduction electron mean free path. This may be introduced as a multiplying factor in the equations above.

Watson and Freeman (1.29) evaluated $J(\underline{K},\underline{K}')$ for a Gd local moment and conduction electrons treated as orthogonalised plane waves. They found that for Gd, the exchange integral is well approximated by $J(q)$. The form of the spin density obtained in this approximation was found to be different from that obtained in the RKKY expression. They found that although the average density is positive (Zener term) and oscillations are observed for large values of $\underline{r}$, the bulk of the positive density is concentrated, not at the nucleus, but about 1Å away. In a subsequent paper (1.32), a more detailed analysis of the validity of the $J(q)$ approximation is given for Gd and it is shown that for Fe, the $J(q)$ approximation has little validity.

All the calculations up till now have assumed a susceptibility appropriate to a non-interacting free electron gas. This approximation is clearly quite unjustifiable in most host metals and good agreement with experiment is thus unlikely. Wolff (1.28) suggested that the effect of electron - electron interactions in the conduction band of the matrix gives rise to an enhancement of the susceptibility. This was calculated in the random phase approximation as:

$$\chi_{ENH}(q) = \frac{\chi(q)}{1 - I\chi(q)} \quad \ldots\ldots\ldots\ldots\ldots\ldots \quad 1.30$$

where $\chi_{ENH}(q)$ is the observed susceptibility, $\chi(q)$ is the susceptibility associated with a non-interacting host with the same density of states at the Fermi surface, and I is the exchange enhancement constant of the matrix band.

Pd is the best known exchange enhanced metal with an enhancement ~ 10. Rh, Pt (~ 2) and the compounds $LaRu_2$, Ni_3Ga, $LaNi_5$ are others.

Giovannini et al (1.33) considered the effect of the enhanced susceptibility on the spin polarisation for various values of the factor, I, above. They obtained an increase in both the amplitude and the range of the spin polarisation over the free electron RKKY form and used their results to account for the g-shift and line-broadening due to rare-earth impurities in a Pd-Gd host (see ch. 5). Watson and Freeman (1.28) calculated the form of the conduction electron polarisation for a seven-fold enhancement of the host susceptibility and obtained qualitatively similar results. A sketch of their results is shown in fig. (1.5).

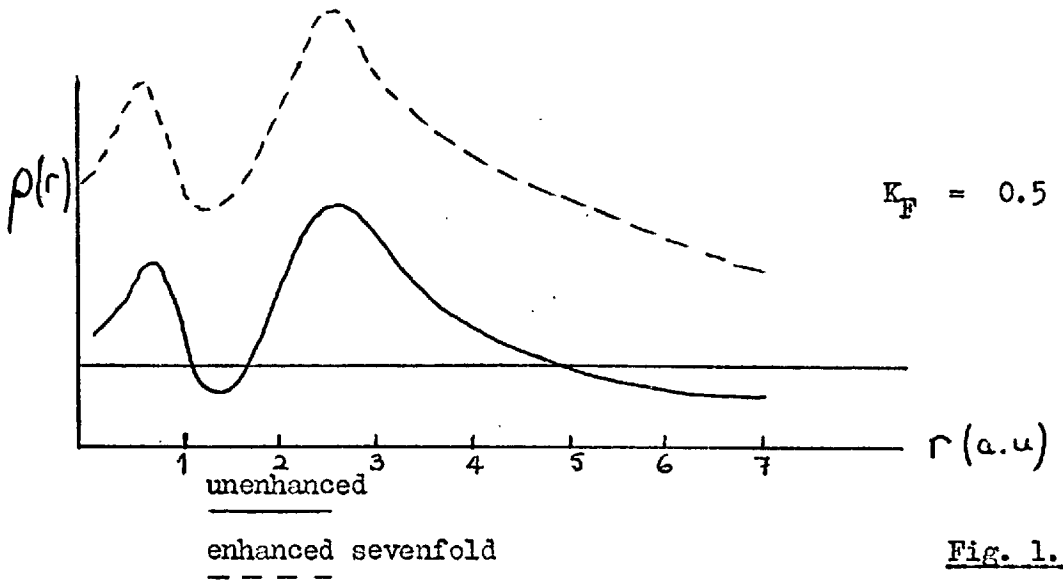


Fig. 1.5

The true exchange integral between the conduction electrons and local moments is positive in sign (equation 1.19). However, the total exchange integral measured by experiment contains other contributions which often give rise to negative coupling and the sign and value of the final exchange

parameter, J, will depend upon the relative magnitudes of the various contributions for a given alloy system.

The admixture term in the Anderson Hamiltonian (equation 1.4) is one possible source of a negative contribution. Schrieffer and Wolff (1.34), following the ideas of Anderson (1.12), Kondo (1.35) and de Gennes (1.31), showed that the mixing term could be written in the magnetic limit as:

$$J_{mix} = \frac{|V_{kd}|^2 U}{Ed\,(Ed + U)} \qquad \text{.....} \qquad 1.31$$

with the usual notation; energies being measured from E_F. This interband or covalent mixing is expected to be fairly small for the well-localised f-electrons in rare-earths and their alloys.

Watson et al (1.36) considered the contribution from this mechanism for a Gd^{3+} ion interacting with orthogonalised plane waves. They believed that the dominant source of interband mixing involves the spherical potential matrix element connecting the 4f shell and the f-like component of the conduction band. The mixing term should thus be greatest for a matrix with maximum f-character at the Fermi surface. Their calculations suggested that for rare-earths, the mechanism might possibly be large enough to outweigh the direct exchange contribution and give a negative value for J. Shaltiel et al (5.8) suggested that the mixing between the f-electrons and the d-band of the host may be the most significant contribution to a negative total exchange.

Whilst these effects may make some contribution, on a priori grounds we would not expect the large negative g-shifts which have been reported for Gd in a number of hosts, e.g., Gd in Pd (see ch. 5). In Gd, the $4f^7$ configuration is extremely stable and the energy denominators in the treatment of interband mixing (1.36) may be ~ 10 eV (1.2). A further possible mechanism may be that (1.37), in transition-like hosts, d - s

hybridisation leads to a polarisation of the s-band antiparallel to the magnetisation of the d-band. If the d-band susceptibility is high, as in exchange enhanced hosts, and there is a true exchange of positive sign between the s-electrons and the 4f shell, a large negative g-shift might be observed. The antiparallel coupling between the s and d-bands is observed in pure ordered transition metals, where neutron diffraction experiments show negative areas of magnetisation between the atoms (1.38, 1.39, 1.40). Phillips (1.41) has found a negative conduction electron polarisation (i.e., 5s antiparallel to 3d and 4d moments) in Pd-Fe alloys, which he estimated as $-1.9 \pm 0.8 \mu_B$ per Fe atom.

Recently, Campbell (1.42) has suggested a further possibility. He argues that the f-electron spin of the rare-earth may create a positive local d-moment through f - d exchange and that d - d interactions with other d-moments are then important as in transition metals. The discussion essentially treats the rare-earth 5d electrons as equivalent to those of a first half transition metal and uses the idea (2.9) that alloys of transition metals in the same half of the transition series give a positive d - d coupling (e.g., NiCo), whilst those from opposite halves give negative antiferromagnetism (e.g., NiCr).

The local moment-conduction electron exchange is reflected in a number of experimental properties of alloys. Peter et al (1.43) showed clearly that, neglecting the effects of the esr bottleneck discussed in chapter 4, the g-factor and moment should be enhanced by the same amount. Neutron diffraction measurements enable a determination not only of the total moment but also its spatial extent (1.44).

The exchange interaction also leads to a spin dependent electron scattering mechanism which contributes to the resistivity (1.31) and leads also to a reduction in the transition temperature, T_c, for superconductivity (1.45) as magnetic ions are added to a pure superconductor. In these two cases, the exchange integral appears as J^2 and thus no direct indication

of the sign of the conduction electron polarisation can be obtained. Furthermore, the values obtained from resistivity and depression of T_C measurements depend upon $J_K(q)$ for all K and q and it is not permissible to compare them numerically with the value J_{K_F} $(q = 0)$ obtained from g-shift and static susceptibility measurements. This has been stressed by Peter et al (1.43). In fact, the main contribution to the resistivity is expected to come from the region $q \sim 2K_F$ and Watson and Freeman (1.29) showed that $J(q)$ may change sign between $q = 0$ and $q = 2K_F$. This may account, for example, for the negative exchange constant suggested by the resistance minimum in the Cu-Mn system, compared with the small positive g-shift in the esr work (see ch. 4).

Nmr measurements also provide a useful tool in the study of the exchange interaction, but again, the value may not agree with those found from static susceptibility and g-shift measurements, since in nmr the conduction electron polarisation is usually measured at the non-magnetic site (e.g. Al in $GdAl_2$).

In table 1.1, below, effective moments P_{eff}, ferromagnetic moments (where appropriate), μ, and g-values are listed for a number of intermetallic compounds. Gd^{3+} ions only have been considered in order to avoid the complicating effects of the crystal field and only compounds where the partner element is not contributing to the total moment are considered.

TABLE 1.1

Compound	P_{eff}	μ	g	Compound	P_{eff}	μ	g
Gd^{3+}	7.94	7.0	1.995	GdNi	8.1	7.4	-
GdAl	8.52	7.0	-	$GdNi_2$	7.82	7.1	-
$GdAl_2$	7.92	-	1.985[x]	$GdNi_3$	-	6.55	-
$GdAl_3$	8.29	-	-	$GdNi_5$	7.9	6.1	1.94
GdIn	8.1	-	-	$GdRu_2$	-	6.35	-
$GdIn_3$	8.2	-	-	$GdRh_2$	-	6.80	1.97
$GdSi_2$	7.8	-	-	$GdPd_3$	8.6	-	2.04[x]
$GdGe_2$	8.1	-	-	$GdOs_2$	-	6.7	-
$GdSn_3$	8.0	-	-	$GdIr_2$	6.8	6.83	1.985
GdCu	8.6	-	-	$GdPt_2$	8.1	6.77	2.03[x]
$GdCu_2$	8.4	6.0	2.013[x]	GdZn	-	6.7	-
$GdCu_4$	-	-	2.01[x]	$GdZn_2$	8.48	-	-
$GdCu_5$	-	-	2.009[x]	$GdZn_{12}$	8.40*	-	1.98[x]
GdAg	8.2	-	-	Gd_2Zn_{17}	7.84*	-	1.995[x]
GdAu	7.92	-	-	$GdCu_6$	-	-	2.03[x]

Values are taken from reference (1.43) and (1.46) except

x this work

* Stewart (2.4)

A clear pattern emerges from this data in good agreement with the model of Coles et al (1.37): partners of Gd with simple metal character tend to give enhanced moments and positive g-shifts, whilst those with transition metal character seem, in general, to give reduced moments and negative g-shifts.

In solid solution alloys, work on the Pd-Gd system indicates, for low concentrations of Gd, a reduction in the ferromagnetic moment of about 20% (3.40, the two values in figs. 2(b) and 2(c) in this reference differ by ~4%; an average has been taken) and a reduction in the paramagnetic moment of 22% (5.8). Guertin and Foner (3.44) find a reduction in the saturated moment of about 8% (see ch. 8).

Alloys of the form $La_xGd_{1-x}Al_2$ have been investigated by a number of workers. Maple and Fisk (1.47) found an effective moment 4 - 7% above the free ion value and observed no resistance minimum. Cooper (1.48) and Maple (1.49) have measured the depression of T_C in $LaAl_2$ on addition of Gd and found good agreement with the expression of Abrikosov and Gorkov (1.45). Their results lead to values of J = 0.073 eV and 0.084 eV respectively. The esr measurements of Lowin (5.24) and those obtained in this work also confirm the positive sign of J in these alloys. The pure compound $GdAl_2$, as shown in the table, gives an enhanced moment but an anomalous negative g-shift and Knight shift (5.6, 5.26).

Alloys of Gd with Y, Lu, Sc and La seem to give enhanced moments. Finnemore et al (3.70) investigated Gd in La and for concentrations of more than 1% Gd, reported a moment enhanced by 6%, whilst GdY and GdLu (1.50, 1.51) both show moments enhanced by about 9%. The Gd Sc system shows an even greater increase in moment (to 30%) at low concentrations (1.52).

The g-values are also positive (5.3, 5.29, 5.30). These alloys do not seem to obey the simple rule above so well, since Y, Sc, Lu and La are transition-like metals with considerable d-character at the Fermi surface. Their behaviour is predicted, however, on the model of Campbell, since the induced d-moments couple ferromagnetically. It seems probable, in conclusion, that both d - d interactions and s - d mixing terms are important in determining the sign of J and it is difficult to predict which is likely to predominate in a given alloy system.

1.3 Divergence of Perturbation Theory - The Kondo Effect

A first order Born approximation of the resistivity (1.26) using an isotropic exchange Hamiltonian for the local moment - conduction electron exchange, leads to a temperature independent contribution to the resistivity and does not explain the phenomenon of the resistance minimum observed at low temperatures in many alloys and reviewed by Van Den Berg (1.53).

Kondo (1.35) made the first step in understanding the phenomenon, by going to second order in the Born approximation. This involves processes which consist of two events, such as:

(i) An electron in state $\underline{K}^+$ is scattered to an unoccupied state $\underline{q}^+$ and then to a final state K'^+.

(ii) An occupied state $\underline{q}^+$ is scattered to $\underline{K}'^+$ and then $\underline{K}^+$ "fills up" the state $\underline{q}^+$ which is empty,

and similar scattering sequences which allow transitions from K^+ to K'^-, K^- to K'^+ and K^- to K'^-.

Summing the total transition probabilities over the impurities leads to an expression for the magnetic resistivity:

$$\rho_M = \rho_o (1 + 4J \rho(E_F) \ln \frac{KT}{D}) \quad \ldots\ldots\ldots\ldots\ldots \quad 1.32$$

where $$\rho_o = \frac{2\pi \rho(E_F) mc}{ZNe^2\hbar} J^2 \underline{S}(\underline{S}+1)$$

is the first Born scattering term, $\rho(E)$ is the density of states and $D \sim E_F$ and Z the number of conduction electrons per atom.

The second term diverges logarithmically as $T \rightarrow 0$ and leads to an infinite resistance at T = 0K. The term arises from the treatment of the problem as a many body effect, through the interference between single electron and two electron scattering processes. For negative J, the second term combined with the phonon term ($\propto T^5$) gives rise to the observed resistance minimum. For positive J, however, the resistance does not show a minimum and continues to decrease. Such behaviour has possibly been observed in Y-Gd and Y-Tb alloys by Sugawara (1.54). Logarithmic terms also appear in other physical properties (1.55), including the esr g-shift (ch. 4), when higher order terms are considered.

Perturbation calculations to infinite order diverge at a temperature T_K, given by:

$$KT_K \sim D \exp\left(\frac{1}{|J| \rho(E_F)}\right) \quad \ldots\ldots\ldots\ldots\ldots\ldots\ldots \quad 1.31$$

for negative J. This defines the Kondo temperature of the system. Considerable theoretical work has been aimed at removing the divergence and calculating the form of the resistivity below T_K. This work is reviewed by Kondo (1.55).

One particularly interesting idea was that of Nagaoka (1.56), who suggested that below T_K, a singlet state is formed with a conduction electron 'cloud' polarised to compensate the impurity moment as the temperature is lowered. Rivier and Zuckermann (1.37) demonstrated the physical equivalence between this concept and the more general picture of a dilute

alloy, non-magnetic in the Friedel-Anderson sense, but where localised spin fluctuations are important.

The effect of second order scattering terms on the RKKY spin polarisation has been investigated by Fullenbaum and Falk (1.58). The correction term is proportional to $\ln 2K_F r$ and calculations show that the term leads to a correction $\sim 10 - 20\%$ at most to equation 1.25 . Considering the other approximation inherent in the RKKY treatment, this latter contribution may be ignored.

Finally, it should be pointed out that Kondo effects are not to be expected in magnetically ordered systems. Here the large exchange field inhibits the free motion of the spin and tends to prevent Kondo scattering. The same is true of a large external magnetic field.

CHAPTER 2

INTERACTIONS BETWEEN MOMENTS AND MAGNETIC ORDERING

In this chapter, various mechanisms for the coupling between magnetic moments will be outlined with reference to their relative importance for 3d transition metal alloys and rare-earth alloys. Conduction electron modulated exchange interactions are considered in the first section of the chapter, whilst in the second, the interactions between neighbouring 3d atoms and the effects of local environment on moment formation will be discussed. In section 2.3, interactions in disordered systems are treated and in the last section, models which seek to account for magnetic ordering and its consequences are described.

2.1 Interactions between Moments via the Conduction Electrons

The RKKY spin polarisation leads to a coupling between two ions of spin $\underline{S}_1$ and $\underline{S}_2$ at a distance $\underline{R}$, the energy of which may be written

$$E_{RKKY} = \frac{9\pi Z^2 J^2}{E_F} F(2K_F.R)\, \underline{S}_1.\underline{S}_2 \quad \ldots\ldots\ldots\ldots\ldots\ldots \quad 2.1$$

and a rough estimate for CuMn nearest neighbours gives $E_{RKKY} \sim 3 \times 10^{-4}$ eV.

For rare-earths, $\underline{S}_1$ and $\underline{S}_2$ will be replaced by $(g_1 - 1)\underline{J}_1$ and $(g_2 - 1)\underline{J}_2$. When the ionic species are the same and including spin - orbit coupling, the total energy of coupling between all the ions in the lattice is

$$E_{RKKY} = \tfrac{1}{2} \sum_{\substack{i,\,J \\ i \neq J}} \frac{9\pi Z^2 J^2 (g-1)^2}{E_F} \times$$

$$F(2K_F(R_{iJ})\, \underline{J}_i.\underline{J}_J \quad \ldots\ldots\ldots\ldots\ldots\ldots \quad 2.2$$

and using the molecular field model (1.31), the paramagnetic Curie temperature, θ is given by

$$K\theta = -\left(\frac{3\pi Z^2 J^2}{E_F}\right)(g-1)^2 J(J+1) \times \sum_{i \neq J} F(2K_F R_{iJ}) \qquad \ldots\ldots\ldots\ldots\ldots \quad 2.3$$

The function $(g-1)^2 J(J+1) = G$ is commonly known as the de Gennes function and from 2.3 it is apparent that for Heisenberg exchange coupling between spins, the values of θ across the rare-earth series for alloys of the same structure should follow the variation of this quantity, so long as J is constant.

The lattice sum in the equation 2.3 has been evaluated for various intermetallic compounds. Buschow et al (2.1) evaluated it for $GdAl_2$ at both rare-earth and Al sites and measured θ in compounds of the form $Gd_xR_{1-x}Al_2$, where R is Y, La or Th. The effect of adding Y and La to $GdAl_2$ is to introduce voids in the summation, whilst addition of Th also increases K_F. By observing the variation of θ with K_F, the location K_F for the compound was estimated. In further papers (2.2, 2.3), the dependence of the exchange integral on K_F for a number of rare-earth compounds (GdAl, $GdAl_3$ and GdCu) was investigated using nmr and susceptibility measurements to obtain consistent values of J and K_F. A change in sign of J was observed in the vicinity of $K_F = 1.3$ Å^{-1}, which agrees with the prediction of Watson et al (1.35) that interband mixing becomes the dominant contribution to J at large K_F. The analysis treats the problem from a free electron point of view, however, and ignores effects due to Brillioun zones which cause the Fermi surface to become far from spherical. Stewart (2.4) has recently pointed out that the results of De Wijn et al (2.3) for J imply that the paramagnetic moment of $GdAl_3$ should be <u>reduced</u> by 28% from the free ion value, whereas the moment in fact is <u>increased</u> by 4% (see Table 1.1). Furthermore, we note that similar analyses to those

above on $GdZn_2$ by Debray et al (2.5) and for $GdNi_5$ by Burzo and Ursu (5.14) do not fall on the curve of J v K_F plotted by Buschow et al.

Blandin and Friedel (1.11) considered a coupling mechanism between magnetised virtual bound states. Since the phase shifts of spin-up and spin-down scattered electrons is different, an oscillating spin polarisation will be obtained at large distances, given by

$$\underline{S}(r) = \tfrac{1}{2}\left[\Delta\rho_+(r) - \Delta\rho_-(r)\right] \quad \ldots\ldots\ldots\ldots \quad 2.4$$

Following the analysis of Friedel above for l = 2,

$$\Delta\rho_+ = \frac{5}{4\pi^2 r^3}\int_0^{K_F} \sin\eta_2 \sin(2Kr + \eta_2)\, 2rdK \quad \ldots. \quad 2.5$$

Blandin and Friedel considered the limiting case when the virtual state is completely split, with spin-down electrons below the Fermi energy and spin-up electrons above, i.e., $\Delta\rho_- = 0$. If we approximate the form of η_2 to a function centred at K_o, which increases from 0 to π over a range K_1, we can perform the integral in 2.5 to give

$$\underline{S}(r) = \frac{5}{4\pi^2 r^3} \frac{\sin K_1 r \cos K_o r}{K_1 r + \pi} \quad \ldots\ldots\ldots\ldots\ldots \quad 2.6$$

and the energy of coupling between two spins separated by R is then

$$E_{BF} = 2S(R)\, V_A\, F \quad \ldots\ldots\ldots\ldots\ldots\ldots\ldots\ldots \quad 2.7$$

where V_A is the atomic volume and F is a parameter $\sim$ J. A rough estimate for Mn nearest neighbours, assuming $V_A \sim 10^{-23} cm^3$, $K_o \sim 0.4 \times 10^{-8}$cm, $K_1 \sim 0.1 \times 10^{-8}$cm, gives $E_{BF} \sim 7 \times 10^{-3}$ eV. Although the polarisation in this mechanism is stronger than in the RKKY result, it decreases more rapidly (as $1/r^4$).

Caroli (2.6) considered a further mechanism which leads to coupling between virtual bound states. In this model, a conduction electron is resonantly scattered from each virtual state in turn.

After scattering from the first virtual state, the wavefunction of the conduction electron may be written for large r as

$$\psi_\sigma(r) = \exp(i\underline{K}.\underline{r}) + \frac{\exp(iKr)}{Kr} \exp(i\phi_1^\sigma) \sin\phi_1^\sigma \qquad \ldots\ldots\ldots\ldots\ldots \quad 2.8$$

where ϕ_1^σ is the phase shift for spin σ. The mixing between the conduction electrons and the d-electrons of the second impurity is characterised, not by a plane wave matrix element as in the Anderson model, but by a term

$$\langle \psi_\sigma | V_2 | d_2 \rangle = V_{Kd_2}\left[\exp(i\underline{K}.\underline{R} + \frac{\exp(iKR)}{KR} \exp(i\phi_1^\sigma) \sin\phi_1^\sigma\right] \qquad \ldots\ldots\ldots\ldots\ldots \quad 2.9$$

where $\underline{R}$ is the separation between the solute atoms. The expression gives rise to a different width and a displacement of the virtual state at the second impurity. Using a Green's function calculation within a Hartree-Fock treatment, Caroli obtains an expression for the energy of interaction between virtual states, E_C, given by

$$E_C(R) = \frac{E_F}{\pi} \sum_\sigma \sin\phi_1^\sigma \sin\phi_2^\sigma \frac{\cos(2K_FR + \phi_1^\sigma + \phi_2^\sigma)}{(K_FR)^3}$$

$\ldots\ldots\ldots\ldots\ldots$ 2.10

for the non-degenerate case and where $T \ll \Delta/K_B$.

In an appendix, Caroli shows that for degenerate d-orbitals, equation 2.10 is multiplied by a factor $(2l+1)^2\sigma^2$.

Equations 2.9 and 2.10 are only valid when $K_FR > 1$ and $K_FR > E_F/\Delta$, in which case the asymptotic form in 2.8 is a valid approximation. For CuMn, $K_FR \sim 4$ and $E_F/\Delta \sim 7$ and thus the conditions are not met.

Caroli derives a more complex expression for the coupling energy E'_C in the regime $1 < K_F R < E_F/\Delta$ and shows that for CuMn nearest neighbours

$$E'_C \sim 4 \times 10^{-2} \text{ eV}$$

The simpler formula, 2.10, is a fairly good approximation, however, giving

$$E_C \sim 7 \times 10^{-2} \text{ eV}$$

The Caroli mechanism thus gives a coupling energy for CuMn nearest neighbours which is some two orders of magnitude greater than the RKKY result. For rare-earth impurities in a real bound state, however, the interaction will be negligible since $\sin \phi \sim 0$ and in this case the RKKY interaction is the most important. Caroli obtained good agreement with the observed values of θ for the Heusler alloys Cu_2MnX, where X = Al, Sn and In, by performing the lattice sum in the expression

$$K_B \theta = \frac{25 E_F}{6\pi} \sum_{K \neq 0} \sum_{\sigma\sigma'} \sigma\sigma' \sin \phi^{\sigma} \sin \phi^{\sigma'} \times \frac{\cos (2K_F R + \phi^{\sigma} + \phi^{\sigma'})}{(K_F R)^3} \quad \ldots\ldots\ldots\ldots\ldots\ldots \quad 2.11$$

and fairly good agreement for $MnAu_2$ and $MnAu_4$. A similar calculation by Dunlop (2.7) for $Zn_{13}Mn$ is described in ch. 3.

2.2 Interactions Between Neighbouring Magnetic Atoms - Local Environment Effects

Alexander and Anderson (2.8) considered the interaction between a pair of neighbouring non-degenerate d ions in a simple metallic host. The total Hamiltonian for the system was written in the same form as that used by Anderson (equation 1.4) for the single added orbital problem, but with the addition of a term H_V which contains a transfer integral, V_{12}, between the two d-states, i.e.:

$$H_d = E_o \sum_\sigma (n_1^\sigma + n_2^\sigma) + U(n_1\uparrow n_1\downarrow + n_2\uparrow n_2\downarrow) + H_V \quad \ldots\ldots\ldots\ldots\ldots \quad 2.12$$

and

$$V_{12} = V_{21}^* = \int \phi_1^* (\underline{r}) \phi_2(\underline{r}) H_d d\underline{r} \quad \ldots\ldots\ldots\ldots\ldots\ldots\ldots\ldots \quad 2.13$$

where E_o is the self energy of the localised states in the absence of interactions.

Following the same lines as the treatment of Anderson, using a Green's function technique and within the Hartree-Fock approximation, they examined the effect of the direct coupling through V_{12} in a number of limiting cases. When the levels are symmetrically disposed about the Fermi level, an antiferromagnetic coupling ($\sim \frac{V_{12}^2}{U}$) was found to exist. When one of the two (single impurity) virtual levels is much closer to the Fermi surface than the other, however, a parallel alignment is favoured. Furthermore, it was found that in the case of antiferromagnetic coupling, the criterion for magnetism derived for the single impurity problem was made more stringent (accounting perhaps for the relatively small number of metallic antiferromagnets), whilst the condition for magnetism in the case of ferromagnetic alignment became less stringent.

Moriya (2.9) extended this work to the more realistic case of five-fold degenerate d-orbitals and his results are summarised in fig. (2.1), where the exchange energy in units of $-\frac{V^2}{2\Delta}$ is plotted against the number of localised d-electrons on the first atom, for several values of the number of localised d-electrons on the other impurity. In the case shown here, $U + 4J = 10\Delta$, but the results are not altered qualitatively for different values of these parameters.

The figure shows that atoms with nearly half-filled d-shells have a tendency towards nearest neighbour antiferromagnetic couplings, but that as the number of d-electrons increases, there exists an increasing tendency towards ferromagnetism.

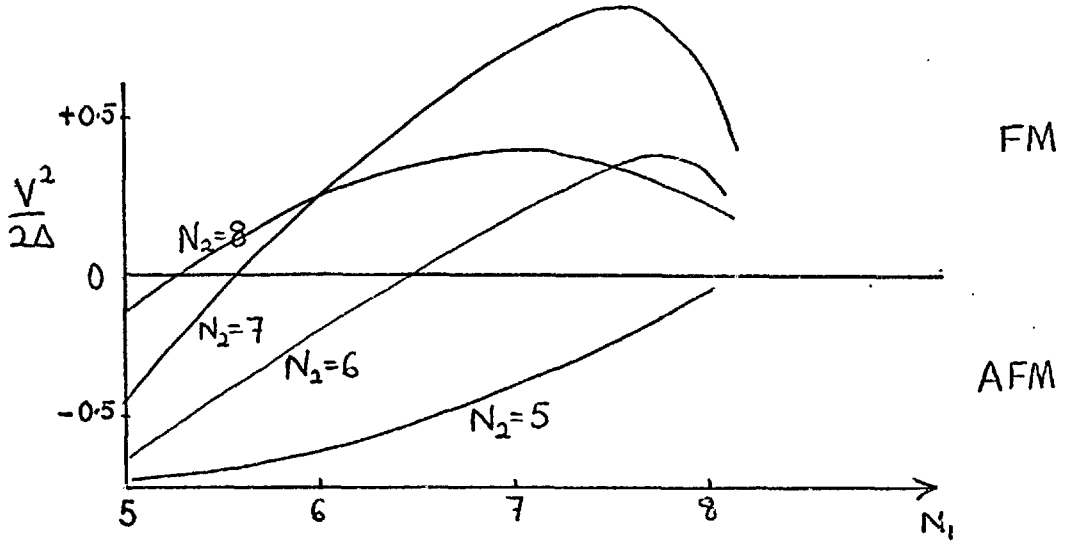


Fig. 2.1

Moriya used this to account for the ferromagnetism of Fe, Co and Ni compared with the antiferromagnetism of the middle row elements Cr and Mn. The estimated exchange energies for these 3d metals compared fairly well with the observed ordering temperatures. The properties of the alloys between these elements were also found to be in good agreement with the predictions of the theory.

Moriya went on to consider the case where one of the two atoms is non-magnetic when isolated, but which is polarised magnetically due to interaction with the neighbouring magnetic ion, and concluded that atoms with nearly half-filled d-shells have a tendency to be polarised anti-ferromagnetically, whilst those with nearly full d-shells have a preference for ferromagnetic polarisation. Likewise, a magnetic ion with a nearly half-filled d-shell tends to polarise neighbours antiferromagnetically, whilst one with a nearly full d-shell prefers ferromagnetism. This principle is used qualitatively to explain, for example, the different behaviours of Fe and Cr in Pd.

Jaccarino and Walker (2.10) suggested from nmr experiments on the Pd-Rh-Co system that the formation of a localised moment depends crucially upon the local atomic environment of the impurity, i.e. that a moment on a particular site will only be stabilised if there are more than

Z nearest neighbours of a particular type. Kim (2.11) considered this suggestion in more detail using the same Hamiltonian as Alexander and Anderson, but extended to finite concentrations, and including the Coulomb interaction between the host conduction electrons.

When other impurities are present, the density of states at the ith impurity is modified from $\rho_i^{\circ}(0)$ to $\rho_i(0)$, and the condition that nearest neighbours may stabilise a moment on an otherwise non-magnetic impurity may be written

$$U_i \rho_i^{\circ}(0) < 1 \text{ but } U_i \rho_i(0) \geqslant 1 \quad \ldots\ldots\ldots\ldots\ldots\ldots \quad 2.14$$

which can be re-written for the case where the impurity state is close to the Fermi level, in the form

$$\frac{U_i}{\pi \Delta_i^{\circ}} < 1 \text{ but } \frac{U_i}{\pi(\Delta_i^{\circ} + \delta\Delta_i)} \geqslant 1 \quad \ldots\ldots\ldots \quad 2.15$$

where the width of the impurity state has changed from Δ_i° to $\Delta_i^{\circ} + \delta\Delta_i$.

This change in width, $\delta\Delta_i$, consists of three components resulting from different contributions to the interaction energy.

$$\text{i.e.} \quad \delta\Delta_i = \delta\Delta_i^{(1)} + \delta\Delta_i^{(2)} + \delta\Delta_i^{(3)} \quad \ldots\ldots\ldots \quad 2.16$$

$\delta\Delta_i^{(1)}$ comes from the indirect inter-impurity interaction through the host conduction electrons (2.6) and is given by

$$\delta\Delta_i^{(1)} \simeq \pi V_J^2 \times \Delta\rho' \quad \ldots\ldots\ldots\ldots\ldots\ldots \quad 2.17$$

where $\Delta\rho'$ is the change of density of states of the host conduction electrons at the ith impurity site due to the surrounding impurities. It can be either positive or negative. Kim shows that $\delta\Delta_i^{(1)}$ may be written:

$$\frac{\delta\Delta_i^{(1)}}{\Delta_i^{\circ}} = \frac{1}{K_F^2} \sum_{J \neq i} \frac{\cos(2K_F R_{iJ})}{R_{iJ}^2} \qquad \text{.....} \quad 2.18$$

or for Z_i nearest neighbours on a simple cubic lattice, lattice constant, d

$$\frac{\delta\Delta_i^{(1)}}{\Delta_i^{\circ}} = 4Z_i \frac{\cos(2K_F d)}{(2K_F d)^2} \qquad \text{.....} \quad 2.19$$

$\delta\Delta_i^{(2)}$ is the contribution due to the direct transfer interaction between impurities and is always positive. Making the assumption that each virtual level is half full, we may write

$$\delta\Delta_i^{(2)} = \sum_{J \neq i} V_{iJ}^2 \frac{1}{\Delta_J^{\circ}} \qquad \text{.....} \quad 2.20$$

If we further assume that $V_{iJ} = V$ for nearest neighbour pairs and zero otherwise, and that $\Delta_J^{\circ} = \Delta^{\circ}$, then

$$\frac{\delta\Delta_i^{(2)}}{\Delta^{\circ}} = Z_i \left(\frac{V}{\Delta^{\circ}}\right)^2 \qquad \text{.....} \quad 2.21$$

Kim shows from a rough numerical approximation, that either $\delta\Delta_i^{(1)}$ or $\delta\Delta_i^{(2)}$ may be dominant in a given alloy system but that $\delta\Delta_i^{(3)}$, which is a cross term, may be neglected. Assuming $\delta\Delta_i^{(1)} \gg \delta\Delta_i^{(2)}$, he shows that the results of Jaccarino and Walker on Co in Pd_xRh_{1-x} may be understood on the basis of the above theory. Beck (2.12) has discussed the role of local environment effects in the Fe-Al, Au-V and Cu-Ni alloy systems.

For alloys like Pd-Ni, where the Ni atoms do not have a local moment and the alloy is not ferromagnetic at any temperature below a critical concentration (3.67), Kim showed, by calculating the susceptibility of

the host metal and localised states within a Hartree-Fock approximation, that the formation of a moment on the Ni site and the onset of magnetic order of the entire alloy should occur at the same impurity concentration (or temperature).

Finally, it should be stressed again that the models presented in this section rely upon a Hartree-Fock approximation for their solution and, as was emphasised in ch. 1 for the single ion problem, the approximation may drastically alter the conditions for magnetism. Furthermore, the omission of the effects of localised spin fluctuations may lead to unphysically sharp transitions.

2.3 Interactions in Disordered Systems

The fact that the interactions between moments in a metal, in general, fluctuate in sign and magnitude as a function of separation of the impurity atoms, leads in random alloys to a continuous statistical distribution of internal field P(H,T). Marshall (2.13) first considered the effects of this distribution in relation to the specific heat data in the Cu-Mn system obtained by Zimmerman and Hoare (2.14). The alloys exhibited a large excess specific heat compared to pure copper and they found this excess to be independent of Mn concentration and to increase linearly with temperature. By analogy with the work of Kittel and Abrahams (4.18) on the dipolar linewidth in magnetic resonance, Marshall concluded that P(H,T) should be of cut-off Lorentzian form with a width proportional to concentration. At low temperatures, he suggested that correlations between spins would lead to a dip in the Lorentzian at H = 0. The excess specific heat is a consequence of the fact that there is a substituted number of Mn spins which remain unaligned (i.e., see a low effective field) and the mechanism predicts the observed temperature and concentration dependence.

Klein and Brout (2.15, 2.16) extended and justified more rigorously the ideas of Marshall. They showed, using an Ising model and writing the partition function for a single spin in terms of the probability distribution of the effective field that, neglecting spin correlations, the distribution function is indeed a Lorentzian with a width proportional to concentration. However, they find that if they exclude the contribution of impurities closer to the origin than the lattice parameter, the distribution becomes a Gaussian with a width proportional to concentration.

Klein and Brout then correct for spin correlations in the limit as $T \rightarrow 0$ and assume that impurities are fully or partially correlated to the spin chosen as origin, if they are located within some correlation sphere of radius R_C. If they lie outside this radius they are screened by the intermediate spins. They show that

$$R_C(0) \simeq 0.5C^{-1/3}\, d \qquad \text{2.22}$$

where d is the lattice parameter and C the percentage of sites occupied by impurities. As the concentration decreases therefore, the correlation radius becomes larger and the average number of spins is kept constant (~ 3.3 including the central spin). The solid may thus be pictured as being composed of small inter-related clusters of interacting spins.

The effective field, H_o, at the origin is given by the convolution of the probability distributions $P(H_1)$ and $P(H_2)$ from correlated and uncorrelated regions respectively. Klein (2.16) suggests that the character of $P(H_o)$ is primarily determined by $P(H_1)$ and that the outside region $P(H_2)$ provides the spread in fields which changes $P(H_o)$ from a discreet to a continuous function.

The concentration and temperature dependence of $P(H_o)$ may be visualised by subdividing the correlated volume into three regions, the region furthest from the origin, 0,contributing the smallest fields (fig. (2.2)).

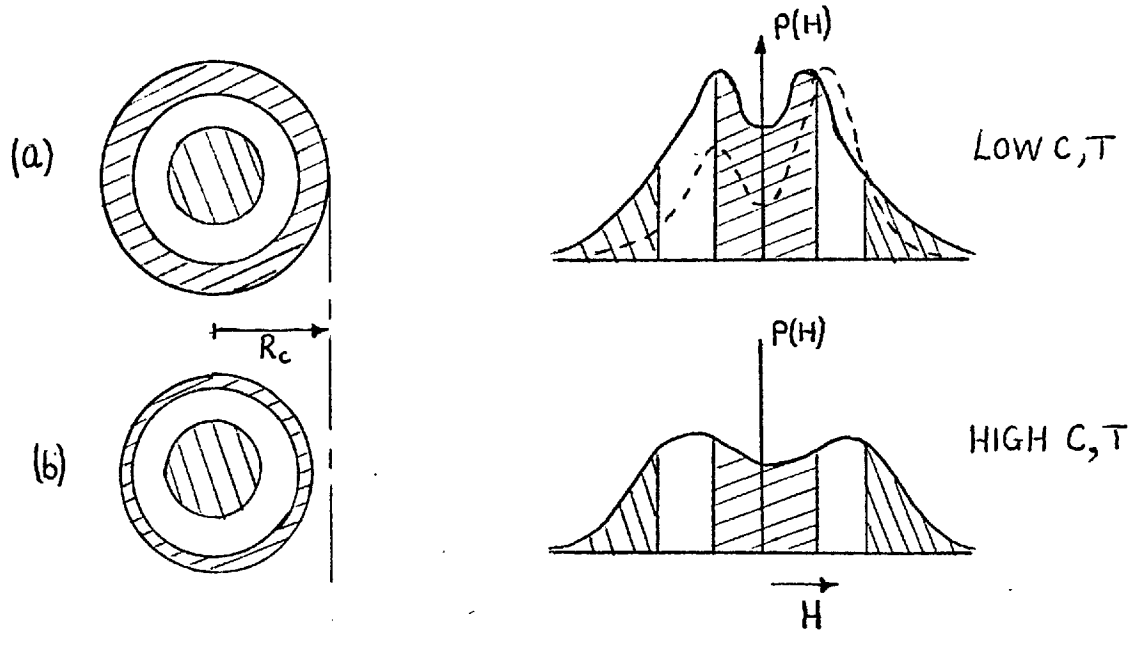


Fig. 2.2

As the concentration is increased, the correlation radius decreases according to equation 2.22 and the normalised P(H) curve takes the form (b). Similarly, as the temperature is raised, the weakly correlated spins at a distance $\sim R_c$ from the origin become randomised first, decreasing R_c, and again leading to a distribution of the form (b). The effect of an external field (dotted) is to introduce an asymmetry into the distribution, due to magnetisation of the spins surrounding the one located at the origin. Klein (2.17) has computed the form of $P(H_o)$ for a number of concentrations and temperatures and the distribution appears to give good agreement with the low temperature specific heat data.

Liu (2.18) has criticised Klein and Brout's model on two counts:

(1) For high concentrations (greater than about 1%), correlation functions beyond the two spin term should be included.

(2) Klein and Brout argue that as the temperature is increased, the most probable field (i.e., P_{max}) moves to higher values. Liu suggests that as the temperature increases, it is equally possible that the screening of the intermediate spins is reduced, the value of R_C is increased and thus the most probable field decreases.

Early Mössbauer work (2.19) seemed to support Klein and Brout's hypothesis whilst later work favours that of Liu (2.20).

Liu reverts to a semiquantitative analysis similar to Marshall's (2.13). He takes a distribution of the form

$$P(H) = \frac{a}{(H - b)^2 + C^2} + \frac{a}{(H + b)^2 + C^2} \qquad H < H_C$$

$$= 0 \qquad H > H_C$$

..... 2.23

where a is a normalising factor, b is the value of the most probable field and C is the width of the distribution. The factor b is taken to vary with temperature in the same way as the reduced average magnetisation per spin, whilst C is assumed temperature independent. Both parameters have a complicated concentration dependence. At low concentrations, however, a linear relation is assumed for both parameters. Using equation 2.23, Liu is able to predict the form of the specific heat and susceptibility with varying temperature and concentration, and also accounts for the effect of an applied field on the specific heat.

The situation outlined, where true long range order does not appear to exist but where, at high enough concentrations, interactions lead to correlations between moments at low temperatures, has been termed by Coles "magnetic glass behaviour". In simple metal hosts such systems show little net spontaneous magnetisation and interactions of both signs are probably present. Perhaps the most interesting property of the

magnetic glass state is that cooling in an external field appears to "freeze in" a moment when the field is reduced to zero at low temperatures. This indicates the presence of "loose" spins (already postulated to account for the specific heat data). This effect, along with the broadness of susceptibility and resistance anomalies, seems to offer some criterion for the existence of magnetic glass behaviour. At present, the central question of the differences between these materials and true long range ordered systems has not been answered. The theories of Klein, Brout, Marshall and Liu have some success in explaining some experimental observations, but it should be stressed that this complex magnetic state is far from understood. For example, it is not justifiable to assume that low-lying excitations can be described in terms of the rotation of individual moments against their internal fields. The esr results of Griffiths (5.49) on the Cu-Mn system, point clearly to the existence of more complex excitations.

Some further experimental manifestations of magnetic glass behaviour will be given in ch. 3.

2.4 Magnetic Ordering

As the temperature is lowered, the interactions described above lead, for the alloys discussed in this thesis, to a spontaneously magnetised state.

The simplest model which accounts for the ferromagnetically ordered state is the Weiss molecular field model. Here, a single magnetic ion is considered and the effect of the other ions in the crystal is replaced by an effective field, H_E, proportional to the magnetisation. The single atom Hamiltonian has the form

$$H_i = -g\mu \underline{S}_i \cdot \underline{H}_e$$

where $$\underline{H}_e = \frac{2zJ}{Ng^2\mu^2}\underline{M} = \gamma \underline{M} \qquad \text{.....} \qquad 2.24$$

This straightforward model is able to predict the spontaneous magnetisation, its temperature dependence, the high temperature form of the susceptibility (Curie-Weiss law) and predicts a change in specific heat at the ordering temperature. It fails, however, in predicting that the magnetic specific heat should vanish above the Curie temperature, and the wrong temperature dependence of the low temperature magnetisation is obtained. The theory predicts that near the Curie point, the magnetisation should vary as $(T_C - T)^N$ where $N = \frac{1}{2}$, whereas experimentally $N = 1/3$ has been obtained.

Various attempts have been made to improve the Weiss model by including some of the properties of the S.S interaction between spins. In the Oguchi method (2.21), the exchange interaction between a pair of atoms is considered explicitly and the effect of all the other atoms is then replaced by an effective field, again proportional to the magnetisation. In this case, the pair Hamiltonian is written

$$H_o = -J\mathcal{S}_i.S_J - g\mu(S_{iz} + S_{Jz})\ H \quad \ldots\ldots\ldots\ldots\ldots \quad 2.25$$

where H includes the applied field.

This model leads to slightly lower transition temperatures than the Weiss model and predicts that the internal energy of the sample may be reduced by short range order above the Curie point. Whereas the Weiss theory predicts $\theta/T_C = 1$, the Oguchi theory allows $\theta/T_C > 1$ (1.05 and 1.03 for simple cubic and body centred cubic lattices respectively). Like the Weiss model, it again fails to predict the correct behaviour of the magnetisation at low temperatures or in the vicinity of the Curie temperature.

These theories may be refined by lifting the restriction that the effective field should be proportional to the magnetisation. In the constant coupling approximation, H_e is taken to be a general function of the magnetisation and temperature and is determined through a self-consistency condition. In the Bethe - Peierls - Weiss (B-P-W) theory, attention is focussed on a cluster of atoms consisting of an arbitrary central atom of spin S_0 and its z nearest neighbours of total spin S_1 which are acted upon by an external field from all the other atoms. It is assumed that there are no interactions between the z shell atoms, and the cluster Hamiltonian is written:

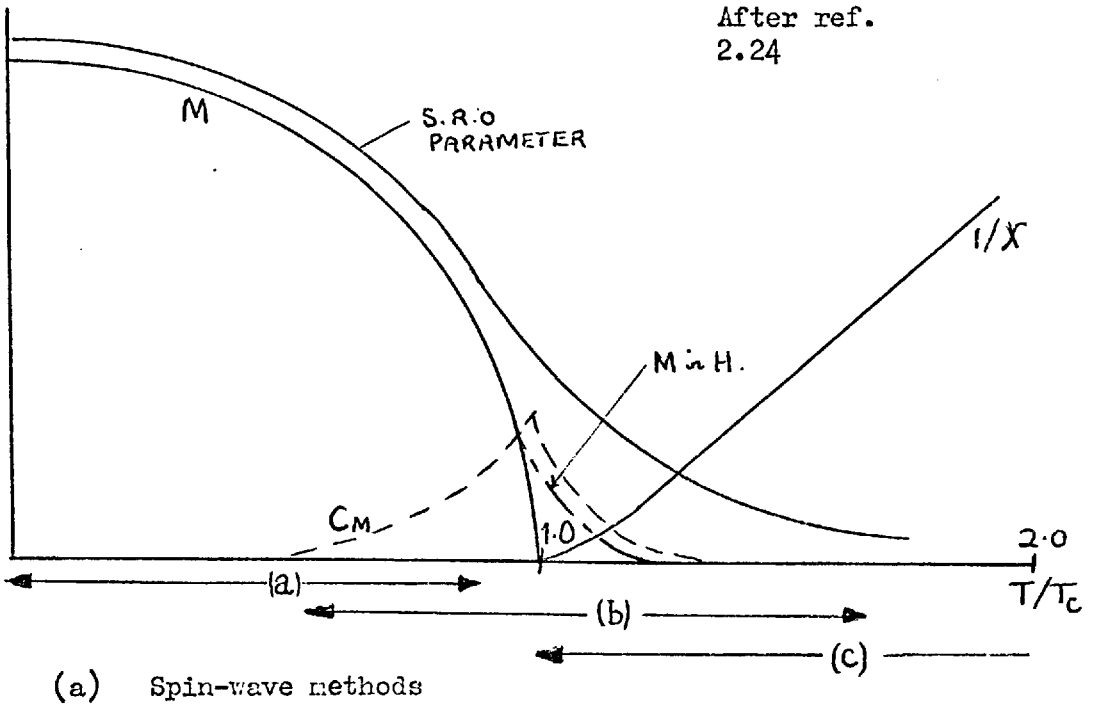
$$H_{C1} = -J\underline{S}_o.\underline{S}_i - g\mu H_o S_{oz} - g\mu H_1 S_{1z} \quad \ldots\ldots\ldots\ldots \quad 2.26$$

The consistency condition that the average moment of the central atom is the same as the average moment of the atoms in the shell, allows the magnetic properties to be evaluated. The B-P-W method is not applicable much below the Curie temperature and at low temperatures, indeed, an anti-Curie point is predicted.

The behaviour of ferromagnets above T_C may also be investigated using series expansions of the partition function in ascending negative powers of T, from which the corresponding rapidly-convergent series for susceptibility and magnetic specific heat may be derived. The calculations include the entropy of the short range order above T_C and they predict that near the Curie point $\chi \propto (1 - T_C/T)^{-4/3}$. This line of approach has been reviewed by Domb (2.22), and by Domb and Miedema (2.23) with an emphasis on the experimental results.

At very low temperatures, where the magnetisation decreases much more rapidly with increasing temperature than the molecular field theory predicts, a decrease in magnetisation may be achieved by creating a long wavelength spin wave which requires an energy $\sim JS\,a^2k^2$, where k is the wavenumber and a is the distance between neighbouring spins. This compares with an energy $\sim 2zJS$ required to flip a single spin. Thus, at low temperatures, spin wave theory (for example 2.24) is required to account for the temperature dependence of the low temperature magnetisation.

Fig. (2.3) shows the ranges of temperature over which the various approximations are valid.



(a) Spin-wave methods

(b) Cluster (effective field) approximations

(c) Series expansion methods

Fig. 2.3

In the simplest treatment of the antiferromagnetic state, the lattice is split into two sublattices, A and B, such that atoms on A have nearest neighbours on B only and vice versa. Two molecular fields,

H_A and H_B, must therefore be included in the theory. The results of this treatment predict a Curie-Weiss law for the susceptibility above T_N, with $T_N = -\theta$. This clearly contradicts the experimentally obtained results for many antiferromagnets (see ch. 4 and ch. 8).

The theory may be improved in two ways: structures such as the fcc lattice cannot be split into two simple sublattices and the theory must be extended to an n-sublattice system; furthermore, exchange beyond nearest neighbours should be included. Smart (2.21) shows that in this generalised theory, θ (which is determined by the strength of the exchange interactions) is given by

$$\theta = \frac{2S(S+1)}{3K} \sum_{m=1}^{N'} Zm\, Jm \qquad \ldots\ldots\ldots\ldots\ldots\ldots \quad 2.27$$

where Z_m is the number of the mth nearest neighbours, Jm is the exchange interaction between mth neighbours and N' is the number of pairs for which $J_m \neq 0$. Smart goes on to show that consideration of second nearest neighbours for a bcc lattice requires the lattice to be divided into four sublattices, whilst the fcc structure must be split into eight. In this way, value of $\frac{\theta}{T_N}$ from +1 to -3 in the first case, and +1 to -5 in the second, may be achieved. The various types of order may be predicted by plotting $\theta/T_{C,N}$ against J_1/J_2.

Antiferromagnets may also be treated in the Oguchi, constant coupling and B-P-W approximations. One interesting point which emerges from the constant coupling treatment (2.24) is that for $S = \frac{1}{2}$, the entropy changes occurring above T_N are 0.496 kln 2 and 0.257 kln 2 per ion for the simple cubic and bcc lattices respectively whilst, for the ferromagnetic case, the equivalent figures are 0.314 kln 2 and 0.199 kln 2, suggesting that short range order persists over a greater temperature regime above T_N than above T_C.

The arguments above have all led to the prediction of collinear structures. Some materials, however, exhibit spiral ordering or helimagnetism. If we specify each magnetic lattice point by a vector $\underline{R}$ from an arbitrary magnetic site:

$$\underline{R} = n\underline{a}_1 + m\underline{a}_2 + l\underline{a}_3$$

below the ordering temperature, the expectation value of the spin at R' will be given by:

$$\langle \underline{S}_{R'} \rangle = \frac{2S\,(S+1)}{3kT} \sum_{R' \neq R} J_{RR'} \langle \underline{S}_R \rangle \quad \ldots\ldots\ldots\ldots\ldots \quad 2.28$$

for an s-state ion, and if we assume that, in general, the ordering may be described by:

$$\langle \underline{S}_R \rangle = e^{i\underline{q}\cdot\underline{R}}\, \underline{S}_o \quad \ldots\ldots\ldots\ldots\ldots\ldots\ldots\ldots \quad 2.29$$

where $\underline{S}_o$ is the average of the spin operator at the origin and $\underline{q}$ is a characteristic wavevector, the moment remains the same in magnitude but rotates in a spiral on advancing from one moment to the next.

Substituting 2.29 into 2.28 we obtain,

$$\left(\frac{3kT}{2\underline{S}\,(\underline{S}+1)} - \sum_{\underline{R} \neq \underline{R}'} J_{\underline{R}\underline{R}'}\, e^{i\underline{q}\cdot(\underline{R}' - \underline{R})} \right) \underline{S}_o = 0 \quad \ldots\ldots \quad 2.30$$

which defines a transition temperature $T_{C,N}$ given by

$$T_{C,N} = \frac{2S\,(S+1)}{3k}\, J^*(\underline{q}) \quad \ldots\ldots\ldots\ldots\ldots\ldots\ldots \quad 2.31$$

where $$J^*(\underline{q}) = \sum_{\underline{R}' \neq \underline{R}} J_{RR'}\, e^{i\underline{q}(\underline{R}' - \underline{R})} \quad \ldots\ldots\ldots\ldots\ldots\ldots \quad 2.32$$

and the ordering then occurs for the value Q which makes $J^*(\underline{q})$ a maximum,

since this minimises the energy ($\sim - NJ^*(\underline{q})S^2$) for the spiral structure of N atoms. When $J^*(q)$ is replaced by $J^*(o)$, equation 2.31 gives an expression for θ .

Smart (2.21) has applied the general molecular field treatment to a body centred tetragonal lattice. He considers an exchange interaction between centre and corner atoms (J_1) and between the body centred atom and nearest neighbours along the x- and z-axes (J_2 and J_3). He finds, by calculating $J^*(q)$, one ferromagnetic mode, three antiferromagnetic modes and an incommensurate spiral. Both MnO_2 and $MnAu_3$ have a body centred tetragonal lattice and show helical ordering.

The heavy rare-earth metals exhibit exotic forms of spiral ordering in some temperature regimes(2.25) and here the effects of anisotropy are important. The subject of ordering in the pure rare-earth metals has been reviewed by Elliott (2.26) and Yosida (2.27).

In metallic systems the interactions are long range via the RKKY mechanism. Mattis and Donath (2.28) investigated the modes of ordering of a simple cubic lattice assuming the free-electron RKKY model with a delta function s - f interaction. They found that as the product $K_F a$ is increased, the initial ferromagnetic state is replaced by two 'antiferromagnetic' structures at $K_F a = 0.5\pi$ and 0.7π and a final 'true' antiferromagnetism at $K_F a > 0.85\pi$. Fedro and Arai (2.29) have pointed out, however, that these predictions depend critically on the assumed q-dependence of the s - f exchange interaction.

When a material becomes magnetically ordered, a new exchange field will act on the conduction electrons and this has a symmetry different from the lattice, i.e., the electrons will move in a potential which is the sum of the crystalline Coulomb potential and the ordered periodicity of the magnetic lattice. The new periodicity leads to a Brillioun zone

structure for the conduction electrons known as superzones, with splittings proportional to magnetisation. Slater(2.3) first considered such a possibility for a row of atoms which order in a simple antiferromagnetic structure, with alternate spins up and down. In such a case, if the first Brillioun zone is initially half full, the effect of ordering through the formation of superzone band gaps would be to form an insulator. The idea was extended to real alloy systems by Coles (2.31) who suggested that if the resistivity is written, as a crude approximation, in the form

$$\rho = (P_A + P_S + P_T)\ F \quad \ldots\ldots\ldots\ldots\ldots\ldots \quad 2.33$$

where P_T, P_A and P_S represent the perturbation produced by the thermal and atomic disorder of the lattice and the perturbation due to disordered spins respectively, the effect of an energy discontinuity would be to decrease the factor, F, which represents the 'freedom' of the conduction electrons and depends upon the number of carriers, their effective mass and the number of states to which they can make transitions.

The idea was used by Coles to interpret the form of the resistance data in Au-Mn compounds.

Elliott and Wedgwood (2.32), applied the idea of superzones to the heavy rare-earths and were able to account quantitatively for the variation of ordering wavevector with temperature.

CHAPTER 3

PREVIOUS WORK AND REVIEW OF MAGNETIC ORDERING IN INTERMETALLIC COMPOUNDS AND SOLID SOLUTION ALLOYS

In this chapter an account of previous experimental work on the systems studied in this thesis will be presented (with the exception of esr results which appear in ch. 5). The chapter is divided into two parts: the first deals with intermetallic compounds, whilst in the second a more general review of the onset of order in dilute solid solutions is given.

3.1 Intermetallic Compounds

(a) Rare Earths

Some data has already been discussed in relation to the sign of the exchange coupling between the conduction electrons and local moments in rare earth intermetallic compounds. Many of the references drawn upon in this section have been taken from the comprehensive review of the subject given by Taylor (1.46). A summary of much of the magnetic data appears in Appendix (2).

The rare earth dialuminides were first investigated by Williams et al (3.1) who reported that the alloys are ferromagnetic with the exception of those of La, Lu and Yb. They reported from susceptibility measurements that $GdAl_2$ orders at 176K and that the values of T_C across the series follow the de Gennes function quite closely (as do those of θ). Mader and Wallace (3.2) deduced from their susceptibility measurements that Eu in $EuAl_2$ is divalent (confirming the esr measurement of Jaccarino et al (5.6)) and found T_N = 15K, $\theta \sim$ OK with deviations from Curie-Weiss law behaviour at about 40K. They suggested that the existence of two

forms of antiferromagnetism below 40K may be responsible for this behaviour. $EuAl_2$ was found to be a metamagnet, a field of 10KGauss being required to disrupt the antiferromagnetic order.

Nereson, Olsen and Arnold (3.3) studied the Dy, Nd and Pr compounds by neutron diffraction and confirmed the ferromagnetic behaviour at low temperatures. In $DyAl_2$ they observed extra peaks at temperatures below 24K and suggested that the compound showed weak helical antiferromagnetism in addition to the ferromagnetism.

The results of resistivity measurements on $GdAl_2$ are in disagreement. Mydosh et al (3.4) found a sharp break in their plot of resistivity against temperature at 150K, with deviations from high-temperature linearity at about 180K. Van Daal and Buschow (3.5), however, observe a sharp change of slope in their data at 173K.

Deenadas et al (3.6) measured the specific heat of the Gd dialuminide and found a broad bump, quite unlike a λ-anomaly, with a maximum at about 153K and a tail extending to about 180K. They suggested that the transition in $GdAl_2$ may be only weakly co-operative.

Recently, Hacker et al (5.12) have made careful susceptibility measurements on $GdAl_2$ close to the Curie temperature. They found deviations from linearity in $1/\chi$ v T below 190K and, between 170K and 180K, fitted the inverse susceptibility to the form

$$\chi^{-1} \propto (T - T_c)^{1.03}$$

where T_c was identified as 167.8 ± 0.6K.

The magnetic properties of the equiatomic rare earth aluminium compounds were first studied by Kissell and Wallace (3.7), who found that PrAl and NdAl were antiferromagnetic, whilst CeAl was metamagnetic, with a critical field of about 8KGauss. Barbara et al (3.8) extended these measurements to other rare earths and showed that all the equi-atomic compounds are antiferromagnetic with the exception of HoAl, which is a ferromagnet. GdAl orders at 42K with $\theta = 85$K, but shows a pronounced

'kink' at about 200K in the plot of $1/\chi$ v T. The authors, by X-ray diffraction, found no sign of second phase, although the temperature at which the kink appears is suspiciously close to the ordering temperature of the metallurgically stable dialuminide. TbAl shows deviations from the Curie-Weiss law at about $2T_N$, but shows no sign of a 'kink'. The values of θ and T_N show no systematic variation across the rare-earth series.

The magnetic structure of the compounds has been elucidated by Becle et al (3.9) in a number of neutron diffraction studies. They showed that the Ho, Er, Tm, Tb and Nd compounds all order into similar non-collinear structures. Only the structures for TbAl and NdAl, however, are identical.

Magnetostatic measurements on the RAl_3 compounds by Buschow and Fast (3.10), show that $NdAl_3$ and $ErAl_3$ are ferromagnetic, whilst $HoAl_3$, $DyAl_3$, $TbAl_3$ and $GdAl_3$ are antiferromagnetic. The remaining compounds show no signs of order. The Neel temperature for the Gd compound is 17K with θ = -89K and it appears to obey a Curie-Weiss law to within a few degrees of the ordering temperature; however, no data is given for $T > 55K$ and thus deviations beginning at higher temperatures would not be immediately apparent. The varying forms of magnetic order taken up by these compounds may be understood from the changes in atomic structure on moving across the rare earth series (Appendix (2)).

Eu forms a further compound $EuAl_4$ and magnetic measurements on this have been made by Wernick et al (5.9) and Mader and Wallace (3.2). The Eu is divalent with an effective moment of $8.02\mu_B$ and the compound orders antiferromagnetically at 13K with θ = 12K. The plot of $1/\chi$ v T shows a kink at about 40K, somewhat reminiscent of that observed in GdAl. The compound has, in fact, been found to be metamagnetic with a change to ferromagnetic order setting in at applied fields greater than about 15KGauss.

The RIn_3 compounds have been studied by Buschow et al (3.11), who found that the Ce, Nd, Sm, Gd, Tb, Dy and Ho compounds order antiferromagnetically with T_N and θ , following the variation of the de Gennes function. $GdIn_3$ orders at 45K with θ = -85K and follows a Curie-Weiss law down to its ordering temperature with no sign of significant deviations. Nereson and Arnold (3.12) made neutron diffraction measurements on $TbIn_3$ and $HoIn_3$. By measuring the intensity of the largest magnetic peaks as a function of temperature, they found values of the ordering temperatures to within 1K of those found by Buschow et al but, in addition, found evidence of some short range order above the Neel point in both compounds, extending for perhaps 5K in the case of $TbIn_3$, where T_N = 37K.

A considerable amount of experimental data is available on the equiatomic compounds of rare-earths with the noble metals. Walline and Wallace (3.13) plotted $1/\chi$ v T for GdCu, and found deviations from Curie-Weiss behaviour at about 170K. No sharp increase in $1/\chi$ was observed at any temperature below this, but the authors suggested that antiferromagnetic order sets in at 41K (θ = -26K). De Wijn et al (3.14), however, find small deviations in the inverse susceptibility at about 100K but of opposite sign to those of Walline and Wallace. Their low temperature data looks similar, however, with a possible $T_N \sim$ 40K. They find θ = -75K. The deviations, it is suggested, may be due to instability of the CsCl structure at low temperatures. The susceptibility measurements of Pierre (3.15), however, led him to quote values of T_N = 140K and $\theta = -70 \pm 10$ and neutron diffraction and X-ray measurements at low temperatures showed only pure CsCl phase. Pierre's value of T_N is further supported by the resistivity measurements of Chao (3.16), who claims that CuGd orders antiferromagnetically at 135K– 145K, where there is a pronounced change in slope of the resistivity.

There is somewhat better agreement for the RAg compounds. Walline and Wallace (3.13) find a 'kink' in the inverse susceptibility (rather like that in GdAl) at about 200K, and find a value of 138K for T_N with θ = -84K. Pierre and Pauthenet(3.17) likewise find deviations from Curie-Weiss behaviour at about 175K and suggest values of $T_N = 150 \pm 3$K and $\theta = -70 \pm 5$K. Chao (3.16) again finds a change in slope of the resistivity, this time at 137K—140K.

The values of both θ and T_N for the RAg and RCu compounds follow the factor $(g - 1)^2 J(J + 1)$ closely and the absolute values for the heavy rare earths correspond, despite a difference in lattice parameter $\sim 5\%$.

Cable et al (3.18) performed neutron diffraction experiments on TbCu, ErCu and TbAg and found an antiferromagnetic structure in which adjacent (110) planes of moments are oppositely aligned.

Kissell and Wallace (3.7) performed magnetostatic measurements on the RAu series and reported a Neel temperature for GdAu of 30K—40K and θ = + 29K, with deviations from the Curie-Weiss law at about 80K. Other rare earth compounds, e.g., TbAu (T_N = 43K) also show deviations and these were explained away as crystal field effects, without reference to the GdAu result. Chao's resistivity measurements (3.16) showed a change in slope at about 45K for GdAu.

Far less magnetic data is available on the more dilute rare earth - noble metal compounds. Sherwood et al (3.19) reported that the RCu_2 compounds, with R = Gd, Tb, Dy, Ho and Er, showed metamagnetic behaviour in fields up to 80KGauss. $GdCu_2$ orders antiferromagnetically in zero field at 41K (note the similarity of this value to the anomalous GdCu result of Walline and Wallace above) and its moment at 4.2K increases steadily to $6\mu_B$ for a field of 80KGauss. The values of T_N do not vary in any systematic way across the series and no values of θ are quoted.

Brun et al (3.20) have performed neutron measurements in zero field on $TbCu_2$ (T_N = 54K, H_{crit} = 22KGauss at 4.2K). They find that Tb moments in an a - c plane form a collinear configuration in which two-thirds of them point along + $\underline{a}$ (sublattice A) and one third along - $\underline{a}$ (sublattice B), with a reversal in adjacent planes. The moments on sublattice A were found to decrease faster than those on sublattice B with a ratio $\sim$ 1:2 at T_N. A molecular field model was used together with the effects of a strong anisotropy field, to explain the results.

Williams (3.21) has measured the susceptibility of the compound Ag_3Gd and finds T_N = 35K, $\theta \sim$ -10K. The compound appears to follow a Curie-Weiss law quite close to T_N.

Buschow et al (3.22) studied RCu_5 compounds of the cubic $AuBe_5$ structure but, unfortunately, not the Gd compound. Tb and Dy were found to be antiferromagnetic and those of Ho, Er and Tm were found to be ferromagnetic, all with transition temperatures below 20K. $DyCu_5$ showed metamagnetic behaviour.

The compounds of the form RPd_3 show a striking contrast in behaviour to the isostructural RIn_3 compounds above. The measurements of Gardner et al (3.23) indicate that only the Gd compound definitely orders magnetically above 2K. It is possible that $TbPd_3$ orders at 2.5 $\pm$ 1.0K where the inverse susceptibility becomes almost constant, but this can be attributed equally well to crystal field effects. Bucher et al (3.24) report that the Pr and Tm compounds order at 1.05 and 0.20K. The inverse susceptibility of Pd_3Gd shows no significant deviations from Curie-Weiss behaviour down to its ordering temperature of 7.5 $\pm$ 0.5K (θ = 1.5 $\pm$ 1.0K). The compound, in fact, is a metamagnet. The magnetisation at 1.5K is linear in field to 7KGauss, where it increases sharply by 50%, and then increases lineary again at higher fields until saturation is achieved at about 26KGauss.

In these compounds, the magnetic interactions are weaker than the effect of the crystal field in the non-s-state ions and Gardner et al suggest that the low exchange interaction is connected with the band structure of the compounds. YPd_3, $LaPd_3$ and $LuPd_3$ are diamagnetic and this indicates that the d-band of the Pd atoms is full, giving rise to a low density of states at the Fermi surface.

Hutchens et al (3.25) have made susceptibility and resistivity measurements on the RPd_3 compounds. They suggest that Pd_3Gd orders ferromagnetically at 7K, (although the resistivity anomaly at this temperature seems to argue strongly for antiferromagnetism). They find no evidence of ordering in the other compounds above 4K.

Harris and Longworth (3.26) have performed Mössbauer and susceptibility measurements on compounds of Eu with Pd. On the Pd rich side of the phase diagram, they find that Eu is trivalent in Pd_5Eu and Pd_3Eu, in agreement with the work of Gardner et al. However, the results suggest that Eu is divalent in Pd_2Eu and the equiatomic compound PdEu. The Pd_2Eu compound shows a linear variation of $1/\chi$ v T in the range 100 - 300K with $\theta \sim$ 80K and an effective moment close to the free ion value, in agreement with the work of Wickman et al (3.27). The PdEu sample, however, shows deviations from Curie-Weiss behaviour at temperatures below 170K. Both compounds are magnetically ordered at 4.2K, but the form of the order and ordering temperatures are not given. Longworth (private communication) has recently investigated the temperature dependence of the Mössbauer spectrum of PdEu and concludes that the compound orders ferromagnetically at about 48K.

The Laves phase compounds of Pt with the rare earths were investigated by Crangle and Ross (3.28), who found them to be ferromagnetic at low temperatures. The Curie temperature of $GdPt_2$ was estimated to be 37K from an Arrott plot (H/M v M^2) and the values of T_C across the series followed the de Gennes function. Wallace and Vlasov (3.29) found

rather higher values of T_C; $GdPt_2$, for example, was reported to order at 46.5K with θ = 32K. These measurements were, however, performed in a field of 19KGauss. No deviations from Curie-Weiss law behaviour were detected above T_C.

Nereson and Arnold (3.14) performed neutron diffraction measurements on $TbPt_3$ and $DyPt_3$ which were reported to have a Cu_3Au structure. They obtained values of T_N = 20.5 $\pm$ 0.5K and 13.2 $\pm$ 0.3K respectively and, as in the case of the RIn_3 compounds, they observed short range order above the Neel point, extending in $TbPt_3$ to about 26K. The compounds order with moments aligned in opposite directions in adjacent (111) magnetic planes.

Debray et al (3.30) have measured the susceptibility of compounds of the form RZn_2. They find that the Ce, Sm, Eu, Tb and Ho compounds order antiferromagnetically whilst the Nd and Gd compounds are ferromagnetic. The shape of the M - H curve, which is concave upwards for fields below 5KGauss, suggests, however, that $GdZn_2$ may be a metamagnet. The inverse susceptibility shows considerable deviations from linearity beginning at about 100K and, finally, shows a transition to an ordered structure at 68K ($\theta \sim$ 70K). The authors point out the deviations, but only suggest that they may "be due to the exchange interaction", which does not seem to be particularly helpful. $TbZn_2$ shows similar behaviour and this has the distinction of apparently ordering into two different antiferromagnetic modes at 55K and 25K. $EuZn_2$ is interesting in that its inverse susceptibility appears to show a gradual change of slope, from that associated with a Eu^{3+} ion at room temperature, to a Eu^{2+} state close to 20K, where it orders.

The dilute compounds RZn_{12} and R_2Zn_{17} have been investigated by Stewart (2.4). Susceptibility measurements on the R_2Zn_{17} compounds showed that when R is Gd or Tb, antiferromagnetism is found at low temperatures, whilst for R = Dy, Ho, Er or Tm no ordering is found down to

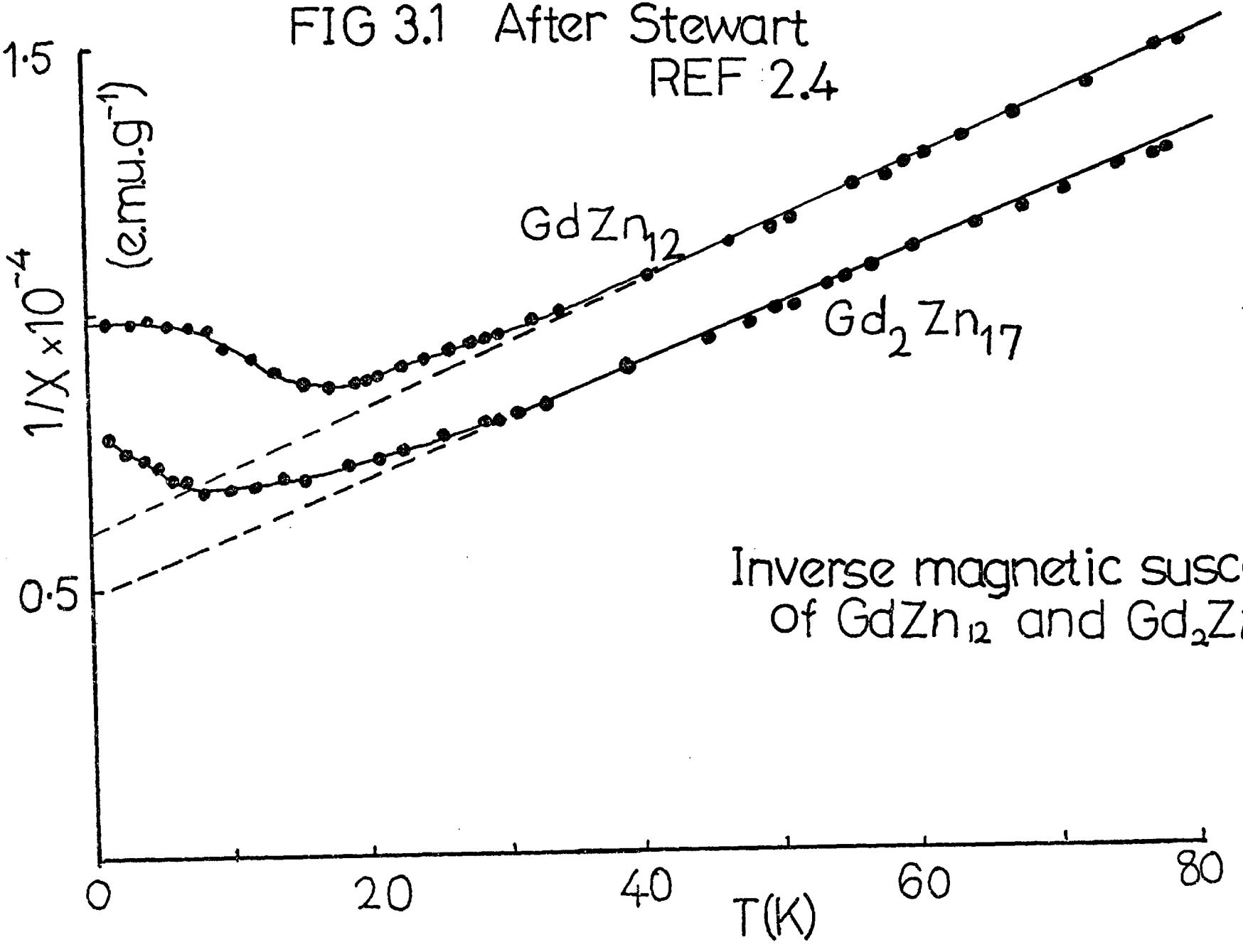
2K. Gd_2Zn_{17} shows sizeable deviations (fig. (3.1)) from Curie-Weiss law behaviour, from just about 30K and orders at about 10K (θ = -53K). Tb_2Zn_{17} shows similar deviations at 90K, well above its ordering temperature of 28K, (θ = -17K). The large difference between the values of θ/T_N in the two compounds may mean that the final modes of order are different.

Stewart measured both the susceptibility and resistivity of the RZn_{12} compounds. $GdZn_{12}$ follows a Curie-Weiss law only down to 50K where deviations begin (fig. (3.1)). The compound orders at 16K (θ = -58K.) The resistance data suggest a value of T_N = 15.25K and the magnetic resistivity obeys a power law $\rho - \rho_0 = AT^n$ below T_N, where ρ_0 is the residual resistivity and $n \sim 3/2$. For a conventional antiferromagnet, a value of $n \sim 4$ is expected. $TbZn_{12}$ shows similar results with departure from linearity in the inverse susceptibility at about 60K, some 46K above the Neel temperature (θ = -38K). The resistivity again follows a $T^{3/2}$ power law below T_N.

Neutron diffraction measurements on $TbZn_{12}$ suggest that the type of order is not simple (e.g., spins at the corner of the tetragonal lattice with spin up, centre spin down). The absence of exponential behaviour in the resistivity (suggesting the absence of an energy gap in the spin wave spectrum) has led Stewart to suggest that the ordered structure may be an incommensurate spiral.

Coles and Griffiths (3.31) measured the susceptibility of the compound GdB_6 and established that it ordered antiferromagnetically at 13K with θ = -60K. Deviations from Curie-Weiss law behaviour were observed at a temperature $\sim$ 100K (fig. (3.2)). Resistance measurements in a further paper by Coles et al (3.32) confirmed the value of T_N found above and showed similar anomalous behaviour between 14K and 80K where the value of the resistance is lower than the curve expected in the absence of ordering.

FIG 3.1 After Stewart
REF 2.4



Inverse magnetic susceptibility of $GdZn_{12}$ and Gd_2Zn_{17}

Resistivity and inverse susceptibility of GdB_6
After Ref 3.32

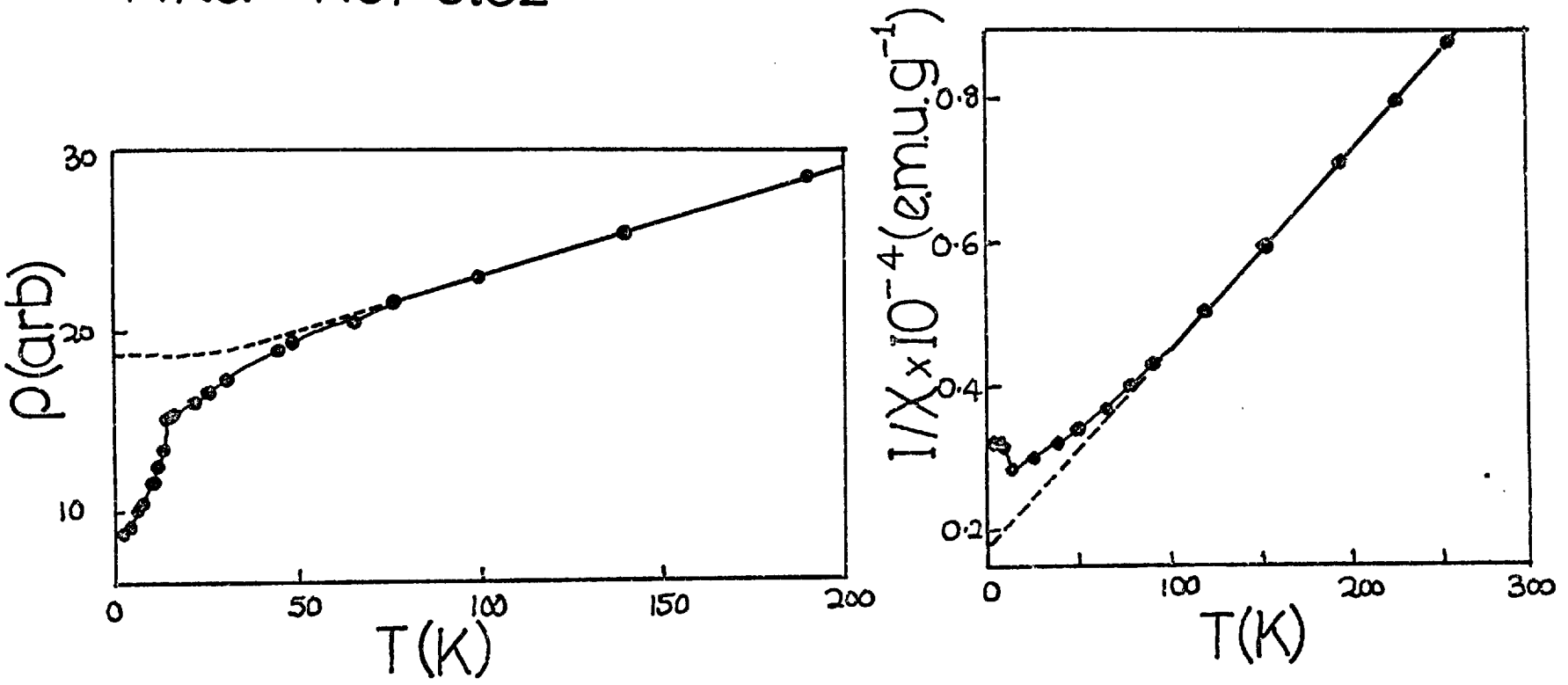


FIG 3.2

Fisk (1.6) has made a thorough study of the rare-earth hexaborides and has found that, with the exception of EuB_6, they order antiferromagnetically and that the Curie-Weiss θ's follow the de Gennes function well. The values of T_N, however, do not, and Fisk suggests that this may be due to anisotropic exchange.

The striking deviations in the inverse susceptibility above T_N were also observed in TbB_6 where, like the Tb_2Zn_{17} compound above, θ/T_N is much lower (~ -1.5) than its Gd counterpart. Fisk speculated that the deviations may be due to the formation of superzone band gaps. This will be discussed in greater detail in ch. 8.

Westrum (3.33) reports a λ -anomaly in the specific heat of GdB_6 at 16K and a Schottky anomaly at 30K, which is best fitted with an upper level about $60cm^{-1}$ above the ground state. He was unable to offer an explanation for this latter effect.

The compound EuB_6 is particularly interesting. The Eu is divalent and the compound is a semiconductor. It is the only hexaboride which is ferromagnetic and Fisk (1.6, 3.34) finds $T_C = 8K$, $\theta = 9K$. He accounts for this anomalous behaviour using a modification of the RKKY interaction suggested by Bloembergen and Rowland for semiconductors.

The heavy rare-earth tetraborides all order antiferromagnetically and Fisk found an ordering temperature of 42K for GdB_4 with $\theta = -60K$. The values of θ again follow the variation of the de Gennes function in contrast to the values of T_N which show no systematic variation.

(b) Transition Metals

The compound Au_3Mn was shown by Meyer (3.35) to be antiferromagnetic with a Neel temperature of 145K, $\theta \sim 200K$. The Mn ion carries a moment of $4.2\mu_B$. Deviations from Curie-Weiss behaviour appear to set in at 250K - 300K (3.36).

The Heusler alloys have been studied extensively by Webster and

Tebble (3.37) using neutron diffraction and susceptibility measurements. Pd_2MnSn, the compound studied in this work, orders ferromagnetically at $189 \pm 3K$ with $\theta = 201 \pm 3K$ and the Mn ion carries a moment of $4.23 \pm 0.07\mu_B$. The inverse susceptibility obeys the Curie-Weiss law to about 240K, below which deviations from linearity set in. Pd_2MnIn is antiferromagnetic with $T_N = 142 \pm 3K$. Neutron diffraction measurements suggest a magnetic structure similar to that of MnO, with adjacent (111) planes coupled antiferromagnetically, but with the Mn atoms within each plane aligned parallel to each other. It is interesting to note that, in this case, $\theta/T_N \sim + 1/3$. Deviations from Curie-Weiss behaviour do occur at about 220K, but the neutron diffraction results indicate a small amount of random atomic disorder for this compound (ch. 6). Webster (3.38) has recently reviewed the metallurgy and magnetism of the Heusler alloys.

Nakagawa et al (3.39) investigated the magnetic properties of various dilute Zn-Mn intermetallic compounds containing from 15 - 35% Mn. The susceptibility of the ϵ phase, which has an hcp structure and is stable at temperatures above 400C, was fitted to a Curie-Weiss law for a number of compositions in its phase field, over temperature ranges from 570K to 960K. The 15% alloy had a Curie temperature of 260K (θ = 150K) and the Mn carried a moment of $3.6\mu_B$. As the concentration of Mn was increased, θ decreased almost linearly to a value of -190K at 35% whilst the moment on the Mn ions increased to $4.3\mu_B$ for a 25% alloy, thereafter showing no further increase. The α' phase, which has a Cu_3Au structure, was found to have θ = 110K and a moment of $3.7\mu_B$, ordering antiferromagnetically at 150K. The γ phase containing 20% Mn has θ = 70K and a moment of $5.4\mu_B$.

Dunlop (2.7) has recently made a careful study of the magnetic properties of the ζ phase $Zn_{13}T$ compounds where T is Mn, Fe or Co. Susceptibility measurements on the compounds show a gradation of magnetic behaviour. $CoZn_{13}$ has a temperature independent diamagnetic susceptibility,

whilst $FeZn_{13}$ shows enhanced Pauli paramagnetism. $MnZn_{13}$, the compound studied here, obeys a Curie-Weiss law from room temperature to about 120K, below which deviations from linearity set in (fig. (3.3)). The high temperature data give θ = + 36.5K and an effective moment of $1.82 \pm 0.05\mu_B$. A plot of magnetisation against temperature in 7KGauss suggests that the compound orders (perhaps between 10K and 30K) and an Arrott plot indicates an ordering temperature of 22.9 ± 0.3K. A magnetisation curve at 4.2K leads to an (almost) saturated moment of $0.3\mu_B$ at 8KGauss. This behaviour contrasts with that of $Mn_{0.05}Fe_{0.95}Zn_{13}$, where 5% of the Fe atoms in $FeZn_{13}$ have been replaced by Mn atoms. In this case, the full paramagnetic moment for dilute alloys of Mn in Zn ($4.0\mu_B$) is observed and the compound follows a Curie law down to 20K.

Specific heat measurements were also made, and below 3.5K the data from all three compounds could be fitted to $C = \gamma T + \beta T^3$. A spin-wave contribution to the value of γ ($62.3 mJ.mole^{-1}.K^{-1}$) for $Zn_{13}Mn$ was not ruled out.

The resistivity of $Zn_{13}Mn$ follows a $T^{3/2}$ beahviour (like $GdZn_{12}$) at low temperatures, whilst at higher temperatures it obeyed a power law (to 19K)

$$\rho - \rho_0 = CT^{3/2} + DT^{7/2}$$

The magneto resistance is large and negative and, when plotted against temperature, peaks sharply at 20K.

The substituted $Mn_{0.05}Fe_{0.95}Zn_{13}$ compound shows a resistance minimum at 19K with a logarithmic temperature dependence from 14K to 7K below which a maximum is observed. The position of the minimum corresponds with the position of the minimum found by Collings et al (5.60) in Zn 0.4at% Mn.

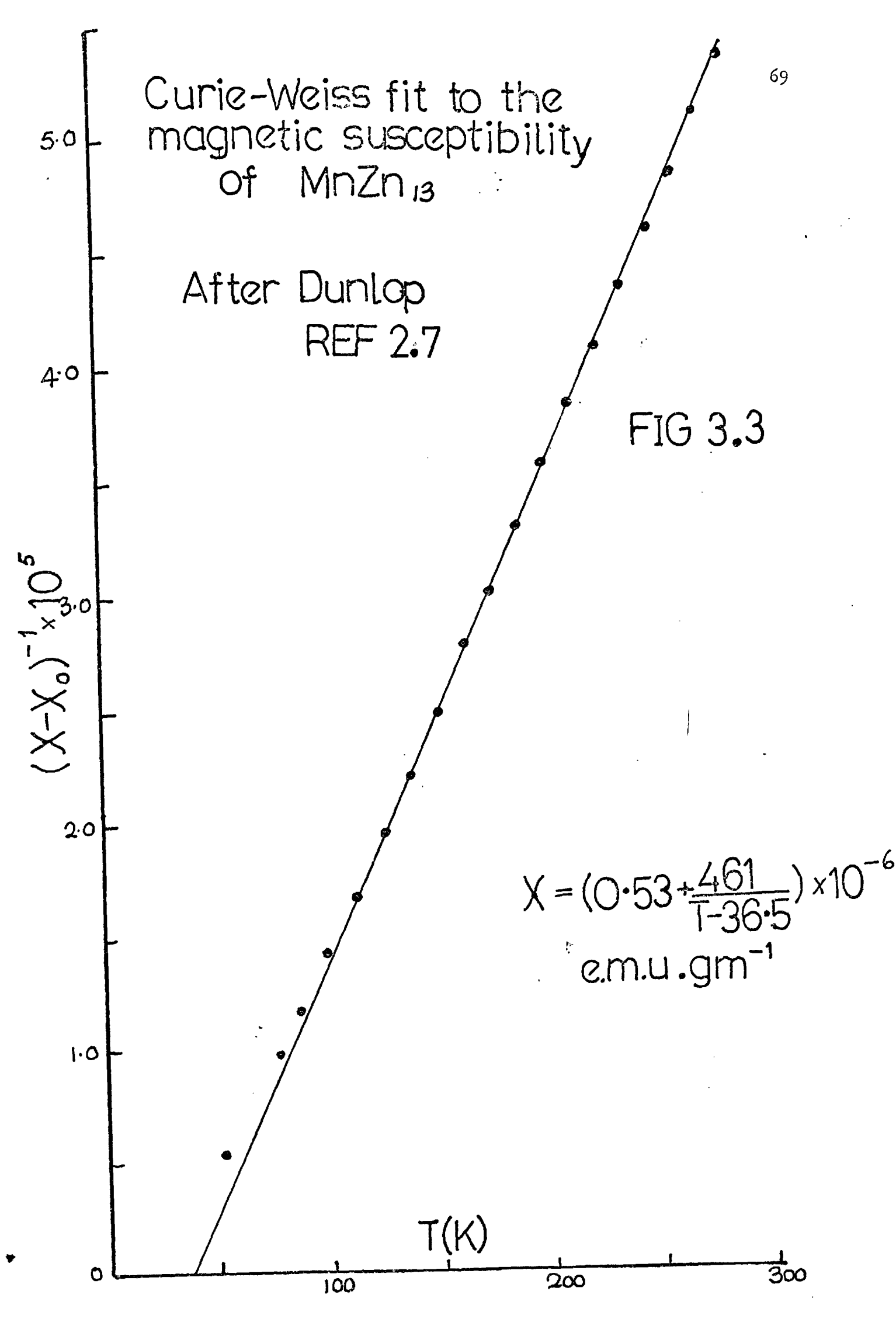

Curie-Weiss fit to the magnetic susceptibility of $MnZn_{13}$
After Dunlop
REF 2.7
$(X-X_0)^{-1} \times 10^5$
5·0
4·0
3·0
2·0
1·0
0
T(K)
100
200
300
$X = (0{\cdot}53 + \frac{461}{T-36{\cdot}5}) \times 10^{-6}$
e.m.u.gm^{-1}

FIG 3.3

Solute / Matrix	1 Bound State good (4f) moment	2 Virtual bound state with good (3d) moment	3 Anomalous moments (Kondo-LSF)	4 Virtual bound state with little or no moment
A Simple (sp) metal	Au-Gd Ag-Er	Cu-Mn Cu-Cr Ag-Mn Au-Mn, Au-Cr, Au-Fe Zn-Mn	Cu-Fe Cu-Co Au-V, Au-Co ZnCr ZnFe	Cu-Ni ZnCo, ZnNi AlMn, AlCr, AlFe, AlCo
B Simple Transition Metal	Zr-Gd Ti-Gd Zr-Er $LaAl_2$-Gd	Mo-Fe Ti-Mn Pt-Fe Pt-Co	RhFe IrFe RhMn PtCr PtNi	Ti-Mn, Ti-Fe VFe, VCo NbFe RuFe IrCo RhCo
C Enhanced Transition Metal	Pd-Cd	Pd-Fe Pd-Mn Pd-Co	PdCr PdNi	PdV
D Anomalous $\chi(q)$ of band structure origin	Sc-Gd Y-Gd Y-Tb etc. La-Gd	Cr-Fe	Y-Ce	Cr-Mn

FIG 3.4

Preliminary neutron diffraction data on a polycrystalline sample of $Zn_{13}Mn$ does not show extra lines at low temperatures which might be associated with antiferromagnetic or spiral ordering.

Dunlop performed the sum in the Caroli interaction (2.6) to a radius of 50Å as a function of ϕ for various values of k_F and found the best agreement with the observed value of θ for a virtual bound state containing six electrons. It was suggested that the low paramagnetic and ordered moments, compared with the substituted alloy, indicates that the translational symmetry of $MnZn_{13}$ modifies the virtual bound state by increasing the overlap between the spin ↑ and spin ↓ halves. The broadening of the halves of the virtual bound state was attributed to coherent hybridisation between the conduction electrons and d-electrons.

3.2 Solid Solution Alloys

It would be beyond the scope of this thesis to attempt to summarise, in any detail, the vast amount of experimental data which has been collected on all dilute alloy systems. In this section will be presented a broad classification of the various situations which occur when a 'solute' atom is dissolved in host metals of various character, plus a more detailed review of experimental work on those sections of the classification of direct relevance to the work in this thesis. The chapter concludes with a brief discussion of a few other 'interesting' systems.

The classification shown in fig. (3.4) has been formulated by Coles. The types of solute configuration have been discussed in some detail in ch. 1, but some comments are required on the types of solvent labelled A - D.

Row A shows alloys with hosts in which the Fermi surface is mainly s-like and is fairly well represented by a nearly free electron model. B-type solvents are unenhanced transition metals with a large density of states at the Fermi surface, due to the presence of an unfilled d-band.

Row C contains exchange-enhanced transition metals, discussed above, whilst Row D is made up of hosts which are similar in character to those classified under B, but whose band structure is such that $\chi(q)$ favours complex forms of magnetic behaviour. For example, Y, Sc and La may be considered as 'rare-earths without 4f electrons' and addition of a little rare-earth solute does not perturb the band structure to any marked extent. As in the pure rare-earth metals, the local 4f moment establishes helimagnetism due to the strong response of $\chi(q)$ at a particular value of q.

It should, of course, be emphasised that the 'dilute alloy map' represents only dilute systems and does not include the considerable modifications of behaviour which may be observed with increasing concentration; furthermore, its rather artificial boundaries are in no sense rigid. The three sections which are of most relevance to the dilute alloy work in this thesis are A2, C1 and C2. Experimental work on alloys within these sections will now be reviewed in greater detail.

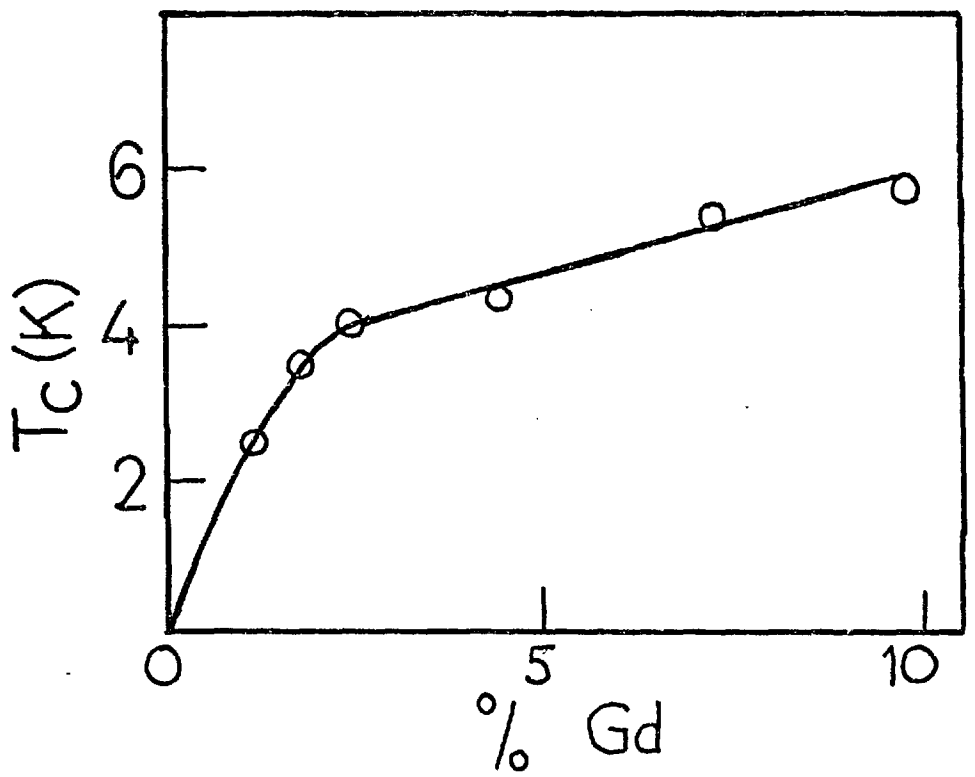
(a) C1: Bound State in Exchange Enhanced Transition Metal

The archetypal alloy system in this category is, of course, Gd in Pd.

Crangle (3.40) performed magnetisation measurements on alloys containing between 1 and 10at% of Gd and reported that all concentrations within this range exhibited ferromagnetism. The Curie temperatures, as a function of concentration, are shown in fig. (3.5). The reported values of the saturation and paramagnetic moments have been discussed in ch. 1.

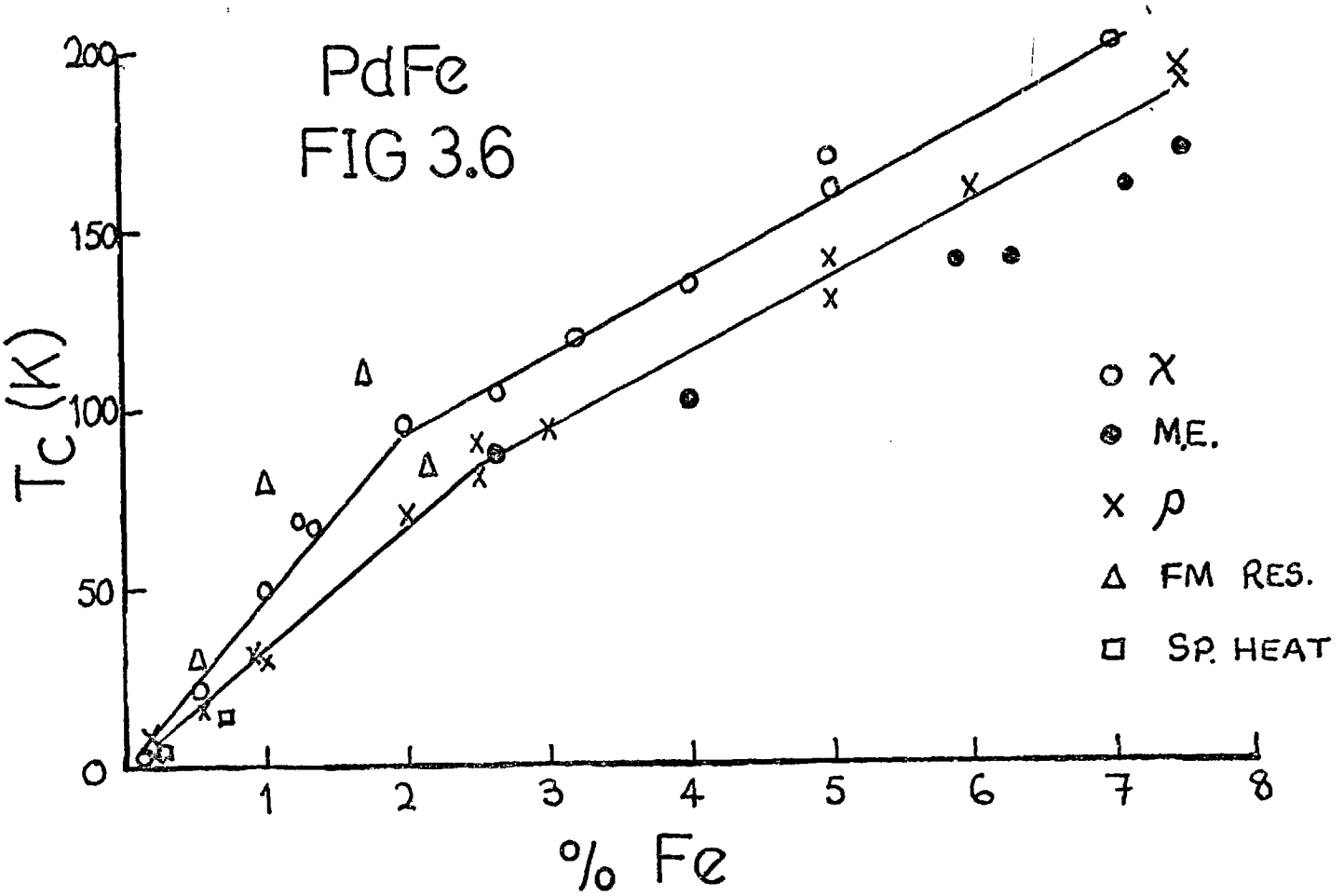
Resistivity measurements on concentrations of 0.5 — 3% Gd were made by Sarachik and Shaltiel (3.41) and showed no sign of any sharp transition which could be associated with the onset of ferromagnetic order and no sign of a Kondo anomaly. On the other hand, more recent resistivity measurements by Chen et al (3.42) have shown a discontinuity of slope

PdGd FIG 3.5



After Ref. 3.42

PdFe FIG 3.6



in 1 at% Pd-Cd and Pd-Nd alloys at 2.4K and 3.5K respectively, the former value being in good agreement with Crangle's data. The authors point out, however, that no signs of ordering are manifested in susceptibility measurements on Pd-Nd and the behaviour of the incremental resistivity below these 'transition' temperatures exhibits a logarithmic temperature dependence. If the measurements are to be interpreted as a Kondo anomaly, the sign of the exchange integral relevant to resistivity measurements must be positive.

Bellarby and Crangle (3.43) measured the specific heat of three PdGd alloys containing 3.0, 5.0 and 7.7at% Gd between 1.5K and 60K. A broad peak was observed at 2.2K, 2.8K and 3.8K respectively. The magnetic entropy was found to correspond to a spin of 2.75 ± 0.4 on each Gd ion; the difference from the value of 3.5, it was suggested, might be attributed to the negative polarisation of the Pd4d band.

(b) C2: Virtual Bound State with Good (3d) Moment in Enhanced Transition Metal

e.g. Pd-Fe, Co, Mn.

The Pd-Fe system has been the subject of considerable research since the early work of Crangle (3.45) who showed that ferromagnetism in the system persists to very low Fe concentrations and that, indeed, extrapolation of the curve of Curie temperature against concentration (which has a remarkably large slope of 30 - 40K per at% Fe) appeared to pass through the origin. The magnetic moment per Fe atom was also found to be larger than could be associated solely with the Fe 3d electrons, reaching 7.4 μ_B/atom at 1.25at% Fe. Crangle suggested that nearest neighbour Pd atoms were polarised ferromagnetically with a moment of 0.4 μ_B/atom.

Cable et al (3.46), from a combination of magnetisation and diffuse neutron scattering on 3at% and 7at% Fe in Pd alloys, deduced that if all Pd atoms carried the same moment, the 3d moment associated with the Fe atoms in both alloys would be $3.0 \pm 0.2\mu_B$, whilst that associated with the Pd atoms would be $0.15 \pm 0.01\mu_B$ and $0.26 \pm 0.02\mu_B$ for the 3 and 7at% alloys respectively.

Following their development of the technique of long wavelength diffuse elastic neutron scattering, through which the spatial distribution of moments may be determined, Low and Holden (3.47) showed that in a 0.25at% Pd-Fe alloy, a polarisation cloud existed with a radial extent of more than 10Å, affecting several hundred Pd atoms. The moment on individual nearest neighbour Pd atoms was estimated to be $\sim 0.05\mu_B$.

Veal and Rayne (3.48) measured the specific heat of a number of Pd-Fe alloys containing from 0.09 to 0.72at% of Fe and found a gentle wedge shaped magnetic peak at temperatures rather lower than is suggested by the magnetisation data of Crangle. An entropy corresponding to a spin of 1.1 was deduced, which is in fair agreement with the single measurement of Coles et al (3.49) (0.19at%) who preferred a value of 1.5 for the spin. The value of the Curie temperature for this alloy was in good agreement with Veal and Rayne's data and with resistance measurements on 0.1at% and 0.5at% alloys, which showed a sharp discontinuity at temperatures corresponding to the peak in the specific heat. The values of T_C deduced from all the measurements are shown in fig. (3.6), including the sharp anomalies found in the incremental resistivity by Williams and Loram (3.50) for concentration of up to 0.9at%. Their results show agreement with the theoretical prediction that $\Delta\rho \propto T^{3/2}$, well below T_C in random ferromagnets.

Ferromagnetic resonance in a 2.2at% alloy reported by Bagguley et al (3.51) gave $g = 2.16 \pm 0.04$ and suggested a value of T_C (derived from a maximum in the linewidth) of $\sim$ 85K, in good agreement with Crangle's data.

At concentrations below about 0.2at%, Crangle and Scott (3.45) claimed that there was a reduction in the moment per Fe atom. They suggested that the long range ordering arises because the polarisation clouds of adjacent solute atoms overlap and thus interact ferromagnetically; at low enough concentrations, however, some complexes become isolated and cease to be coupled to the magnetisation of the whole specimen and thus a drop in moment is observed. At high temperatures the moment is again reduced but, in this case, solute atoms compete with each other for solvent and there is insufficient to complete each polarisation cloud.

Recently, Chouteau and Tournier (3.52) have extended measurements of the magnetisation of Pd-Fe alloys to concentrations as low at 69ppm, at temperatures down to 0.05K and in fields of up to 35KGauss. They find a mean value for the moment per Fe atom below 0.2at% of $10\mu_B$ and an effective moment of $13\mu_B$. Below about 0.1at%Fe, T_C appears to be proportional to the square of the concentration whilst at higher concentrations a linear relation is obeyed. Extrapolation of this linear regime leads to a 'critical concentration' corresponding to an average Fe-Fe separation of 15 - 20Å. Chouteau and Tournier suggest that this may mark the onset of antiferromagnetic interactions at very low concentrations. It is interesting to speculate whether, at low enough temperatures and concentrations, the statistical nature of the alloy will, in fact, lead to magnetic glass behaviour.

The Pd-Co system is very similar to Pd-Fe in its magnetic properties. Bozorth et al (3.53) showed that a 0.1at% Co in Pd alloy is a ferromagnet below 7K and measured a saturation moment of $10.5\mu_B$ per Co atom. The curve of Curie temperature against concentration is broadly similar to that of Pd-Fe, with a slightly greater slope ($\sim$ 50K/at% below 2at%). The neutron diffraction work of Low and Holden (3.47) showed the same polarisation clouds as in Pd-Fe, with similar radial extent. One point of interest arises from the specific heat measurements of Boerstel (3.54) and the resistivity measurements of Williams (3.55a) in that both measurements show less well defined magnetic transitions than the Pd-Fe data. The specific heat peaks are rather broader, and the discontinuity in the incremental resistivity much less sharp. The transition temperatures indicated by esr (3.51) and magnetisation data are, again, higher than those derived from the specific heat and resistivity.

Pt-Fe (3.45) atoms (as might be expected) show only a relatively small increase in moment per solute atom at low concentrations.

Rather surprisingly, whilst its Fe and Co counterparts have received considerable attention, the Pd-Mn system has been relatively neglected. Sarachik and Shaltiel (3.56) measured the resistivity of 0.5, 1.0 and 2.0at% alloys and found sharp transitions, suggesting ferromagnetism, at 1.4, 4.0 and 5.5K respectively. This behaviour was reproduced by Williams and Loram (3.55b) who found a linear regime below T_C, followed by $T^{3/2}$ behaviour at low temperatures. The measurements suggest that dT_C/dc is a decreasing function of concentration in contrast to Pd-Co and Pd-Fe.

Rault and Burger (3.57) confirmed the ferromagnetic behaviour at low Mn concentrations by magnetisation and susceptibility measurements. They found that the Curie temperature increased as a function of concentration up to 2.5% Mn, but then decreased as the concentration was further increased. Above about 8at% the alloys were found to be antiferromagnetic.

They suggested that the behaviour of the system is similar to that of Pd-Fe and Pd-Co but that antiferromagnetic Mn-Mn interactions on the model of Moriya (2.9) begin to dominate, as the likelihood of nearest neighbour Mn atoms is increased. The authors also added hydrogen to their alloys and found that, for concentrations of less than 8at%, the ferromagnetism was reduced whilst, for the higher concentration, the paramagnetic susceptibility was strongly increased. This latter observation is difficult to explain.

Boerstel (3.54) measured the excess specific heat of five Pd-Mn alloys containing from 0.08at% to 2.45at% Mn, both in zero field, and in fields of up to 27KGauss. For the higher concentrations with peaks within the temperature range of the measurements, a rather remarkable cusped peak is observed in zero applied field, which looks intermediate in character between the peaks in Pd-Fe and Pd-Co and a true λ-anomaly. Boerstel points out that no similar peak has ever previously been reported in a dilute alloy. The temperatures at which the peaks occur are compounded with the other measurements on the system in fig. (8.14); again, the specific heat data indicates lower values of T_C. Application of a magnetic field of 27KG broadens out the cusp and moves the peak to higher temperatures (from 4.5K to 9.5K for a 1.35at% alloy). The total entropy associated with the magnetic transition was found to correspond to a mean spin $\sim 2.35 \pm 0.1$.

Sarachik and Shaltiel (5.56) quoted a private communication which ascribed a moment of $5.6\mu_B$ per Mn atom to a Pd2Mn alloy, and this agreed well with the value of $6.3\mu_B$ obtained for the effective moment by Shaltiel et al (5.8). Accordingly, it was long considered that the moment of Mn in Pd is close to the free ion value. Very recently, however, Star et al (3.58) have reported that Mn in Pd has a 'giant' moment of $7.5\mu_B$ per Mn atom for concentrations of less than 0.5at%. The fields of up to 210KGauss were, at 4.2K, insufficient to saturate alloys with Mn concentrations about 0.5at%.

(c) A2: Virtual Bound State with Good 3d Moment in a Simple Metal

This constitutes one of the most widely studied groups of alloys and includes, for example, Mn in Cu, Ag and Au; Fe in Au and Mn in Zn.

Owen et al (5.45) measured the static susceptibility of a number of alloys of Mn in Cu with concentrations from 0.03 to 11.1at%, and found maxima in the susceptibility indicative of antiferromagnetism. These maxima became increasingly broad as the concentration was increased and, for a 5.6at% alloy, the authors were only able to define a transition region, extending from 30K to 60K. Extrapolation of the inverse susceptibility from the Curie-Weiss region gave positive intercepts on the temperature axis and the authors reported that, for the 1.4 and 5.6at% alloys, a spontaneous magnetisation was observed at 4K, whose magnitude depended on the magnetic field in which the alloy was cooled.

Kouvel (3.59) investigated this latter effect in some detail for both Cu-Mn and Ag-Mn alloys with concentrations above 5%.

Alloys cooled in zero field to 1.8K showed very little remanence but, with increasing temperature, the remanence and magnetisation passed through maxima, the temperature of which was a linear function of concentration. However, if the samples were cooled in a magnetic field the behaviour was greatly changed, with the appearance of a thermoremanent magnetisation and a hysteretic magnetisation curve displaced along the field axis. The assymetry and thermoremanence decreased with increasing temperature and became zero when the hysteresis losses went through a maximum; these, in turn, decreased to zero in the region of the susceptibility maximum. The largest values of the remanent magnetisation were observed for concentrations $\sim$ 12at%, independent of the size of the field in which the alloys were cooled. Kouvel proposed a model to explain this behaviour, in which the net moments of clusters of antiferromagnetically

aligned, nearest neighbour Mn atoms, are aligned antiparallel in the absence of an applied field, but where the effect of field cooling is to 'lock' the moments of the clusters to the field direction. Strong local anisotropy then maintains this metastable configuration at low temperatures, even when the applied field is removed. Kouvel also measured the resistivity of the samples between 4.2 and 700K and found a drop in resistivity at low temperatures and a gradual transition to a linear behaviour at higher temperatures. The region of transition (and the rather arbitrary value of transition temperature defined by Kouvel) are far higher than those indicated by the susceptibility measurements of Owen et al, and increase at a rate of about 10K per at%.

The magnetic specific heat discussed in ch. 2 shows a very broad peak at temperatures roughly corresponding to the susceptibility peak.

The Au-Fe system also seems to show a region of complex magnetic character. The magnetisation measurements of Crangle and Scott (3.45) showed normal ferromagnetic behaviour above about 12% Fe but, below this concentration, plots of $\frac{H}{M}$ v M^2 suggested that no finite Curie temperatures could be defined. They suggested that the Curie temperatures reported by Borg et al (3.60) from Mössbauer measurements on alloys with concentrations from 0.84 to 11.5at% were, in fact, associated with short range magnetic effects in the vicinity of the absorbing Fe nucleus.

The susceptibility measurements of Lutes and Schmit (3.61) and Cannella et al (3.62) show broad peaks in the susceptibility for low concentrations whilst, at higher concentrations, the peaks become sharper, until above about 12 - 15% the susceptibility rises slowly at low temperatures and then falls quite sharply, suggestive of a ferromagnetic transition. The resistance data of Mydosh et al (3.63) is similar to that for Cu-Mn at low concentrations with a broad transition region. The 'ordering' temperature rises at about 4K per at% up to about 12at%, above which the slope increases to about 15K per at%. Below 12at% the susceptibility

and Mössbauer measurements indicate lower values of the ordering temperature than the resistivity data (as in Cu-Mn), but there is a smaller discrepancy, (in the case of Au-Fe the maximum in $d\rho/dT$ is used to define the transition temperature).

Since the behaviour of Au-Fe at high concentration (> 12%) is ferromagnetic, whilst Cu-Mn takes on increasing antiferromagnetic character, a comparison of the concentration dependence of the various properties is not expected to show parallel behaviour.

It would appear that no field cooling experiments have been reported on the Au-Fe system.

The behaviour of the Zn-Mn system is limited by the restricted solubility of Mn in Zn (ch. 6). Collings et al (3.64) suggest from susceptibility data that a 0.4% alloy shows signs of antiferromagnetic order at about 6K. Alloys containing less than 0.2at% showed Curie-Weiss behaviour to the lowest temperature at which measurements were made ($\sim$ 3K). An effective moment of $4.0\mu_B$ was deduced, corresponding to S = 3/2. The same authors showed that Zn-Mn alloys show a Kondo effect with a resistance minimum at about 20K in a 0.4at% alloy.

Martin (3.65) examined the specific heat of alloys containing from 0.02 to 0.2at% Mn, in the temperature range 0.4K to 30K. The measurements show maxima in the magnetic contribution to the specific heat, the temperature of which (about 2K for a 0.1at% alloy) increases linearly with increasing concentration. The associated entropy indicates a spin of 3/2 for the Mn atoms.

(d) Some Other Interesting Systems

Murani and Coles (3.66) have studied the systems Rh-Fe and Rh-Mn (B3). For concentrations above 3at% Fe, susceptibility maxima are found which are rather like those in Au-Fe at lower concentrations. Field cooling shifts the M - H plot from the origin, as in Cu-Mn. In the

dilute limit, the incremental resistivity falls anomalously at low temperatures whilst at concentrations in excess of about 5at%, minima are observed at temperatures roughly corresponding to the susceptibility peak.

The slow rate of increase of the 'ordering' temperature at low concentrations suggests that there is some tendency towards a delay in the onset of magnetic order. The authors suggest that, at low temperatures, isolated solute atoms are non-magnetic, but are capable of spin fluctuations of increasing lifetime as the temperature is raised. The fluctuations are stabilised by interactions at higher concentrations, leading to behaviour resembling that of solutes which possess a magnetised virtual bound state.

Rh-Mn shows similar behaviour in all respects except that resistivity minima are not observed at high concentrations. Both alloy systems give an anomalous positive magnetoresistivity.

Unlike the Pd-Fe and Pd-Co systems, the Pd-Ni system requires a finite concentration of solute atoms before ferromagnetism is stabilised. Tari and Coles (3.67) have recently shown, by fitting the resistance data at liquid helium temperatures to the expression $\rho - \rho_0 = AT^N$ and plotting the coefficient A against concentration, that the para to ferromagnetic transition occurs at a critical concentration of 2.32 $\pm$ 0.03at%. Below this concentration, spin-spin correlation lifetimes increase as the concentration increases. Certain properties of the system are well described in terms of low frequency spin fluctuations or paramagnons which scatter the conduction electrons. The effects have been described by Lederer and Mills (3.68) in terms of a model in which addition of Ni to Pd produces a localised exchange enhancement in the Ni cell. This model leads to a prediction that $\rho - \rho_0 = AT^2$, with the coefficient A linear in susceptibility χ. Such behaviour has been observed by Schindler et al (3.69).

The solubility of rare earths in Cu, Ag and Au is probably too low to allow magnetic glass behaviour. There does, however, exist some evidence to suggest that such behaviour may occur in the system $La_{1-x}Gd_xAl_2$, where Maple (.149) has found that, below about 12at%Gd, the 'ordering' temperature no longer decreases linearly with decreasing concentration. In La-Gd, Finnemore et al (3.70) observe a maximum in the susceptibility similar to those in Cu-Mn and report that the superconducting transition temperature intersects the curve for magnetic 'ordering' at 0.5K and 1at%Gd. The coexistence of an 'ordered' state and superconductivity has also been reported in the $Ce_{1-x}Gd_xRu_2$ and $La_{1-x}Gd_xOs_2$ systems (see p.629, Taylor review article 1.46). It would clearly be of great interest to investigate these systems in greater detail to determine whether Cu-Mn type behaviour is exhibited.

CHAPTER 4

THEORY OF ELECTRON SPIN RESONANCE

4.1 Basic Theory

The application of a magnetic field $\underset{\sim}{H}_0$ to an ion of magnetic moment $\underset{\sim}{\mu}$ produces an interaction energy $-\underset{\sim}{\mu}.\underset{\sim}{H}_0$; the Hamiltonian for the system is thus:

$$H = -\underset{\sim}{\mu}.\underset{\sim}{H}_0 \quad \ldots\ldots\ldots\ldots\ldots\ldots\ldots\ldots\ldots\ldots \quad 4.1$$

For an ion with angular moment $\underset{\sim}{J}\hbar$

$$\underset{\sim}{\mu} = -g_J\mu_B\underset{\sim}{J} = \gamma\hbar\underset{\sim}{J} \quad \ldots\ldots\ldots\ldots\ldots\ldots\ldots\ldots \quad 4.2$$

where g_J is the Landé g-factor

μ_B is the Bohr Magneton $(\frac{e\hbar}{2mc})$

γ is the gyromagnetic ratio.

If $\underset{\sim}{H}_0$ is taken along the z-direction, then

$$H = g_J\mu_B J_Z H_0 \quad \ldots\ldots\ldots\ldots\ldots\ldots\ldots\ldots\ldots\ldots \quad 4.3$$

For a transition $\Delta J_Z = \pm 1$

$$\Delta E = g_J\mu_B H_0 \quad \ldots\ldots\ldots\ldots\ldots\ldots\ldots\ldots\ldots\ldots \quad 4.4$$

To obtain absorption of electromagnetic radiation of frequency ω, the condition

$$\hbar\omega = \Delta E = g_J\mu_B H_0 = \gamma\hbar H_0 \quad \ldots\ldots\ldots\ldots\ldots\ldots \quad 4.5$$

has to be satisfied.

It is thus clear that if the value of $\hbar\omega$ (or more conveniently, the field H_0) is varied, absorption of energy will occur between a pair of energy levels when the resonance condition 4.5 is satisfied.

4.2. Longitudinal Relaxation

Consider a system of spins with $S = \frac{1}{2}$. The energy level diagram for this system is shown in fig. (4.1).

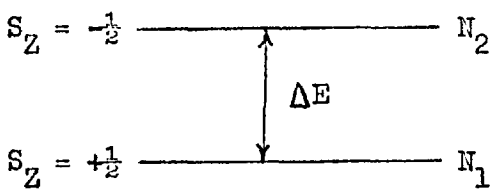


Fig. 4.1

Let N_2 be the number of spins in the higher energy level (antiparallel to the applied field) and N_1 the number in the lower level. Application of a microwave field will cause the populations N_1 and N_2 to change as transitions between the energy levels are induced. If the probability of inducing an upward transition is denoted by W_{12} and a downward transition by W_{21}, we may write

$$\frac{dN_1}{dt} = N_2W_{21} - N_1W_{12} \quad \ldots\ldots\ldots\ldots\ldots\ldots\ldots\ldots \quad 4.6$$

If the transition probabilities are equal to W

$$\frac{dN_1}{dt} = W(N_2 - N_1) \quad \ldots\ldots\ldots\ldots\ldots\ldots\ldots\ldots \quad 4.7$$

and putting

$$\begin{aligned} N &= N_1 + N_2 \\ n &= N_1 - N_2 \end{aligned} \quad \ldots\ldots\ldots\ldots\ldots\ldots\ldots\ldots \quad 4.8$$

equation 4.7 reduces to

$$\frac{dn}{dt} = -2Wn \quad \ldots\ldots\ldots\ldots\ldots\ldots\ldots\ldots \quad 4.9$$

If n(0) is the initial population difference, after time t

$$n = n(0)e^{-2Wt} \quad \ldots\ldots\ldots\ldots\ldots\ldots\ldots\ldots \quad 4.10$$

Thus an initial population difference will disappear and the resonant absorption of energy will eventually stop.

We postulate, therefore, that transitions between N_1 and N_2 may be induced by a coupling of the spins to an energy 'reservoir' at temperature T, which tends to establish a population difference between the energy levels corresponding to the reservoir temperature. In this case there will be a preference for downward transitions. If the probability of this mechanism

incuding an upward transition is W_a and a downward transition W_e, we may write for the rate equations in this case:

$$\frac{dN_{1,2}}{dt} = \pm N_2 W_e \mp N_1 W_a \quad \ldots\ldots\ldots\ldots\ldots\ldots\ldots \quad 4.11$$

When thermal equilibrium is achieved with populations N_1^0 and N_2^0

$$\frac{N_2^0}{N_1^0} = \frac{W_a}{W_e} = e^{-\Delta E/kT} \quad \ldots\ldots\ldots\ldots\ldots\ldots\ldots \quad 4.12$$

Substituting 4.8 in 4.11 gives

$$\frac{dn}{dt} = N(W_e - W_a) - n(W_e + W_a) \quad \ldots\ldots\ldots\ldots\ldots\ldots \quad 4.13$$

and this may be re-written in the form

$$\frac{dn}{dt} = \frac{n_0 - n}{T_1} \quad \ldots\ldots\ldots\ldots\ldots\ldots\ldots\ldots \quad 4.14$$

$$\text{where } n_0 = N\left(\frac{W_e - W_a}{W_e + W_a}\right) \quad \ldots\ldots\ldots\ldots\ldots\ldots\ldots\ldots \quad 4.15$$

$$\frac{1}{T_1} = (W_e + W_a)$$

T_1 is termed the "spin-lattice relaxation time" or "longitudinal relaxation time". The solution to 4.14 is:

$$n = n_0 + Ae^{-t/T_1} \quad \ldots\ldots\ldots\ldots\ldots\ldots\ldots \quad 4.16$$

Where n_0 is the thermal equilibrium population difference and T_1 may be seen as the characteristic time associated with the approach to thermal equilibrium.

The two rates for $\frac{dn}{dt}$ may be combined to give the transition rate for both thermally induced transitions and those induced by the microwave field.

$$\frac{dn}{dt} = -2Wn + \frac{n_0 - n}{T_1} \qquad \text{.....} \qquad 4.17$$

so that in the steady state:

$$n = \frac{n_0}{1 + 2WT_1} = \frac{P}{h\omega W} \qquad \text{.....} \qquad 4.18$$

It may be seen from this analysis that if $2WT_1 \ll 1$ the system will absorb more power, P, as the amplitude of the incident radiation is increased. As $2WT_1 \rightarrow 1$, however, the power absorbed will level off and saturation is reached.

4.3 The Bloch Model

The model proposed by Bloch (4.1) for nuclear magnetic resonance described the interaction of an assembly of interacting moments in the presence of a magnetic field and is equally relevant to the case of electron spin resonance. Before describing and solving the phenomenological equations proposed by Bloch, a simple picture of the resonance process will be sketched in terms of an analogy with the classical mechanical system of a spinning top or gyroscope. Slichter (4.2) has shown in a rigorous quantum mechanical description that the expectation value of the moment follows the classical equations of motion, whilst the instantaneous value is subject to normal uncertainty relations.

If energy is to be coupled into a precessing top, a torque is applied in the direction of the locus of the motion. In the case of an electron precessing about a static magnetic field, energy is coupled by a correctly phased, circularly polarised, magnetic field perpendicular to the axis

of the static field. For maximum torque, the rotating magnetisation should lag 90° behind the rotating field.

If the frequency of the rotating field, ω , is held slightly lower than that of the precessional frequency of the magnetisation, ω_0, the angle of 90° is reduced as the magnetisation catches up with the rotating field, and the torque is reduced to zero when the angle between them becomes zero. Subsequently, the magnetisation overtakes the rotating field and energy is transferred in the opposite direction. Thus, over many rotations no net transfer of energy takes place. This situation is altered, however, by a second relaxation mechanism known as the transverse relaxation time, T_2. This has the effect of de-phasing the rotating moments and destroying their coherence. If this process occurs before the magnetisation can catch up with the rotating field, it is clear that a transfer of energy from the microwave field to the spin system is achieved, i.e. if

$$\omega_0 - \omega < 1/T_2 \qquad \text{4.19}$$

there is a net energy transfer.

T_2 thus determines the linewidth of the esr signal.

The moment will thus precess, on average, at an angle which is less than 90° behind the rotating field and this angle will be determined by the frequency difference $|\omega_0 - \omega|$. Fig. (4.2(a)) shows the amplitude and phase relative to the rotating field of the net rotating moment.

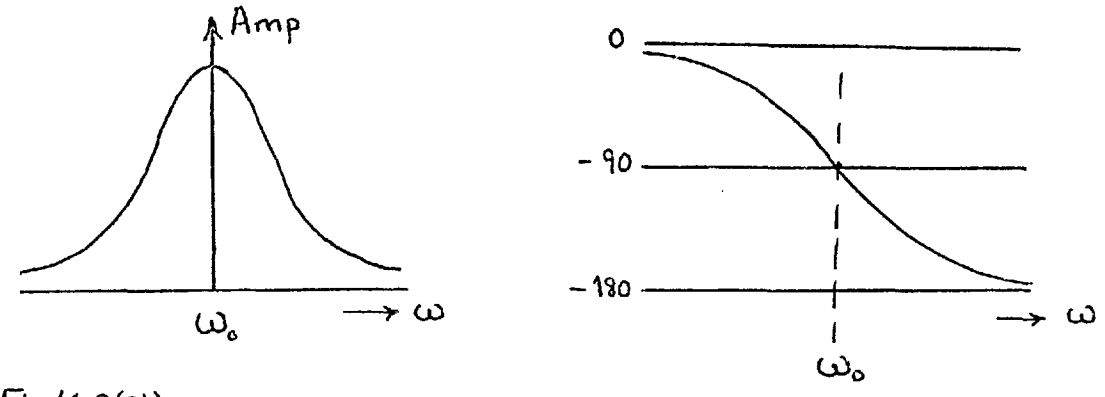


Fig (4.2(a))

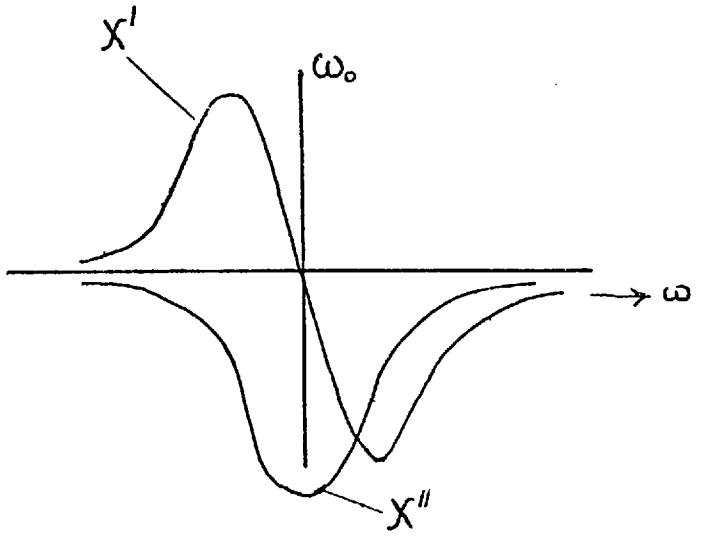


Fig (4.2(b))

A complex susceptibility (for low amplitude rotating fields) may be defined:

$$\chi = \chi' + i\chi'' \qquad \ldots\ldots\ldots\ldots\ldots\ldots\ldots\ldots \quad 4.20$$

where χ' represents a component of susceptibility in phase with the rotating field and χ'', a quadrature component. The variation of these two components as a function of frequency is shown in fig. (4.2(b)). The in-phase term χ' gives no torque and is thus not normally observed (see ch. 7).

The ideas above were formulated by Bloch into a set of equations. He proposed that the magnetisation of the paramagnetic system, M, decays from an initial non-equilibrium magnitude and orientation towards an equilibrium value M_0 and assumed an exponential form for this decay, thus:

$$\frac{dM_z}{dt} = \frac{M_0 - M_z}{T_1} + \gamma (\underline{M} \wedge \underline{H})_z$$

$$\frac{dM_x}{dt} = \gamma (\underline{M} \wedge \underline{H})_x - \frac{M_x}{T_2} \qquad \ldots\ldots\ldots \quad 4.21$$

$$\frac{dM_y}{dt} = \gamma (\underline{M} \wedge \underline{H})_y - \frac{M_y}{T_2}$$

where $\underline{H}(t) = \underline{H}_0 + \underline{H}_1(t)$ 4.22

$\underline{H}_1(t)$ is the magnetic component of the microwave field and is small enough compared to $\underline{H}_0$ to be regarded as a perturbation.

The solutions to these equations are obtained most simply by transforming into a frame of reference rotating with the microwave field, i.e., at frequency ω. Pake (4.3) shows that in such a frame the effective static field is given by

$$H_{eff} = H_0 - \omega/\gamma \quad \ldots\ldots\ldots\ldots\ldots\ldots\ldots \quad 4.23$$

and the equations then become (with primes indicating the rotating frame):

$$\frac{dM'_z}{dt} = -\gamma M'_y H_1 + \frac{M_0 - M'_z}{T_1}$$

$$\frac{dM'_x}{dt} = \gamma M'_y H_{eff} - \frac{M'_x}{T_2}$$

$$\frac{dM'_y}{dt} = \gamma\left[M'_z H_1 - M'_x H_{eff}\right] - \frac{M'_y}{T_2} \quad \ldots\ldots\ldots\ldots \quad 4.24$$

Solving these equations and re-transforming back to the laboratory frame gives:-

$$\chi' = \frac{\chi_0}{2}\,\omega_0 T_2\,\frac{(\omega_0 - \omega)\,T_2}{1 + (\omega - \omega_0)^2 T_2^2} \quad \ldots\ldots\ldots\ldots \quad 4.25$$

$$\chi'' = \frac{\chi_0}{2}\,\omega_0 T_2\,\frac{1}{1 + (\omega - \omega_0)^2 T_2^2} \quad \ldots\ldots\ldots\ldots \quad 4.26$$

The average rate, A, at which energy is absorbed per unit volume by the sample from the H_1 field may be written:

$$A = \frac{\omega}{2\pi}\int_0^{2\pi/\omega} \underline{H}\cdot\frac{d\underline{M}}{dt}\,dt$$

$$= 2\omega\chi'' H_1^2 \quad \ldots\ldots\ldots\ldots\ldots\ldots\ldots\ldots \quad 4.27$$

and this leads to

$$\omega = \omega_0 \pm 1/T_2 \quad \ldots\ldots\ldots\ldots\ldots\ldots\ldots\ldots \quad 4.28$$

for the half-power points.

Thus the half-width at half-power of the Lorentzian line may be written

$$\Delta\omega_{\frac{1}{2}} = 1/T_2 = \gamma \Delta H_{\frac{1}{2}} \quad \ldots\ldots\ldots\ldots\ldots\ldots\ldots \quad 4.29$$

and this is related to the full width of the experimentally observed derivative line, H (see fig. (7.6)) by

$$H = \frac{2\Delta H_{\frac{1}{2}}}{3^{\frac{1}{2}}} \quad \ldots\ldots\ldots\ldots\ldots\ldots\ldots\ldots \quad 4.30$$

Pake (4.3) shows that when the amplitude of the microwave field is not small enough to be regarded as a perturbation, an extra term $\gamma^2 H_1^2 T_1 T_2$ is added to the denominators of equations (4.25) and (4.26). In the limit of very large H_1

$$A_{max} = \lim_{H_1 \to \infty} 2\omega H_1^2 \chi''$$

$$= \frac{\chi_0 H_0^2}{T_1} \quad \ldots\ldots\ldots\ldots\ldots\ldots\ldots\ldots \quad 4.31$$

This is known as the saturation limit.

4.4. The Spin Hamiltonian

The complete Hamiltonian for a free ion in a magnetic field may be written as a sum of a number of terms of decreasing energy:

$$H = H_1 + H_2 + \ldots\ldots H_6 \quad \ldots\ldots\ldots\ldots\ldots\ldots \quad 4.32$$

We will consider each of these terms individually.

H_1 represents the part of the Hamiltonian which is spin-independent (thus it does not contribute to the spin Hamiltonian).

It may be written in the form:

$$H_1 = \sum_i \left(\frac{p^2}{2m_0} - \frac{Ze^2}{r_i}\right) + \sum_{i<k} \frac{e^2}{r_{ik}} \quad \ldots\ldots\ldots\ldots \quad 4.33$$

and has an energy $\sim 10^5 cm^{-1}$.

The two terms H_2 and H_3 vary in magnitude depending upon the ion under consideration. H_2 is the term due to the crystal field of the neighbouring ions and in the first transition series, where the magnetic 3d electrons lie on the 'outside' of the ion, the crystal field interactions are $\sim 10^4 cm^{-1}$. However, in the rare-earth series where the magnetic 4f shell is screened by the 5s and 5p electrons, this energy is reduced by about two orders of magnitude. H_3 is the contribution from the coupling of the orbital and spin moments and may be represented by a term $\lambda \underline{L}.\underline{S}$; it has a magnitude $\sim 10^2 - 10^3 cm^{-1}$. In the transition metal series the large crystal field must be considered first, the orbital moment is quenched, and the magnetic properties are due almost entirely to the spin.

However, in the rare-earth series the reverse order obtains. $\underline{J}$ is a good quantum number and at low temperatures in these ions the effect of the crystal field is to raise the $(2\underline{J} + 1)$ fold degeneracy. Williams and Hirst (4.4) and Murani (4.5) have measured the effects of the crystal field on rare-earth metals in Au and Ag through the deviation of the magnetic susceptibility from the Curie-Weiss law at low temperatures and from resistance measurements. Williams and Hirst elucidated the lowest lying crystal field levels and the values of the crystal field parameters C_4 and C_6. In cubic crystals, there are eight possible levels into which the ground state may be split and these are labelled $\Gamma_1 \ldots\ldots \Gamma_8$. Ions with integral $\underline{J}$ can split into states Γ_1 to Γ_5 and those with half integral $\underline{J}$ (which obey Kramer's theorem) can split into states Γ_6 to Γ_8. The allowed splittings are determined from symmetry considerations using group theory. Resonances from the Γ_7 ground state

in Dy, Er and Yb have been reported and recently a resonance has been observed from the Γ_8 quartet level of Dy in Au, using a single crystal. These measurements are described in ch. 5. No resonances have so far been observed for integral $\underline{J}$;* though the Γ_4 and Γ_5 triplet states may produce a resonance. (Γ_1 and Γ_2 are singlets; Γ_3 has no Zeeman splitting). Pr may be a candidate for a resonance from an integral $\underline{J}$ ion.

The ions Mn^{2+}, Fe^{3+}, Gd^{3+} and Eu^{2+} constitute a special case from the point of view of crystal field theory, as they have no orbital momentum. In the case of Gd, the crystal field splittings are $\sim 0.1 - 1 cm^{-1}$ only (4.6).

The term H_4 in the Hamiltonian is the Zeeman term mainly responsible for paramagnetism and may be written

$$H_4 = \mu \underline{H}.(\underline{L} + 2\underline{S}) \quad \ldots\ldots\ldots\ldots\ldots\ldots\ldots\ldots \quad 4.34$$

for an ion with angular momentum. For a field $\sim$ 3KGauss, a splitting $\sim 0.5\ cm^{-1}$ is expected.

H_5 is that part of the Hamiltonian which represents the exchange between the local moment and the conduction electrons and is discussed in detail in ch. 1. The discussion so far in this chapter has been concerned with general theory equally applicable to insulators doped with a paramagnetic ion or to a magnetic impurity in a metal. The term containing H_5 relies explicitly on the metallic nature of the host.

H_6 is the term representing the interaction of the magnetic ion with the magnetic moment of the nucleus and is $\sim 10^{-2} cm^{-1}$. This term is not important from the point of view of the present work, but some reference will be made to its recent observation in a metallic host and to its apparent absence in other cases. The interaction may be written

* in a metallic host

in the form:

$$H_6 = A' \underline{I}.\underline{s} \quad \ldots\ldots\ldots\ldots\ldots\ldots\ldots\ldots\ldots\ldots \quad 4.35$$

The nuclear moment is space quantised and may take up $(2\underline{I} + 1)$ orientations, where $\underline{I}$ is the nuclear spin quantum number. Thus, for example, a nucleus with $\underline{I} = 3/2$ will split a doublet ground state into four components for each value of m_J and thus the selection rule $\Delta m_I = 0$, will give four equally spaced hyperfine satellites about the central esr line.

There may be further contributions to the total Hamiltonian, equation 4.32, such as a term from nuclear Zeeman splitting and the term responsible for diamagnetism. These terms will give rise to splittings of less than $10^{-3}cm^{-1}$ and are unimportant here.

Although the splittings have been quoted in this section as an absolute value, in esr it is conventional to express the energy splitting as an effective g-value, which regards all splittings as though they derived from the interaction between the spin and the applied field, i.e.,

$$H_{eff} = -g_{eff}\mu \underline{S}.\underline{H} \quad \ldots\ldots\ldots\ldots\ldots\ldots\ldots\ldots\ldots\ldots \quad 4.36$$

and for single crystal measurements g_{eff} is a tensor.

4.5 The g-Shift and Linewidth of Ions in Metals

(a) First Order and Second Order g-Shifts

Owen, Browne, Knight and Kittel (5.46) used a simple molecular field theory to obtain the g-shift of magnetic ions in a metallic host and their simple derivation will be used here.

We suppose that a d or f shell is present in a matrix of Pauli susceptibility χ_s (equation 1.23). If λ is the molecular field coefficient for the local moment conduction electron interaction, M_s is the magnetisation of the conduction electrons and M_d the magnetisation of the localised moment

at a specific field and temperature,

$$M_s = \chi_s(H + \lambda M_d) \quad \ldots\ldots\ldots\ldots\ldots\ldots\ldots \quad 4.37$$

where $$\lambda = \frac{J(0)}{g\mu_B^2}, \quad \ldots\ldots\ldots\ldots\ldots\ldots\ldots \quad 4.38$$

$$M_d = \chi_d H,$$

The field acting on the d shell (say), H_d, is given by

$$H_d = H(1 + \lambda\chi_s + \lambda^2\chi_s\chi_d) \quad \ldots\ldots\ldots\ldots\ldots \quad 4.39$$

and thus from the resonance condition

$$g_{eff} = g(1 + \lambda\chi_s + \lambda^2\chi_s\chi_d) \quad \ldots\ldots\ldots\ldots\ldots \quad 4.40$$

we get a first order g-shift:

$$\Delta g_1 = J(0)\rho(E_F) \quad \ldots\ldots\ldots\ldots\ldots\ldots\ldots\ldots \quad 4.41$$

and a second order shift:

$$\Delta g_2 = J^2(0)\frac{2\rho(E_F)S(S+1)}{3kT}C \quad \ldots\ldots\ldots\ldots\ldots \quad 4.42$$

where C is the concentration of impurity.

A rough calculation shows that the ratio of the second order to first order shift for 1% Mn in Cu at 100K would be ~ 1. In fact, in Cu-Mn the second order g-shift was not observed. Kittel and Mitchell (4.7) argued that the shift should be observable if the spin lattice relaxation time of the conduction electrons, T_{sL}, was shorter than the relaxation time, T_{ds}, due to s - d exchange. Yosida (1.26), however, argued that the shift can never be seen since the conduction electron polarisation by the d-shell follows the magnetisation of the d electron spin adiabatically, so that the effective field $\lambda^2\chi_s M_d(t)$ cannot produce a torque on $M_d(t)$. No second order g-shift has been identified in esr measurements to date.

(b) Indirect g-shift

A number of measurements have been made which involve the additional g-shift of Gd ions due to the addition of other rare-earth ions. The contribution of the second rare-earth may be analysed in the same way as the direct g-shift above and, assuming no second order g-shift, equation 4.39 becomes

$$H_{Gd} = H(1 + \lambda\chi_s + \lambda_1\lambda_2\chi_s\chi_{R.E}) . \quad \ldots\ldots\ldots\ldots \quad 4.43$$

and this leads to an extra shift:

$$\Delta g_3 = \frac{J_1(0)}{g\mu_B^2} \times \frac{J_2(0)}{g\mu_B^2} \chi_s \langle S_z \rangle \quad \ldots\ldots\ldots\ldots \quad 4.44$$

where $\chi_{R.E}$, $J_2(0)$ and λ_2 are appropriate parameters for the second ion and

$$\langle S_z \rangle = \frac{(g_J - 1)\, g_J^2 \mu_B^2\, J(J+1)}{3kT} \quad \ldots\ldots\ldots\ldots \quad 4.45$$

thus this shift is inversely proportional to the temperature and, because of the term $(g_J - 1)$, this g-shift is expected to be negative for the light rare-earths and positive for the heavy rare-earths.

(c) Hasegawa's Treatment - the esr Bottleneck

Hasegawa (4.8) studied the problem of why g-shifts are not observed in some systems, and obtained expressions for the g-shift and linewidth in terms of the strength of the thermal contact between local moments, conduction electrons and the lattice as illustrated in fig.(4.3)

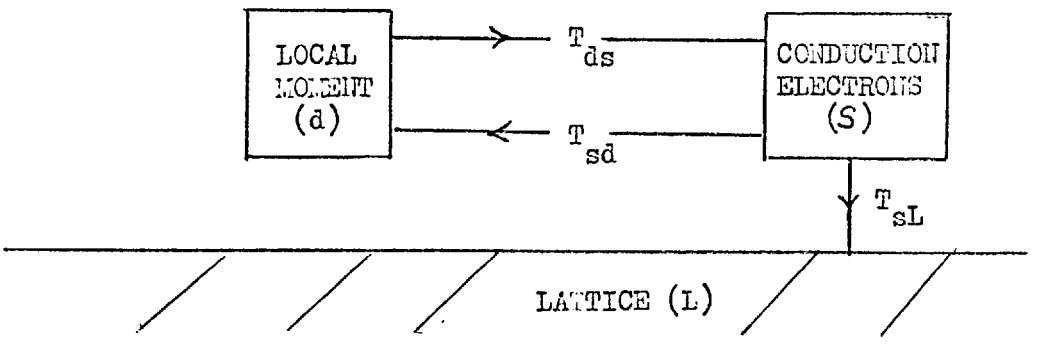


Fig. 4.3

He considered phenomenological equations of the Bloch form:

$$\dot{M}_s = \gamma M_s \wedge (H + \lambda M_d) - \frac{1}{T_{sL}} (M_s - \bar{M}_s) - \frac{1}{T_{sd}} M_s + \frac{1}{T_{ds}} Md \quad \ldots\ldots\ldots\ldots\ldots\ldots \quad 4.46$$

and

$$\dot{M}_d = \gamma' M_d \wedge (H + \lambda M_s) + \frac{1}{T_{sd}} M_s - \frac{1}{T_{ds}} Md \quad \ldots\ldots\ldots\ldots\ldots\ldots \quad 4.47$$

where T_{sd} and T_{ds} are the relaxation times from the conduction electrons to the d-cores and vice versa via s - d exchange, M_s is the final value towards which the relaxation M_s proceeds, and he assumed that in equilibrium each magnetisation M_s and M_d has a definite value M^o_s and M^o_d satisfying a law of detailed balance:

$$\frac{M^o_s}{T_{sd}} = \frac{M^o_d}{T_{ds}} \quad \ldots\ldots\ldots\ldots\ldots\ldots\ldots\ldots\ldots\ldots\ldots\ldots \quad 4.48$$

Only in equilibrium does $\bar{M}_s = M^o_s$.

Solving these equations Hasegawa showed that the g-shift should correctly be written:

$$\Delta g = g_0 \frac{\left(\frac{T_{sd}}{T_{sL}}\right)^2}{\left(1 + \frac{T_{sd}}{T_{sL}}\right)^2 + \left(\gamma \lambda M^o_d T_{sd}\right)^2} \quad \ldots\ldots\ldots \quad 4.49$$

and the broadening:

$$\frac{1}{T_{2eff}} = \frac{\left(1 + \gamma \lambda M^o_d T_{sd}\right)^2 \frac{T_{sd}}{T_{sL}} + \left(\frac{T_{sd}}{T_{sL}}\right)^2}{\left(1 + \frac{T_{sd}}{T_{sL}}\right)^2 + \left(\gamma \lambda M^o_d T_{sd}\right)^2} \frac{1}{T_{ds}} \quad \ldots \quad 4.50$$

and $$\frac{1}{T_{1eff}} = \frac{T_{sd}}{T_{sL} + T_{sd}} \frac{1}{T_{ds}} = B. \frac{1}{T_{ds}} \quad \ldots\ldots\ldots\ldots\ldots \quad 4.51$$

where B is termed the bottleneck factor.

The values of Δg, T_2 and T_1 are thus dependent upon the relaxation times. T_{sd} and T_{ds} may be obtained by considering the exchange coupling between d and s electrons and using the Golden Rule for transition probabilities. At temperatures greater than a fraction of a degree Kelvin (4.9, 4.10)

$$\frac{1}{T_{ds}} = \Delta_{ds} = \frac{2\pi}{\hbar} 2(\rho(E_F)(J))^2 kT \quad \ldots\ldots\ldots\ldots\ldots \quad 4.52$$

and $$\frac{1}{T_{sd}} = \Delta_{sd} = \frac{2\pi}{\hbar} 2(\rho(E_F)(J)^2) C \frac{2}{3} S(S+1) \quad \ldots\ldots\ldots \quad 4.53$$

These expressions, derived initially for nuclear relaxation, are known as the Korringa and Overhauser rates respectively. Orbach (4.17) quotes expressions which are valid for the extreme low temperature limit.

The expressions above, 4.49 and 4.50, may be evaluated for two limiting cases:

(1) $T_{sL} \ll T_{sd}$

In this limit the full g-shift should be observed and the linewidth ΔH is given by

$$\Delta H = \Delta_{ds} = \frac{k\pi}{g_s \mu_B} (\Delta g)^2 T \quad \ldots\ldots\ldots\ldots\ldots\ldots \quad 4.54$$

This is known as the Korringa or unbottlenecked limit and equation 4.54 is known as the Korringa relation. It is plotted in Appendix 3(a).

A number of assumptions are made in using equation 4.54 as it stands:

(a) We assume that the Korringa relaxation mechanism is the only source of line broadening. In practice, the residual linewidth (see below) is normally subtracted from ΔH and the slope of the temperature in the paramagnetic regime $\frac{d\Delta H}{dT}$ is measured.

(b) Moriya (4.12) showed that in an exchange enhanced host, the full enhanced g-shift is obtained but the relaxation is less strongly effected. The enhancement factor for the relaxation is an average of $\left[1 - I\chi_s f(q)\right]^{-1}$ over all q which span the Fermi surface. Narath (4.13) shows that the correct form of the Korringa relation for an exchange enhanced host is:

$$\frac{d\Delta H}{dT} = \frac{k\pi}{g_s\mu_B} (\Delta g)^2 K(\alpha) \quad \ldots\ldots\ldots\ldots\ldots\ldots\ldots \quad 4.55$$

where $$K(\alpha) = \left[\frac{(1-\alpha)}{1-\alpha f(q)}\right]^2$$

and $$\alpha = I\chi_s$$

(c) Even in the case of an unenhanced host, the assumption is made that the relaxation, like the g-shift, measures $J(q = 0)$. Peter et al (1.43) have pointed out that this is not necessarily true.

We must conclude from these remarks that equations 4.54 and 4.55 are only likely to be obeyed approximately and it is not surprising that in the present work, even for alloys which are expected to be fairly free electron-like, the Korringa relation is not rigorously obeyed.

(2) $T_{sL} \gg T_{sd}$

Here the g-shift is not normally observed for s-state ions, being reduced from the full value by a factor $(T_{sd}/T_{sL})^2$.

The linewidth is given by

$$\Delta H = \frac{1}{\gamma} \frac{T_{sd}}{T_{ds}} \frac{1}{T_{sL}} \quad \ldots\ldots\ldots\ldots\ldots\ldots\ldots \quad 4.56$$

and since from equation 4.52 and 4.53

$$\frac{T_{sd}}{T_{ds}} = \frac{3}{2} \frac{\rho(E_F)\, k}{S(S+1)} \frac{T}{C} \quad \ldots\ldots\ldots\ldots\ldots\ldots \quad 4.57$$

we note that the linewidth in this limit is inversely proportional to the concentration of the magnetic ion and this is a useful means of identifying bottlenecking in a solid solution alloy system.

The behaviour outlined above may be pictured in a simple way. In order to maintain thermal equilibrium with the lattice, the local moment attempts to couple some of its energy to the lattice via the conduction electrons. When the conduction electron - lattice relaxation rate is large enough, the linewidth is governed only by the rate at which the local moment can transfer energy to the conduction electrons and the unbottlenecked (Korringa) behaviour is observed. If, however, the conduction electron - lattice relaxation rate is small, energy "piles up" in the spin system and the resonance frequency is that of the coupled system.

If the concentration of the local moment is increased, the bottleneck becomes stronger since there is more energy to be coupled out; however, if impurity atoms are added, the bottleneck may be eased by increasing the conduction electron - lattice relaxation rate. These effects and their consequences will be further described in the experimental review below.

In summary, we may thus expect to identify a bottlenecked system from the following observations:

1. The g-value for an s-state ion will be close to $g = 2$; any increase or reduction in the effective magnetic moment from the free ion value as indicated by static susceptibility measurements (ch. 1) will not be observed in the g-value. For a bottlenecked system the value of J_{s-d} or J_{s-f} calculated from the g-value will be underestimated.

2. The slope of linewidth v temperature deduced from the Korringa relation using a 'reasonable' value of J will be <u>much</u> lower than predicted, allowing where necessary for the effects of exchange enhancement.

3. The linewidth at a given temperature will be inversely proportional to the concentration of the magnetic impurity.

4. Addition of non-magnetic impurities will broaden the line at a given temperature.

(d) Extensions of Hasegawa's Work

Peter et al (1.43) carried the molecular field treatment to its completion by introducing not only lattice relaxation to the instantaneous local field, as in Hasegawa's work, but they also introduced relaxation to the instantaneous local field for the localised - conduction electron exchange relaxation. Their equations of motion were also designed to include the ion - lattice relaxation explicitly and to satisfy the condition that the energy absorption must be positive definite (which, they showed, Hasegawa's equations did not). Despite these refinements to the model, equations 4.49 to 4.57 give essentially correct answers.

Apart from the two limits explored above, there also exists an intermediate regime where so-called "dynamic effects" are expected (see Appendix 3(b)) to occur. This regime was investigated experimentally and theoretically by Cottet et al (5.19) and Davidov and Shaltiel (5.21). They found that when Δ_{sd} is of the same order of magnitude as Δ_{sL}, the g-shift is reduced from its full unbottlenecked value, as either the concentration is increased or the temperature reduced. Davidov and Shaltiel in their work on Gd doped $LaNi_5$ (the results of which are presented in the experimental review) derive an expression of the form

$$\Delta g = \frac{(\Delta_{sL})^2 \Delta g_0}{(\lambda \gamma X_i H)^2 + (\Delta_{sL} + \Delta_{sd})^2} \quad \ldots\ldots\ldots\ldots \quad 4.58$$

to describe the dynamic behaviour. It is also observed that the effects

are field dependent, the shift being reduced in high external fields (corresponding to Q-band measurements for example).

Recent theoretical work has been reviewed by Dupraz et al (4.14). The problem has been treated from a microscopic point of view using Green's function techniques. A particular result of interest has been the prediction of a Kondo g-shift (4.15) in the unbottlenecked limit such that

$$\frac{\Delta g^{(2)}}{g} \sim (\rho(E)J)^2 \left[1 - \ln \left| \frac{\pi kT}{D} \right| \right] \quad \ldots\ldots\ldots\ldots\ldots\ldots \quad 4.59$$

The effect will be small; a rough calculation suggesting that, typically

$$\left[\frac{\Delta g^{(2)}}{g}\right]_{4.2K} - \left[\frac{\Delta g^{(2)}}{g}\right]_{1K} \sim 2 \times 10^{-3}$$

There have been no reported observations of such a shift, but the best candidate would presumably be a non s-state ion in a host where J_{sf} is large and negative (e.g., Yb in Au).

4.6 Hyperfine Splitting

If the nucleus has a net magnetic moment, a hyperfine structure is normally observed in the esr of ions in crystals. Until recently (5.64) hyperfine structure had never been observed for an ion in a metallic environment; hyperfine structure was, for example, absent in the resonance line obtained from single crystals of Mn in Cu, even though the central linewidth was much narrower than the predicted splitting (5.48).

Barnes et al (4.16) have attempted to explain this behaviour. Adopting the molecular field equations of Cottet et al (5.19), they add to the effective field acting on the moments a further term which arises from their own nuclei, and solve the resulting equations for the simplest case of $I = \frac{1}{2}$ (i.e., hyperfine field either parallel or antiparallel to the applied static field.) The results are then generalised

to arbitrary nuclear spin.

Three regions of interest are identified:

1. In the case of weak exchange coupling (i.e., the unbottlenecked regime), hyperfine splittings are predicted with the same character as those of an ion in a crystal.

2. In the opposite (bottlenecked) limit of large exchange coupling such that $\omega_{HF} \ll \Delta_{ds}$, where ω_{HF} is the electronic hyperfine splitting frequency, it is predicted that hyperfine structure will be suppressed.

3. This region corresponds to sufficiently large values of the exchange coupling for a resonance bottleneck to obtain, but where $\omega_{HF}/\Delta_{ds} \gg 1$. Here they predicted that hyperfine structure should be observed, but with the width of each hyperfine component reduced from the value which would be observed for the same ion in an insulator, by a factor of $\left[\frac{2I}{(2I+1)}\right]$.

It is suggested that the recent observations correspond to region 1, but that in other systems (e.g. Cu-Mn) which are well bottlenecked, the reduction of Δ_{ds} at very low temperatures ($<1K$) might enable at least partially resolved hyperfine structure to be observed. This would allow an estimate of the exchange coupling to be made, even in the presence of bottlenecking.

4.7 Residual Linewidth

In the sections above, expressions have been derived for the temperature dependent part of the esr linewidth. In addition to this, there is normally a residual linewidth, which is defined as the value of ΔH at $T = 0K$, extrapolated from the high temperature data. Thus, in the paramagnetic regime, the linewidth can often be expressed in the form:

$$\Delta H = A + BT \quad \ldots\ldots\ldots\ldots\ldots\ldots\ldots\ldots\ldots\ldots \quad 4.70$$

Any contribution to the linewidth from inhomogenous broadening may contribute to the $T = 0K$ linewidth. In the analysis above, a single

value of the magnetic field for resonance has been assumed but, in fact, this field is only the average of the local fields, H_i, which are experienced by the individual ions. The lineshape is therefore an envelope of the individual resonance lines from each ion. The spread in the values of the local fields seen by the ions is given by the $\langle H_i^2 \rangle$, which is called the second moment of H_i.

The sources of this broadening may be due to a number of factors. In very narrow lines of the order of one Gauss or less, such as are observed for free radicals, inhomogeneities in the static field or modulation broadening may be of importance, but in the case of ions in metals three sources of residual linewidth are expected to be important:

1. Unresolved fine or hyperfine structure.
2. Variations in the local field due to defects in the lattice.

In this case the residual linewidth increases monotonically with the concentration of defects, but may be reduced by a suitable anneal.

3. The effect of interactions between ions.

Van Vleck (4.17) showed that the exchange interaction between ions does not contribute to the second moment since the total spin commutes with it, but that it enters the fourth moment $\langle H_i^4 \rangle$. There will be a residual width due to dipole - dipole interactions between impurities, and the effect of the exchange narrowing is to modify the Gaussian dipolar line into the form of a Lorentzian.

A theory of the residual linewidth due to interactions between impurities in a metallic host has yet to be developed. In addition to the dipolar width and the direct exchange contribution, the effect of the conduction electron modulated exchange and the screening of the dipolar width by the conduction electrons will have to be included. Using the expression derived by Van Vleck (4.17) for a lattice of spins in a powder sample:

$$\langle \Delta H^2 \rangle = 0.6\, S(S+1)\, g^2 \mu_B^2 \sum r_{ij}^{-6} \quad \ldots\ldots\ldots\ldots \quad 4.71$$

where r_{ij} is the separation of the ith and Jth ion, a very rough calculation for the unscreened dipolar width of 1% Gd in Pd would suggest a value of several hundred Gauss.

In a more rigorous analysis of dipolar width for randomly sited impurities, Kittel and Abrahams (4.18) suggested that for concentrations in excess of about 10% the residual linewidth is proportional to $f^{\frac{1}{2}}$, where f is the fractional occupation of the lattice points by the ions. For concentrations of less than about 1% the width is proportional to f.

Anderson and Weiss (4.19) introduced the "random frequency modulation" model for exchange narrowing. It is assumed in this model that a magnetic ion absorbs a single frequency ω_o which varies over a distribution ω_p, determined by the dipolar local field, but which varies randomly in time at a rate, ω_e, determined by the exchange interaction. They derived a linewidth (in terms of frequency) of

$$\Delta\omega = c\frac{\omega_p^2}{\omega_e} \quad \ldots\ldots\ldots\ldots\ldots\ldots\ldots\ldots \quad 4.72$$

A further mechanism for residual linewidth which may be of some importance for 3d ions was suggested by McElroy and Heeger (5.52). They proposed that the admixture of conduction band wave functions into the localised 3d impurity function described by Friedel and Anderson (ch. 1) allows the localised d-spin to be sensitive to the spin-orbit interaction at distant impurity sites, leading to a non-vanishing relaxation to the lattice via this interaction even at T = 0K. Being a wave function effect, it might be expected to be temperature independent and proportional to the spin-orbit spin flip scattering cross-section of the impurity atoms and to the average admixture matrix element V_{kd}^2.

The interaction above was represented by the matrix element,

$$\langle d\uparrow|\lambda \underline{L}.\underline{S}|d\downarrow\rangle = \sum_{kk'} \frac{\langle d^{\circ}\uparrow|V|k\uparrow\rangle\langle k\uparrow|\lambda \underline{L}.\underline{S}|k'\downarrow\rangle\langle k'\downarrow|V|d^{\circ}\downarrow\rangle}{(E_d^{\circ} - E_k')(E_d^{\circ} - E_k)} \quad \ldots\ldots \quad 4.73$$

where $|d^{\circ}\rangle$ and E_d° are the unperturbed wave function and energy for a pure d-orbital on a Mn ion in the metal.

Using the Golden Rule:

$$\Delta H = 1/\gamma \frac{2\pi}{h} |\langle d\uparrow|\lambda \underline{L}.\underline{S}|d\downarrow\rangle|^2 \rho_d(E)$$

and in the approximation that ρ_d is given by a Lorentzian distribution and that the K-states are Bloch functions, they obtained :

$$\gamma \Delta H_{res} \sim 2.5 \frac{V_{kd}^2}{K_F\, a\, \rho_s(E_F)^2 E_F^4} \frac{N_i}{T_{sL}} \quad \ldots\ldots\ldots\ldots \quad 4.74$$

where a is the lattice spacing and N_i is the number of impurity atoms.

4.8 Ferromagnetic and Antiferromagnetic Resonance

The work in this thesis is primarily concerned with paramagnetic materials but measurements have been made below the ordering temperature in many cases. In this section the basic theory of ferromagnetic and antiferromagnetic resonance will be presented, followed by an outline of some esr measurements which have been made in the transition regime between the paramagnetic and magnetically ordered states.

(a) Ferromagnetic Resonance

The field for resonance in a ferromagnet was first treated by Kittel (4.20). He considered a specimen of a cubic ferromagnetic insulator in the form of an ellipsoid. Components of a demagnetisation

field N_x, N_y, N_z were introduced to relate the components of the internal field H^i to the applied field H,

i.e., $H_x^i = H_x - N_x M_x$ etc.

Solution of the equations of motion led to the ferromagnetic resonance frequency

$$\omega_o^2 = \gamma^2 \left[H_o + (N_y - N_z) M \right] \left[H_o + (N_x - N_z) M \right] \quad \ldots\ldots \quad 4.75$$

for the frequency of the uniform mode, where all the moments precess together with frequency ω_o.

If we consider the demagnetisation factors explicity for various geometries:

for a sphere, $N_x = N_y = N_z$

$$\text{so} \quad \omega_o = \gamma H_o \quad \ldots\ldots\ldots\ldots\ldots\ldots\ldots\ldots\ldots\ldots \quad 4.76$$

for a flat plate with H_o perpendicular to the plate, $N_x = N_y = 0$, $N_z = 4\pi$

$$\text{so} \quad \omega_o = \gamma (H_o - 4\pi M) \quad \ldots\ldots\ldots\ldots\ldots\ldots \quad 4.77$$

or for a flat plate with H_o parallel to the surface in the xz plane, $N_x = N_z = 0$, $N_y = 4\pi$

$$\text{so} \quad \omega_o = \gamma \left[H_o (H_o + 4\pi M) \right]^{\frac{1}{2}} \quad \ldots\ldots\ldots\ldots\ldots \quad 4.78$$

For most samples the conditions derived above are too simple since they do not include the effect of anisotropy. Kittel replaced the effects of the anisotropy energy by an equivalent magnetic field which can be written into the equations of motion as an effective demagnetisation factor, N^e.

The resonance condition then becomes:

$$\omega_o = \gamma \left[(H_z + (N_y + N_y^e - N_z) M_z) \times (H_z + (N_x + N_x^e - N_z) M_z) \right]^{\frac{1}{2}}$$

$$\ldots\ldots\ldots\ldots\ldots \quad 4.79$$

and the values of the demagnetisation factors N_x^e and N_y^e are determined for each experimental situation. For a sphere, if the anisotropy energy density is of the form $K\sin^2\theta$ where θ is the angle between the magnetisation and the Z-axis, the ferromagnetic resonance frequency is:

$$\omega_o = \gamma(H_o + H_A)$$

where $$H_A = \frac{2K}{M} .$$

In the case of a powder sample the demagnetisation factors will run over all values, depending upon the shapes of the individual particles, and some average shift will be expected. The linewidth will become the envelope of the shifted lines and thus might be expected to become extremely broad.

(b) Antiferromagnetic Resonance

The theory for resonance below the Neel point was established by Nagayima and Kittel, and Keffer in 1951 (4.21).

Keffer and Kittel considered a uniaxial antiferromagnet with spins on two sublattices in the presence of an anisotropy field H_A. Using the molecular field approximation and solving the equations of motion, they obtained a value of the antiferromagnetic resonance frequency

$$\frac{\omega_o}{\gamma} = H_o \pm \left[H_A (H_A + 2H_E)\right]^{\frac{1}{2}} \quad \ldots\ldots\ldots\ldots\ldots\ldots \quad 4.80$$

When the exchange field is much greater than the anisotropy field H_A, 4.80 reduces to

$$\frac{\omega_o}{\gamma} = H_o \pm (2H_A H_E)^{\frac{1}{2}} \quad \ldots\ldots\ldots\ldots\ldots\ldots\ldots\ldots \quad 4.81$$

In antiferromagnetic crystals such as MnF_2, $H_E \sim 10^6$G and $H_A \sim 10^4$G so the shift $(2H_A H_E)^{\frac{1}{2}}$ is expected to be $\sim$ 100KGauss (280 Gc/s).

Except in cases where the anisotropy field or exchange field is very small and the shift is less than 2KGauss, antiferromagnetic resonance would not be observed with the present apparatus.

(c) Theories and Measurements just above the Critical Temperature

(i) Antiferromagnet

Various attempts have been made to describe theoretically the temperature dependence of the linewidth above T_N, due to the effects of short range magnetic order. Mori and Kawasaki (4.22) find the esr linewidth for a uniaxial antiferromagnet near the Neel point to be given by

$$\Delta H = (\Delta H)_\infty \left[\frac{T}{(T - T_N)}\right]^{\frac{3}{4}} \quad \ldots\ldots\ldots\ldots\ldots\ldots \quad 4.82$$

where $(\Delta H)_\infty$ is the high temperature limit.

Mori (4.23) using an improved approximation suggested that

$$\Delta H \propto \left(\frac{C}{T\chi_\perp}\right)\xi^p \quad \ldots\ldots\ldots\ldots\ldots\ldots\ldots\ldots \quad 4.83$$

where $\xi = \text{const}\left[\left(\frac{T}{T - T_N}\right)\right]$

and Kawasaki (4.24) obtains

$$\Delta H \propto (T - T_N)^{-p} \quad \ldots\ldots\ldots\ldots\ldots\ldots\ldots\ldots \quad 4.84$$

where $p = 5/3$.

Experimentally, Maxwell and McGuire (4.25) investigated the antiferromagnets Cr_2O_3, MnO, MnTe and MnSe above T_N and found that whilst the g-value remained roughly constant over the whole paramagnetic regime, the linewidth broadened well above T_N. In MnO, the temperature $T_{\Delta H\min}$ at which the increase in linewidth set in, is nearly four times the ordering temperature. The results are summarised in Table 4.1.

TABLE 4.1

	Structure	T_N	$\lvert\theta\rvert/T_N$	$T_{\Delta Hmin}/T_N$
MnO	fcc	116	5.3	~ 3.5
MnS	fcc	160	3.3	~ 2
MnTe	hex	307	2.3	> 2
MnSe	hex	130	~ 2.3	~ 1.6
Cr_2O_3	Complex	307	1.58	~ 1.05

In the limited number of results displayed here, we notice that $T_{\Delta Hmin}/T_N$ is largest where $|\theta|/T_N$ is largest. Zimmerman et al (4.26) studied a single crystal of $CuCl_2.2H_2O$ (T_N = 4.34K) and observed signs of broadening at 20K. They identified two temperature regimes. From 4.34 to 4.8K the data was fitted to a curve of the form predicted by Kawasaki (above) but the value of the index, p, was found as 0.58 ± 0.07 for each axis; this temperature regime was identified with the existence of critical fluctuations. The regime above 4.8K was associated with short range order. Zimmerman et al argued that the broadening of the line below 20K is caused by the decrease in the fluctuation frequency, ω_e, on the model of Anderson and Weiss, above, by the short range order. The consequent reduction in exchange narrowing leads to a broadened line.

Seehra and Castner (4.27) examined the critical broadening in MnF_2 up to $2T_N$ (T_N = 67.4K). They were able to fit their linewidth data to Kawasaki's expression with p = 1.20.

Battles (4.28) has recently attempted to fit MnS and MnO linewidth data to the expressions above, and obtains a good fit to equation 4.84 from about T_N + 10K to T_N + 100K for both compounds, with p = 0.75. He obtained, however, the best fit to an expression

$$\Delta H = \frac{CT}{T - T_N} \quad \ldots\ldots\ldots\ldots\ldots\ldots\ldots\ldots \quad 4.85$$

for $T > T_N$ + 10K, with C = 80 for MnS and 280 for MnO.

(ii) Ferromagnets

The position with respect to short range order in the esr linewidth of ferromagnets above T_C, is far less clear. Particularly in powder measurements, the demagnetisation corrections are difficult to determine and tend to mask the true behaviour. Salamon (4.28) has followed the ferromagnetic resonance of Ni into the paramagnetic regime and claims to have identified a regime from T_C + 30K to T_C + 66K where the change in slope of the linewidth may be fitted to an expression of the form 4.84 . However, no satisfactory theory has yet been proposed which correctly predicts the change of linewidth above T_C.

CHAPTER 5

EXPERIMENTAL REVIEW OF ESR OF IONS IN METALS

There has been no experimental review of the esr of magnetic ions in metals since the article of Peter et al published in 1968 (1.43), in which an account was given of the results of all previous investigations. In the present work, an attempt has been made to review all experimental work on the esr of ions in metals published up till April 1972 and a comprehensive list of papers appears in Appendix 4, classified by magnetic impurity and by host matrix. The survey is divided, rather arbitrarily, into sections dealing with s-state rare-earth ions, transition metal ions and non s-state ions and each of the sections is subdivided according to the type of host. In the final section of the chapter the technique of transmission electron spin resonance (tesr) is discussed.

5.1 Rare-Earth S-State Ions

(a) Pure Rare-Earth Ions

The first observation of paramagnetic resonance in Gadolinum metal was reported by Kip (5.1), working with a small disc of metal. He found a paramagnetic g-value of 1.95 ± 0.03 (c.f. $g = 1.995$ in insulators). A g-shift was observed to set in at about 50C and moved continuously to lower fields as the sample became ferromagnetic (T_C = 16C). The half-power, half-width also showed an increase from about 400 Gauss at 40C to more than 2KGauss at 0C, below which temperature the line was too broad for further measurement.

Chiba and Nakamura (5.2) extended the work in the paramagnetic regime to 600C and found a linear relation between linewidth and temperature above about 350C. A temperature independent g-value of 1.97 was found. Popplewell and Tebble (5.3) in their work on the Y-Gd

system (see below), obtained a value of $g = 1.96 \pm 0.03$ for the g-value of pure Gd in the paramagnetic regime, but were unable to quote a value below the Curie temperature because of uncertainty over demagnetisation corrections.

Careful work above and below T_C using a single crystal enabled Rodbell and Moore (5.4) to obtain a g-value of 1.94 ± 0.02 for the paramagnetic regime and a value of $g = 2.00 \pm 0.02$ below T_C.

Europium metal, which is known to order in a complex antiferromagnetic arrangement with a Neel temperature of 94K, was investigated by Peter and Matthias (5.5). Between room temperature and 120K they found $g = 1.985 \pm 0.015$ and $\Delta H = 1300$ Gauss. Below 120K, however, the line was found to 'broaden and disappear'. The 'free ion' g-value for Eu is 1.993.

(b) Rare-Earth Intermetallic Compounds

Peter and Matthias (5.5) made the first observation of resonance in an intermetallic compound in their work on $GdIr_2$. They failed to observe a resonance in $EuIr_2$ and considered this to be evidence that Eu is trivalent in this compound. They extended this work (5.6) to the compounds $EuAl_2$ and $GdAl_2$ between 100K and 300K. Allowing for admixture of the real and imaginary parts of the susceptibility (see ch. 7) and for demagnetisation corrections, they arrived at a value of $\Delta H = 900 \pm 30$ Gauss for the half power width of the line and $g = 1.982 \pm 0.003$ ($J \sim -0.03$ eV) in the case of $GdAl_2$. For $EuAl_2$ they found $g - 1.994 \pm 0.003$ at 300K, which is close to the Eu free ion value. In corresponding nmr measurements on $(R.E)Al_2$ alloys, they observed Knight shifts consistent with a negative exchange interaction but which varied in magnitude across the series. This was the first measurement of the sign of conduction electron polarisation in a magnetic metal. Neither the inconstancy of the nmr data nor the sign of the exchange was explained. Peter (5.7), however, showed that addition of other rare-earths to $GdAl_2$ led to a broadening of the line due to RKKY interactions between the impurities

and the Gd ions and found that the line broadenings had the same relative values as the shifts in the nmr work.

Shaltiel et al (5.8) in the course of their extensive work on resonance in s-state ions, measured the g-value and linewidth of the two $CaCu_5$ structure compounds, $GdNi_5$ and $GdCu_5$ at 78K and 65K respectively. They obtained a g-value of 1.942 ± 0.007 and $\Delta H = 905 \pm 90$ Gauss for the Ni compound and $g = 2.009 \pm 0.007$, $\Delta H = 875$ Gauss for the Cu compound. They did not investigate the temperature dependence. The negative g-shift in the $GdNi_5$ compound was interpreted as being due to the high density of states in the almost full d-band of this compound, whilst the positive shift in $GdCu_5$ was ascribed to true atomic exchange.

The compound $EuAl_4$ was investigated by Wernick et al (5.9). Their magnetisation measurements at 4.2K showed that the compound was a metamagnet undergoing a transition to ferromagnetism at a field of about 15KGauss. A plot of $1/\chi$ v T suggests antiferromagnetism at temperature below 6K but $\theta = 14$K. Esr measurements were made between 1.8K and 295K and a high temperature g-value of 1.995 ± 0.04 with half-width at half-power of 430 Gauss was obtained. The resonance was followed below the nominal ordering temperature and at 1.8K the line had broadened to over 3KGauss.

Vijayaraghavan et al (5.10) performed nmr measurements on compounds of the form $(R.E)Pt_2$ and $(R.E)Pt_5$, where (R.E) = Ce, Pr and Nd. They obtained different Knight shifts from the inequivalent Pt sites in the $(R.E)Pt_5$ compounds. All the values of J obtained from these measurements were positive, but this was found to be in disagreement with the negative value obtained from esr on Pt_2Gd, where a g-value of 1.873 ± 0.007 (corrected for lineshape and demagnetisation) was obtained. However, Davidov and Shaltiel (5.11) contradicted this latter result, obtaining a large positive shift ($g = 2.032$). These latter authors also measured the g-value of the compounds $GdAl_2$, $GdRh_2$, $GdMn_2$ and $GdIr_2$ and

found negative g-shifts for these, the value for $GdAl_2$ agreeing well with the previous measurement (5.6). In nmr experiments on the same compound they distinguished between two hyperfine fields: the first resulting from the polarisation of the conduction band due to the Gd ion of the same nucleus, and the second from the conduction electron polarisation arising from the same ions, estimating this second contribution to be ~15% of the first. Allowing for core polarisation, they obtained fairly good agreement between the relative values of the hyperfine field and esr g-shifts, and they also accounted for the positive g-shift in $GdPt_2$ by assuming that, as in $LaPt_2$, the d-band is full in this compound.

Very recently Hacker et al have obtained a value of $g = 1.984 \pm 0.003$ for $GdAl_2$ at room temperature, in excellent agreement with the results above.

Okuda and Date (5.13) measured what they presumed to be a dilute solution of Gd in Cu. The form of their results, and the fact that the data did not change with concentration, suggests that the resonance was, in fact, due to an intermetallic compound. Comparison with the data on Cu_6Gd obtained in this work further confirms this view. They found that the g-value was constant at the room temperature value (not quoted) down to about 60K where the field for resonance shifted to lower values. At about 10K the shift was ~ 2.5KGauss. The linewidth data were linear at high temperatures with a slope of about $5G.K^{-1}$. A fairly sharp minimum in the linewidth was found at 50K and the line subsequently broadened to about 2KGauss at 10K.

The temperature dependence of the g-value and linewidth in the compound $GdNi_5$ has been investigated by Burzo and Ursu (5.14) between 100K and 300K. They found a g-value of 1.944 ± 0.006 (in good agreement with Shaltiel et al (5.8)) which was temperature independent, and obtained a value of $6.4G.K^{-1}$ for the high temperature slope of the linewidth. A value of $K(\alpha)$ in equation 4.55 of 0.1 was assumed to bring the measured

values of Δg and $d\Delta H/dT$ into good agreement.

Esr measurements on the compound GdB_6 were first performed by Coles et al (5.15) and, more recently, Miller and Hacker (5.16) have also measured this compound. Coles et al found a g-value of 2.01 at both room temperature and 77K and a 20% broadening in the linewidth between these temperatures. At 4.2K they did not observe a resonance. Miller and Hacker used a computer fit of Lorentzian dispersion and absorption components to correct their g-value and obtained values of 1.994, 1.992 and 1.992 at 77K, 195K and 295K respectively, with half-power linewidths of 733, 609 and 630 Gauss at the same temperatures.

(c) Intermetallic Compound Hosts with Rare-Earth Impurities

Shaltiel et al (5.8) substituted 5 mole% Gd on the A sites of the compounds of stoichiometry AB_5 listed below. They observed negative g-shifts at 20K in all the compounds except $LaPt_5$ and YCu_5. The largest shifts were obtained in the compounds containing Ni.

	g	H
$LaNi_5$	1.877 ± 0.007	550 ± 10%
YNi_5	1.900 "	525 "
$ThNi_5$	1.913 "	525 "
UNi_5	1.953 "	470 "
$ThIr_5$	1.973 "	640 "
YCu_5	2.000 "	350 "
$LaPt_5$	2.022 "	860 "

As the signs of the g-shifts in YNi_5 and YCu_5 were opposite, the two compounds were alloyed. At the composition $YNi_{4.5}Cu_{0.5}$ a maximum in the g-shift and a minimum in the linewidth were obtained, but as extra Cu was added the g-value moved back to $g = 2$. The addition of other Rare-Earths substituted on the A sites gave an increase in g-shift for elements to the right of Gd in the rare-earth series and a decreased g-shift

for those to the left.

A plot of linewidth against temperature for 2at% Gd dissolved in the compound UPd_3 gave a linear relation between about 60K and 240K with a rapid broadening at low temperatures. It was concluded that this increase in linewidth was due to magnetic ordering. The g-value increased from 2.02 at 300K to 2.10 at 4.2K.

A number of conclusions were drawn from the above observations:

1. The similarity of the $(Ni\text{-}Cu)_5$ La g-shift measurements with measurements in the (Pd-Ag), (Pd-Rh) - Gd systems suggested that $LaNi_5$, YNi_5 and Pd are very similar hosts.

2. It was observed that when the trivalent La and Y in the Ni_5 compounds are replaced by tetravalent Th and hexavalent U, the g-shifts are reduced. This was attributed to filling of the d-band.

3. It was also observed that when Ni was replaced by Ir and Pt, smaller g-shifts were obtained. This decrease was explained by the fact that these elements are the 5d analogs of Co and Ni and show only weakly enhanced paramagnetism in the elemental state.

4. The large negative g-shifts were explained on the basis of the d-f interaction mechanism discussed in ch. 1. The small positive shifts observed for the other compounds were taken as an indication that in these alloys, 'true' s-f exchange was stronger than d-f exchange.

In a further paper, Shaltiel et al (5.17) made a systematic investigation of the sign and magnitude of the g-shifts of 1 - 5% Gd substituted into AB_2 Laves phase compounds on the A site, where A = Sc, Y, La, Th, U and Zr. The B sites were occupied by 4d and 5d elements with an almost full d-band (Ru, Rh, Ir and Pt). The g-shifts are shown below:

$ZrRu_2$	-0.02	$LaRh_2$	-0.01
$ScRu_2$	-0.05	$LaIr_2$	-0.02
YRu_2	-0.06	$LaPt_2$	+0.01
$CeRu_2$	-0.03	$La_{0.5}Th_{0.85}Ru_2$	-0.07
$ThRu_2$	-0.03	$LaAl_2$	0.00
$LaRu_2$	-0.13		

When these g-values are plotted as a function of increased filling of the B element d-band, i.e. Ru/Os, Rh/Ir and Pt, a trend from large negative g-shifts to small positive shifts becomes clear.

Both esr and nmr experiments (5.18) were carried out on the $La_{1-x}Th_xRu_2$ system with 1 at% Gd substituted on the La site. The g-shifts and Knight shifts, K, were found to vary with x at 20K, both showing a minimum shift at a composition x = 0.5. A linear relation was found to exist between both Δg and K and between K and the susceptibility of the x = 0 compound as the temperature was varied. From these measurements a value of -0.05 eV was estimated for the effective exchange between the Gd f-electrons and the d-band.

Cottet et al (5.19) investigated compounds of the form $La_{1-x}(R.E)_xRu_2$ by susceptibility and esr measurements. On substituting 6% Gd, they found that the alloy became ferromagnetic at 9.5K with θ = + 16K. Addition of Tb and Pr to the Gd alloy increased the susceptibility in the first case and reduced it in the second. Esr on the Gd alloy showed some temperature dependence, exhibiting a broad minimum at about 25K, where g = 1.88. Addition of 1% Pr shifted this curve to lower values of g and addition of 1% Tb shifted it to higher values. The increase in linewidth and shift back towards g = 2 in the ferromagnetic regime was attributed to dynamic effects.

Davidov et al (5.20, 5.21) looked at compounds of the same form containing 0.5, 1.0, 3.0 and 10% Gd, and the compound $LaNi_5$ with additions of 0.1, 1.0, 2.0 and 5% Gd. In the first case they found that for concentrations of 3.0 and 10% there was, again, considerable temperature dependence of the g-value, their results being broadly similar to those of Cottet et al. At low concentrations they found that Δg was almost temperature independent and equal to -0.15. On the addition of 1% of Pr to a 0.25% Gd alloy the additional g-shift varied approximately as 1/T, indicating that the g-shift was proportional to the Pr susceptibility.

The g-shift results for the $LaNi_5$-Gd alloys are shown in fig. (5.1). The main features of the results are as follows:

(1) For Gd concentrations of less than 1% the g-shift was almost temperature independent but for higher concentrations a shift back to g = 2 sets in at temperatures increasing with increasing concentration.

(2) The linewidth displayed a strong concentration dependence increasing from 100 Gauss at the lowest concentration to about 600 Gauss at 3% and then flattening out. There was also a large field effect; measurements at X-band ($\sim$ 3KGauss) giving a linewidth of about half that at Q-band (14KGauss).

(3) The g-shift measurements also showed a pronounced field effect. The g-shift was greater at X-band and the largest differences were observed for high concentrations.

Dynamic effects were again invoked to explain this behaviour as described in ch. 4 and ch. 8. However, the increase in linewidth with concentration and field was not explained by the above theory; instead it was assumed that local clusters of Gd ions resulted in inhomogenous broadening, with exchange narrowing at higher concentrations.

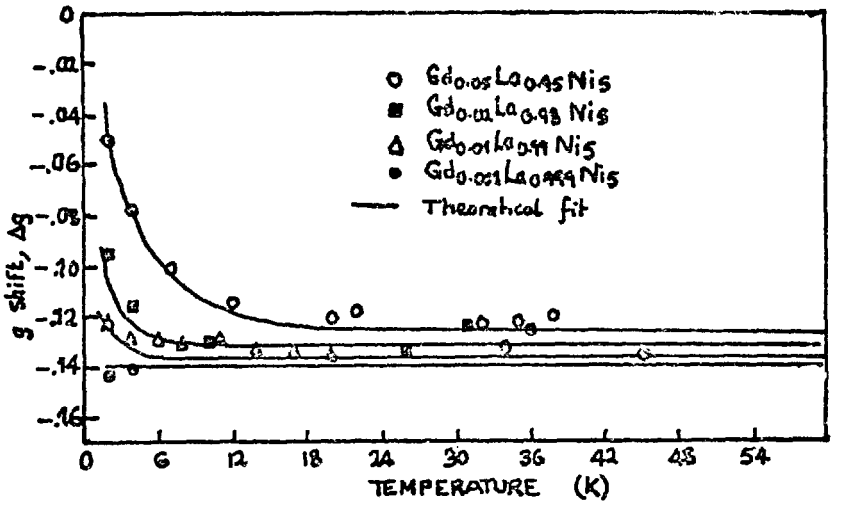


FIG 5.1
AFTER
REF 5.21
$(GdLa)Ni_5$

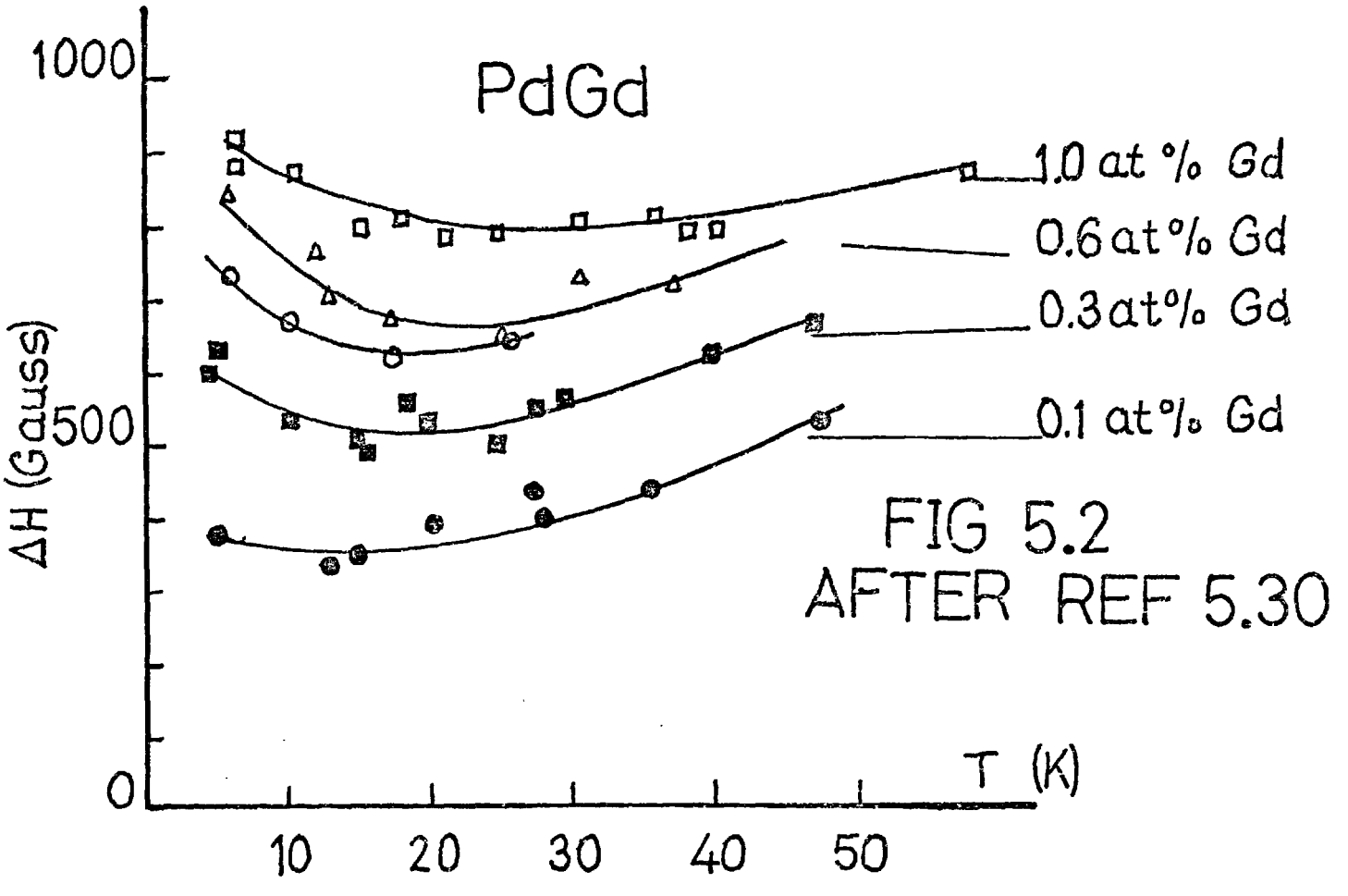
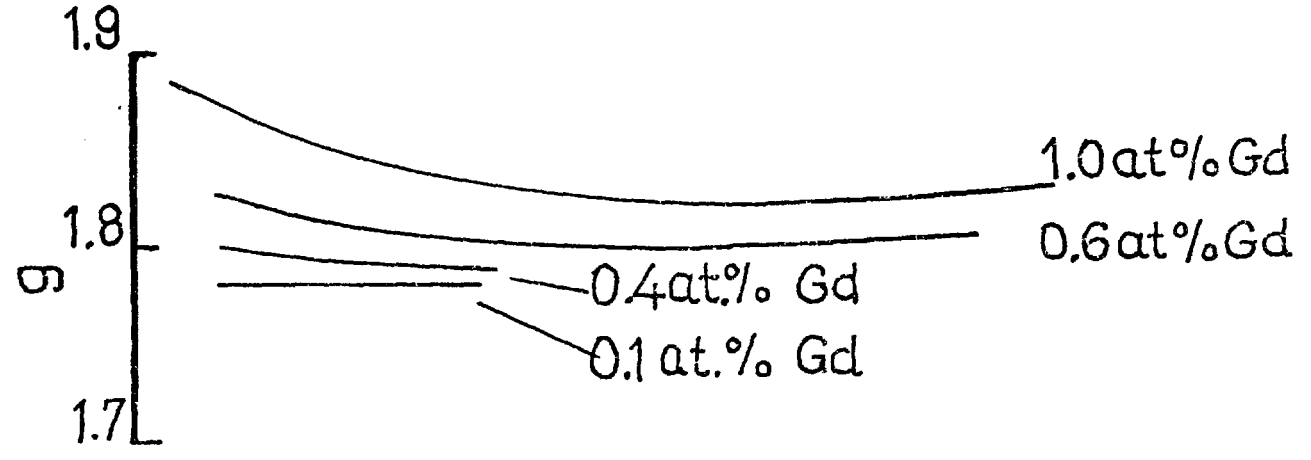


FIG 5.2
AFTER REF 5.30



Davidov et al (5.22) also investigated the system $Gd_xZr_{1-x}Zn_2$ ($x = 0.06$, 0.05 and 0.03). Susceptibility measurements on the compound containing 6% Gd gave $T_C = 20K$ and $\theta = 23K$. The esr measurements showed a broad maximum in the linewidth at 40K decreasing to a minimum at 60K, with a high temperature slope of $3G.K^{-1}$. A negative g-shift was observed with a maximum at 30K and a shallow minimum at 50K, decreasing asymptotically at higher temperatures. Fairly good correspondence was obtained between the shape of the curves of g v T and ΔH v T for different concentrations, although for lower concentrations the absolute value of the linewidth was less and the minimum in the g-value more pronounced. They claim that a fairly good fit to the data above 20K may be obtained by consideration of dynamic effects.

Schäfer et al (5.23) observed the resonance of from 0.3 to 5% Gd in the compound YAl_2. They observed no measurable g-shift and found that ΔH varied linearly with temperature, with a slope inversely proportional to the Gd concentration. They took these observations, and the fact that addition of Th increased the slope of the linewidth, as a strong indication that the system was well bottlenecked.

Lowin (5.24) has recently obtained a g-value of 2.045 ± 0.015 for $LaAl_2$ - 0.5 at% Gd at 4.2K and this is in disagreement with the negative value of Δg observed for these alloys in previous work (5.8). The slope of the linewidth with temperature was found to be 42 ± 5 $G.K^{-1}$.

Finally, Davidov et al (5.25) have reported measurements on compounds of the form $U_xTh_{1-x}Pd_3$ which they believe may indicate the existence of a spin compensated state in the system. Susceptibility data on the compounds show a number of anomalies which could possibly be explained, it was suggested, by crystal field splittings, band structure considerations, the antiferromagnetic alignment of U atoms or the existence of a spin compensated state. Esr measurements on a $U_xTh_{0.94-x}Gd_{0.06}Pd_3$ compound showed no linearity between Δg and χ when the temperature was varied,

but did show linearity at constant temperature as the Uranium concentration was varied. These esr data were shown to be incompatible with the first three hypotheses, but it was claimed that the existence of a spin compensated state of the Uranium could explain both the susceptibility and the esr data.

(d) Rare-Earths in Pd and Pd Binary Alloys

The first observation of resonance in the much studied Pd-Gd system was made by Peter et al (5.26a). They found $g = 1.887 \pm 0.007$ for 3% Gd in Pd at 20K and plotted the linewidth against temperature at different frequencies. At high temperatures a linear relation was observed with a slope of about 5 $G.K^{-1}$ for 1% and 3% Gd in Pd at all frequencies. At 10K, 12K and 20K they found broad minima for the 1% alloy at 9 Gc/s, the 3% at 12 Gc/s and the 3% at 50 Gc/s respectively, with strong broadening in the higher concentration alloys, from about 600 Gauss at the minimum to 1800 Gauss at 2K.

On dissolving Gd in a number of hosts from pure Rh($g = 1.89 \pm 0.007$) through Rh-Pd and Pd-Ag alloys to pure Ag ($g = 1.995 \pm 0.007$) i.e. effectively varying the atomic number of the host from 45.0 (pure Rh) to 47.0 (pure Ag), they found a strong minimum in the g-value measured at 20K and 78K, and a peak in the linewidth at a host atomic number slightly on the Rh side of pure Pd. This minimum corresponded well with peaks in the electronic specific heat and susceptibility obtained by Budworth et al (5.26b). In a further paper (5.27), Peter et al discussed the effect of adding other rare-earths to the Pd-Gd host. They found that the addition of the light rare-earths increased the g-shift, whilst addition of heavy rare-earths decreased it. They also showed from susceptibility measurements of Tb in Pd and Pr in Pd, that the g-shift was proportional to the susceptibility of the added rare-earths. The measurements suggested that the range of the polarisation in Pd was far greater than the range of the RKKY polarisation in simple unenhanced hosts (see ch. 1).

Shaltiel et al (5.8) extended their previous work by adding small concentrations of Tb, Sm, Pr and Ce to a Pd 3% Gd alloy and measuring the g-shift as a function of temperature. Below about 20K the g-value of the alloy containing Tb shifted to 2.10, whilst that of the Pr alloy dropped to 1.75. The Sm and Ce doped alloys showed anomalous behaviour; the Sm behaved as though it were a heavy rare-earth giving a g-value of 2.00 at 2K, whilst no additional shift was observed in the case of Ce. The g-value of Gd in Pd was found to be approximately concentration independent over the range 1 to 3% Gd, but addition of Tb and Nd to an alloy containing 2% Gd gave a g-value which increased with increasing Tb content and decreased on the addition of Nd.

When Ni was added to a Pd 3% Gd alloy, the g-shift and linewidth were found to increase linearly with the concentration of Ni. No separate resonance from the Ni ions was observed. Concentrations of up to 0.3% Fe and Co were also added and in the case of Co impurities, the g-shift at 20K increased from the value observed for Gd in pure Pd but became smaller than the Pd-Gd g-shift as the temperature was lowered. The first effect was attributed to an increase in the Pauli susceptibility (as in the Ni case), whilst the second effect suggested a negative sign for the exchange interaction between the Co ion and the conduction electrons. No resonance from Co was observed. The measurements on alloys containing Fe were hampered by a strong Fe ferromagnetic resonance signal.

Resonance was also observed from 2% Gd diluted in a series of Pd-U hosts containing up to 20% U. On the addition of U the g-value increased to g = 2, reaching this value at 9% U, at which concentration there is also a minimum in the Pd-U susceptibility data. When the Pd-U g-shift data were plotted on the same electron concentration scale as Pd-Ag, the two sets of values were found to correspond. The linewidth in the Pd-U-Gd system was found to be fairly independent of concentration up to about 9% but then increased rapidly from 400 Gauss to 1200 Gauss at 15%.

Shaltiel (5.28) further investigated the effect of filling the Pd d-band by hydrogenating a Pd-Gd alloy. In a short note he confirmed that in this case the g-value returned to $g = 2$. Addition of other rare-earths gave no extra shift.

Higher concentrations of Gd in Pd (4.4 - 6.2%) were found by Harris et al (5.29) to give constant g-values of 1.86 ± 0.03 in the paramagnetic regime.

Cottet and Peter (5.30, 5.31) have worked extensively on the Pd-Gd and binary Pd-Gd systems. They find that at 0.1% the g-value of Gd in Pd is temperature independent at $g = 1.78$ and that this increases linearly with concentration to 1.88 at 2.5% Gd in Pd. Cottet (5.30) plots a family of curves for ΔH v T and g v T for concentrations of 0.1, 0.4, 0.6 and lat% Gd in Pd (fig. (5.2)). In the high temperature regime ($> 30K$) the linewidth increases linearly with a slope of about $6G.K^{-1}$ and each curve shows a fairly weak minimum between 10K (0.1%) and about 30K (1.0%). Above about 0.4% the g-value shows a slight curvature towards higher g-values at low temperatures.

Addition of Ni or Rh to the Pd host gave an increased g-shift to $g \sim 1.73$ for 1% Ni or 2-5% Rh. It was found that for Pd alloys doped with Cr, Pt and Ag, where the susceptibility of the host is lower than in pure Pd, the g-value was proportional to the host susceptibility at 4.2K. The same was also true for Ni doped alloys where the susceptibility is higher than pure Pd, but here a new constant of proportionality was found. In the case of Rh this proportionality was no longer observed. When, however, the g-shift was plotted against the high temperature susceptibility (250K), simple proportionality was observed for all the systems. They suggested that both Ni in Pd and Rh in Pd are partially localised and that the temperature independent part of these solutes in Pd corresponds to the de-localised part of the susceptibility which largely controls the g-shift. The localised part influences the linewidth and

here it was found that whilst addition of Ni and Rh broadened the line considerably, addition of Pt and Ag had little effect.

Praddaude and Gärtner (5.32) measured the g-values of 0.2 - 2% Gd in Pd using specimens in the form of thin plates. Their lowest observed g-value was 1.826 and they suggested that the lower values of Cottet and Peter were obtained on the basis of powder work where demagnetisation corrections are more difficult to apply.

Very recently, Shaltiel et al (5.33) have completely resolved fine structure in the spectrum of Gd in single crystals of Pd at a concentration of 430 ppm at 1.47K. They exhibited resonance data showing a decrease in resolution with increasing concentration and temperature. A sample of 1300 ppm Gd was partially resolved and the g-value was found to be 1.806 ± 0.005 for the central line. The slope of the linewidth at high temperatures was larger (at 9.3 ± 0.5 $G.K^{-1}$) than the figure for powder samples quoted by Cottet (5.30).

(e) Gd in Y, Lu, Sc and La

Popplewell and Tebble (5.3) measured the g-value of Gd-Y alloys containing from 3.7at% Gd to pure Gd, in eleven concentration steps. The g-values were found to be concentration dependent ranging from 1.96 ± 0.03 at pure Gd to 2.13 ± 0.05 for the 3.7at% alloy, passing through the free-ion value at about 30at% Gd. They observed that cooling through the Curie point broadened the line until the width became indeterminate some 100K below T_C and the line was shifted to lower fields. In the alloys with concentrations between 25 and 60% Gd, where in addition to ferromagnetic order there exists a regime of antiferromagnetic order, two lines were observed. One of these lines broadened and disappeared above T_N whilst the other appeared to be a ferromagnetic resonance. They suggested that these double lines were due to ferromagnetic clusters of Gd. For a 64% alloy at high temperatures a slope of about 15 $G.K^{-1}$ was observed in the linewidth

and a minimum was found about 40K above T_c.

In further papers (5.29, 5.34) they alloyed Gd in Lu, Sc and La as well as Y. In the Lu-Gd system the g-value in the paramagnetic regime becomes positive at 80% Gd and, for the lowest concentration measured (8.3at%), is equal to 2.015 ± 0.01. The linewidth again exhibited a minimum some 40K above the paramagnetic Curie point for an alloy containing 70% Gd and continued to broaden below T_c. The large positive g-shift (to 0.13) quoted above (5.3) for small concentrations of Gd in Y was revised in the present work to a figure closer to the free ion value, and the g-value for an alloy containing 8% Gd was given as 1.998. The g-values for dilute Gd in La and Sc were both quoted as being equal to the Gd free ion value.

Cottet (5.30) investigated the behaviour of alloys of Y, La and Sc containing less than 2% Gd. He quoted the following g-values at 4.2K:

Y-Gd	2.04 ± 0.02
La-Gd	2.03 ± 0.02
Sc-Gd	2.00 ± 0.02

A plot of $d\Delta H/dT$ against concentration in the paramagnetic regime showed an increase in $d\Delta H/dT$ at low concentrations in all three systems, but was particularly large in Y-Gd (from 35 $G.K^{-1}$ at 2% to 100 $G.K^{-1}$ at 0.2%). Plots of ΔH against temperature for 4.2% and 3.5% Gd in Y showed a broad minimum at 30K and 20K respectively, with strong broadening of the lines at low temperatures. The temperatures of the minima in these alloys correspond quite well with the Curie temperature. Cottet concluded from the absence of appreciable g-shift and the behaviour of $d\Delta H/dT$ V concentration that the Y-Gd system was well bottlenecked and that the other two systems were partly bottlenecked.

Addition of 3% Ce to an Y 1% Gd alloy gave a g-value of 2.12 ± 0.02 at 4.2K which moved towards g = 2 as the Kondo temperature of the Y-Ce system was approached. Cottet surmised that this may have been a manifestiation of the Kondo effect in esr.

Recently, Salamon (5.35) has observed resonance in a single crystal of 500 ppm Sc in Gd and found that the g-value varied from 1.988 to 2.07 with orientation and that the linewidth passed through a minimum at an angle of approximately 60° between the DC field and the C-axis. Salamon attempted to explain his results in terms of an anisotropic g-value, whereas Tao et al (5.40) suggest that the results are better interpreted in terms of unresolved fine structure.

(f) Rare-Earth Ions in Other Hosts

Nakamura et al (5.36) prepared a series of alloys containing 0.15, 0.44 and 0.5at% Gd in Ag and found that the linewidth was linear with temperature down to the lowest temperatures, with a slope of 4 $G.K^{-1}$ for the low concentration alloy. The g-value for all the alloys was close to the Gd free ion value. Addition of Al was found to increase strongly the slope of the linewidth and to increase the g-values. These observations were attributed to the breaking of the esr bottleneck by the impurities.

The g-values obtained above agreed quite well with the single Ag 0.8at% Gd alloy examined by Coles and Griffiths (5.37) in their paper on Er in Ag. Here they found g = 2.005 ± 0.005 and ΔH = 158 Gauss at 4.2K.

Ehara (5.38) measured an alloy of 0.5at% Gd in Mg and obtained a g-value of 2.03 ± 0.005 with a linewidth of 260 ± 30 Gauss, at 4.2K. It was suggested that this positive g-shift provided evidence for the interpretation of the behaviour of the incremental resistivity (which shows a logarithmic increase with increasing temperature) in terms of a Kondo effect with positive J. Williams (5.39) has, however, emphasised once again the dangers of comparing the sign of J obtained in different measurements.

Tao et al (5.40) have recently observed the resonance of 500 ppm of Gd in a single crystal of Mg at 1.4K and 4.2K measured at both X-band and Q-band. They report strongly anisotropic g-values which are temperature dependent and negative at 1.4K for all angles. This appears to cast some doubt on Ehara's result. As in the case of Salamon above (5.35), a minimum in the linewidth is observed and $g \sim 2.0$ for an angle of about 60° between the field and the C-axis. They propose that both their results and those of Salamon may be best described in terms of unresolved fine structure.

The sign of the g-value for Gd in Mg is further confused by the report of Burr and Orbach (5.41) of a positive g-value for both Gd and Eu in Mg. They declined to give a precise value, however, "due to deviations from Dysonian lineshape".

The first resolved fine structure of a localised moment in a metal was observed by Chock et al (5.42) in single crystals containing 1000, 300 and 150 ppm of Gd in Au. At 4.2K they observed a single line at all angles, but with considerable angular variation of the linewidth. At 1.4K, however, they resolved fine structure at certain angles. The resonance position of the "line" at 1.4K also showed an angular variation of 30 ± 5 Gauss. For minimum linewidth a g-value of 2.05 ± 0.01 was found, which is equal to that obtained from powder samples of the same concentration. At the angle for minimum linewidth they were able to fit the line to a form $A(C) + BT$ where $B = 8\ G.k^{-1}$, which again is the same as powder samples. The value of A (17 ± 3 Gauss) at 150 ppm was, however, larger by a factor of four for powders of the same concentration. The observed resonance did not display the character expected for resolution of the seven Gd fine structure lines and a theory of line narrowing from spin - spin couplings and localised conduction electron exchange was outlined. Addition of 1 - 2% Pt increased the value of A and decreased B, thus suggesting that the system was not bottlenecked, despite a small increase of B with decreasing concentration.

Recently, Davidov et al (5.43) have observed the resonance of a number of rare-earths in Th, including Gd. For the Gd alloy they found that both splat-cooled and powder alloys with concentrations of from 95 - 1300 ppm of Gd obeyed a relationship A(C) + BT with B = 31 $\pm$ 5 $G.K^{-1}$. The alloys had g-values of 2.01 $\pm$ 0.01.

Finally, we consider the work of Schäfer et al (5.44) who dissolved up to 10% Eu in Yb. A signal was observed from 1.6K to 77K and measurements were made at both X-band and Q-band. A value of g = 1.970 $\pm$ 0.005 was obtained at all temperatures and the alloys all showed the same slope $\sim$ 24 $G.K^{-1}$ in the linewidth above about 30K, below which the alloys ordered. Good correspondence was obtained between the values of J calculated from the g-shift and from the temperature dependence of the linewidth.

5.2 Transition Metal S-State Ions

(a) Mn in Cu, Ag and Au

The first observation of an impurity resonance in a metal was made by Owen et al (5.45, 5.46) on Mn in Cu. They observed resonance from alloys containing from 0.07% to 11.1% Mn at 2K, 4K, 77K and 295K. They also studied an alloy of 4.2% Mn in Ag. The linewidths increased with temperature in the paramagnetic regime and g-values for the alloys were all in the range g = 1.99 to 2.01, after correcting approximately for lineshape. At low temperatures in the alloys containing more than about 1 at% Mn in Cu, they observed from susceptibility measurements what appeared to be antiferromagnetic ordering at temperatures increasing from about 12K for a 1.4at% alloy to about 100K for the 11.1% alloy. In addition, they observed a spontaneous magnetisation at 4K from the higher concentration alloys, the value of which appeared to be a function of the field in which the alloy was cooled. Below the Néel point the esr line was observed to move to lower fields, the largest shift being obtained

in the highest concentration alloys (at 4.2K, the 5.6% Mn alloy had shifted by 1170 Gauss, the 1.4% alloy by ~ 190 Gauss). These shifts were found to be well described by the relation:

$$H = (H_o^2 - H_C^2)^{\frac{1}{2}}, \quad H_C = (2H_E H_A)^{\frac{1}{2}}$$

which is of the same form as equation 4.80, for antiferromagnetic resonance with H perpendicular to an anisotropy axis.

Measurements on a single crystal of 5.6at% Mn in Cu showed the line to be isotropic to within $\pm$ 30 Gauss in the (111) and (110) planes.

Field cooling was also found to have a strong effect on the esr measurements. Cooling the 5.6at% alloy from 77K to 4K in a field of 5KGauss shifted the line back to higher fields by 670 Gauss, compared to a measurement at 4K taken after cooling in zero field. Hysteresis effects and gradual field dependent shifts were also found when the alloy was held at 4K and the field was varied.

The absence of an appreciable g-shift and the observed widths of the resonant lines was taken to indicate that the s - d exchange in the alloys was 1/5 - 1/10 less than might be expected for Mn in Cu. A molecular field model for the antiferromagnetic resonance was presented, where the anisotropy field was replaced by a small molecular field arising from the magnetisation of the conduction electrons.

Shaltiel and Wernick (5.47) observed the resonance of 2% Mn in Au, Cu and Ag and confirmed the g-values obtained by Owen et al in Cu and Ag. They found a value of $g = 2.005 \pm 0.005$ in the Au-Mn alloy with a broad line of 725 Gauss at 20K (c.f., Cu-Mn = 140 Gauss, Ag-Mn = 120 Gauss).

Geschwind et al (5.48) made measurements on a 0.1at% Cu-Mn single crystal. They observed a line which narrowed to 40 Gauss at low temperatures but were unable to find evidence of hyperfine structure. Anisotropy in the Cu-Mn g-value was put at less than one part in four thousand from these measurements.

Griffiths (5.49), using the present spectrometer, carefully investigated the behaviour of alloys containing 4at% and 15at% In in Cu, as a function of their magnetic history.

In the 4at% alloy cooled in zero field, a well defined maximum in the plot of amplitude (A + B) against temperature was observed at 43 ± 2K. At about the same temperature (50K) the linewidth showed a weak minimum and a lineshift became apparent. The more concentrated alloy showed similar behaviour, the corresponding temperatures being 115 ± 3K for amplitude and 135K for linewidth.

The g-values and linewidths obtained by Griffiths agreed well with those of Owen et al except for the room temperature linewidth of the 4at% alloy which Griffiths found to be considerably narrower than Owen's value, although both samples were annealed. Griffiths also found a smaller shift in resonant frequency for his 4at% alloy (700 ± 20 Gauss).

Cooling the alloys in a field of 5KGauss radically altered the behaviour on a subsequent warm-up run. The temperature of the amplitude maximum was the same as the zero field value, but showed, in addition, a pronounced minimum at 21K and 60K for the 4% and 15% alloys respectively. There was a maximum in the linewidth at these temperatures and a reduction in the shift in resonant field at low temperatures. The 4at% alloy was, for example, only shifted 460 ± 20 Gauss from g = 2 at 4.2K. By plotting the parameter $(A + B)(\Delta H)^2$ against temperature, it was evident that a 1/T dependence of the signal intensity did not hold. The form of the curves for both zero and field cooled samples was similar. Using the expression $H^2 = H_o^2 - H_C^2$ used by Owen et al, Griffiths found a good linear relation between H_C and T for the zero field data and noticed that the extrapolated value of T corresponding to $H_C = 0$ was in both cases close to the observed amplitude maximum.

Griffiths pointed out the fact that whilst these characteristic temperatures agree with those obtained from static susceptibility measurements, they are much lower than anomalies found in the resistance data for Cu-Mn alloys. The esr results were thought to support Kouvel's theory of ferromagnetic/antiferromagnetic interactions and the characteristic temperatures to correspond to the onset of ferromagnetic interactions.

Gossard et al (5.50) studied the temperature dependence of the esr linewidth of 0.3 and 1.5at% Mn in Cu alloys from 1.4K to 240K with the addition of 0.01 to 0.15at% Tie, Fe, Co and Ni. They estimated, on the basis of the Korringa formula, that the slope of the linewidth should be $\sim 2000T$ Gauss compared with an observed value some two hundred times less for a 0.3at% alloy and eight hundred times less for a 1.5at% alloy. They attributed this difference to bottlenecking. When non-magnetic impurities (Ti and Ni) were added, the linewidth was observed to broaden and the slope of the linewidth to increase by an amount roughly proportional to the impurity concentration. This was interpreted as evidence of the breaking of the bottleneck by increased conduction electron relaxation from spin - flip scattering at the impurity sites. When Fe or Co were added, the broadening was an order of magnitude greater still and this was attributed to the extra relaxation involving the transfer of spin energy from the Mn to the Fe and Co spins. Further work investigated the effect of Al and Mg impurities. The spin - flip scattering cross-sections were deduced and tabulated for the various impurities.

Okuda and Date (5.51) added Ni and Al to a Cu-5% Mn alloy and found that the slope of the linewidth was five times greater for Ni. They also found that in the antiferromagnetic regime, in a Cu 2% Mn alloy, addition of Ni increased the lineshift whilst addition of Al had little effect upon it.

In a further paper (5.51), the same authors presented detailed measurements on alloys of 1.4, 2.0, 3.0 and 4.0 at% Mn in Cu below 77K and the results were in good agreement with those of Owen et al and Griffiths. It was observed that the concentration dependence of the lineshift at 4.2K was linear with a slope of 140 $G.K^{-1}$ at X-band. They suggested that the anisotropy field originated from the nuclear spin of the Mn^{55}. It was shown that this field had the correct temperature dependence and the temperature dependence of the sublattice magnetisation was deduced. ENDOR experiments on Ag-Mn alloys were performed and some effect attributable to nuclear anisotropy was observed.

In further work on the effect of a third element they extended their previous work to Co, Fe, Pd, Ti and Zn, finding that the first three elements behaved like Ni in the antiferromagnetic regime whilst the last two were like Al.

McElroy and Heeger (5.52) observed that residual linewidths in the Cu-Mn system were unchanged for Mn concentrations of from 0.1 to 1.5at% and this ruled out Mn-Mn interactions as being the main contribution. They found that the addition of non-magnetic impurities such as Si or Al to a 0.1at% Mn in Cu alloy increased the residual width by 72 G per % Si and 38 G per % Al and accounted for this by the mechanism discussed in ch. 4. In their analysis they obtained a value of $V_{dk} \sim 1$ e.V., by substituting the value for the spin - flip scattering time for Si, obtained from a plot of linewidth against temperature for different Si impurity concentrations. Good agreement was obtained with the results from addition of Al.

Nakamura and Kinoshita (5.53) investigated a number of Cu-Mn alloys with concentrations from 0.03 to 2% and found that, below about 1% Mn in Cu, there was a rapid increase in linewidth for decreasing concentration, with a slope rather less than inversely proportional to concentration. They observed that the residual linewidth was concentration independent for less than 1% Mn but decreased above this concentration. All their alloys gave $g = 2.01 \pm 0.01$ in the paramagnetic regime.

Gossard et al (5.54) studied the esr behaviour of Ag-Mn alloys and found good qualitative agreement with the Cu-Mn results. They worked with etched slabs of the material and with filed powders and observed that even after stress annealing, the linewidth in the filed powders increased at a sharper rate with temperature than in the slabs. In a slab containing 0.26% Mn the linewidth increased at ~ 10 G.K^{-1} whilst in a 1.3% alloy, the linewidth increased at 3 G.K^{-1}, thus suggesting that the system is bottlenecked. Both alloys gave $g \sim 2$ in the paramagnetic regime and it was found (as in Cu-Mn) that the addition of non-magnetic impurities increased the slope of the linewidth. The spin - flip scattering cross-sections for Zn, Ga, Cd, Pt and Au were evaluated.

The importance of metallurgical treatment in Cu-Mn alloys was highlighted by the work of Miyako et al (5.55). They annealed their samples at 850C in a vacuum of 10^{-8} torr and claimed that this had a pronounced effect on the linewidth of their alloys. They found that the use of a vacuum of only 10^{-6} torr doubled the linewidth of a 4.3% Mn in Cu alloy at room temperature and that bringing the vacuum up to 10^{-3} torr pushed the linewidth up by a further factor of about five. Differences were found to be much smaller at lower temperatures. Contrary to the work of Owen et al and Griffiths, they claimed to find pronounced maxima in linewidth for high vacuum annealed samples at temperatures corresponding to Kouvel's anomalies in the resistance ($\sim$ 100K for 4.3% and 40K for 2.0%).

A detailed study of the Ag-Mn system with Mn concentrations of from 0.19 to 18at% was carried out by Elliston (5.56). In the antiferromagnetic regime, behaviour similar to the Cu-Mn results of Griffiths was observed, the Neel temperatures suggested by the esr measurements again being considerably lower than values estimated from resistivity measurements.

Oda and Asayama (5.57) plotted the linewidth against temperature and residual linewidth against concentration for very dilute (0.05, 0.3 and 1.5%) Mn in Cu doped with between 0.006 and 0.5% Fe, Ni and Co. They claimed that their results, using McElroy and Heeger's analysis, suggested the existence of an s - d quasi-bound state with high Kondo temperature for Co in Cu.

Recently, Nagashima and Abe (5.58) have opened the bottleneck in Cu-Mn using a different approach. They evaporated thin films of Cu-Mn on to thin glass plates and observed the increase in linewidth as the film thickness was reduced. They calculated a value of 0.04 as the probability of a spin disorientation with a surface collision.

(b) Mn in Pd

The first esr measurements in the Pd-Mn system were reported by Shaltiel and Wernick (5.47). They found $g \sim 2.10$ for a 2at% sample at 4.2K and 20K and a gradient in the linewidth of about 50 $G.K^{-1}$. The linewidth at 4.2K was quoted as 680 Gauss. When 1% Pr was added to the alloy, the g-value increased to 2.195 whilst the addition of 0.2% Ho decreased it to 2.055. This indicated that, as in the case of Pd-Cd, the light rare-earths increase the g-value whilst addition of the heavy rare-earths decrease it. Comparison of the values of J for the two systems were in fairly good agreement. The broadening of the line on adding the rare-earth was in this case much greater than for the Pd-Cd system.

Cottet (5.30) measured the temperature dependence of the linewidth in the paramagnetic regime for concentrations of 0.23, 0.5, 1.0, 1.5 and 2.0% Mn in Pd and found a slope of 75 $G.K^{-1}$ for the 2% alloy, increasing slightly to about 90 $G.K^{-1}$ for the lowest concentration. He observed a g-value of about 2.12 $\pm$ 0.01 for the 1.5at% alloy at 5K and g = 2.17 for the 0.23% alloy.

(c) Mn in Zn, Mg and Al

Owen et al (5.45) performed one experiment on a 0.67% Mn in Mg alloy and obtained a g-value of 2.02 and linewidth of 270 Gauss at 4.2K, which showed some signs of Cu-Mn type antiferromagnetic behaviour below 4K. Single crystal measurements in this regime suggested some signs of anisotropy.

Collings and Hedgcock (5.59) made a thorough study of esr in a 0.6at% Mn in Mg alloy. They reported g = 2.00 $\pm$ 0.01 from 70K to about 6K and a shift in the resonant field of 300 Gauss at 2K which was double the value reported by Owen et al. A temperature independent linewidth of about 300 Gauss was reported up to 20K, with a slope of 6 $G.K^{-1}$ above this temperature. The amplitude of the signal also gave a broad peak at about 6K. No change in the esr data was observed by cooling to 2.6K in a 3KGauss field. The same authors found no resonance for 1 at% Mn in Al.

Observation of a resonance line between 4K and 15K in a Zn 0.4at% Mn alloy was claimed by Collings et al (5.60). A linewidth of 800 $\pm$ 100 Gauss was reported with a shallow minimum at roughly 10K. A small lineshift to lower field below the same temperature led them to the conclusion that some form of antiferromagnetic order was present. Above 10K it was stated that a g-shift was observed but no value was quoted.

Miyako (5.61) claimed to have observed resonance from 0.5at% and 1.0at% Mn in Zn. A temperature independent g-value of 2.05 $\pm$ 0.01 was reported below 90K with a linewidth of 800 Gauss at 4.2K which broadened at

higher temperatures. Addition of Al and Cu impurities to the higher concentration alloy increased the residual width and the slope of the linewidth.

(d) Other Transition Metals

Collings and Hedgcock (5.59) reported the absence of any resonance in Al-Fe and Mg-Fe alloys at 4K.

Salamon and Feigl (5.62) claimed to have observed a resonance from iron in dilute Cr-Fe alloys but considerable doubt has now been cast upon this result.

5.3 Non S-State Resonances

The first observation of a non s-state paramagnetic resonance in a dilute alloy was made in a Ag 0.3at% Er alloy by Griffiths and Coles (5.37) using the spectrometer described in this thesis. A resonance line with $g = 6.73 \pm 0.1$ was obtained at 2.5K close to the value (6.78) observed for trivalent Er in cubic non-metallic matrices, where the $^4I_{15/2}$ state is split by the crystal field to give a ground state doublet. The linewidth was observed to broaden from 60 Gauss at 2K linearly to 160 Gauss at 14K. Over this temperature range the signal intensity ($(A + B)\Delta H^2 T$) showed little temperature dependence. A 1.5at% sample showed weaker temperature variation of the linewidth but had the same g-value.

In a further paper (5.63) g-values of 6.80 ± 0.07 were reported for Ag 0.28at% Er and a g-value of 3.30 ± 0.10 was found for a 0.9at% Yb in Au alloy. A g-value of 3.43 is expected for a Γ_7 doublet of Yb^{3+} in a cubic environment.

The linewidths for the alloys were found to be of the form $A + BT$, where $A = 42$ Gauss and $B = 9.2$ $G.K^{-1}$ for the Ag-Er alloy, whilst $A = 370$ Gauss and $B = 12$ $G.K^{-1}$ for the Au-Yb, implying $J = 0.15$ e.V. and 0.03 e.V. respectively. No resonances were observed in powder samples of AgDy, AgYb or from the ions Tm, Ho and Tb. The absence of a resonance in AgYb

was attributed to a divalent state for Yb in this alloy, as was suggested by the small and weakly temperature dependent susceptibility.

Lowin (5.28) confirmed the g-values obtained above and searched for further non s-state resonances in various hosts. He failed to observe any signal from 2% Tm, 2% Ho or 0.9% Ce in $LaAl_2$ or from Ce in the compound $CeAl_2$.

A resonance from Er in a single crystal of Mg was reported by Burr and Orbach (5.41). The observed signal was characteristic of a uniaxially distorted Γ_7 doublet of the free ion $^4I_{15/2}$ multiplet, the principal values of the g-tensor being $g_{//} = 8.90 \pm 0.1$ and $g_{\perp} = 5.77 \pm 0.1$. They observed that the broadening of the line with temperature was anisotropic varying from 120 ± 20 Gauss in the parallel direction to 140 ± 20 Gauss in the perpendicular direction at 4.2K. Analysis of these values was taken to suggest that the conduction electron - localised moment exchange interaction was isotropic with a value of 0.031 e.V.

The first observation of hyperfine splitting of a localised moment in a metal was made by Chui et al (5.64) for concentrations of from 65 to 1500 ppm of Er in Ag. They estimated a value of $A' = 75 \pm 10$ for the hyperfine coupling constant, in good agreement with values for Er^{3+} in an insulator. They found that the form A + BT used by Griffiths and Coles fitted their linewidth data (central line) and that A was concentration dependent. They attributed the absence of hyperfine splitting in the previous work as due to the larger residual linewidth together with the thermal contribution at the lowest temperatures (total $\sim$ 70 Gauss at 2K) which caused the central line to mask the inner hyperfine lines.

In a further paper (5.65) hyperfine splitting was observed in dilute Eu-Er (to 50 ppm) and Au-Yb (to 500 ppm) alloys. The value for the hyperfine coupling constant for Au-Er was found to be 75.5 ± 0.5 Gauss (c.f. value of 73.8 for Er^{3+} in ThO_2), the central line gave $g = 6.80 \pm 0.04$ and the linewidth obeyed the relation A + BT with $B = 2.4 \pm 0.2$ $G.K^{-1}$.

The hyperfine structure in Au-Yb corresponded to the Yb^{171} isotope with $I = \frac{1}{2}$, and A' was found to be 575 ± 10 Gauss (c.f. $A' \sim 549$ for Yb in CeO_2). The hyperfine structure from the isotope Yb^{173} which has about the same abundance as the Yb^{171} ($I = 5/2$) was not observed and this was attributed to the reduction in intensity on division between the six satellites. A g-value of 3.34 ± 0.06 was found for the central line but the value of the temperature dependent contribution to the linewidth of 42 ± 7 $G.K^{-1}$ was higher by a factor of three than the value reported by Hirst et al (5.63) for the slightly more concentrated alloy. The increase in A' for both alloys over the values in insulators was attributed to the spin polarisation of the conduction electrons. They evaluated the localised moment - conduction electron exchange from the temperature dependence of the linewidth and using a value estimated by Shaltiel et al (5.18) for the 6s contribution to the hyperfine coupling constant, they separated out the atomic and covalent mixing contributions to J for both alloys. By this method, they obtained a value for the covalent mixing contribution in Au-Yb some twenty times larger than is theoretically predicted and they speculate (bearing in mind the diamagnetism of AgYb) that the difference in covalent mixing is due to the close proximity of the 4f level to the Fermi level in this alloy.

The values quoted above have recently been corrected (5.66) in work on enriched samples of Er^{167} and Yb^{171}. The revised hyperfine constants were given as 75 ± 0.5 and 575 ± 10 and the temperature dependence of the linewidth as 2.7 ± 0.5 and 40 ± 10 $G.K^{-1}$ respectively.

Davidov et al (5.67) reported the resonance of Dy in Ag at concentrations of from 0.05% to 1% at temperatures in the helium range. They obtained a value of $g = 7.80 \pm 0.3$ which is close to the value expected for the Γ_7 state in a cubic environment (c.f. $g = 7.55$ in CaF_2). The linewidth followed the usual linear relationship with temperature, in this case $A(C) = 230$ Gauss for a 0.4% alloy and 130 Gauss for a 0.1%

alloy with B = 40 ± 15 $G.K^{-1}$. These figures give a value of J = + 0.25 ± 0.1 eV. No hyperfine structure was observed.

The same authors (5.68), in a further paper, investigated the resonance of Er in Th, Rh, Pt and Cu; their results are shown below:

	C(ppm)	g	A	B
ThEr	100	6.84 ± 0.05	27	15 ± 2
RhEr	700	6.78 ± 0.1	63	4 ± 2
PtEr	1000	6.50 ± 0.3	500	-
CuEr	200	6.86 ± 0.07	54	10 ± 2

Hyperfine structure was observed in the ThEr system but (presumably due to the larger residual linewidths) was not observed in the other alloys. A value of J = + 0.2 ± 0.05 eV was calculated for CuEr.

The first observation of a Γ_8 quartet resonance was reported by Davidov et al (5.69) in AuDy single crystals with concentrations of 500 and 1000 ppm Dy. The 500 ppm sample displayed two lines both exhibiting appreciable angular dependence in resonant field. The 1000 ppm sample showed only one line with angular variation similar to one of the 500 ppm sample lines. The data were fitted to crystal field parameters with B_4/B_6 = 1300 ± 30. This value is much larger than the value $B_4/B_6 \leqslant 340$ (deduced from the work of Hirst and Williams) for a AgDy alloy and the difference was attributed to the larger virtual d-level width in Ag, reducing the contribution to B_4 from the d-like screening electrons.

The nearly linear increase with temperature of the linewidth of the strongest line in the dilute crystal was used to evaluate J = 0.14 ± 0.05 eV. This value (larger than AuEr) was taken to be evidence, along with previous measurements (above), of the increasing tendency to covalency in moving across the rare-earth series from Gd to Yb.

A further paper by the same authors (5.70) analysed the behaviour of Er in various hosts, extending their previous measurements (5.68). Powder samples of Er in Pt gave broad lines with $g = 6.5 \pm 0.3$ as found previously, but splatted samples gave a narrow line at $g = 5.95 \pm 0.05$. Hyperfine structure was observed with $A' = 75 \pm 2$ Gauss. All concentrations from 250 to 1020 ppm gave a linewidth linear in temperature with $B \sim 8$ G.K.$^{-1}$.

PdEr gave two lines in powder samples with Er concentrations from 200 ppm to 10,000 ppm. The g-values were quoted as 7.5 ± 0.5 and 4.5 ± 0.5. It was found that splatting reduced the intensity of the first line and increased the second (low g), and hydrogenation of the alloys caused the second line to vanish. From these observations the broad line in the PtEr powder samples and the $g = 7.5$ line in the PdEr samples were attributed to intermetallic compounds.

It was argued that although the Γ_6 level has $g = 5.95$, the associated value of the hyperfine coupling constant A' would be 12% lower than the observed value. Since Er in seven other hosts gave a value of A' less than 1.5% from the expected value, it was argued that the Er resonance observed in Pd must be due to the Γ_7 level but shifted from the free ion value of 6.78 by some 34%. A plot of Gd and Er g-values against host (Rh, Pt, Pd) susceptibility yielded a pair of straight lines. The values of the g-shifts, however, do not predict through equation 4.55 the observed temperature dependence of the linewidth.

These observations constitute the only tentative identification of a non s-state resonance in an intermetallic compound.

Davidov et al (5.43) have also investigated Er and Dy in Th as well as Gd in Th reported above.

In ThEr alloys of concentration from 40 to 2600 ppm, a linear plot of linewidth against temperature was again obtained with slope 14 ± 3 G.K^{-1}.

The measured g-value of the alloys was 6.84 ± 0.05 (as previously reported for a 100 ppm sample). Hyperfine structure was resolved with $A' = 75 \pm 2$ Gauss. In ThDy alloys with concentrations of from 180 to 3250 ppm Dy, values of $g = 7.61 \pm 0.1$ and $B = 33 \pm 7$ $G.K^{-1}$ were obtained.

The temperature dependence of the linewidth was used to calculate J for the alloys with an assumed enhancement factor of $K(\alpha) \sim 0.4$. The values obtained were within the errors of the values calculated from the g-shift (except for ThGd) and showed a constant value ~ 0.044 eV for all three alloys, in good agreement with values obtained from previous superconducting transition temperature measurements.

5.4 Transmission Electron Spin Resonance

The investigations in the previous sections of this chapter have all made use of the reflection technique in esr. A few experiments on dilute alloys have, however, made use of the technique of transmission electron spin resonance (tesr).

In these measurements a thin sheet is held between two resonant cavities. At resonance, electrons in the skin depth of the surface exposed to an rf magnetic field develop a transverse magnetisation and, via a diffusion process, carry the magnetisation to the other side of the sample, where power is radiated into the 'receiver' cavity. The process can only occur if the diffusion length δ_s in the relaxation time T_2, is greater than the sample thickness. This, itself, must be sufficiently thick that negligible power is transmitted.

If randomly distributed dilute magnetic moments with a g-value g_d close to the conduction electron value g_s are present in the sample and if, in addition, the cross relaxation rates are larger than those to the lattice (i.e. the bottleneck limit), a single resonance line is observed.

The most important parameter in this case is the ratio χ_r of the impurity static susceptibility χ_d to the conduction electron susceptibility χ_s. When $\chi_r > 1$, the resonance is dominated by the local moment properties (i.e. at low temperatures or high concentrations), but when $\chi_r < 1$, the conduction electron system dominates. A solution of Bloch-like equations, modified for diffusion and exchange (5.73) yield

$$g_s - g_o = \frac{(g_s - g_d)\chi_r}{(1 + \chi_r)} \quad \ldots\ldots\ldots\ldots\ldots\ldots \quad 5.1$$

and

$$\frac{1}{T_{eff}} \left(\propto \Delta H_{obs} \right) = \frac{1}{T_{sL}} \frac{1}{1 + \chi_r} + \frac{1}{T_{dL}} \frac{\chi_r}{1 + \chi_r} \ldots \quad 5.2$$

in the limit above, where g_o is the observed g-value of the 'system'.

TESR Results

The technique was first applied to the dilute alloy problem by Cowan (5.71) who studied the Cu-Mn system. The g-value of an alloy containing 100 ppm Mn at 1.5K was found to be 2.011 ± 0.005 which is the same value as that obtained by conventional techniques. This result is not surprising since $\chi_r > 1$. No sign of hyperfine splitting was observed even in a 40 ppm sample.

Schultz et al (5.72) studied the Cu-Mn system from 1.4K to 35K, for concentrations ranging from 13 ppm ($\chi_r \sim 3$ at 1K) to 250 ppm. In the low concentration limit, the g-value of 4K was 2.024 and this approached the pure Cu cesr value of 2.033 at higher temperatures. The more concentrated alloy made a far slower approach towards the Cu value with increasing temperature. The results on the Cu-Mn system were found to be in good agreement with the simple theory above. One Ag-Mn alloy was also studied. In this case, whilst the general form of the behaviour was in accord with theory, the high temperature g-value appeared to saturate at a value (~ 1.999) far from the pure Ag g-value (1.983) and no explanation was offered for this.

The behaviour of the linewidth as a function of temperature for the alloys was also in good agreement with theory, and Schultz and his co-workers deduced values of T_{dL} and T_{sL} from their measurements.

In a further paper, Monod and Schultz (5.73) performed tesr on alloys of Cu containing 4 to 36 ppm of Cr. The same form of behaviour for the variation of g-value with temperature was observed as in the Cu-Mn and both the g-value and linewidth were again in good agreement with theory. The value of the spin flip scattering cross-section for Cr obtained from the present work was in excellent agreement with the values obtained previously for Ti, Ni and Mn by indirect methods (5.50, 5.51).

CHAPTER 6

METALLURGY

A wide variety of solid solutions and compounds has been investigated in this work. In this chapter, a brief discussion of alloying theory is followed by a section dealing with some of the experimental techniques used in the preparation and analysis of the samples and, finally, each alloy system studied is discussed individually. Appendix 2 contains structural data on many of the systems.

6.1 General Alloying Theory

The approach to the alloying behaviour of metals is still rather empirical, but there are some general rules relating to the solid solubility of one element in another and the existence and structure of intermetallic compounds. These classical rules of alloying behaviour were first enunciated by Hume-Rothery (6.1) as follows:

(a) Size Factor

If a solute atom is substituted into the lattice of a solvent atom, and there is a wide disparity in atomic "size", a significant strain field is set up around the solute atom and at the limit second phase is precipitated. Hume-Rothery considered that a difference in atomic radii of greater than 15% severely restricts solubility, even when other factors are favourable.

Laves (6.2) examined the ease with which different types of atom may be stacked to form various structures when the radii of the atomic species are different. The Laves phases ($MgZn_2$, $MgCu_2$, and $MgNi_2$),

for example, occur for radius ratios between 1.1 and 1.4, the ideal theoretical ratio for close packing being 1.225. Dwight (6.3) showed that the major factor controlling the formation of rare-earth Laves phases and related structures is the ability of the partner elements to expand or contract so that the ideal ratio is approached. He further suggested that electronic factors are important in determining the stable structure in a given system.

(b) Electron Concentration

Hume-Rothery observed that in alloys of Cu, Ag and Au with elements such as Sn and Zn, certain structures existed with a fixed electron to atom ratio. These "magic" ratios correspond to the maximum number of electrons which can be contained in the first Brillioun zone without overlapping into the second zone. In the case of these "electron compounds", at the point of contact of the Fermi sphere with the zone boundary, a new structure becomes energetically more favourable. The Brillioun zone of this new structure can accomodate a larger Fermi surface. These ideas are discussed at some length in most metallurgical texts.

The extension of these ideas from simple monovalent metals to rare-earth and transition metal systems involves great difficulties. The ideas of Hume-Rothery have, however, been extended to other systems (6.3, 6.4, 6.5) including the Laves phases, and the general importance of the factor in more complex systems has been reviewed by Wernick (6.6).

(c) Electrochemical Factor

When the difference in electronegativity between two elements is large, a very stable compound is usually formed and this tendency to compound formation limits the extent of solid solution. Considerations of electronegativity are esentially qualitative, but an attempt to combine the size factor and electrochemical factor in the form of a Darken-Gurry

plot has led to some success in predicting the solubility of one element in another.

The factors described above operate to determine which of a variety of structures occur for a given alloy system, but their relative importance varies, and the fact that the difference in energy between various structural forms is often marginal, means that second order effects may determine the final equilibrium form. In the discussion of the alloy systems below, reference will be made where possible to the relative importance of these effects. It is usually most obvious when size effects are of greatest importance.

6.2 Purity of Materials

The purity and form of the elements used in this study are indicated below:

Pd	Johnson Mathey, Specpure powder
Gd	Koch-light 3N ingot
Mn	Koch-light 4N5 electrolytic flake (cleaned before use in dilute HNO_3)
Zn	Koch-light 5N rod
La	Koch-light 3N ingot
B	Koch-light 2N8 sponge
Tb	Koch-light 3N ingot
Ag	Koch-light 5N rod
Au	Johnson Mathey Specpure powder
Al	Johnson Mathey Specpure rod
Cu	Johnson Mathey Specpure rod
Pt	Johnson Mathey Specpure sponge and Engelhard 4N sponge
In	Koch-light 5N ingot
Sn	Koch-light 5N rod
Fe	Koch-light 4N8 wire

The purities are, in general, those stated by the manufacturers, although the Pd and Ag were analysed by emission spectroscopy in the Analytical Services Laboratory of Imperial College. The results show that impurity levels in both cases are well below 10 ppm.

6.3 Furnaces

An argon arc furnace was used for preparing some of the alloys. This type of furnace employs a water cooled hearth and tungsten electrode, and melting is performed, after flushing twice with clean argon gas, in two-thirds of an atmosphere of argon. A titanium getter is heated for a minute or two before each melt in order further to purify the atmosphere in the furnace. Generally, unless otherwise specified, nominal currents of about 80 amps are employed and the ingots held in the molten state for about thirty seconds before turning over and remelting a number of times. In some cases, the alloys were cast *in situ* into sticks (40mm x approx. 2mm in diameter) using a suction device described by Stone (6.7).

The furnaces used at temperatures below about 1200C are constructed from silicon carbide "Crusilite" elements and temperatures are held steady to about 2C by "Ether" and "Eurotherm" controllers, calibrated against a Pt - Pt 13 at. % Rh thermocouple.

6.4 Metallurgical Examination of Samples

A number of techniques were used to check the composition, homogeneity and structure of the samples.

(a) Metallographic Examination

Samples were set in mounting plastic and ground and polished on successive grades of emery paper until all surface scratches were removed. They were then etched and examined under magnifications of up to x400. This enabled amounts of second phase and grain size to be estimated.

(b) Hardness

Measurements were made using a Vickers microhardness tester. Several indentations across a specimen allow areas of second phase to be confirmed and homogeneity to be checked. With suitable standards a rough estimate of composition in dilute systems may sometimes be made.

(c) "Wet" Analysis

Quantitative chemical analysis was performed on Zn-Mn alloys by the Analytical Services Laboratory of Imperial College and on the Pt-Gd intermetallic compounds by Dr. I. R. Harris at the University of Birmingham.

(d) Electron Microprobe Analysis

In this form of analysis, an electron beam a few microns in diameter is moved across the surface of the sample; from the characteristic X-rays emitted, the elements present in the sample may be determined. From variations in intensity, homogeneity may be checked.

(e) X-ray Analysis

X-ray powder patterns of a number of the intermetallic compounds were obtained. By comparison with published data, the presence of specific phases of a given atomic structure could be checked.

6.5 The Intermetallic Compounds

(a) Ag-Gd

Steeb et al (6.8) found that there existed two silver rich phases in this system, corresponding to compositions Ag_3Gd and Ag_2Gd; the Ag_3Gd compound melts congruently at a temperature in the region of 900 to 940C.

Gschneider (6.9) confirmed the existence of these phases, but preferred a true stoichiometry of $Ag_{51}Gd_{14}$ for the dilute phase.

The "Ag_3Gd" sample investigated in this work was prepared by arc-melting the starting materials. A fairly large weight loss ($\sim$3%) was observed. The ingot was etched with a mixture of equal proportions of NH_4OH and H_2O_2 and the observed microstructure closely resembled fig. (c) and (d) in the paper of Gschneider et al, showing a two phase structure. The majority phase ($\sim$80%) was shown by electron probe analysis to be the required phase; the rest appeared to be a eutectic mixture.

Steeb et al originally suggested that the compound took up the Ag_3Pu structure type which has a hexagonal unit cell containing 64 atoms. Gschneider et al, however, believe that, whilst the structure is hexagonal, it is a new structure type which they call $Ag_{3.6}Gd$. McMasters et al (6.10) find a similar structure in the Au-Gd system. Full structural details are yet to be published.

(b) Al-Gd

An X-ray diffraction and thermoanalytical investigation of the rare-earth aluminium system was carried out by Buschow and Van Vucht (6.11). Their phase diagram (fig. 6.1) shows the presence of three intermetallic compounds on the Al-rich side: GdAl, $GdAl_2$ and $GdAl_3$.

Samples of $GdAl_2$ were prepared by melting the Gd and Al together in the arc-furnace. The resulting ingots were exceedingly brittle and shattered on re-melting, thus making the estimation of weight losses impossible. The compound melts congruently at 1500C and is the most stable phase in the system; it can thus be easily prepared as single phase. This was confirmed by electron probe and metallographic analysis. $GdAl_2$ has the cubic $MgCu_2$ Laves phase structure with space group Fd3m.

Attempts to make the other two compounds in the system were less successful. A number of GdAl ingots were arc melted and various heat treatments were given. The best specimen was obtained by annealing

the ingot for three days at 750C. Examination under the microscope revealed a white matrix (~70%) with darker areas. Electron probe analysis suggested that the white majority phase was indeed the monoaluminide but that the darker areas were Al rich and probably the dialuminide. Unfortunately, no useful data could be obtained from this sample since the esr signal from $GdAl_2$ is extremely strong. A few filings were in fact taken from the ingot (which was not very brittle) and mounted in the esr spectrometer; a room temperature sweep showed a slightly distorted $GdAl_2$ signal!

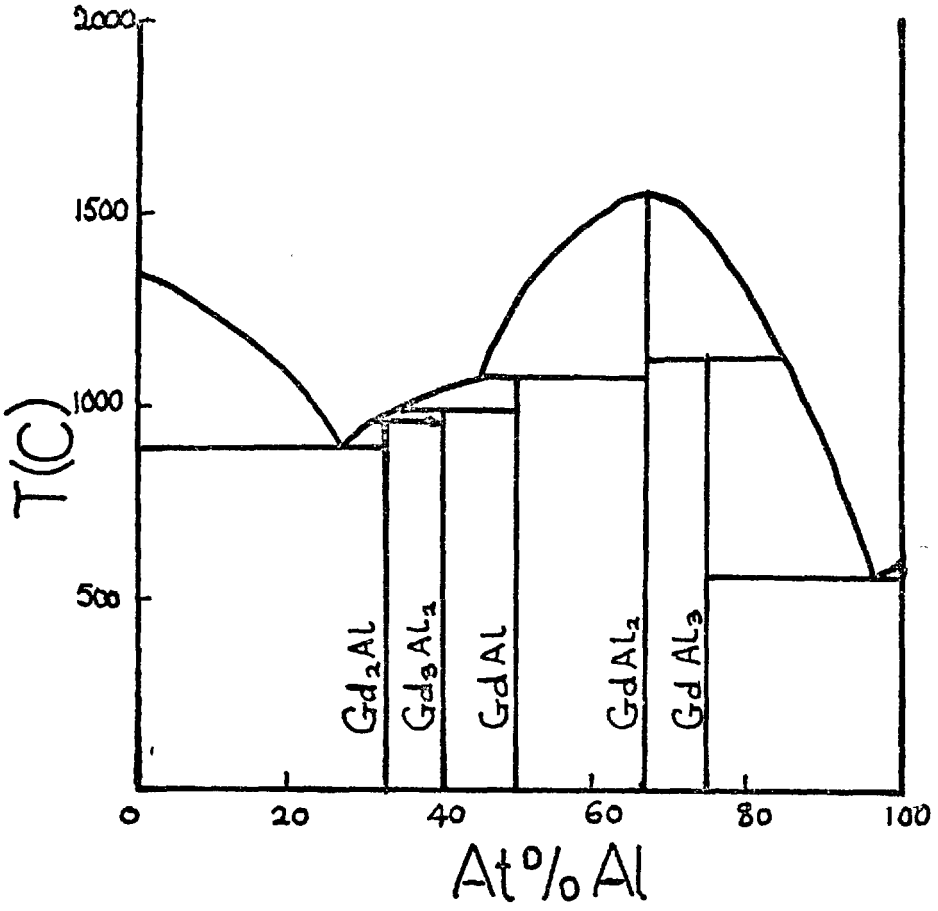
The monoaluminide has an orthorhombic lattice (6.12) and is classified as of the ErAl structure type (space group Pmma), the structure of which is not known. It may be transformed by suitable heat treatment to a metastable modification (GeAl type).

A number of attempts were also made to form the trialuminide, but this was not formed as majority phase. Visual and electron probe analysis of these samples showed a mixture of three phases: a majority of $GdAl_2$, perhaps 20 - 30% of $GdAl_3$ and what appeared to be pure Al.

Runnals and Boucher (6.13) claim the existence of a further Al rich phase at composition $GdAl_4$ which decomposes by a peritectoidal reaction at about 400C to form α-Al and $GdAl_3$. Buschow and Van Vucht (6.11) maintain, however, that the $(R.E)Al_4$ (they prefer $(R.E)_3Al_{11}$) phase only exists for La, Ce, Pr, Nd and Sm.

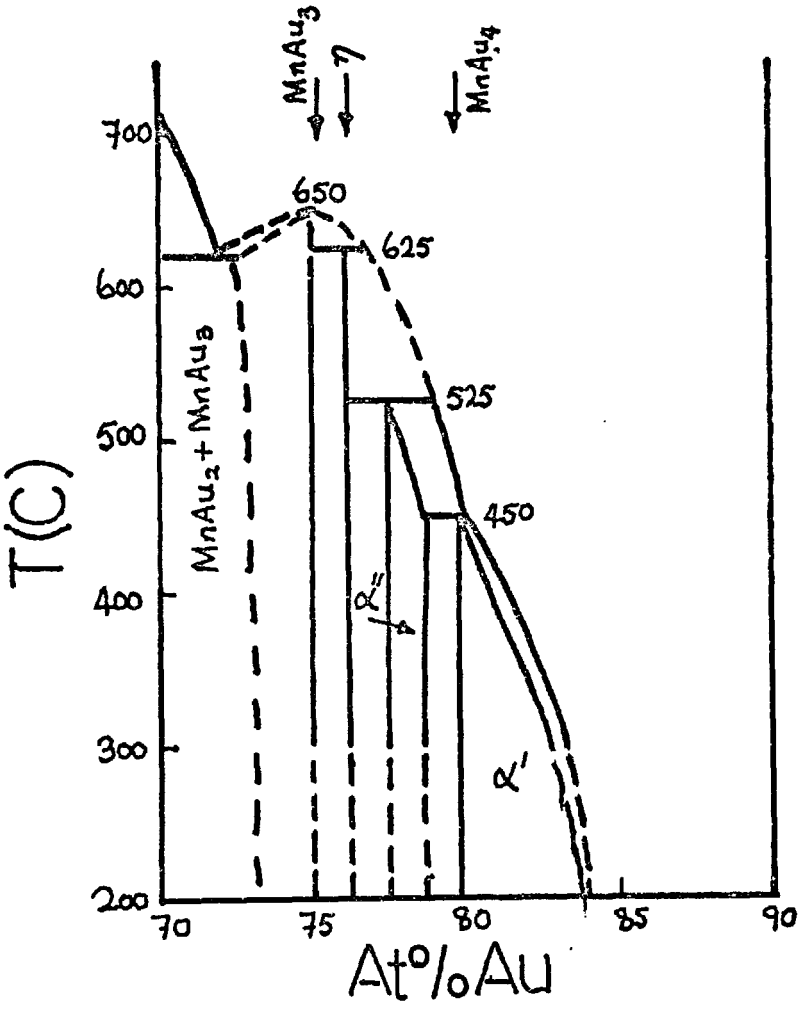
The structure of the $(R.E)Al_3$ compounds has a number of forms. Up to and including Gd, the hexagonal Ni_3Sn type structure is formed (6.13) with space group $P6_3/mmc$, but the heavier rare earths take up a variety of different structures (see Appendix 2). This wide variety of structural forms, on moving across the rare earth series, suggests that atomic size is of great importance in deciding the stability of structures in these systems.

FIG 6.1 THE GD-AL PHASE DIAGRAM



REF 6.11

FIG 6.2 THE MN-AU PHASE DIAGRAM



REF 6.14

(c) Au-Mn

The Au rich end of the Au-Mn phase diagram is shown in fig. (6.2) This is reproduced from "The Constitution of Binary Alloys" by Schunk (6.14). Between the stoichiometry Au_3Mn and the Au richest compound α'-Au_4Mn, there exist two intermediate phases and this has led to considerable confusion in the literature. The phase referred to by Watanabe (6.15) as Au_3Mn, for example, has since been shown to be the α''- phase which forms peritectoidally at about 21%Mn.

Morris et al (6.16, 6.17), in X-ray diffraction studies, distinguished three alloys at the composition Au_3Mn. They formed the disordered face centred cubic alloy by quenching rapidly from 700C, a metastable ordered structure produced by an anneal of a few minutes at 445C followed by quenching, which they labelled Au_3MnI, and a stable ordered structure formed after a long anneal at 445C, which they called Au_3MnII.

Because of the complexity of the system, a number of alloys were prepared in this work. The disordered phase was prepared by arc-melting the components (a small ($\sim$ 0.3%) weight loss being observed) and homogenising the ingot for five days at 850C, followed by a rapid quench. The resulting alloy was not brittle and hardness measurements further suggested that the solid solution had been retained. X-ray diffraction data was obtained on this sample and the lines observed corresponded to the data for the disordered structure given by Morris et al (6.17). Some very faint super-lattice lines were observed.

The ordered phase was formed by again arc-melting the elements and then annealing for three days at 550C. This sample was fairly brittle and much harder ($\sim$200 on the Vickers scale compared with $\sim$70 for the disordered structure). The X-ray diffraction data showed strong super-lattice lines. Comparison with the data of Morris et al (6.17) suggested

that a mixture of the Au_3MnI and Au_3MnII forms were present.

The stable Au_3MnII phase is a tetragonally distorted modification of the face-centred cubic (Au) structure, whilst the metastable Au_3MnI compound, which transforms at room temperature slowly back to the Au_3MnII structure, appears to be orthorhombic. Morris and Hughes were unable to distinguish between a 2 x 4 x 1 superlattice cell or a 1 x 1 x 10 cell for the stable compound.

(d) B - Gd, Tb, Er

All the rare earths form isostructural hexaborides and tetraborides. These interstitial compounds are metallic and highly refractory.

Some of the measurements made in this study were performed on samples prepared by Dr. Z. Fisk, but the majority of the work was performed on samples of GdB_4, GdB_6, TbB_4, TbB_6 and ErB_4 prepared in this laboratory.

All the borides were prepared by arc-melting. Tetraborides were prepared fairly easily by this technique and microscopic, X-ray and electron microprobe analysis on the as-cast ingots suggested that they were all better than 90% single phase. The light blue-greyish ingots were heavily faceted and hardness measurements were variable but gave values of about 2000 on the Vickers scale. No estimate of weight loss was made as the samples spluttered on re-melting.

The tetraborides appear to be the most stable of the rare earth borides and preparation of the hexaborides was more difficult. Initial attempts to prepare them by arc melting stoichiometric proportions of the rare earth metal and boron sponge in a pile on the arc-furnace hearth, using currents of up to 150A, in general proved unsuccessful. Finally, a procedure was adopted in which an excess of boron (20 - 30%) was used and the elements pressed into a pellet, using a hardened steel die.

The samples were then arc-melted about four times at increasing currents up to 170A, turning over after each melt. Some of the excess boron was lost on pressing and melting but Fisk (1.6) showed that using even quite large excesses (to composition $(R.E)B_9$) had no effect on magnetic data. Comparison of esr data obtained in this work on samples formed with different amounts of excess boron further supported this view.

Visual examination of the Gd and Tb hexaborides indicated three phases: a whitish phase normally present in very small quantities which microprobe analysis suggested was the diboride, the tetraboride and the shiny blue hexaboride. Samples of GdB_6 were prepared with 5 ÷ 10% second phase, whilst the best that could be done with the TbB_6 was about 10 - 15% second phase. Attempts to form ErB_6 as majority phase were unsuccessful. The hardness of the hexaborides lay in the range 3000 - 5000 on the Vickers scale.

The 3 gram samples of the Tb borides, used in the neutron diffraction experiments, were prepared from the separated isotope B^{11} obtained in sponge form from 20th Century Electronics and quoted as being 95% B^{11}.

The hexaboride structure can be conceived as a CsCl type structure with a rare earth atom replacing the Cs ion, and a B_6 octahedron in place of the chloride ion. The structure type is CaB_6 with space group Pm3m.

Longuet-Higgins and Roberts (6.18) considered, using molecular orbital theory, how many electrons were required to bond the octahedra of boron atoms to the rare earth. They showed that twenty electrons were required. The boron atoms can supply eighteen, so the rare earth must provide the remaining two. The remaining electron thus gives rise to the metallic properties of the hexaborides.

The tetraborides have a tetragonal ThB_4 structure (6.19) with sixteen atoms per unit cell and space group P4/mbm. The structure is rather complex, being essentially a combination of the CaB_6 structure and the AlB_2 structure, with a three dimensional network of boron atoms formed among the metal atoms. Lipscomb and Britton (6.20) suggest that, in the rare earth tetraborides, the same type of bonding scheme operates as in the hexaborides, and that the rare earth again contributes two electrons to stabilise the boron network.

(e) Cu-Gd

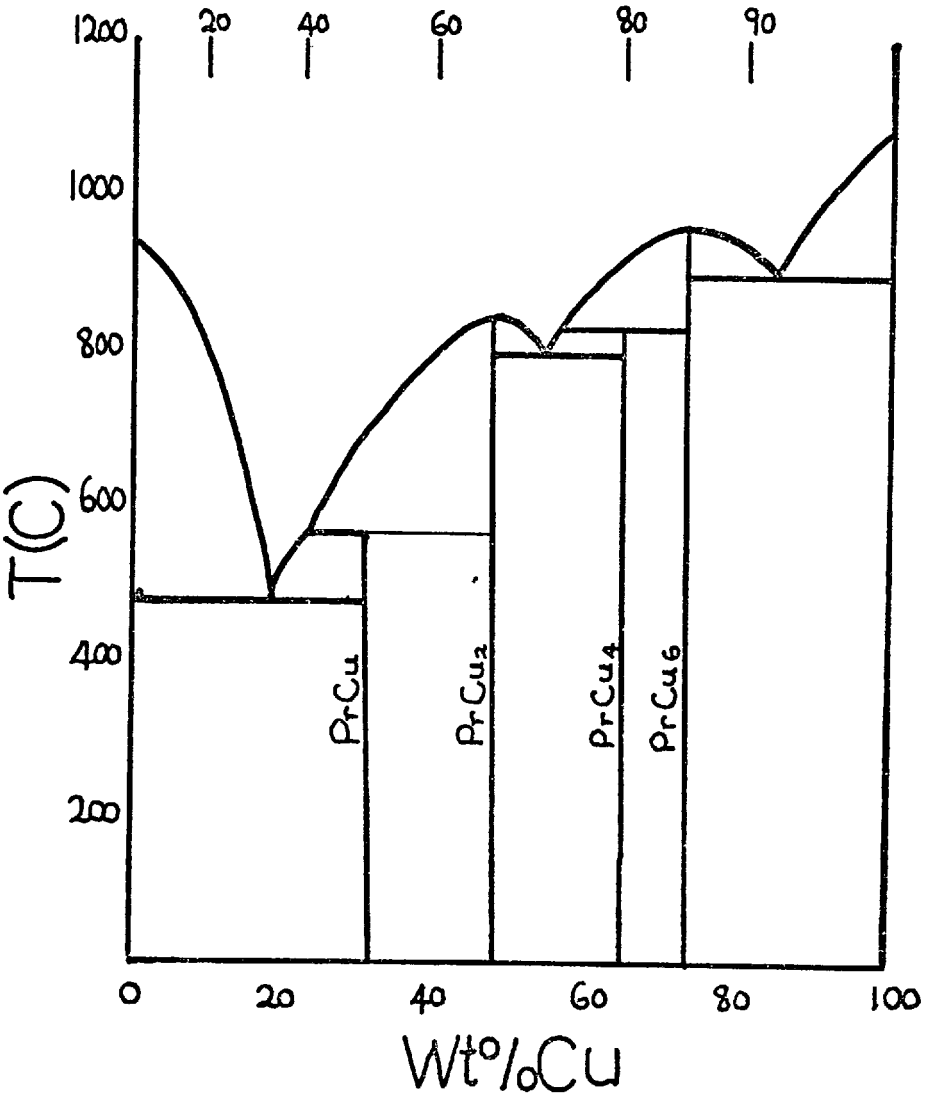
No phase diagram has yet appeared for the Cu-Gd system and there is some disagreement as to the existence of a number of phases reported in the literature.

The existence of the compound Cu_2Gd is well established and analogs exist for all the rare earth metals. It forms congruently from the melt at about 900C in the case of Gd. In this work, the compound was formed by arc-melting the components. The resulting alloy was exceedingly brittle, making the estimation of weight losses impossible. Metallographic examination showed the alloy to be almost entirely single phase.

This compound crystallises in the $CeCu_2$ type structure (6.21) which is orthorhombic with space group Imma. Each Ce atom has four nearest neighbours with a Ce-Ce distance greater than 3Å.

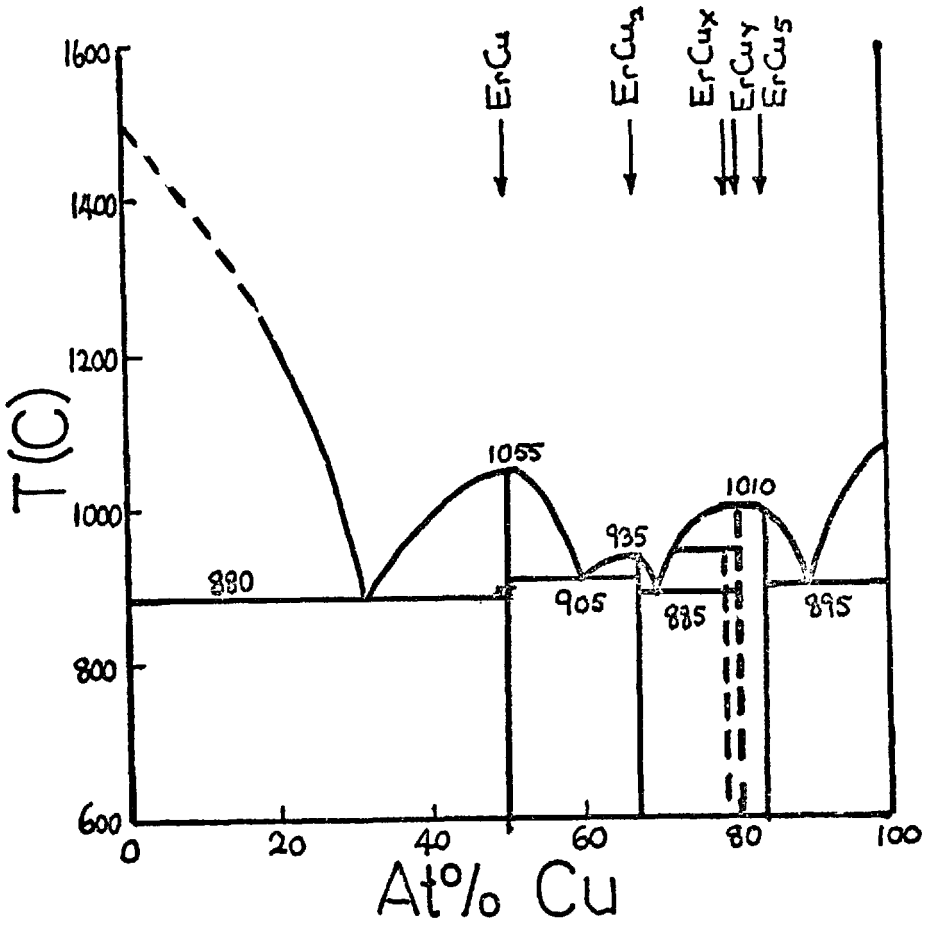
In the Pr-Cu (fig. (6.3)) (and La-Cu) system (6.22) there exist two further compounds: $PrCu_4$, which forms peritectically at 824C and $PrCu_6$, which melts congruently at 926C. Buschow (6.23) has investigated the Er-Cu system in some detail and his tentative phase diagram is shown in fig. (6.4). He finds three compounds beyond $ErCu_2$: $ErCu_5$, which forms peritectically at 1005C, and two unidentified compounds which he calls Cu_xEr and Cu_yEr, both existing at about 20 at.% Er. The Cu rich compound (Cu_yEr), he believes, is formed congruently from the melt at 1010C, whereas the Cu_xEr compound is formed peritectically at 940C.

FIG 6.3 THE PR-CU PHASE DIAGRAM



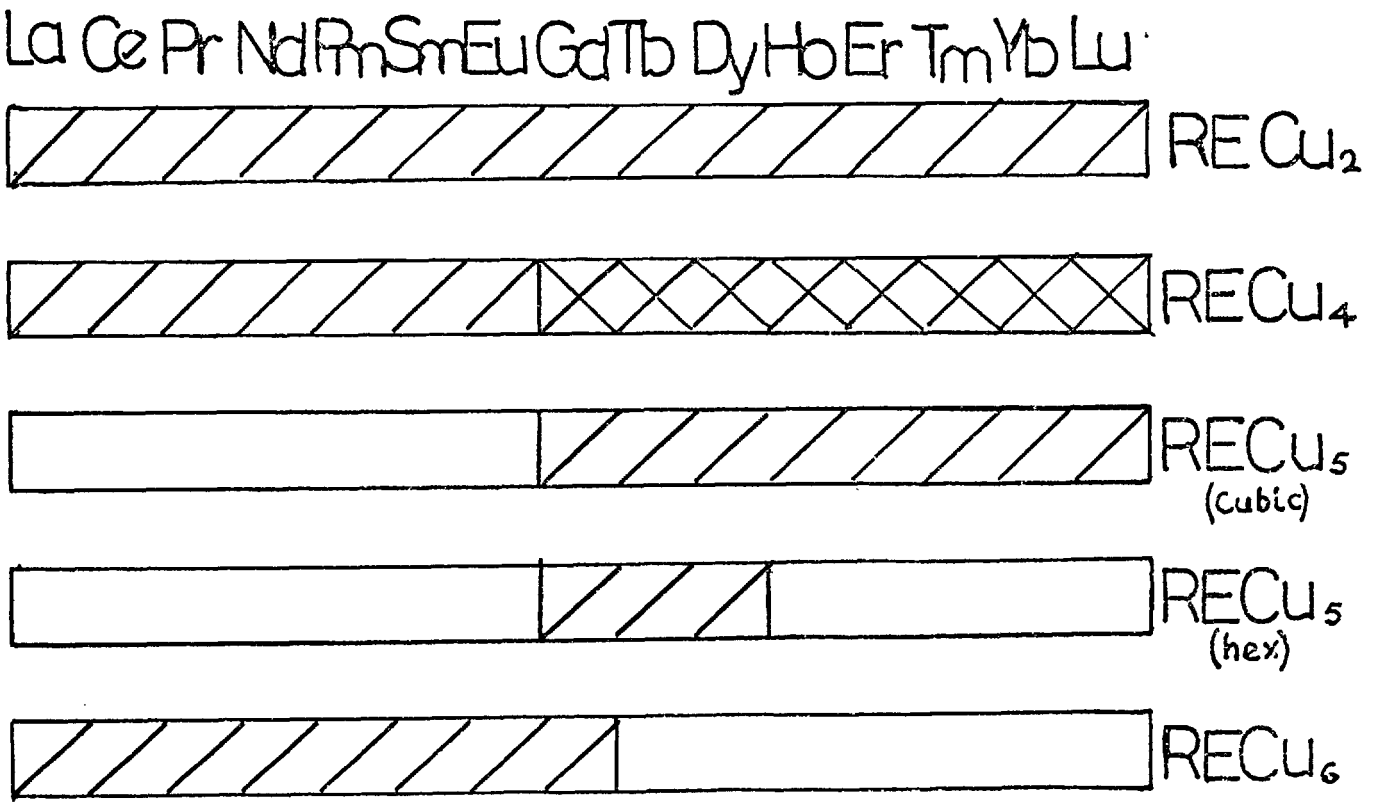
REF 6.22

FIG 6.4 THE ER-CU PHASE DIAGRAM



REF 6.23

FIG 6.5 EXISTENCE OF RE(CU) PHASES



He finds no evidence for the existence of a phase with composition Cu_6Er.

These striking differences between light rare-earth-Cu and heavy rare-earth-Cu phase diagrams suggest that size effects are probably a large factor in the determination of the structural forms in the rare-earth-Cu series. The position of Gd in the middle of the series means that it lies in the transition region for various structures.

Moriarty and Baenziger (6.24) identified a compound Cu_4Gd and suspected the presence of Cu_5Gd and Cu_6Gd. Buschow et al (6.25) found by X-ray diffraction the existence of two structure types for the (R.E)-Cu_5 alloys. For Tm, Er, Ho and Dy the compounds crystallise in the $AuBe_5$ structure type which is cubic with space group $F\bar{4}3m$, but for the compounds of Gd, Tb, Dy and Y the hexagonal $CaCu_5$ structure, space group P6/mmm, was observed in addition. Buschow and Van Der Goot (6.26) in a further paper, confirmed the existence of the (R.E)-Cu_6 phase for Pr, Nd, Sm and Gd and showed that it had the Orthorhombic $CeCu_6$ structure described by Croner et al (6.27). This structure has space group Pnma and is closely related to the $CaCu_5$ structure; there are no Ce-Ce nearest neighbours. Buschow found no such phase for Tb and Dy.

In this work attempts have been made to form compounds at compositions Cu_6Gd, Cu_5Gd and Cu_4Gd. The possible existence of the various rare-earth-Cu phases is summarised in fig. (6.5).

Sample (1): This was arc-melted at composition Cu_6Gd and the ingot homogenised at 750C in vacuo in an etched silica tube. The ingot was etched in dilute HF and both metallographic and electron probe analysis suggested the presence of two phases, the latter indicating a mixture of Cu_6Gd and Cu_5Gd ($\sim$70%) stoichiometries. An esr run on this sample confirmed this view, a mixture of two signals being observed below 77K with a single line at higher temperatures which did not correspond to the line obtained from a sample of fairly single phase Cu_6Gd (Sample (2)).

Sample (2): A Darken-Gurry plot suggests that the solubility of the rare earths in Cu is negligible and therefore an attempt was made to form the Cu_6Gd phase by arc-melting amounts of starting materials corresponding to a structure Cu_8Gd. This alloy (and subsequent alloys formed in this way) gave low ($\sim$0.5%) weight losses on melting and were quite brittle. Examination under the microscope suggested that the alloy was over 90% single phase and electron microprobe analysis confirmed that this phase was of approximate composition Cu_6Gd.

Sample (3): This sample was formed by arc-melting at composition Cu_4Gd. The ingot was annealed in vacuo in a silica tube for fourteen days at 700C. It appeared about 90% single phase on examination under the microscope, and, for three alloys prepared in this way, the electron microprobe analysis suggested a nominal concentration which would correspond to a compound with stoichiometry $Cu_{3.8}Gd$; it confirmed the existence of small inclusions of second phase. The sample was not very brittle.

X-ray analysis confirmed that Sample (2) had the $CeCu_6$ structure reported by Buschow. No structural details are available for the compound $GdCu_4$ and Sample (3) did not give a sharp X-ray powder pattern. It was also not possible to determine whether the predominant phase in Sample (1) was of the $AuBe_5$ or $CaCu_5$ structure type.

(f) In-Gd

The 'most probable' phase diagram for Ce-In and Pr-In is given in Hansen (6.28) and this shows that the compounds most dilute in rare-earth form congruently at composition (R.E)-In_3. This is confirmed for Gd by Moriarty and Baenziger (6.24).

The compound was prepared by arc-melting the constituents. A weight loss of about 2% was obtained for both the compounds produced.

Examination under the microscope revealed fairly large grains of intermetallic compound with a little second phase deposited in the grain boundaries. Both the alloys prepared in this way were rather less brittle than the majority of intermetallic compounds and one of the alloys was stress annealed for two hours at 250C in an etched pyrex tube in vacuo, after crushing.

The compound has been shown (6.29) to crystallise in the cubic Cu_3Au type structure, space group Pm3m.

(g) Pd-Eu

Measurements were made on two compounds in the Pd-Eu system: PdEu and Pd_2Eu. Harris and Longworth (3.26) have shown that the Eu is in a divalent state in both these compounds. The alloys were supplied by Dr. I. R. Harris of the University of Birmingham who prepared them by arc-melting. Chemical analysis and metallographic examination showed the two alloys of the appropriate compositions, although susceptibility measurements on the Pd-Eu phase have indicated the presence of some second phase (G. Longworth, private communication).

X-ray diffraction data of Harris shows that Pd_2Eu takes up the $MgCu_2$ structure Laves phase. The structure of PdEu is, however, not known.

(h) Pd-Gd, Er, Yb

These alloys were again prepared by Dr. I. R. Harris. The measurements in this work were made on the materials prepared for the magnetic measurements of Gardner et al (3.23).

The three compounds measured, Pd_3Gd, Pd_3Yb, and Pd_3Er, were all prepared by arc-melting the elements and homogenising them at 900C for one week. The compounds are shown to form congruently at temperatures

in excess of 1400C from an approximate form of the (R.E)-Pd phase diagram given by Gardner et al. The Pd_3Gd and Pd_3Er were extremely brittle and appeared single phase under the microscope.

The Pd_3Yb sample, however, was not brittle (no magnetic measurements were published for this sample). Further attempts were made to form this compound as single phase in this laboratory, but without success. On early attempts it was found that large arc furnace currents (>120A) were required to fuse the elements and that they then tended to separate again on further melting. The large currents were leading to considerable volatalisation of the Yb metal and therefore a number of melts were made with compositions up to 35 at.% Yb to try to allow for loss. None of the alloys was brittle and they showed a Vickers hardness nearer the value expected for a solid solution. Electron probe analysis showed a wide variation of concentration (as much as 10 - 15%) across the sample and averagely low levels of Yb for each of the two samples analysed by this method. Examination under the microscope failed to reveal any features, although a variety of etching reagents were tried.

Harris and Raynor (6.30) showed that all the $Pd_3(R.E)$ compounds crystallise in the $AuCu_3$ structure.

(i) Pt-Gd

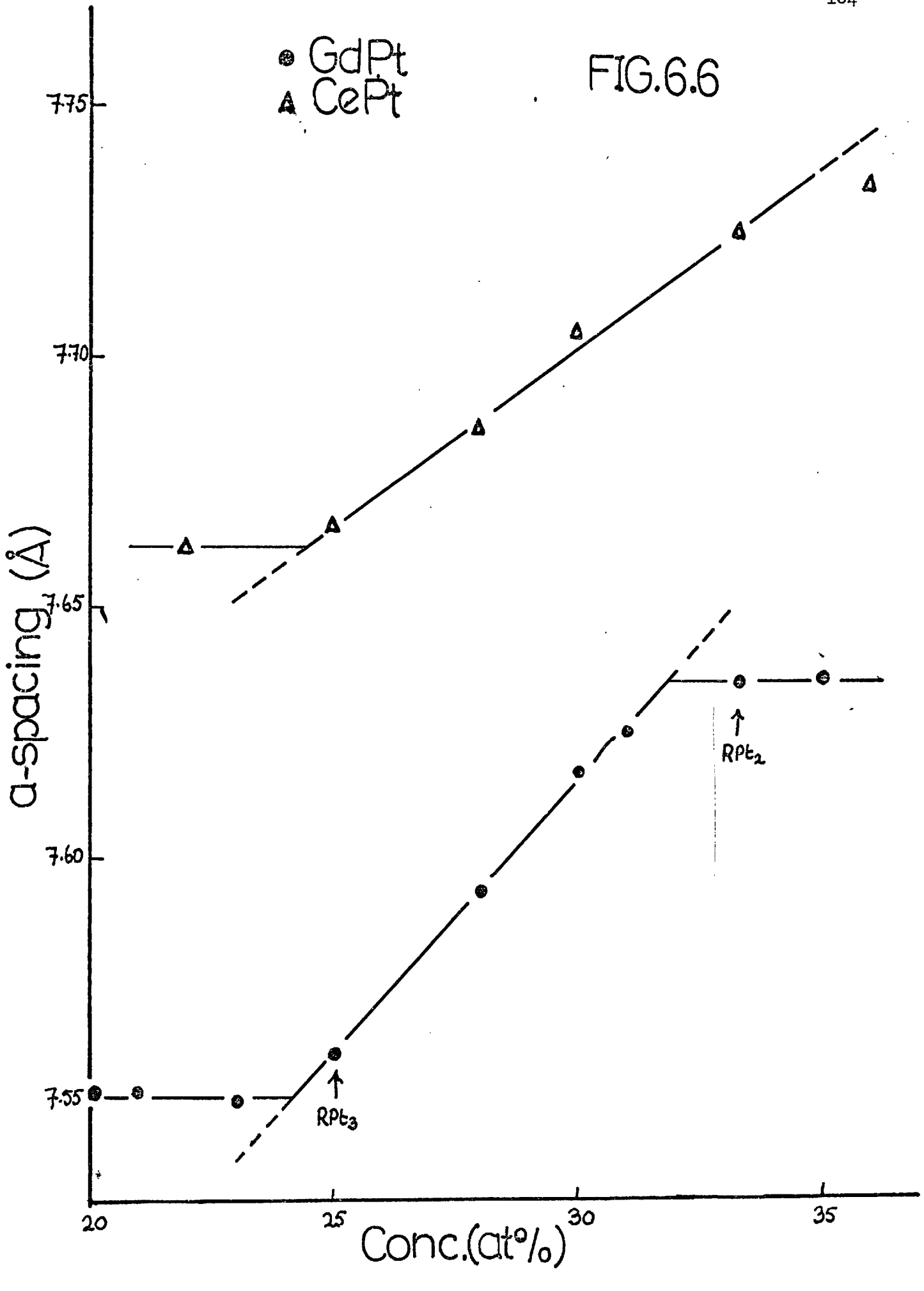
ESR measurements were made on the intermetallic compound Pt_2Gd, which was formed by arc-melting the starting materials, the Pt sponge being first melted into a small button. Weight losses were not measurable due to the extreme brittleness of the compound. Visual and electron probe analysis showed the alloys melted at this composition to be single phase. Attempts were also made to prepare the compound $GdPt_3$, the existence of which was reported by Moriarty and Baenziger (6.24).

The compound produced at this composition also appeared to be single phase and was again very brittle. X-ray diffraction measurements were made by Dr. I. R. Harris on both compounds and he found that the so-called Pt_3Gd was, in fact, the same phase as the Pt_2Gd, both giving sharp X-ray lines corresponding to the $MgCu_2$ Laves phase structure but with a difference in lattice parameter $\sim$1.6%. The value of the lattice parameter for the 'true' Pt_2Gd compound agreed well with previous work (6.24).

Harris (6.31) reported similar behaviour in a number of light rare-earth-Pt compounds and investigated the variation of a-spacing with concentration in the Pt-Ce alloys. A similar analysis has been carried out in the case of Pt-Gd for concentrations from 20% Gd (Pt_4Gd) to 35% Gd ($Pt_{1.85}Gd$) and the results are shown in fig. (6.6) along with the results for the Ce compounds. The values of the a-spacing obtained at 296K in the "arc-melted" condition are shown below:

Atomic % Gd	a-spacing ($\pm$ 0.0005Å)	Previous Work
35.0	7.6359	
33.3 ($GdPt_2$)	7.6348	7.6349 (6.24)
31.0	7.6245	
30.0	7.6166	
28.0	7.5928	
25.0 ($GdPt_3$)	7.5597	7.577 (6.31)
23.0	7.5498	
21.0	7.5525	
20.1	7.5524	

It can be seen that there is a significantly steeper variation of a-spacing with composition in the case of the Gd-Pt alloys and the alloy at stoichiometric composition $GdPt_2$ appears, rather surprisingly,


GdPt
CePt
FIG.6.6
7·75
7·70
7·65
7·60
7·55
a-spacing (Å)
RPt2
RPt3
20
25
30
35
Conc.(at%)

to lie within the two phase region. It appears that the limits of the Laves phase are at 24.2 and 31.8%Gd, compared with 24.3 and 34.5% Ce for the Ce-Pt alloys. Harris has found that rare-earths heavier than Gd have a Cu_3Au structure in the arc-melted condition.

It is surprising that the Laves phase for the $(R.E)Pt_2$ alloys should exist over such a wide range of composition since, in other systems such as the $(R.E)Al_2$ alloys, the Laves phase exists over a very limited range of compositions. It would appear that, in the system investigated here, the smaller Pt atoms are occupying rare-earth sites; this would explain the reduction in a-value as the alloys become Pt rich. This suggestion might be confirmed by measurements of absolute density and these are now proceeding.

(j) Zn-Gd, Er

Measurements were made on three dilute Zn-Gd intermetallic compounds: $Zn_{12}Gd$, $Zn_{12}Er$ and $Zn_{17}Gd_2$. These alloys were prepared by Stewart (2.4) and a detailed discussion of the Zn-Gd system is given by him.

The compounds richest in Zn are formed peritectically at about 750C from the Zn rich melt and the $(R.E)_2Zn_{17}$ compounds. Stewart prepared these alloys by heating the elements in vacuo in pyrex for three weeks at 500C. Extensive analysis showed the $Zn_{12}Gd$ and $Zn_{12}Er$ compounds to be almost entirely single phase.

The $(R.E)Zn_{12}$ compounds have a body-centred tetragonal $ThMn_{12}$ lattice, space group I 4/mmm. Each rare-earth atom is surrounded by four Zn atoms at 3.1Å and eight Zn atoms at 3.2Å, with a further eight at 3.4Å. The rare-earth ions are never nearest neighbours and the distance between any pair is not less than 5Å.

The $(R.E)_2Zn_{17}$ compounds exist in two structural forms: the rhombohedral Th_2Zn_{17} type structure, when formed from the melt, and the Th_2Ni_{17} structure, when formed by prolonged heating between 420 and 600C.

Stewart prepared the Th_2Zn_{17} compounds which form congruently from the melt by heating the pure metals in an evacuated silica tube for ten hours at 1070C and quenching in air. The Gd_2Zn_{17} sample was again almost entirely single phase.

The Th_2Zn_{17} structure has space group $R\bar{3}m$. No magnetic atoms are nearest neighbours and they are again separated by at least 5Å.

Size effects (6.32) seem to be the primary consideration in the form of structure exhibited by these compounds.

(k) Zn-Mn

Measurements were made on a number of Zn-Mn intermetallic compounds which were prepared by Dr. J. B. Dunlop. A detailed discussion of the system and the preparation of the alloys is given by him (2.7).

The compounds richest in Zn (ζ-phase) have a composition MZn_{13}, where M is Mn, Fe and Co. These are formed peritectically. Dunlop prepared the compounds by dissolving the transition metal at a temperature 50C above the relevant liquidus and quenching in cold water. The alloys were then annealed at temperatures below the peritectic for three or four weeks and slowly cooled. The $FeZn_{13}$ alloy was held at 500C and the $Zn_{13}Mn$ alloy was annealed at 420C. Examination under the microscope showed the Fe and Co compounds to be fine grained and single phase, whilst the $Zn_{13}Mn$ compound showed up to 5% second phase, which microprobe analysis showed to be solid solution. X-ray analysis was used to confirm that the structures were ζ-phase.

The compounds have a monoclinic structure with space group C2/m. This structure may be visualised as a transition metal atom surrounded by twelve Zn atoms at the vertices of a slightly distorted icosahedron, and these are linked together to form chains parallel to the c-axis, which are packed in a hexagonal array with extra Zn atoms between the chains.

The transition metal atoms are never nearest neighbours and are separated by a minimum of 5Å.

Runs were carried out on Dunlop's samples (135) and (1334).

The δ-phase was also formed in the Zn-Mn system. This is more concentrated than the ζ phase compound and has a composition equivalent to $Zn_{10}Mn$. The specimen was prepared in the same way as the ζ-phase compound, the final anneal again being carried out at 420C. Microscopic examination showed the alloy to be almost single phase.

The structure is exceedingly complex with a hexagonal unit cell containing about 550 atoms.

A run was also carried out on an alloy of composition $Mn_{0.05}Fe_{0.95}Zn_{13}$, where 5% of the Fe atoms have been replaced at random by Mn atoms. The alloy was prepared in exactly the same way as the $Zn_{13}Fe$ compound. Examination under the microscope showed this alloy to be single phase.

(1) Pd_2MnSn

This ternary Heusler alloy was made by arc-melting the elements in stoichiometric proportions. There was a 2.5% weight loss for the first alloy prepared in this way and examination in the as-cast state showed the alloy to be a 50% mixture of two phases. Following the procedure of Webster and Tebble (3.37), the ingot was annealed for twenty-four hours at 800C and then quenched. Metallographic examination showed roughly the same proportion of the two phases but with a coarser structure.

A second alloy was arc-melted and this time, using a low value of arc current (nominally 70 amps), the losses were less than 0.5%. Examination of this ingot, both under the microscope and by electron probe analysis, showed that it was about 95% single phase with a few specks of second phase.

X-ray and neutron diffraction analysis of Pd_2MnX (X = Sn, In, Sb) Heusler alloys show that the structure of the In compound is very sensitive to heat treatment. The Sn alloy is well ordered with only a slight amount of random disorder, irrespective of heat treatment.

The structure is best described in terms of four interpenetrating fcc sublattices. There are no nearest neighbour Mn atoms, which are separated by ~ 6.4Å.

6.6 Dilute Solid Solutions

(a) Pd-Gd and Pd-Ni-Gd

Solid solutions were prepared by arc-melting. Samples with concentrations from 0.02% to 7% Gd were prepared in this way with no second phase visible. Harris (6.33) estimated that the solubility limit of α Pd-Gd solid solution was 11.3% at 900C. This seems large, since the ratio of the atomic radii is $\sim 30\%$. Harris suggests that this enhanced solubility can be attributed to the expansion of the Pd lattice by filling of the 4d states by the solute valency electrons. This would suggest a much more open lattice than that expected from a simple substitutional solid solution.

Losses on melting were in general very small ($\sim 0.1\%$) but electron probe analysis suggested that, especially in alloys containing less than 0.5 at.% Gd, compositions were considerably less than nominal and that, even after re-melting five or six times, there existed considerable heterogeneity. This latter result is in disagreement with the work of Cottet (5.30) who did not apparently homogenise his alloys.

For concentrations of less than 4 at.% a master alloy was prepared and diluted with excess Pd. The alloys were then homogenised in a vacuum of 10^{-5} torr in a clean silica tube for periods in excess of two days. Analysis showed that the alloys prepared in this way were fairly homogenous. Before filing, the alloys were cleaned in aqua regia to

which had been added a few drops of H_2O_2. They were then filed and stress annealed at 300C for 2 - 3 hours (although subsequent runs showed that, at least for alloys with concentrations less than 0.5% Gd, this anneal had no effect on the esr linewidth).

Satisfactory results were obtained on alloys of 4 at.% and 0.25 at.% but in experiments on a 0.02% sample the 'true' signal was superimposed on a broad background signal. Careful analysis of the 0.25 at.% trace showed some signs of this background but at very low levels compared to the 'true' signal. Cottet observed no such effect in his work on similar concentrations and it was concluded that the effect must be due to contamination.

No significant levels of impurity were found in the Pd powder; runs were also performed on specimens which had not been stress annealed and these showed comparable levels of contamination. It was finally found that when samples were homogenised in Alumina crucibles instead of silica tubes, no background 'signal' was observed. This suggests that the effects observed were due to the reaction of the silica glass with the Gd in the sample, giving what in the light of subsequent experience appeared to be a ferromagnetic resonance. A number of Gd-Si intermetallic compounds are ferromagnets with high Curie temperatures.

The Pd-Ni-Gd alloy was formed by arc-melting Ni into the 0.4 at.% ingot of Pd-Gd and homogenising again at 1200C in an Alumina crucible prior to filing and stress annealing.

(b) Pd-Mn

Alloys of 0.4, 0.9, 2.3, 2.5, 3.7, 4.5, 6.0, 7.0, 8.6, 12 and 20 at.% Mn in Pd were prepared by arc-melting. Only very small (typically $\sim 0.2\%$) weight losses were experienced.

The ingots were then homogenised at about 800C for 3 - 4 days and quenched. This temperature is somewhat less than might be expected from consideration of the Pd-Mn phase diagram (6.28), which would suggest

higher temperatures ~ 1200 - 1300C. The lower temperature is chosen to maintain a balance between adequate homogenisation and the avoidance of Mn loss from the surface of the ingot, which may occur at high temperatures, leading to a Mn depleted surface layer.

After quenching, ingots were etched in aqua regia and the surface layer filed off with a clean file kept only for this purpose.

Metallographic examination of the samples showed that all but the most concentrated alloy were single phase. The phase diagram suggests that the solubility of Mn in Pd at 1000C is ~28%. Electron probe analysis confirmed the nominal concentrations and showed good homogeneity.

After filing, the alloys were stress annealed for three hours at 350C.

(c) Zn-Mn

A number of experiments were performed on dilute alloys of Mn in Zn. Phase diagrams (6.28) indicate that the maximum solubility of Mn in Zn is ~0.4 at.%.

Sample (1): This sample was a nominal 0.4 at.% Mn in Zn and was obtained from Dr. A. D. Caplin. The ingot was etched in dil. HNO_3, filed and stress annealed at 150C for two hours.

Sample (2): This sample was prepared by sealing the elements in an etched pyrex tube and holding it at 510C for one hour, shaking regularly. The sample was quenched and re-sealed prior to homogenisation for two days at 400C (falling to 330C) and again quenched. Hardness measurements showed a Vickers hardness of 550 , compared to 35 for pure Zn. Metallographic examinations showed no sign of second phase.

Samples (3a) and (3b): These samples were nominally 0.4 at.% Mn and were obtained from Dr. C. Rizzuto of the University of Genoa. The alloy was homogenised for two days at 400C in an etched pyrex tube in vacuo. After filing, Sample (3a) was stress annealed for two hours at 180C. Sample(3b) was not stress annealed. Hardness measurements again gave a

value ~50 and measurements of the resistance ratio gave $R273/R_{4.2}$~2.3, which is close to the value expected for the nominal concentration.

Samples (4a) and (4b): A nominal Zn0.1 at.% Mn alloy was also obtained from Dr. C. Rizzuto. They were heat treated in exactly the same way as Samples (3a) and (3b).

(d) Rh-Mn

Alloys of 5 and 10 at.% Mn in Rh were obtained in powder form from Dr. A. P. Murani.

CHAPTER 7

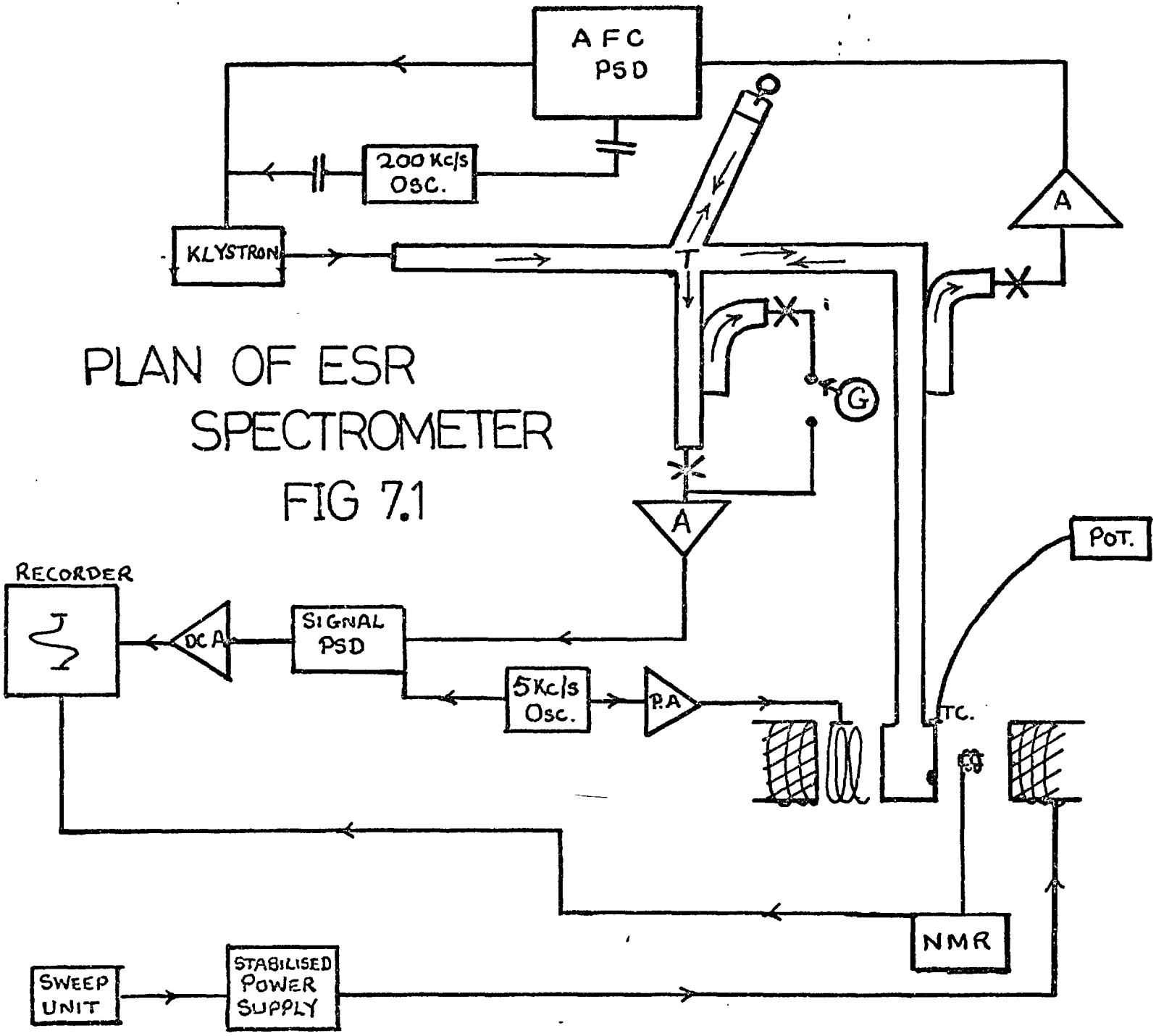
APPARATUS AND EXPERIMENTAL METHOD

7.1 The ESR Spectrometer

The spectrometer was built by Dr. D. Griffiths and is a conventional homodyne X-band reflection spectrometer. A plan of the apparatus is shown in fig. (7.1).

Microwave power is supplied by an R9689 EMI-Varian tunable klystron. This operates at 8950 Mc/s and supplies about 25mW of microwave power. This is fed through an isolator and wavemeter to a hybrid Tee, where the incident power is split equally between the balance arm and the cavity arm. The cavity arm waveguide is coupled by a circular fixed iris to the microwave cavity which is positioned between the poles of the electromagnet. The amplitude and phase of the microwaves in the balance arm may be adjusted by means of an attenuator and variable short circuit. This "bucking" signal and the reflected power from the cavity re-combine in the hybrid Tee and pass to an AEI type CS10B receiver crystal via a directional coupler. Another detector crystal and a variable screw probe in this arm enable the power reflected from the crystal to be minimised.

The output from the detector is fed through a matching transformer into a low-noise head amplifier and then through a cascade of wide band amplifiers. The signal is finally passed through a tuned 5.1 Kc/s amplifier and a phase sensitive detector. The amplifier chain yields a maximum final gain $\sim 10^7$. The output is traced on a Honeywell x-t pen recorder with a chart speed of 0.085 cm/sec.



PLAN OF ESR SPECTROMETER

FIG 7.1

FIG 7.2 Ag0·2Gd

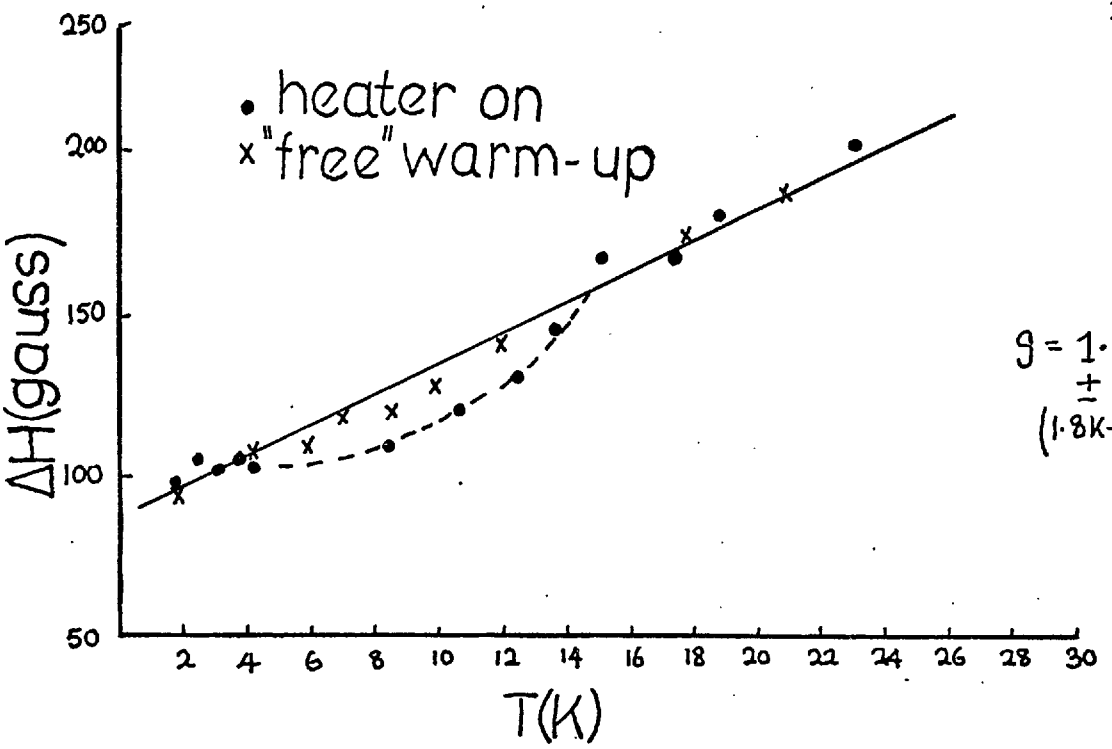
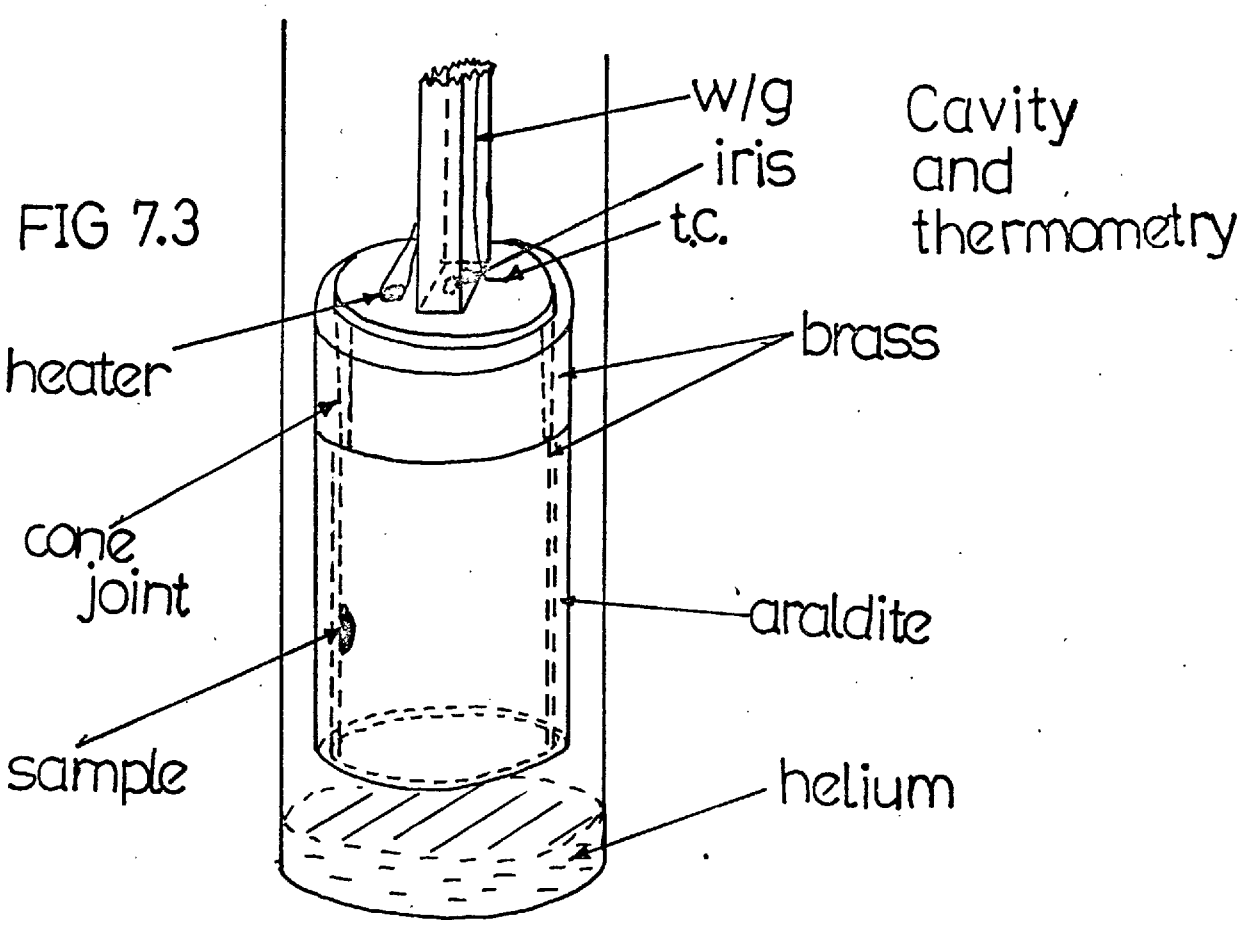


FIG 7.3



The klystron frequency is locked to the cavity frequency by an automatic frequency control (AFC) loop. A little of the reflected signal is coupled into the AFC loop and detected by an AEI type CSB4 diode; this signal is amplified and passed through a phase sensitive detector and DC amplifier feeding back to the klystron reflector, which is modulated by a 200 Kc/s oscillator.

A magnetic field of up to about 8KGauss, with a pole gap of 6½cm, is achieved with a Newport type D electromagnet, operating from a 2kw Wareham magnet power supply (type C298). The field is homogenous over a wide area; a 3KGauss field (corresponding to $g = 2$) at the centre of the pole-faces decreases by only 2 Gauss at a distance of 7cm from the centre of the pole-faces. The field is swept by a unit which sweeps from zero to full field in settings of ½-minute to 16 minutes. On the settings used in a typical esr sweep, the unit is linear in both directions of the sweep to 1%.

The field is modulated at 5.1 Kc/s by a pair of Helmholtz coils driven by a Quad II power amplifier. Variable settings of the modulation amplitude are available with a maximum of 15 Gauss. Since this amplitude is small compared with a typical linewidth, the pen recorder traces the derivative curve.

7.2 Thermometry

Temperatures below 4.2K were generally measured by recording the helium vapour pressure with a mercury manometer. Below about 2K, oil pressure readings were taken. An Allen-Bradley 50Ω carbon resistor was also used on occasions in this temperature range and was calibrated against the manometer readings.

Temperatures from 4.2K to room temperature were measured using a Au 0.03% Fe-Chromel thermocouple (annealed) referenced to room temperature. Below 77K the calibration curve of Rosenbaum (7.1) was employed, whilst about 77K the data of Berman (7.2) was used.

During the course of the work on the Pd-Mn system (see Ch. 8), a discrepancy between the measured temperature and the actual temperature of the sample was suspected between 4K and about 12K. Since this temperature regime is of particular interest in the work on the Pd-Mn and Pd-Gd dilute alloy systems, it was decided to investigate the effect carefully.

A number of measurements (5.36) have shown that for a dilute system of Gd in Ag, the linewidth is linear with temperature and, for a 0.2 at.% sample, should have a slope of 4 Gauss K^{-1}. The linewidth behaviour of this system is thus useful for checking thermometry in this temperature range.

A small ingot of nominal Ag 0.2 at.% Gd was prepared by arc-melting the constituents and annealing the ingot for five days at 670C in a clean silica tube. Microprobe analysis confirmed the nominal concentration and microscopic examination showed the ingot to be over 90% single phase.

Two runs were performed on this sample and the results are shown in fig. (7.2). In the first case the heater used to boil off the liquid helium was left running at a low setting during the warm up and, in the second experiment, a 'free' warm up took place. It is noticeable that, in the first case, there is a pronounced deviation from straight line behaviour, suggesting that a nominal temperature of 7K corresponds in fact to a temperature of nearer 5K. In the second case, the discrepancy appears to be about half this value.

The effect may be understood by reference to fig. (7.3). When the helium level is above the cone joint, the sample and thermocouple are at the same temperature; however, as the level of the helium drops to the bottom of the cavity and the warm up begins, there exists a temperature gradient up the cavity, causing the thermocouple to register a higher temperature than the actual temperature of the sample. Extra local heating from the heater used to boil off the helium accentuates the effect. A further run on this specimen was made with the heater hanging below the cavity in the helium. In this way, cold helium gas could be boiled off in short bursts to even out the thermal gradient. This appeared to give a slight improvement, but there remains an uncertainty of as much as -1K on points in this temperature regime. In practice, the warm-up points from 4K to about 15K have been obtained without the use of the heater.

7.3 Measurement of Magnetic Field

Lowin (5.24) monitored the magnetic field during a sweep by measuring the potential across a standard resistor in series with the magnet, and periodically calibrated the field in terms of current, using an nmr apparatus.

During the present experiments the magnetic field is measured using a Bell 620 Gaussmeter, with Hall probe mounted close to the dewars. The field was monitored on a Solartron LM1420.2 digital Voltmeter. Field calibration marks were obtained using a chart marking facility designed and built by D. Griffiths (7.3). This device closes a relay circuit within a millisecond or so of the start of the first counter display period, which contains an initiating digit, and causes the pen recorder to "blip".

These reference points are then calibrated in terms of the magnetic field, using proton resonance in rubber. The nmr frequency is adjusted to beat with one of a series of standard crystal oscillators and, when beats are achieved, the magnetic field is swept until the proton resonance is observed on an oscilloscope. This process is repeated three or four times in each run and on each occasion five crystal oscillators are used.

Comparison of the proton nmr unit with a commercial instrument, using a Lithium resonance, gave agreement at 3KGauss to within 1 Gauss. The zero stability and full scale deflection calibrations of the Gaussmeter and voltmeter do not drift by more than one part in a thousand during a run and, allowing for the manufacturer's specification for the probe itself, the present system should measure a field of 3KGauss to within about 8 Gauss.

7.4 The Resonant Cavity

The original cavity built for the spectrometer consisted of a rectangular TE_{102} mode cavity made of thinned brass waveguide, cast in araldite for thermal mass. Samples were inserted in a side tube and could be changed at low temperatures through an air-lock device. This enabled runs to be performed on a number of samples without returning to room temperature, but had the great disadvantage that impurities tended to build up in the cavity giving a background signal.

Lowin (5.24) discussed in detail the factors influencing the choice and design of cavities. He concluded that the most suitable for use with the present system was a cylindrical TE_{112} mode cavity.

The first such cavity built for this rig was fabricated by Dr. L. L. Hirst. It was formed by electroplating gold on an aluminium mandril and casting this in araldite, before dissolving away the aluminium with sodium hydroxide. This produced a cavity fairly free from extraneous signals and a high unloaded quality factor, Q ($\sim$ 7000), but it was found that on thermal cycling the araldite tended to crack.

The cavity used at present was constructed by Lowin. Naval brass (which is relatively free from both magnetic and superconducting impurities) was machined to give walls 8 thou thick. This was etched and cast in araldite. It gave an unloaded Q $\sim$6000 and withstood repeated thermal cycling. A number of checks were made during the course of the present work (apart from negative results) to ensure that no appreciable level of extraneous impurity had built up to produce background signals. Runs were performed on filed, arc-melted Ag-Au alloys and at no time was a significant background signal observed at any temperature.

There is another type of signal which is not due to the sample and this arises from the currents induced in the walls of the cavity by the modulation. These currents interact with the static DC field and thus cause mechanical vibrations of the cavity walls. This "Wall-breathing" signal, as it is called, being at the modulation frequency, is within the band-pass of the narrow band amplifier and phase sensitive detector and yields a signal whose amplitude increases monotonically with field, thus causing a continuous shift in baseline.

Fig. (7.4) shows how a dispersion signal may be mixed with an absorption signal and how the spectrometer responds to fluctuations in frequency which are faster than the response time of the AFC.

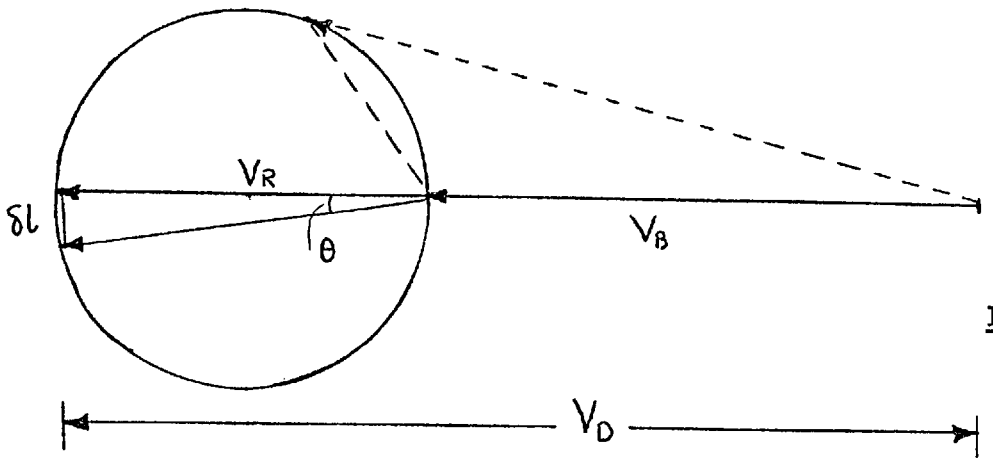


Fig. 7.4

V_B represents the bucking signal from the klystron and V_R the signal reflected from the cavity. V_D is the resultant reaching the detector. The absorptive part of the signal causes the vector V_R to move radially, whilst the dispersive component causes V_R to move round the circumference of the circle that V_R describes as the frequency is varied. To set the spectrometer such that the absorptive part of the signal only is observed, V_D is made perpendicular to the circumference (i.e., $\theta = 0$). In this configuration the variation of V_R due to an absorption signal has a first order effect on the length of V_D, whilst a small dispersion signal only has an effect to second order. If the dispersion signal were required, V_D would be set tangential to the circle (dotted).

If a frequency drift occurs during the course of an experiment, the tip of V_D moves round the circle, θ increases, and the dispersion signal is no longer fully suppressed. From Fig. (7.4) it may be seen that fluctuations in frequency modulate V_D with full force, in the case of the dispersion signal, but have no effect to first order on the absorption signal. We thus see that a small frequency drift, (typically a few Kc/s in the course of an experiment), may have an inordinately large effect upon the total noise level arising from fluctuations in frequency.

In the case of "wall-breathing", the fluctuations may be reduced by a proper alignment of the cavity with respect to the DC field. Feher (7.4) observed that 'squeezing' the broad face of a TE_{10} mode rectangular cavity increases the frequency, whilst 'squeezing' the narrow face reduces it. Thus two positions (180° apart) may be found for the magnet at which the effects cancel. A similar mechanism seems to exist for a cylindrical TE_{112} mode cavity, but the effects appear to be smaller.

Lowin (5.24) made measurements on the cylindrical cavity used in these experiments both before and after casting in araldite. He observed that the signal from "wall-breathing" was reduced by a factor of ten after 'potting'. He plotted the amplitude of the "wall-breathing" signal at a constant field against the bucking signal phase for a number of orientations of the magnet and found, at unfavourable magnet orientations, a sine curve for the dispersive phase signal; in addition, he found a small signal which appeared to be independent of magnet angle, but which was reduced by potting. Lowin suggested that some mechanism involving the modulation of the coupling of the cavity to the feed wave guide, by changes in radiation losses through the iris or by changes in losses at the cone joint, may be responsible.

The effect of "wall-breathing" was reduced in these experiments by the simple expedient of fixing a copper tube on the tail of the helium dewar in a position below the cone joint, but well clear of the specimen. Measurements with a search coil showed that the shield reduced the modulation by a factor of about twenty. When the copper tube was positioned round the feed wave guide a small reduction in "wall-breathing" signal was observed, but as it was lowered to cover the iris and cone joint a reduction by a factor of almost two was achieved. The presence of the shield had no effect on the shape or position of the resonance lines from the samples.

7.5 Sensitivity

The sensitivy of an esr spectrometer is usually quoted as the minimum number, N_{min}, of spins detectable under certain conditions. The following factors must be considered:

(a) Microwave frequency:

Feher (7.4) shows that:

$$N_{min} \propto \frac{1}{\omega^{7/2}} \qquad \ldots\ldots\ldots\ldots\ldots\ldots \quad 7.1$$

where ω is the microwave frequency of the system.

This relation means that, theoretically, a Q-band spectrometer should be capable of detecting about eighty times fewer spins than an X-band spectrometer. In practice, however, this is compensated by the larger amount of sample used at X-band, the increased performance of the microwave components at the lower frequency, and the use of lower magnetic fields.

(b) Microwave power:

The signal is proportional to the square root of the power, P, incident on the sample, (7.4), the limit being set by the occurrence of saturation at high power levels, with consequent saturation broadening.

(c) Cavity quality factor and filling factor:

ΔQ_L, the change in the loaded Q of the cavity due to paramagnetic absorption is given by (7.4):

$$\Delta Q_L = 4\pi \chi'' \eta \, Q_o^2 \qquad \ldots\ldots\ldots\ldots\ldots\ldots \quad 7.2$$

where Q_o is the unloaded cavity Q and η is the filling factor, which is very approximately equal to the ratio of sample volume to cavity volume. This, for the greatest sensitivity, Q_o should be as high as possible. The amount of sample (and hence η) in the present system is determined by the conditions for optimum matching of the cavity and feed waveguide.

(d) Temperature:

The size of the signal is a function of temperature in two ways. The first of these is through the relative population of the energy levels of the system.

In the case of a doublet, the signal amplitude, A, is proportional to the population difference $n_1 - n_2$ between levels, and has the form:

$$A = A_o \left(\frac{n_1 - n_2}{n_1 + n_2}\right)$$

$$= A_o \left[\frac{1 - \exp\left(\frac{-h\nu}{kT}\right)}{1 + \exp\left(\frac{-h\nu}{kT}\right)}\right] \quad \ldots\ldots\ldots\ldots\ldots\ldots \quad 7.3$$

where A_o is the signal amplitude as $T \rightarrow 0$.

For energy levels separated by $\Delta E \sim 1/3$ cm^{-1} (i.e., 6×10^{-24} J) and since $k \sim 1.4 \times 10^{-23}$ J.K^{-1}, for values of T greater than a degree or two, the exponential term above may be expanded in a power series and the sensitivity is inversely proportional to temperature.

The second effect is due to the change in Q of the cavity.

$$Q_o \propto 1/\delta$$

and $$\delta \propto \rho^{\frac{1}{2}}$$

where δ is the microwave skin depth and ρ the resistivity of the cavity walls.

For pure copper:

$$\frac{\rho_{300}}{\rho_{4.2}} \sim 1000 \text{ and } \quad \frac{Q_{300}}{Q_{4.2}} \sim 30$$

For brass:

$$\frac{\rho_{300}}{\rho_{4.2}} \sim 1.7 \text{ and } \quad \frac{Q_{300}}{Q_{4.2}} \sim 1.3$$

Thus for a cavity with pure metals walls (e.g. the cavity fabricated by Hirst), the effect of temperature is very great, but for brass is far less significant.

(e) Time constant:

Sensitivity is proportional to the square root of the ultimate time constant, τ , of the electronics. With the usual time constant setting of the system, a recording band width of $\frac{1}{2}$ c/s is employed.

The effect of the time constant on the line is discussed again in section (7.9).

(f) Modulation:

Signal size is directly proportional to the amplitude of the modulation Δ Hmod. Increase in the amplitude is restricted by the condition that it should be small compared to the linewidth. If this condition is not observed, modulation broadening sets in and the true derivative signal is not obtained. This sets a maximum of about 15 - 20 Gauss for the modulation in resonances from metals where typical linewidths are of the order of 100 - 500 Gauss.

(g) Linewidth:

The number of spins present is equal to the area beneath the absorption curve. For the same number of spins, it is clear that a narrow signal should have greater amplitude than a broad signal. For the derivative signal, the sensitivity is proportional to the inverse square of the linewidth. A common intensity plot is $(A + B)\ \Delta H^2$ v T, where A and B are defined in fig. (7.6).

(h) Signal to noise ratio:

The sensitivity is a function of the number of spins divided by the signal to noise ratio of the line. The factors influencing the noise level will be discussed in section (7.6) below.

A number of results have been analysed (table 7.1) with a view to obtaining a rough figure for the sensitivity of the present apparatus.

The DPPH sample was crystallised from Benzene solution to avoid deterioration of the sample (7.4) and measurements were made at room temperature to avoid the considerable distortion of the line due to antiferromagnetic ordering in DPPH at low temperatures and to enable a larger and more manageable crystal to be used. The modulation was reduced for the measurement on DPPH by using the copper shield described above.

Bearing in mind the discussion above, a suitable formula for the sensitivity of the system (P, γ and Q_L fixed) is:

$$\text{Sensitivity} = \frac{(\text{no. of spins})(\Delta H_{\text{mod.}})\ 4.2}{(S/N)\ \Delta H^2\ T_{obs}} \quad \ldots\ldots\ldots \quad 7.4$$

where T_{obs} is the temperature at which the measurement is made.

Extrapolating from the data in Table 7.1 to a signal to noise ratio of about five, which might be considered the smallest value at which a signal could be identified, the minimum number of ions detectable for a linewidth of (say) 200 Gauss at 4.2K would be $\sim 3 \times 10^{14}$.

TABLE 7.1

	Pd0.1Gd	Cu5Mn	Diphenyl Picryl Hydrazil (DPPH)
Temperature	4.2	300	300
Quantity of sample	$\sim 10^{-2}$gm	$\sim 7.5 \times 10^{-3}$gm	-
Radius of particles	$\sim 4 \times 10^{-3}$cm	$\sim 4 \times 10^{-3}$cm	-
Surface Area $(\frac{3v}{2r})$	$\sim$ 0.45cm^2	$\sim$ 0.3cm^2	-
Resistivity	0.4 $\mu\Omega$ cm	16 $\mu\Omega$ cm	-
Skin depth (10Gc/s)	3×10^{-5}cm	2.2×10^{-4}cm	-
No. of ions in skin depth	10^{15}	3×10^{17}	3.2×10^{16} *
S/N ratio	70	20	300
ΔH	125	420	3
ΔHmod	15	15	0.2
Q_L	3000	3000	3000
Power	25mW	25mW	25mW
γ	1	1	1
Sensitivity	$\sim 1.4 \times 10^{10}$	$\sim 1.8 \times 10^{10}$	$\sim 3 \times 10^{10}$

* deduced from volume of monoclinic single crystal measured under a microscope.

7.6 Possible Improvements in Sensitivity

For the work in this thesis, the present spectrometer has, in general, been sufficiently sensitive to give lines with a good signal to noise ratio. There are, however, cases such as measurements in the extreme dilute limit, resolution of hyperfine structure and searches for non-S-state resonances where extra sensitivity might be desirable. In this section, possibilities for achieving this will be described and discussed:

(a) Improved signal to noise ratio of the microwave components and electronics

Torrey and Whitmer (7.5) showed that P_N, the noise power at the output of the detector in an esr system, may be written:

$$P_N = (GN_k + F_{AMP} + t - 1)\, kT\, \Delta\nu \qquad \ldots\ldots\ldots\ldots\ldots \quad 7.5$$

where G is the conversion gain of the detector and is directly proportional to its efficiency;

N_k is the noise figure at the output of the detector due to the microwave source;

t is the noise temperature of the detector, and

F_{AMP} is the noise figure of the amplifier.

The relative importance of the terms in the expression above depends upon the level of microwave power at the detector (i.e., size of the bucking signal). This has been discussed in some detail by Wilmshurst (7.6).

For low levels of bucking signal, the noise contribution from the amplifiers is the chief contribution to the noise in the system. At higher levels of microwave drive, the detector efficiency increases but the effect of crystal flicker (1/f) noise and, to a lesser extent, klystron noise, becomes important. There is, thus, an optimum value for the microwave drive which gives the best signal to noise ratio for a given system and Wilmshurst (7.6) states that in practice this coincides with the transition point between the square law and linear regions of the detector crystal characteristic.

In the light of these remarks, specific possibilities for improved performance will be considered:

(i) The detector crystal:

This is probably the main source of noise in the present system and this is largely 1/f noise. There is an advantage, therefore, in using modulation at the highest possible frequency, subject to the conditions that the modulation has to penetrate the cavity walls and that RF heating should be minimised to achieve a fairly slow warm up.

New generations of low noise crystals, such as the Mullard BAV 22, are now available and replacement of the present crystal with a low noise diode would probably be a relatively simple and useful modification.

(ii) The klystron and power supply:

The klystron is not a perfectly coherent, monochromatic source of radiation; its output contains a sharp peak superimposed on a broad background that extends for tens of megacycles. There appears to be little, however, published about the magnitude of klystron noise. The noise generated by a klystron is particularly sensitive to fluctuations in the reflector voltage and, to a lesser extent, in the accelerator voltage. Experience gained in modifying the smoothing circuits in the present power supply, which were found

to have a figure of merit ~40 at 50 c/s, suggests that some improvement could be gained from this source.

(iii) 'Magic' hybrid Tee:

One factor which was not considered in equation 7.5 was the effect of the magic tee. This splits the incident power between the cavity and load and the reflected power between the signal source and detector; in doing so, it reduces the power reaching the detector by a factor of four. Replacement of the hybrid tee by a microwave circulator would avoid this loss.

(b) Improved performance of the cavity

A higher Q cavity could be fabricated using the method described below employed by Hirst. New types of araldite have recently been developed for potting superconducting magnets and these are reported to survive rapid and frequent thermal cycling (J. Good, Private Communication).

Alternatively, a silvered glass cavity could be employed. Feher (7.4) used such a cavity and claimed a high Q combined with a very small "wall-breathing" signal

The use of a pure metal conducting surface in the cavity would, as pointed out in section (7.5), restrict the use of the cavity to a limited temperature range, unless corrections were made for changes in Q with temperature. Fabrication of an improved cavity would also provide an opportunity to improve the thermometry of the system by, perhaps, building a thermocouple into the wall of the cavity.

One final useful modification might be to replace the present fixed iris with a variable device, thus enabling the cavity to be more conveniently and efficiently matched. Such devices can introduce extra noise into the system through the effect of vibrations, but a number of fairly rigid designs, which can be used at 4.2K, have been described in the literature (e.g., 7.7).

7.7 Preparation of Specimens

The dilute alloy specimens are prepared from etched ingots of about 1 gm. wt. They are held firmly in the end of a clean copper tube with methacrylate (MHP 1844) mounting plastic and filed under high purity toluene or acetone, using a small stub file which is used once only. The first filings from each ingot are discarded in order to avoid including in the final sample any oxide layer or loose particles from the file. About 200 - 300 mgms of filings are collected and the acetone decanted until only enough remains just to cover the sample. A small magnet is used to pick out any pieces of ferromagnetic material introduced from the file. The filings are then transferred to a quartz tube with a specially drawn neck which has previously been etched for a day in aqua-regia and run through with hydrofluoric acid. The tube is then pumped out, using a rotary pump and, when the acetone has completely boiled off, an ultimate pressure of about 10^{-5} torr is achieved with a diffusion pump and liquid nitrogen trap. The filings are annealed under vacuum to remove stresses caused by the cold working and are quenched by applying a wet cloth to the tube, before being shot into warm Apiezon M-grease and mixed in well using a piece of etched copper wire. The filings are thus exposed to air for less than five seconds during the whole preparation.

Care is taken during filing to avoid any shavings of the mounting plastic from contaminating the samples. A preliminary experiment on a Au-Ag alloy, deliberately contaminated with mounting plastic, gave no detectable signal at room temperature 77K or 4.2K.

Microscopic examination of the filings shows a wide distribution of shapes, and particle sizes are in the range 50 - 100 microns.

The preparation of samples from intermetallic compounds is simpler since these are in general brittle. Samples of about 250 mgms are placed under acetone in an etched agate or glass mortar and pestle and are crushed into a fine powder. These are then transferred to the quartz glass tube and the acetone boiled off before shooting into the vacuum grease. The brittleness of the samples suggests that no stress anneal is necessary for intermetallic compounds and subsequent work confirmed this.

Microscopic examination of the powders formed in this way showed that there existed a wide variety of particle shapes. About 90% of the particles were $\sim$10 microns, with a few in the range of 50 - 100 microns.

7.8 Experimental Procedure

The filings in their grease are attached $\lambda_g/4$ from the bottom of the resonant cavity and aligned with the narrow face of the feed waveguide, so as to be located in maximum microwave magnetic field. The amount of sample used is carefully adjusted to leave the cavity slightly undermatched at room temperature, thus allowing critical coupling to be achieved at low temperatures. A crystal of DPPH is added as a $g = 2$ marker.

A good vacuum seal between the cavity and waveguide is achieved by using a well-greased cone joint, and the cavity arm evacuated. The two dewars are fitted and the interspace flushed three or four times with nitrogen gas before being evacuated with a diffusion pump. The pumping rate is adjusted (using a needle valve) to obtain a steady pressure of about 0.1 torr. This ensures that, when the outer dewar is filled with liquid nitrogen, the cool down rate is sufficiently slow (about two hours) to avoid cracking of the cavity araldite. A few torr of helium exchange gas is then admitted to the cavity arm and liquid helium transferred to the inner dewar.

The klystron is first tuned to the resonant frequency and the cavity matching checked. This is achieved by fully inserting the attenuator in the bridge arm to give no drive power except from the cavity. A 50 c/s modulation is then applied to the klystron reflector, thus sweeping the klystron frequency over a complete mode. If the frequency is far from the resonant value, power is just reflected from the cavity iris and the normal klystron mode (fig. (7.5a)) is observed. Both mechanical and electrical fine tuning are then used to bring the klystron near to the cavity frequency (fig. (7.5b)). This is measured on the wavemeter and converted to frequency from standard tables supplied with Sanders TE_{10} 0.9" x 0.4" waveguide.

The 200 kc/s AFC modulation is applied to the klystron, adjusted in amplitude, and the resultant signal monitored by the detector crystal. The klystron electrical fine control is then again adjusted until the klystron is precisely tuned to the cavity. Finally the AFC loop is closed, thus locking the klystron frequency to the cavity frequency.

The bucking signal is then adjusted in amplitude and phase by means of the attenuator and short circuit to give a 400 kc/s signal only, at the detector, corresponding to the absorption phase alone. At the same time, the receiver crystal current is adjusted to a value of 1.1 μA which gives the best signal to noise ratio for the detector. Reflected power at the crystal is minimised by adjusting the variable screw probe in this arm.

A trial sweep is made and the gain, amplifier time constant and sweep rate are fixed. The field is held at a high value and the magnet rotated to minimise the offset due to "wall-breathing".

Several sweeps are made at 4.2K. Lower temperatures (to 1.5K with two pumps) are achieved by pumping on the helium and the use of a manostat allows the temperature to be held steady at intermediate values.

After the pump down, the pressure is allowed to return to atmospheric pressure and the remaining helium boiled off with the heater. In a typical run, a warm up to 77K takes about two hours, allowing numerous sweeps to be made with typical temperature drifts during the course of a sweep of less than $\frac{1}{8}$K.

In cases where the signal may be followed to temperatures above liquid nitrogen, control of the interspace pressure enables the cooling rate from room temperature to be made slow enough for measurements to be made in this temperature regime. Pumping on the liquid (and solid) nitrogen allows extra points to be taken down to about 55K. In this way, an adequate number of sweeps may be made in the whole range from room temperature to 1.5K.

Over the course of the experimental work described in this thesis the apparatus performed with great reliability. A number of minor modifications and repairs were made to the wide band amplifiers and to the klystron and its power supply. Since a number of the faults which developed were intermittent, two pieces of simple test apparatus were built, in order to check the integrity of the system between runs and, hence, to allow greater confidence in the intercomparison of data taken at different times.

The gain of the amplifier chain is checked before each run using a transformer system which was built for this purpose. This consists of two small screened transformers in series, giving voltage ratios of approximately 10^3:1 and 10^6:1 at the two outputs. By injecting a standard signal from an oscillator, the constancy of the output from the amplifier chain can be checked.

The amplitude of the high frequency modulation is also checked before runs using a small search coil of about 400 turns of 38swg copper wire, mounted on a plastic rod.

FIG 7.5

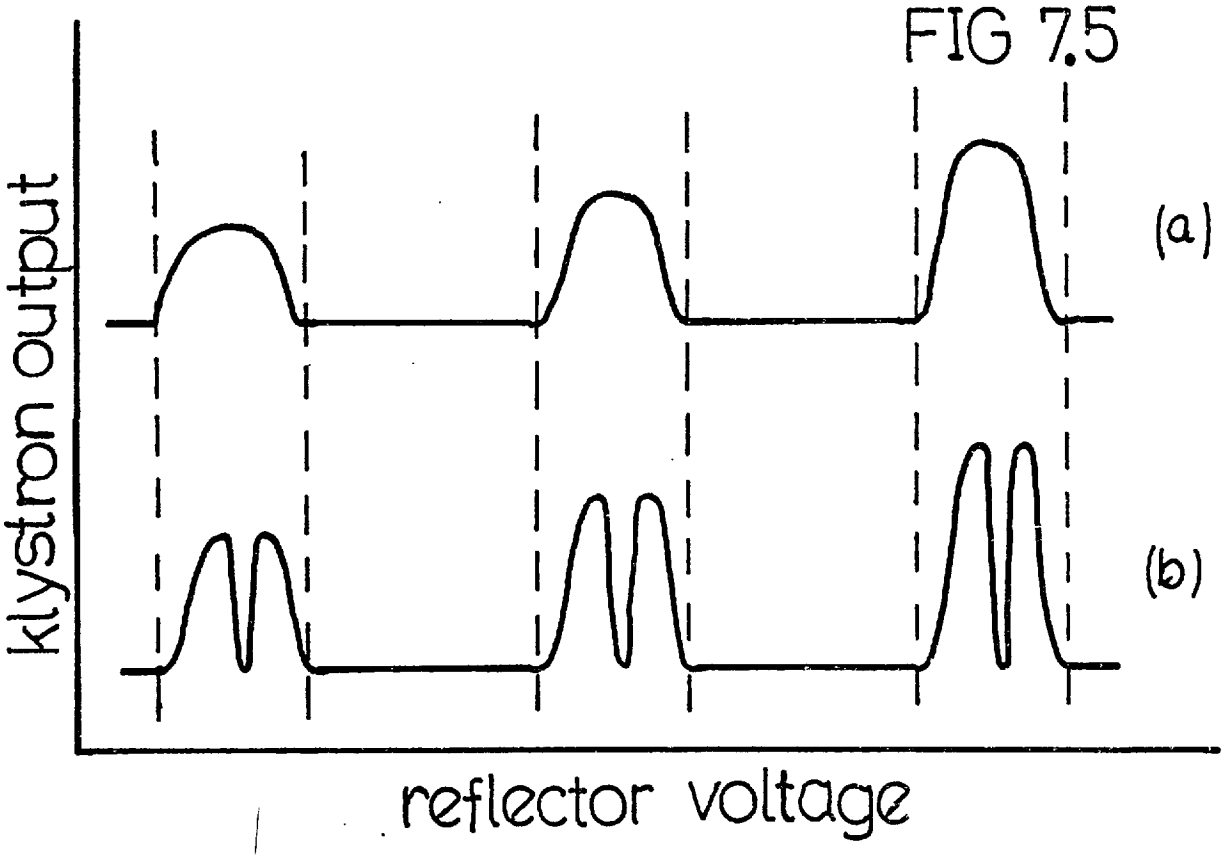
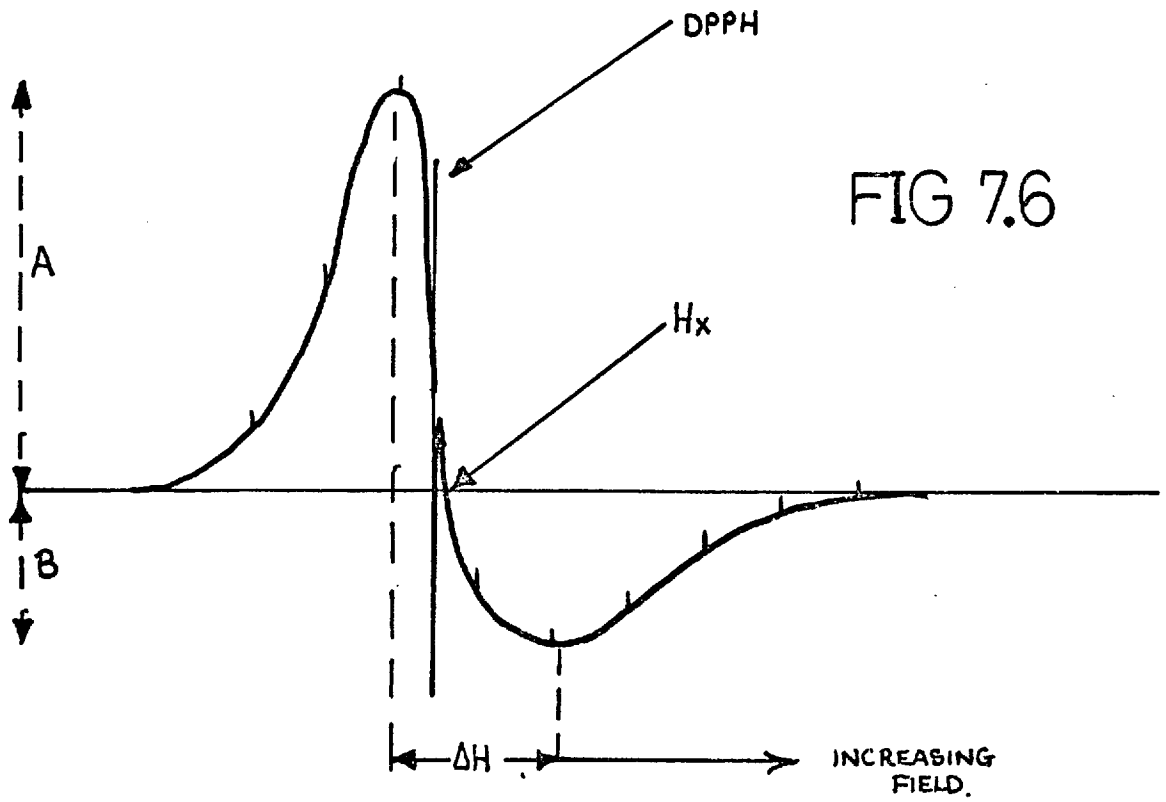

klystron output
(a)
(b)
reflector voltage

FIG 7.6


DPPH
A
Hx
B
ΔH
INCREASING FIELD.

7.9 Shape of Lines - Corrections

Three parameters are measured from the derivative esr line; the linewidth, ΔH, the resonant field, H_x, and amplitude A + B (fig. (7.6)).

The shape of lines in metals was investigated theoretically by Dyson (7.8) and his work confirmed experimentally by Feher and Kip (7.9). Dyson introduced three important parameters into his theory: T_D, the time it takes for an electron to diffuse through the skin depth δ, the time T_T taken by an electron to traverse the sample, and the spin-spin relaxation time, T_2.

For very small particles where $T_T \ll T_D$, the microwave field is not phase shifted in the skin depth and the absorptive part of the susceptibility only is observed. In this case the power absorbed, P

$$= \frac{\frac{\omega H_1^2}{4} (V) \omega_o X_o T_2}{I + (\omega - \omega_o)^2 x \quad T_2^2} \qquad \ldots\ldots\ldots\ldots\ldots\ldots \quad 7.6$$

where V is the sample volume and H_1 the amplitude of the RF magnetic field; X_o is the paramagnetic part of the static susceptibility and ω_o the resonant frequency. This is a Lorentzian line shape and the derivative is plotted in fig. (7.7). A/B = 1 in this case.

As the particle size increases with respect to the skin depth, an increasing fraction β of the dispersive (dotted) component $\frac{dX'}{dx}$ is mixed in and then

$$X = \beta X' + i X'' \qquad \ldots\ldots\ldots\ldots\ldots\ldots \quad 7.7$$

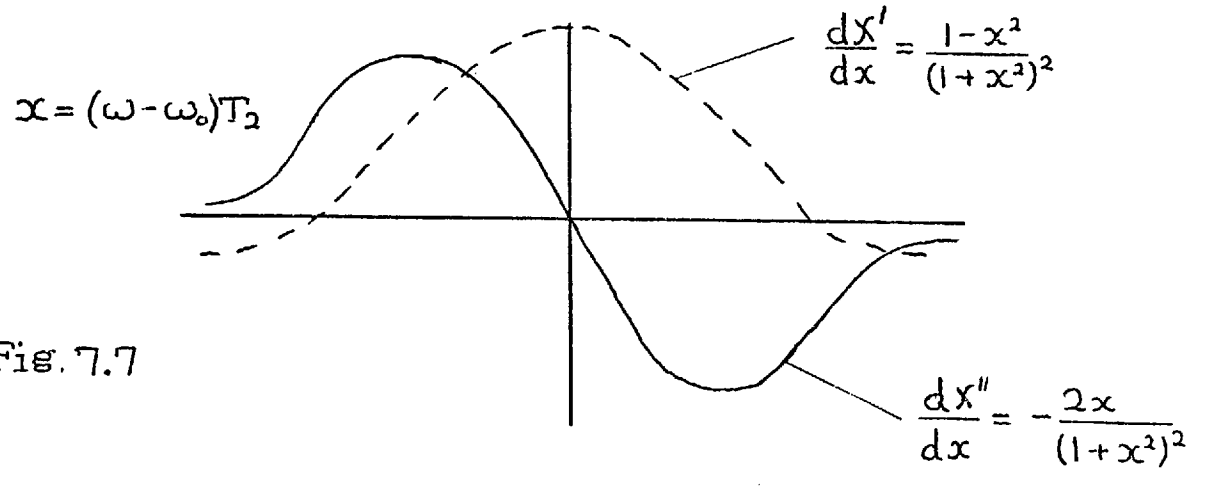


Fig. 7.7

In the present experiments, the skin depth is about two orders of magnitude less than the particle size and for fixed paramagnetic impurities distributed throughout the volume of the metal, we are in the limit:

$$T_T \gg T_D \gg T_2$$

In this case, $\beta = 1$ and Feher and Kip show that the line shape ratio should be 2.55.

Owen et al (5.45) have shown that, for A/B = 2.55, the centre of the true resonant absorption, $H_{x\ true}$, is given approximately by,

$$H_{x\ true} = H_{x\ obs} - \frac{\Delta H_{obs}}{3} \quad \ldots\ldots\ldots\ldots\ldots\ldots \quad 7.8$$

and the peak to peak linewidth ΔH by

$$\Delta H = \frac{1.25}{\gamma T_2} \quad \ldots\ldots\ldots\ldots\ldots\ldots\ldots\ldots \quad 7.9$$

where γ is the free spin gyromagnetic ratio. For $\Delta H \sim 200$ Gauss this gives $T_2 \sim 3.5 \times 10^{-10}$ sec.

The true linewidth is given by

$$\Delta H_{true} = 0.9\ \Delta H_{obs} \quad \ldots\ldots\ldots\ldots\ldots\ldots \quad 7.10$$

This analysis assumes that the spectrometer has been correctly tuned to the absorptive part of the signal but, due to drifts (section 7.4), this is not always the case and the peak heights ratio A/B is in practice sometimes observed to be less than 2.55.

A procedure for obtaining the true values of H_x and ΔH has been devised and is shown in appendix 5 . By measuring the value of A/B from the trace, the corrections may be read from the graph. The calculations were performed by Dr. D. Griffiths.

The correction system assumes a Lorentzian line and this assumption was checked against a number of lines from different samples and found to hold well. The corrections used in this work are referenced to the observed centre of the line, which can be measured accurately, whereas those used by Peter et al (5.26a) were referenced to the first maximum,

which in broad lines is difficult to measure with precision. Baseline drifts, which are troublesome in measurements on weak signals, can give a false value of A/B, and for a broad line this is a major source of error in the quoted g-value.

A second important correction has to be made to allow for the effect of the time constant of the final stage of the amplifier chain, if this is significant compared with the time taken to sweep through the line.

If the input to the final amplifier is V(H) and the observed signal $V'(H)$, τ is the time constant and R the chart speed, we may write

$$V(H) = V'(H) + \tau R \, d/dH \, V'(H) \quad \ldots\ldots\ldots\ldots\ldots \quad 7.11$$

Solving this using the conditions that $V(H_x) = 0$ and that near H_x, $V'(H)$ is linear in H we get,

$$H = H_x + C \quad \ldots\ldots\ldots\ldots\ldots\ldots\ldots\ldots\ldots \quad 7.12$$

where $C = \tau R$

Thus, the true centre of the line corresponds to a point above or below the observed value, depending on the direction of sweep.

This factor is determined experimentally by displaying a signal at a set value of the field and rapidly switching off the modulation. The time taken to decay by a factor of 1/e (i.e., 0.63 x amplitude) is then measured. This correction is only valid if the value of C is considerably less than the value of ΔH. Since in practice $C/\Delta H \sim 1/40$ this condition is amply satisfied.

CHAPTER 8

RESULTS AND THEIR INTERPRETATION

8.1 Gd in Dilute Solid Solution

(a) Pd-Gd

Figs. (8.1) to (8.4) show the temperature dependence of the g-value and linewidth of 0.2, 0.4, 4 and 6at% Gd in Pd and the low temperature g-value of 0.1 and 0.02at% Gd in Pd. Data on the two higher concentrations have been obtained up to 77K, but at lower concentrations the reduced intensity of the signal, combined with the fairly rapid warm up rate in the temperature regime around 30 - 40K, has confined measurements to lower temperatures. The values of g (in the paramagnetic regimes), $d\Delta H/dT$, the minimum in the linewidth ΔH_{min}, and the residual linewidths ΔH_{res}, are presented in table (8.1).

TABLE 8.1

Alloy	g_{PM}	$d\Delta H/dT$	ΔH_{min}	ΔH_{res}
Pd6Gd	1.95 ± 0.01	~ 7.5	600	500
Pd4Gd	1.93 ± 0.01	~ 9	530	400
Pd0.4Gd	1.82 ± 0.01	~ 12	200	50
Pd0.2Gd	1.795 ± 0.005	-	190	-
Pd0.1Gd	1.77 ± 0.07	-	120	-
Pd0.02Gd	1.77 ± 0.02	-	-	-

The high temperature g-values have been corrected for demagnetisation effects (where appropriate) and by the lineshape factor (A.5(a)). The relatively large error put on the 0.02% alloy g-value is due to the distorted signal obtained in this case (see ch. 6).

The form of the data in figs. (8.1) to (8.4) is in broad agreement with the low concentration data of Cottet (5.30, see fig. (5.2)) and the higher concentration data of Peter et al (5.26). The curves of Δg v T show an upturn at low temperatures for concentrations in excess of 0.2at% and the magnitude of this upturn increases with increasing concentration of Gd, giving an effective g-value of about 2.45 at 1.7K in the 4at% and 6at% alloys. Using the M - H plots of Crangle (3.45) for a 7.2% alloy, which orders ferromagnetically at 5K, and applying an average demagnetisation factor $\sim \pi M$ at 3KGauss, we obtain the crosses in fig. (8.4). These are in fairly good agreement with the experimental results. This suggests that the increase in g-value at temperatures more than twice T_C is a result of measurement in a finite magnetic field (see fig.(2.3)). The increase in the linewidth in this temperature regime may be explained in a similar way. The line will be inhomogenously broadened as a result of the distribution of demagnetising factors among the particles of the powder which, as described in ch. 7, show a wide distribution of shapes and sizes. It is noticeable that the linewidth begins to broaden at rather higher temperatures than the temperatures at which the g-values begin to increase. This may indicate the presence of short-range order in the alloys (see 8.2 and 8.3(g)).

Peter et al (1.43) suggested that the shape of these curves may be explained in terms of dynamic effects in the esr bottleneck, and a fit to the present data can indeed be made, over a limited temperature range, using the formula of Davidov and Shaltiel (equation 4.58). The g-shift obtained using this formula, however, can never change sign for an alloy of a given concentration and thus the expression cannot account for the low temperature g-shifts in the 4at% and 6at% alloys, where Δg becomes positive. It seems relevant to question also the analysis of Davidov and Shaltiel (5.21) with respect to the $LaNi_5$ - Gd system (fig. (5.1.)), since the ordering temperature for these alloys was not determined.

We know that the compound $GdNi_5$ orders ferromagnetically at 27K and therefore we might expect that $LaNi_5$ - 5%Gd would, very approximately, order at about 1.5K. Bearing in mind that the Q-band measurements of Davidov and Shaltiel were performed in an applied field of 14KGauss, it seems feasible that demagnetisation effects might become important at 12 - 15K where the upturn in g-value is observed. The behaviour of the alloy is rather similar to that of the 1at% Gd in Pd ($T_C \sim 2K$) alloy measured by Cottet at Q-band. The form of the frequency dependence of the linewidth and g-value at 4.1K in $LaNi_5$ - Gd might also be accounted for in terms of demagnetisation effects, since the inhomogenous broadening is likely to be greater in higher measuring fields, where a wider range of demagnetising fields will be present in the powder. The interpretation of the frequency dependence of the linewidth data is, however, open to some doubt since the frequency dependence of the residual linewidth may be an important factor (see below). Davidov and Shaltiel were only able to account for their linewidth data in terms of clustering effects.

The behaviour of the $LaRu_2$ - Gd system has also been explained on the basis of the existence of dynamic effects (5.20). In this system it is known that an alloy containing 6at% Gd orders ferromagnetically at 9.5K and an upturn in the g-value of a 3at% Gd alloy is observed at $\sim$ 20K in a field of 12KGauss.

It is impossible, of course, to state with certainty that dynamic effects are <u>not</u> present in the Pd-Gd or other systems. Such a statement could only be justified if M - H plots were available at a number of concentrations and temperatures in each system and if g-shift measurements were made on a specimen in a form such that a precise demagnetisation field could be defined.

Various models have been discussed in ch. 1 which seek to explain the large negative g-shifts observed in the dilute Pd-Gd alloys. At the lowest concentration of Gd a g-shift has been observed of 0.225 and this leads, using equation 4.41 and the value of the Pd susceptibility of 9×10^{-6} emu per cc quoted by Peter et al (5.26), to a value $J_{eff} = -0.018$ eV. The values of the g-shifts obtained in this work are in good agreement with those obtained by Cottet, but in disagreement with the recent results of Praddaude and Gartner (5.32) (who obtained $\frac{\Delta g}{g} \sim -8\%$ for a 0.2at% alloy). Particularly puzzling is their remark that the discrepancy may be due to incomplete inclusion of demagnetisation effects in other work, since not only would this tend to increase the discrepancy but, for such low concentrations, such effects are negligibly small at X-band (less than 2 Gauss). The observed shift of -12% found in this work is much less than the reduction in the paramagnetic and saturation moments obtained by Shaltiel et al (5.8) (22%) and Crangle ($\sim$20%) (3.40). However, the recent work of Guertin and Foner (3.44) indicates a reduction of only 7 - 8%, independent of concentration. The discrepancy between this value and that of Crangle, whose magnetisation data on the 7at% alloy at 1.7K look well saturated at fields of from 5KGauss to 20KGauss, is puzzling. One possibility might be that the Pd host is itself contributing an extra moment at the high field (150KGauss) used by Guertin and Foner; however, this possibility appears to be ruled out by the work of Müller et al (3.71) who showed that the magnetisation of Pd at high fields is given by

$$M = \chi H (1 + \beta H^2)$$

up to 325KGauss at 4.2K with $\beta = 6 \times 10^{-14}$ Gauss^{-2}.

If we accept the value obtained by Crangle and by Shaltiel et al, one intriguing possibility might be that a second order g-shift (equation 4.42) is present. For $J < 0$ this will tend to decrease the negative g-shift, since $\Delta g_2 \propto J^2$. A second order shift might also explain the reduction

in Δg on increasing the Gd concentration, since $\Delta g_2 \propto C$. Two facts argue strongly against such a proposition, however:

1. We might expect considerable temperature dependence of the g-value for a given alloy in which second order effects are important, since $\Delta g_2 \propto 1/T$, and such effects are certainly not observed in either Pd 4at% Gd or Pd 6at% Gd in the paramagnetic regime.

2. Cottet (5.30) has added Lu to a 0.1at% Gd in Pd alloy and finds that the g-shift continues to decrease with increasing Lu content. If a second order g-shift were responsible for the reduction in Δg, addition of Lu might be expected to produce no change in g. The reduction in Δg would appear to be a consequence of the filling of the Pd d-band.

The work of Budworth et at (5.26) shows that Ag fills the d-band of Pd at a concentration of about 60%, whereas the De Haas Van Alphen experiments of Vuillemin and Priestly (3.72) suggest that there are $\sim$0.36 holes in the Pd d-band. These results indicate that the naive rigid band model is, even for Ag, far from satisfactory. Addition of Lu, which has a configuration $4f^{14}5d^{1}6s^{2}$, increased the g-value of Gd in Pd at about three times the rate for Ag (fig. (8.5b)) and this suggests that if a rigid band model is applied for the addition of Ag, it is equally applicable for Lu. Addition of Gd, however, appears to increase the g-value rather faster than Lu at low concentrations, showing distinct curvature, but when 6at% Gd has been added, the g-value falls on the Lu curve. It is difficult to account for this behaviour; we only note that complications arise in comparing Gd and Lu since the atomic radius of the latter is smaller by $\sim$4% and thus addition of Lu may have the effect of increasing K_F for the conduction electrons and increasing the width of the d-band.

As the concentration is increased, the temperature dependence of the linewidth appears to decrease. The slope of the lowest concentration alloys is difficult to estimate, but the slope of the 0.4at% alloy is certainly greater than the value of $6G.K^{-1}$ obtained by Cottet, whose

measurements suggest a decrease in slope from $6G.K^{-1}$ for a 0.6at% alloy to about $4G.K^{-1}$ for a 1at% alloy. As discussed in ch. 4, we cannot use the simple Korringa form for an exchange enhanced host but must include a factor $K(\alpha)$ (equation 4.55). In this case, assuming from the large g-shift that the system is not bottlenecked, we obtain $K(\alpha) \sim 1/60$ for the 0.4at% alloy, reducing as $\rho(E_F)$ is reduced, to about 1/8 for the 6at% alloy.

One further interesting fact emerges from the linewidth data. We note from fig. (5.2) that the values of the minimum linewidth observed by Cottet are about twice the values obtained in this work. To check that this was not a metallurgical difference (Cottet did not homogenise his alloys), the 0.2at% alloy used in the present work was measured by the Geneva group, and Q-band and the difference in linewidths confirmed. Careful analysis of the data suggests that the residual linewidth in these alloys is frequency dependent. No explanation can be offered for this behaviour but we note that similar behaviour has been found by Bagguley et al (3.51) in their work on the PdFe alloys; here it was noticed that a plot of linewidth against temperature has the same form but with absolute values scaled by a factor equal to the square root of the ratio of the frequencies (fields) at which the measurements were made. The same would appear to be approximately true in the present case. One measurement made by Peter et al at 50 Gc/s on a 3at% Pd-Gd alloy (fig. (8.5a)) rather surprisingly falls on the 9 Gc/s curve.

(b) Pd-Ni - Gd

The effect of adding 1.3at% Ni to the Pd0.4Gd alloy was investigated and at 4.2K a g-value of 1.72 ± 0.02 (c.f. Pd0.4Gd = 1.82) and $\Delta H = 550G$ was obtained. This result is consistent with the g-values found by Cottet for Gd in Pd-Ni alloys containing up to 1at% Ni (5.30) and with the idea that addition of Ni 'drives' the Pd towards ferromagnetism. From the data above, it cannot strictly be claimed that a Gd content of 0.4at% acts

merely as a 'probe' of the host alloy behaviour and such a claim could certainly not be made for the 3% Gd used by Shaltiel et al (5.8) in their experiments, since this concentration of Gd will appreciably alter the band structure of the host. The concentration used in this work did, however, allow a limited warm-up to be made to about 15K and despite the reduction in amplitude of the signal, it appeared that the alloy showed similar temperature dependence to the original Pd0.4Cd alloy. The absence of a sharply increased slope, $\frac{d\Delta H}{dT}$, (as in Cu-Mn) on the addition of impurity, lends further support to the contention that the Pd-Gd system is unbottlenecked. Cottet (private communication) has found no increase in $\frac{d\Delta H}{dT}$ for alloys doped with other non-magnetic impurities.

(c) $LaAl_2$ - Gd

From twelve sweeps at 4.2K on the $LaAl_2$ - 0.45at%Gd alloy investigated by Lowin (5.24) a g-shift of + 0.027 $\pm$ 0.01 was obtained. This is less than his value of 0.055 $\pm$ 0.015, obtained without the nmr field calibration facility (which is crucial to the accurate determination of g-shifts). Furthermore, it would appear that Lowin applied the simple $\Delta H/3$ lineshape correction factor which is valid only for lines with A/B = 2.55. More realistic corrections for $A/B < 2.55$ lead to smaller positive g-shifts. The present result shows unequivocally that the shift is positive, contrary to the earlier work of Shaltiel et al (5.8) who found a negative g-shift. It is, however, in agreement with the static susceptibility results of Maple and Fisk (1.47). Using the measured susceptibility (corrected for core diamagnetism) of 150 x 10^{-6} emu per mole obtained by Maple, a value of J_{eff} = + 0.017 eV is obtained.

In the present work, the temperature dependence of the linewidth was not investigated but using the value of $\frac{d\Delta H}{dT}$ = 42 $\pm$ 5 $G.K^{-1}$ obtained by Lowin, the simple Korringa relation (equation 4.54) predicts Δg = + 0.040 which is rather higher than the value obtained in this work. The result seems to imply K (α) $\sim$1 and that exchange enhancement is not important for $LaAl_2$.

FIG 8.1

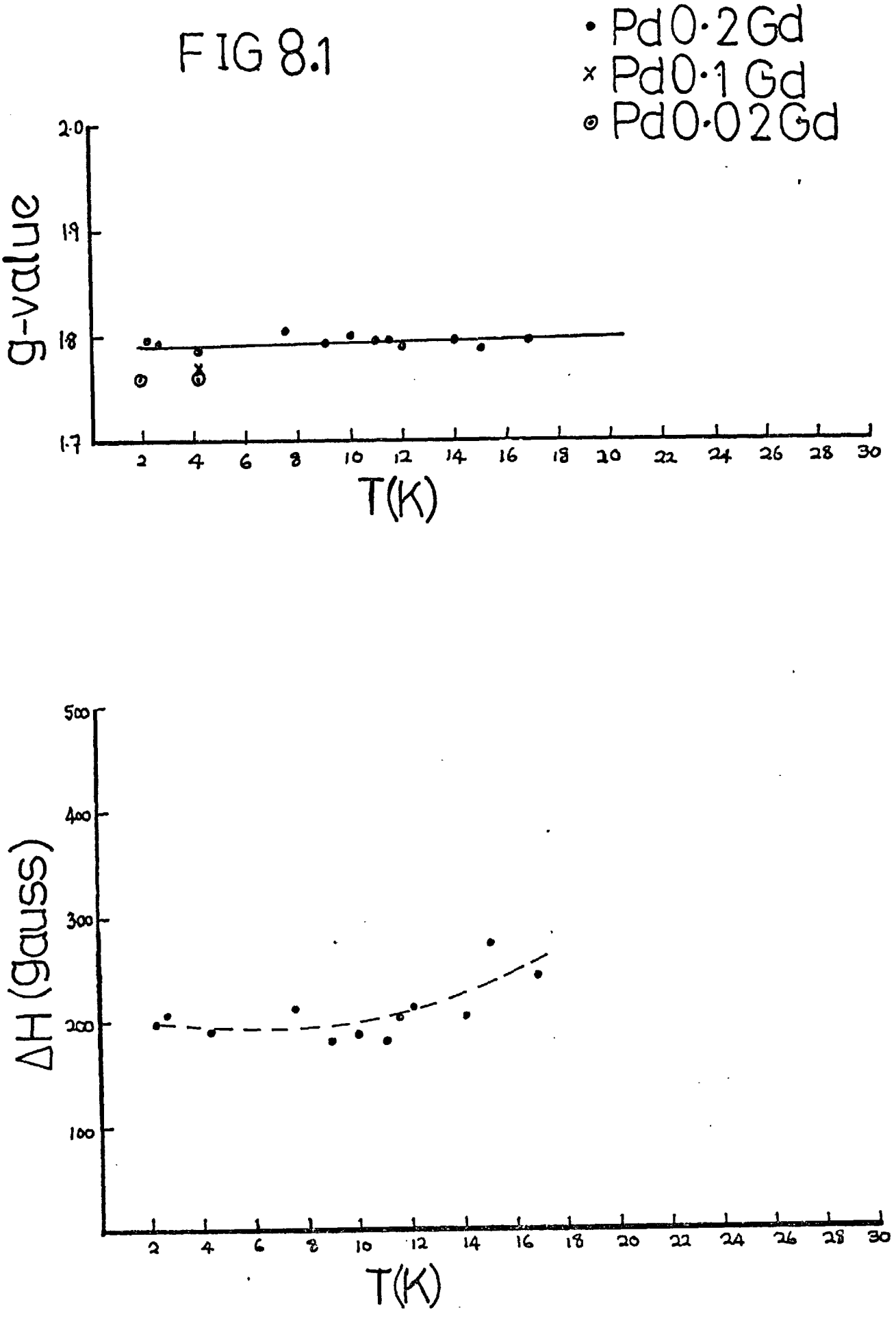
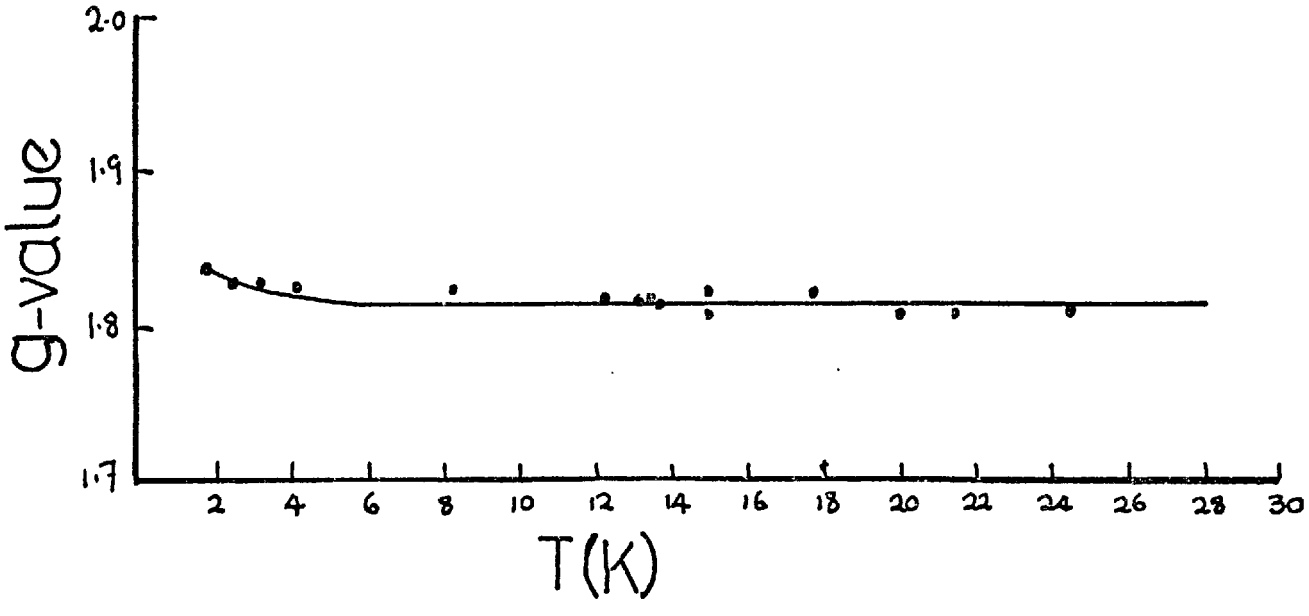

• Pd 0·2 Gd
× Pd 0·1 Gd
⊙ Pd 0·02 Gd
g-value
2·0
1·9
1·8
1·7
2
4
6
8
10
12
14
16
18
20
22
24
26
28
30
T(K)
ΔH (gauss)
500
400
300
200
100
2
4
6
8
10
12
14
16
18
20
22
24
26
28
30
T(K)

FIG 8.2 Pd 0·4 Gd



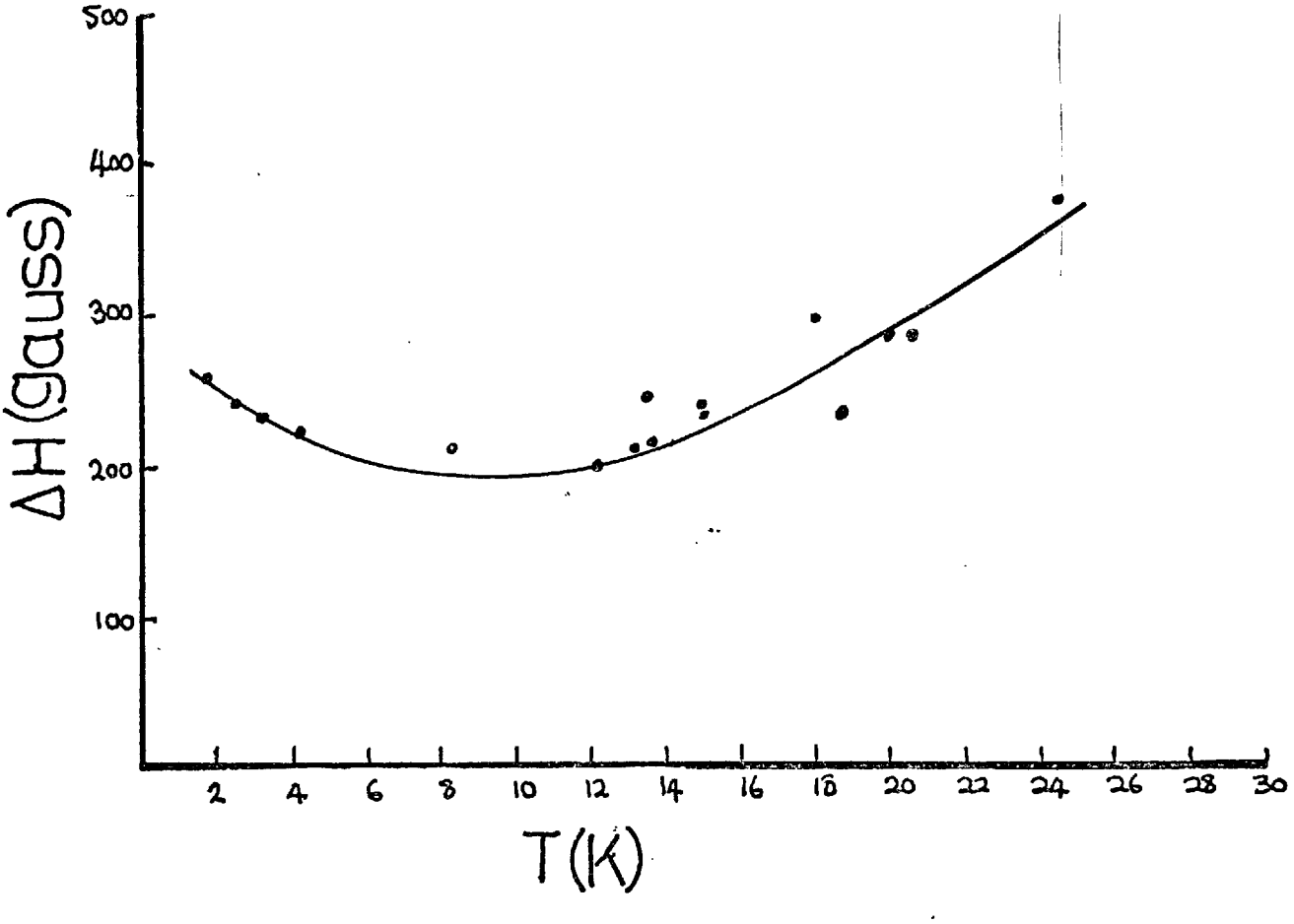
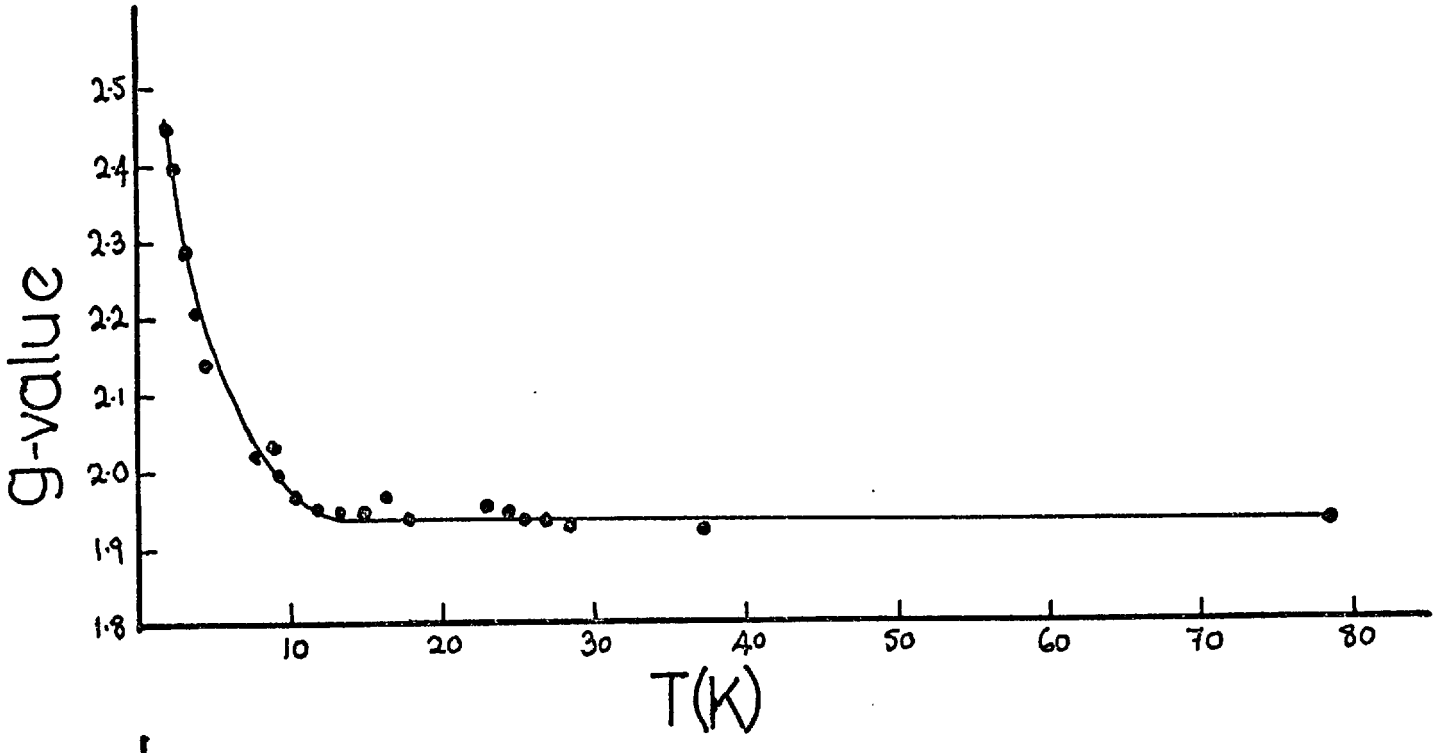


FIG8.3 Pd 4Gd


g-value
2·5
2·4
2·3
2·2
2·1
2·0
1·9
1·8
10
20
30
40
50
60
70
80
T(K)

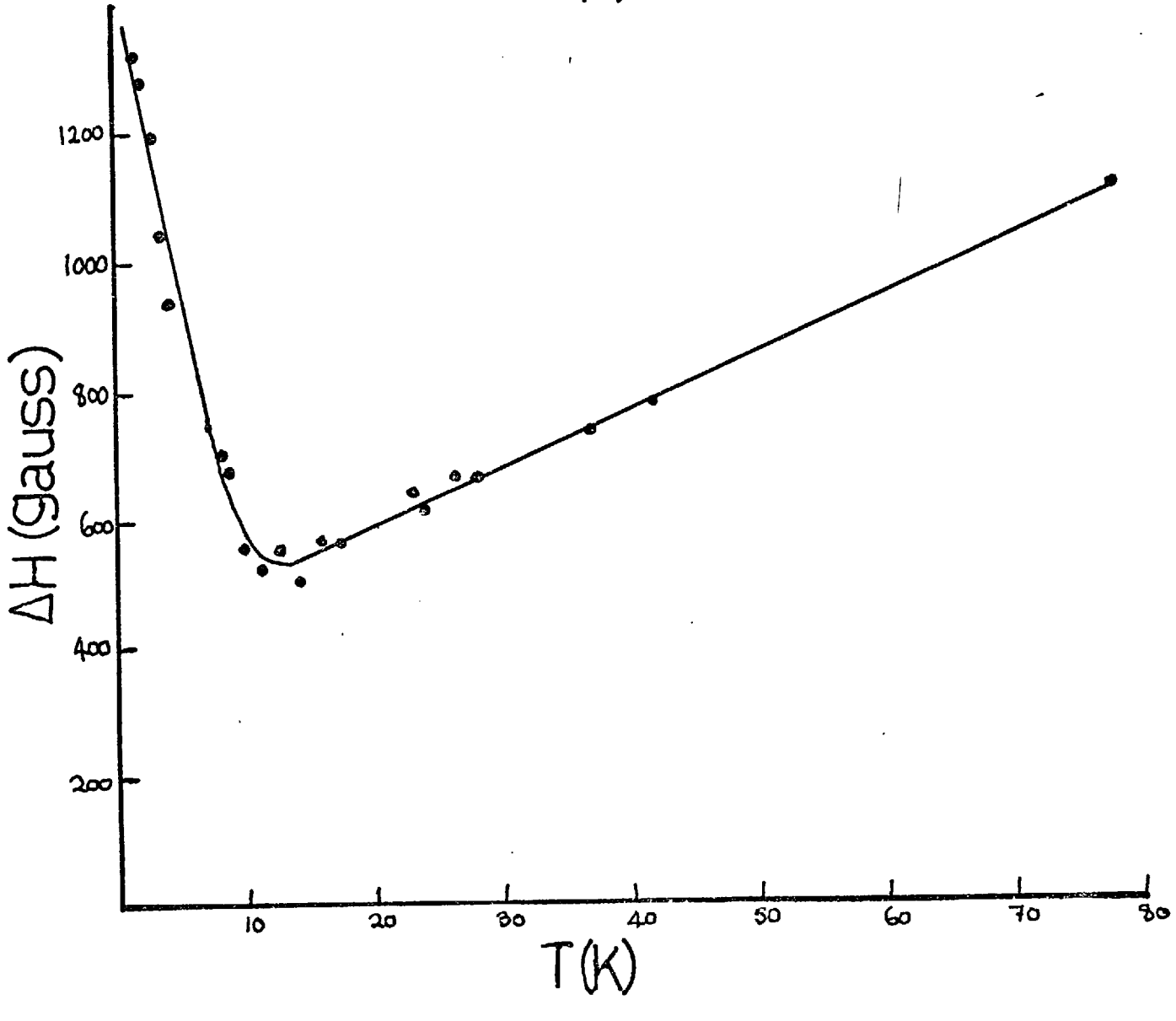
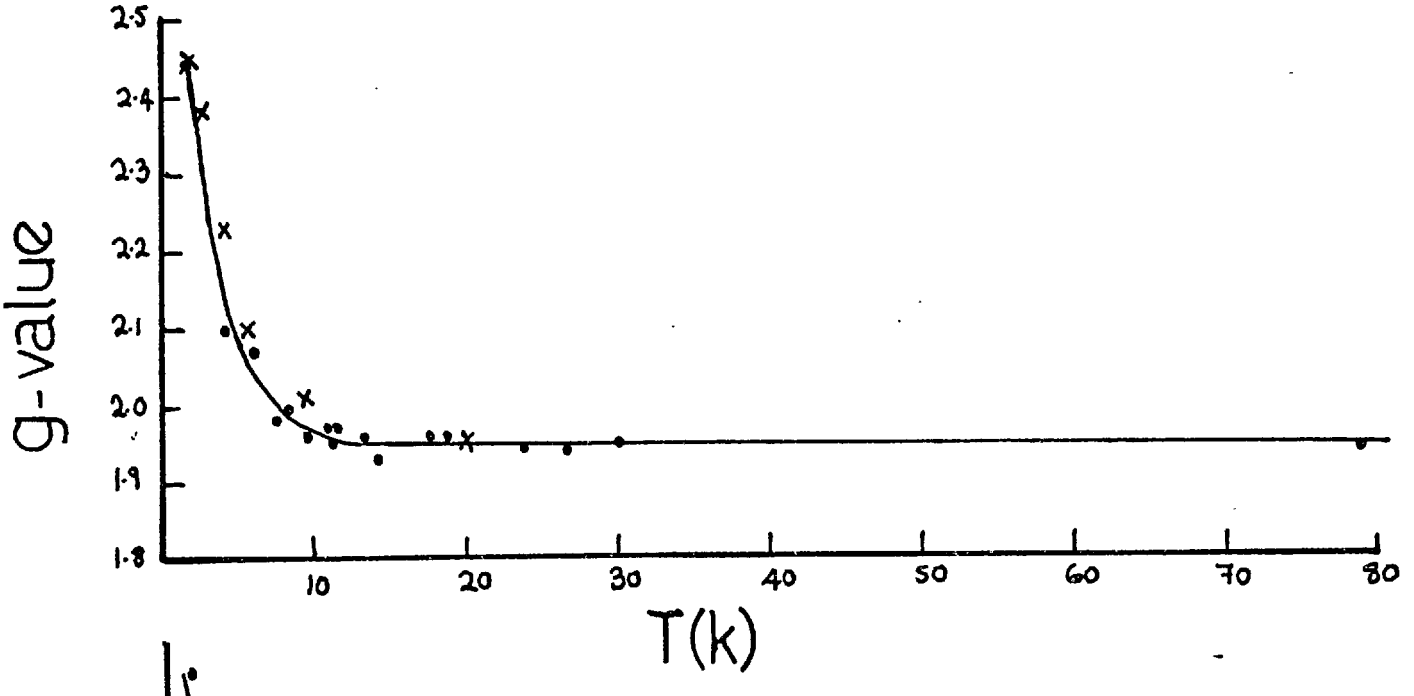

ΔH (gauss)
1200
1000
800
600
400
200
10
20
30
40
50
60
70
80
T(K)

FIG 8.4 Pd 6Gd


g-value
2·5
2·4
2·3
2·2
2·1
2·0
1·9
1·8
10
20
30
40
50
60
70
80
T(k)

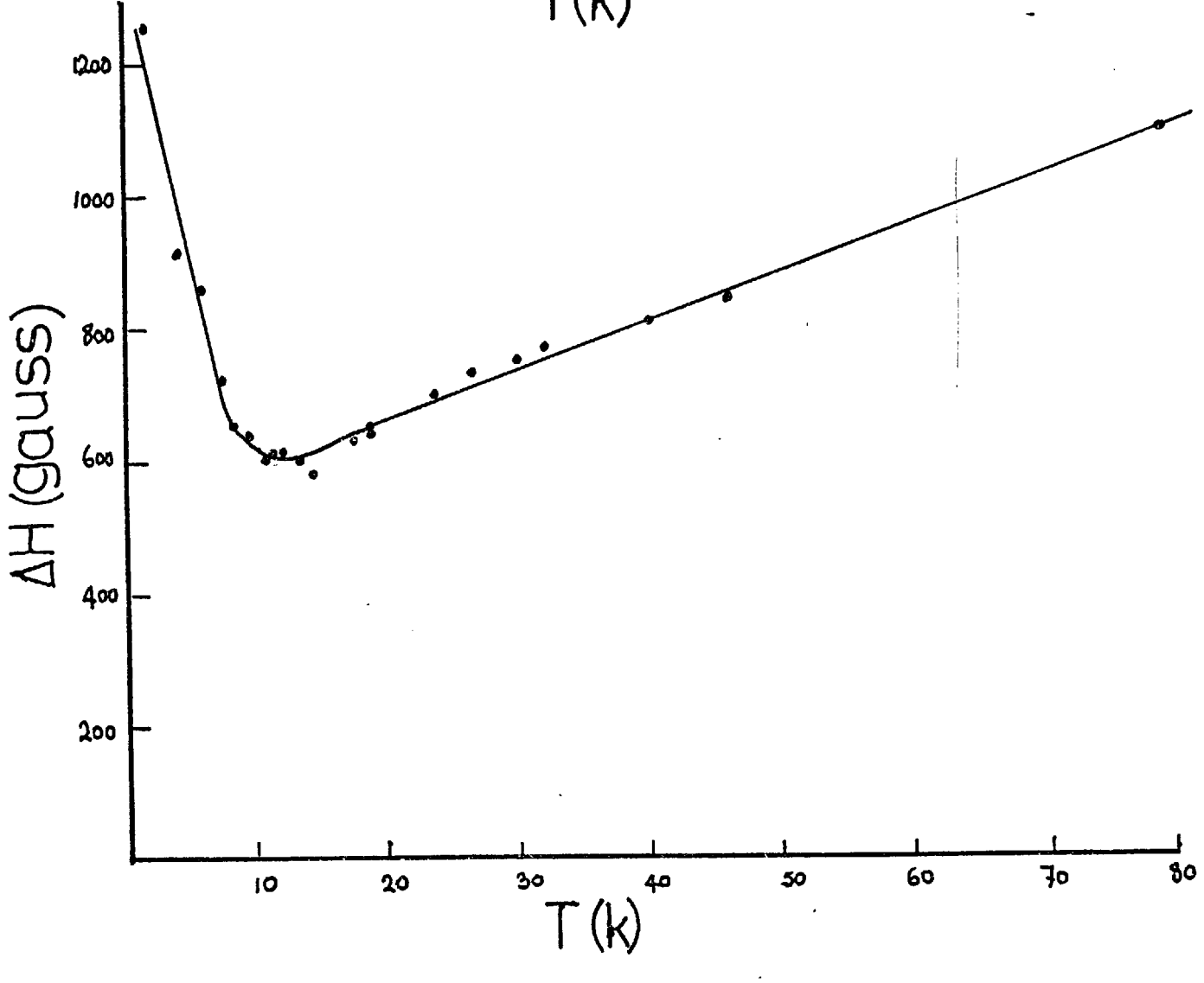

ΔH (gauss)
1200
1000
800
600
400
200
10
20
30
40
50
60
70
80
T (k)

FIG 8.5a

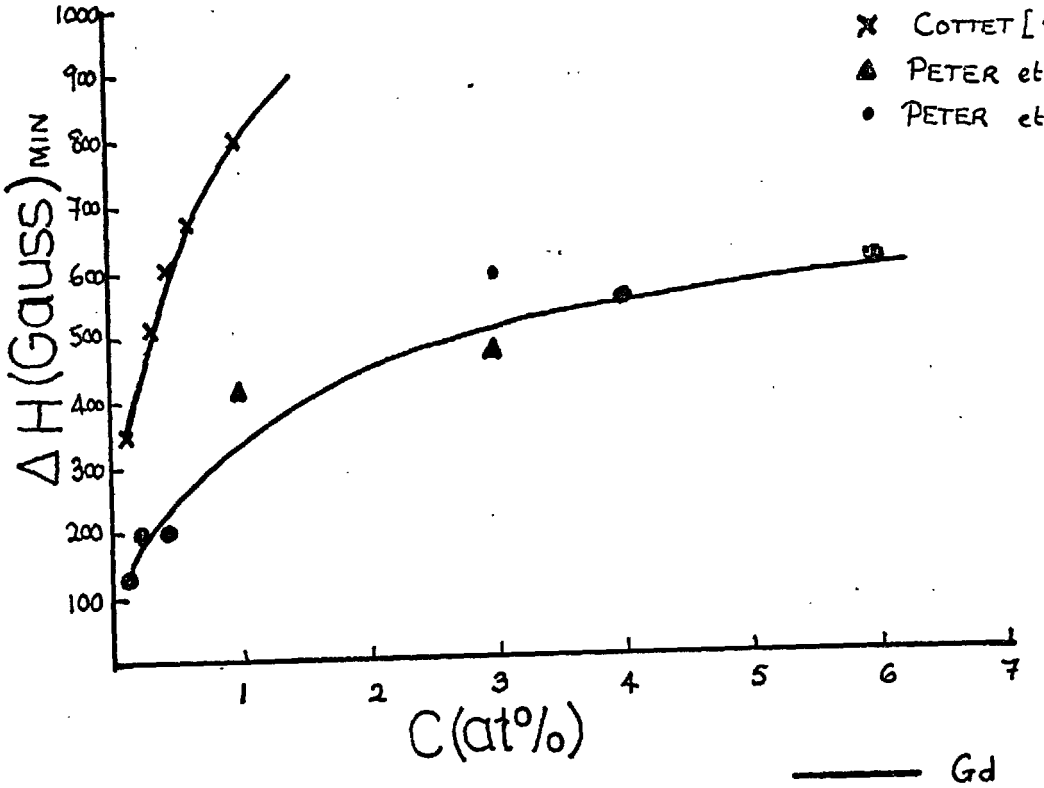
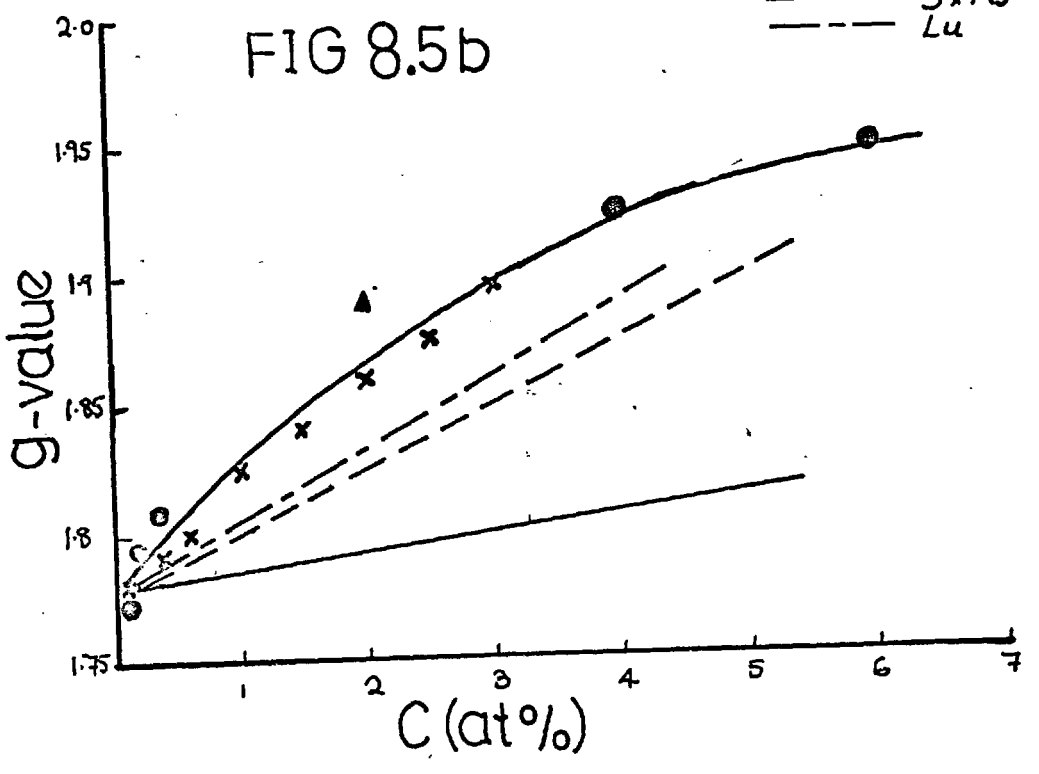


FIG 8.5b



8.2 Solid Solution Alloys containing Mn

(a) Pd-Mn

The esr study of the Pd-Mn system has been carried out in conjunction with Mr. A. Tari who has measured the resistivity of a number of Pd-Mn alloys, and Dr. H. Jamieson who has made susceptibility and magnetisation measurements. The esr runs in which a signal was observed are plotted in fig.s (8.6) to (8.13) and important data are summarised in Table (8.2).

The values of the slope of the linewidth against temperature show no systematic variation with concentration and yield an average value of $52 \pm 7 G.K^{-1}$. This is in good agreement with the result for the 2at% alloy measured by Shaltiel and Wernick (5.47) who obtained $\frac{d\Delta H}{dT} = 51 G.K^{-1}$. Cottet (5.30) investigated alloys containing up to 2at% Mn and found no systematic variation with concentration, but values ranging from about 60 to $75 G.K^{-1}$.

Probably the most notable aspect of the results is the large positive g-value of 2.15 ± 0.01 which leads, using the value of the susceptibility of pure Pd given by Peter et al (5.26), to a value of $J = + 0.012 \pm 0.001$ eV. The g-value is in excellent agreement with the value obtained by Cottet (2.14) but is rather higher than that of Wernick and Shaltiel (2.10). The large positive value of Δg may be explained by the theory of Coles et al (1.37) or by that of Campbell (1.42). In the former model, we argue that as the Mn ion is expected to form a Virtual Bound State, the admixture term in the Anderson Hamiltonian will lead to a negative coupling between the Mn moments and the conduction electrons; d-s hybridisation in Pd as in Pd-Fe (1.41) will then lead to a polarisation of the s-band antiparallel to the magnetisation of the d-band.

The sign of the g-shift is in agreement with the sign of the enhancement of the moment from static susceptibility measurements, but is far less than the value of the saturation moment ($7.5 \mu_B$ per atom) obtained in the high field work of Star et al (3.58). It is, however, in fairly

good agreement with the values obtained by Shaltiel et al (+ 11.5%) and Sarachik and Shaltiel (+ 12%). Taking these latter values we again note the curious fact that the g-value is enhanced by about half the amount obtained from static susceptibility measurements (c.f. $LaAl_2$ and Pd-Gd)

Pd-Mn DATA TABLE 8.2

C	$\frac{d\Delta H}{dT}$	ΔH_{min}	$T_{\Delta Hmin}$	Tg	g
0.6	50	250	2	2	2.15 ± 0.02
0.9	62	265	3.75 ± 1.0	2	2.14 ± 0.01
2.3	55	315	7.75 ± 1.0	5 ± 1	2.13 ± 0.01
2.5	57	330	8.75 ± 1.0	-	2.15 ± 0.01
3.75	40	375	9.5 ± 1.0	7 ± 1	2.14 ± 0.02
4.6	47	500	7.5 ± 1.0	6 ± 1	2.16 ± 0.02
6.0	52	720	8 ± 1.0	8 ± 1	2.16 ± 0.02
7.0	-	1000	8.5 ± 1.5	9 ± 1	2.17 ± 0.03
	Av. 52 ± 7				Av. 2.15 ± 0.01

Using the simple form of the Korringa relation (4.54), we obtain a value of $\frac{d\Delta H}{dT}$ from the measured value of Δg of about $550G.K^{-1}$. This suggests, as expected, that exchange enhancement is present and we obtain a value of $K(\alpha) \sim 1/10$ from equation 4.55.

The residual linewidth shows no systematic variation with concentration and an average value $\sim 110G$ is obtained. It is apparent from fig. (8.6) that in the 2.3at% alloy, which was the first measured in the Pd-Mn series, a small negative residual linewidth is obtained by extrapolating the high temperature data. This seems quite unphysical. It was at this stage that the thermometry experiments on the Ag-Cd alloy described in ch. 7 were carried out. It is clear from fig. (8.8) that to obtain even a zero intercept in the 2.3% data, all points from 6K to 13K would have to be

shifted to lower temperatures by more than 2.5K. This is a greater discrepancy in the measured temperature, extending over a much greater temperature regime, than was found in the Ag-Gd experiment. A further run on a 2.5at% alloy allowing a 'free' warm-up from liquid helium temperatures, which reduced the discrepancy in Ag-Gd, led to similar data with, again, a small negative intercept on the linewidth axis. Negative residual linewidths have also been observed for a number of intermetallic compounds (see 8.3(j), (1)).

It is possible that there is again a frequency dependence of the residual linewidth, since Cottet working at 35 Gc/s found a non-systematic variation in ΔH_{res} from 200 - 650G with an average value of about 400G and Wernick and Shaltiel obtained $\Delta H_{res} \sim$ 500G at 50 Gc/s in their 2at% alloy.

Neither of the previous esr investigations of the Pd-Mn system mention the effect of magnetic ordering. Cottet plots a series of straight lines through his linewidth data for temperatures down to 4.2K which, on the basis of this work, is not justified. It may be seen from figs. (8.7) to (8.13) that there is a well defined minimum in the linewidth and an upturn in g-value for all concentrations above 0.6at%. This we identify, as in Pd-Gd, with the increase in demagnetising fields as magnetic order sets in and the magnetisation increases. These fields, again, both shift the position of the centre of the line and inhomogeneously broaden it. In fig. (8.15) the temperature, $T_{\Delta Hmin}$, of the linewidth minimum and the temperature, Tg, at which the g-value begins to show an increase, are plotted against concentration. Both $T_{\Delta Hmin}$ and Tg increase with increasing concentration below about 2.5at% where the alloys are ferromagnetic at low temperatures, although it is noticeable that $T_{\Delta Hmin}$ rises more steeply than Tg. This may be due to the presence of short range order, which tends to broaden the line without shifting it.

These values seem to correspond fairly well with the concentration dependence of the Curie temperatures of the alloys as indicated by specific heat (3.54), resistivity (3.55(b) and 3.56) and susceptibility (3.57) measurements which are shown in fig. (8.14). As in Pd-Fe and Pd-Co, the specific heat and resistivity measurements seem to indicate rather lower values of the Curie temperature than the susceptibility data. The transition temperature in the Pd-Mn system below about 2% Mn increases at about 3 - 4K per at% compared with the values of 30 - 60K per at% found for Pd-Fe and Pd-Co; this seems to imply that the strength of the interactions is much less in Pd-Mn. The change of slope of the resistivity is very sharp at these concentrations and as discussed in ch. 3, Boerstel (3.54) finds cusped peaks in the specific heat. This latter observation suggests that the matrix is far more uniformly polarised than either Pd-Fe or Pd-Co where a broad scale of interaction strengths leads to far more rounded peaks. The disagreement as to the moment per Mn atom does not enable us to say whether the polarisation is relatively strong, as the results of Star et al (3.58) would suggest, or fairly weak, as suggested by those of Sarachik and Shaltiel (3.56) and Shaltiel et al (5.8). Neutron diffraction measurements are being performed at present by Prof. B. R. Coles et al to determine the form of the polarisation.

Above about 2.5% Mn, the ordering temperature indicated by the resistivity measurements of Tari begins to drop. As the concentration is increased, the point at which the slope of the resistivity changes becomes progressively less well-defined, until above about 4.1% the resistivity becomes a fairly smooth function of temperature and it is no longer possible to determine a transition point. Jamieson, from an Arrott plot, finds an ordering temperature of 1.25K for a 4.6% alloy and this is in good agreement with an extrapolation of the lower concentration resistivity results. Above about 5 - 6% Mn the susceptibility shows a broad peak at low temperatures and the temperature at which this peak occurs increases

with increasing concentration. This is in agreement with the data of Rault and Burger (3.57).

The esr data behave quite differently at these concentrations. Even allowing for the large error bars on the values of $T_{\Delta Hmin}$ and Tg, there is no indication of a drop in these values with increasing concentration. The value of $T_{\Delta Hmin}$ appears to remain fairly steady at about 8.5K between 2.5% and 7% Mn. The linewidth at which the minimum in ΔH occurs, ΔH_{min}, can be seen from fig. (8.16) to increase with concentration at an increasing rate, and indeed no resonance was observable for an 8.5% alloy. No signal was found in alloys containing 12at% and 20at% Mn.

The decrease in 'ordering' temperature obtained from the susceptibility data and the decrease in the magnetisation at 6KGauss measured at 4.2K, found by Rault and Burger for concentrations above $\sim$3at%, may be understood in terms of the increasing probability of Mn atoms to become nearest neighbours as the concentration is increased, leading, on the model of Moriya (2.9), to antiferromagnetic coupling between them through direct exchange. The probability of any Mn atom having another Mn atom as its nearest neighbour at a concentration of 1at% is about 0.12, which rises to $\sim$ 0.50 at 5at% Mn. We may thus say that at low concentrations the Mn atoms tend to couple ferromagnetically via the surrounding spin polarisation clouds, as in Pd-Fe and Pd-Co, but as the concentration of Mn is increased, an increasing antiferromagnetic contribution appears, until at above about 5 - 6at% Mn the antiferromagnetic coupling between Mn nearest neighbours predominates.

It is very difficult to interpret the behaviour of the characteristic temperatures obtained from the esr measurements. Jamieson has determined the magnetisation of a 4.5at% alloy at 4.2K, 3.7K and 1.7K in a field of 3KG and obtained magnetisations of 2.12, 2.36 and 2.86 emu per gm respectively. If we use these values and again assume an average

demagnetisation correction $\sim \pi M$, we obtain fairly good agreement with the observed g-values. However, the magnetisation drops with increasing concentration whilst the g-shift continues to increase. Jamieson finds a magnetisation of 1.58 emu per gm for a 6.5at% Mn alloy in a field of 3KG at 1.7K, whilst the g-value of the 6at% alloy reaches 2.55 at 1.8K, which corresponds in the crude approximation above to a magnetisation ~ 12 emu per gm. This behaviour is summarised in fig. (8.17). It thus appears that the esr measurements show a form which is consistent with <u>increasing ferromagnetic</u> behaviour with increasing concentration.

Jamieson has investigated the effect of field cooling on the alloys. No field cooling effects were found in the 4.5at% Mn alloy, but the 6.5at% alloy, when cooled in 5KGauss, gave a 'frozen-in' moment at low temperatures, similar to that observed in Rh-Fe and Rh-Mn by Murani and Coles (3.66). The M - H plot at 4.2K showed no asymmetry, as is shown in Cu-Mn alloys, but did show some hysteresis and time dependent remanence. An alloy containing 10.5at% Mn showed, on field cooling, signs of asymmetry in its M - H plot. Field cooling experiments have also been performed in esr. The alloys of 4.6, 6, 7, 8.5 and 12at% Mn were cooled to 1.7K in a field of 5KG and the results compared with alloys cooled in zero field. In no case was there any significant difference in the g-value, linewidth, amplitude (A + B), or intensity $(A + B)\,\Delta H^2$, either at 1.7K or in the subsequent warm-up (e.g. fig (8.77)).

This negative result is to be compared with the results of Griffiths (5.49) in the Cu-Mn alloys, where gross effects in all the above properties were observed on field cooling. Since the esr behaviour in Cu-Mn is not understood, it is clearly rather difficult to interpret the present negative results. In Cu-Mn, however, competing interactions exist through the RKKY polarisation, which for the simple matrix gives rise to both ferromagnetic and antiferromagnetic couplings of the Mn moments as well as the tendency towards antiparallel alignment of Mn atoms arising

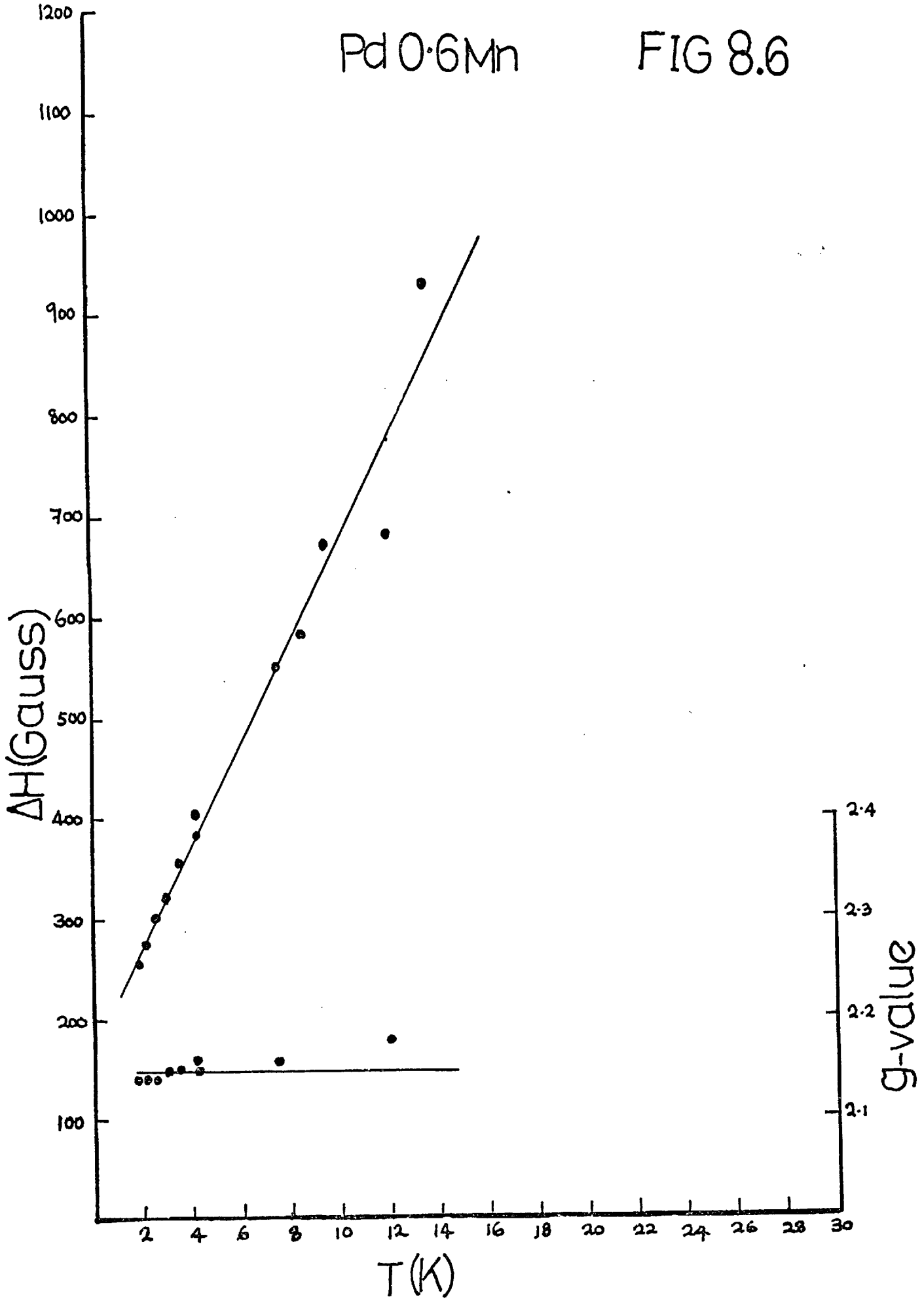
from the direct exchange between nearest neighbours. In Pd-Mn however, as discussed above, the conduction electron modulated part of the exchange is expected to lead predominantly to parallel coupling between moments (except in the lowest concentrations). This constitutes a fundamental difference in the two materials.

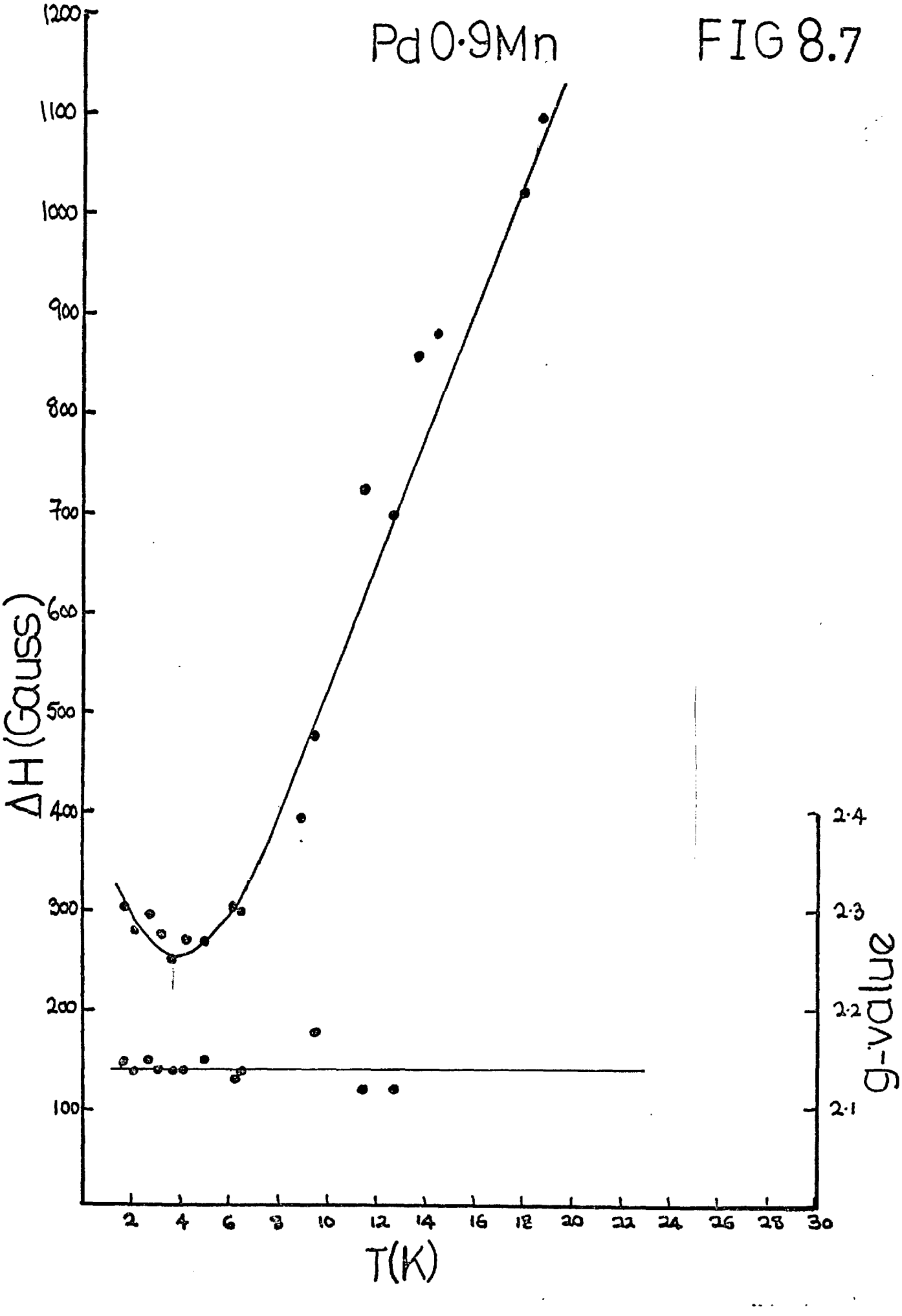
(b) Other Solid Solution Alloys containing Mn

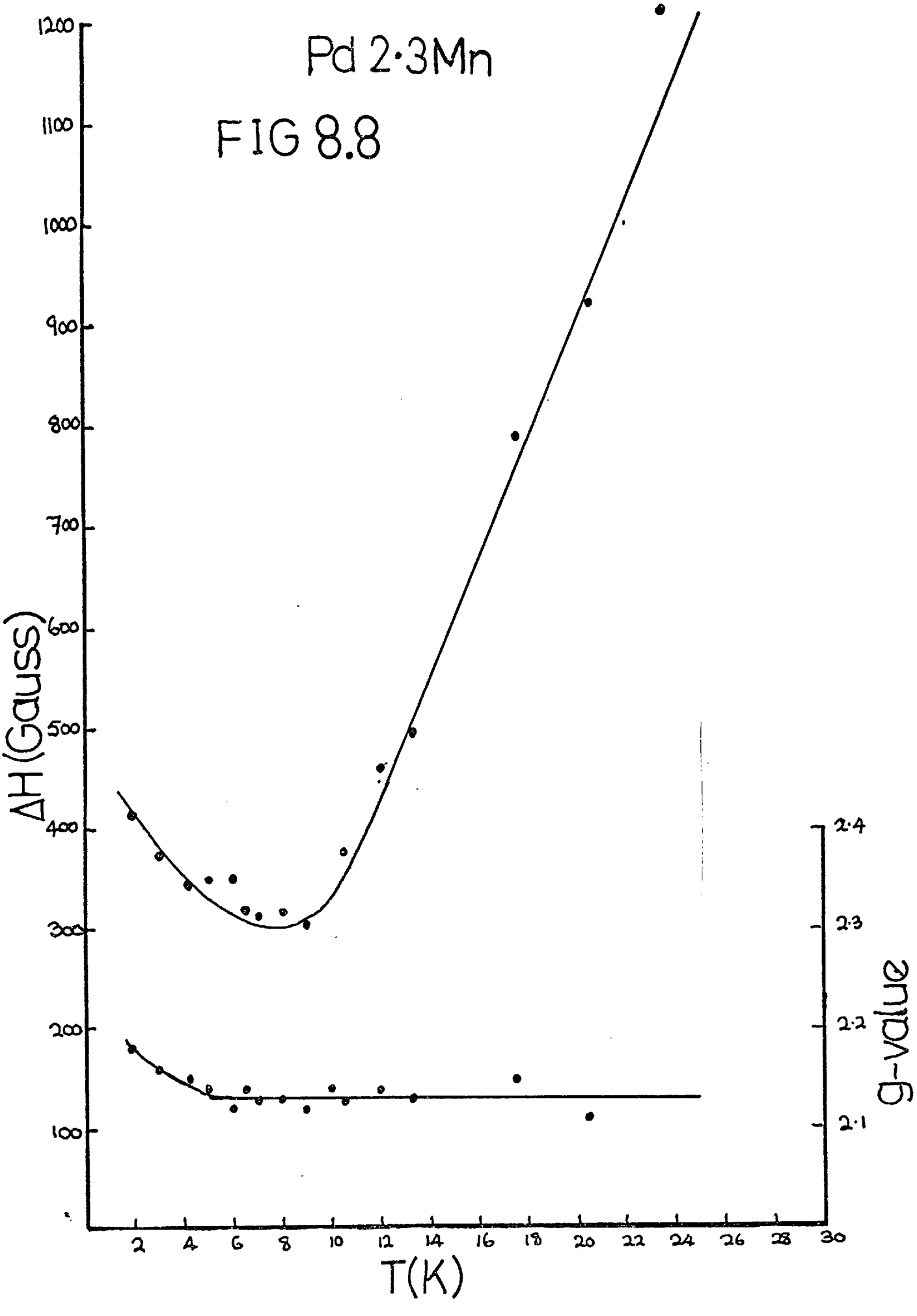
In order to try to gain more information about the effect of field cooling on the esr behaviour of various systems, experiments were carried out on alloys of Rh5% Mn and Rh10at% Mn. As discussed in ch. 3, these alloys show small displacements of their hysteresis curves and frozen-in moments when cooled in a field. The exchange enhancement of the Rh matrix seems to play little or no part in the onset of order and above about 3 at% the magnetic properties show similar behaviour to those of Cu-Mn and Au-Fe at lower concentrations. No esr signal was, however, observed from either sample when cooled in zero field or 5KG. Recently Dr. A. P. Murani has failed to detect a resonance, using the present spectrometer, in a 15% alloy cooled in zero field.

The Pt-Mn system would be an extremely interesting system to investigate. No esr data havebeen published as yet.

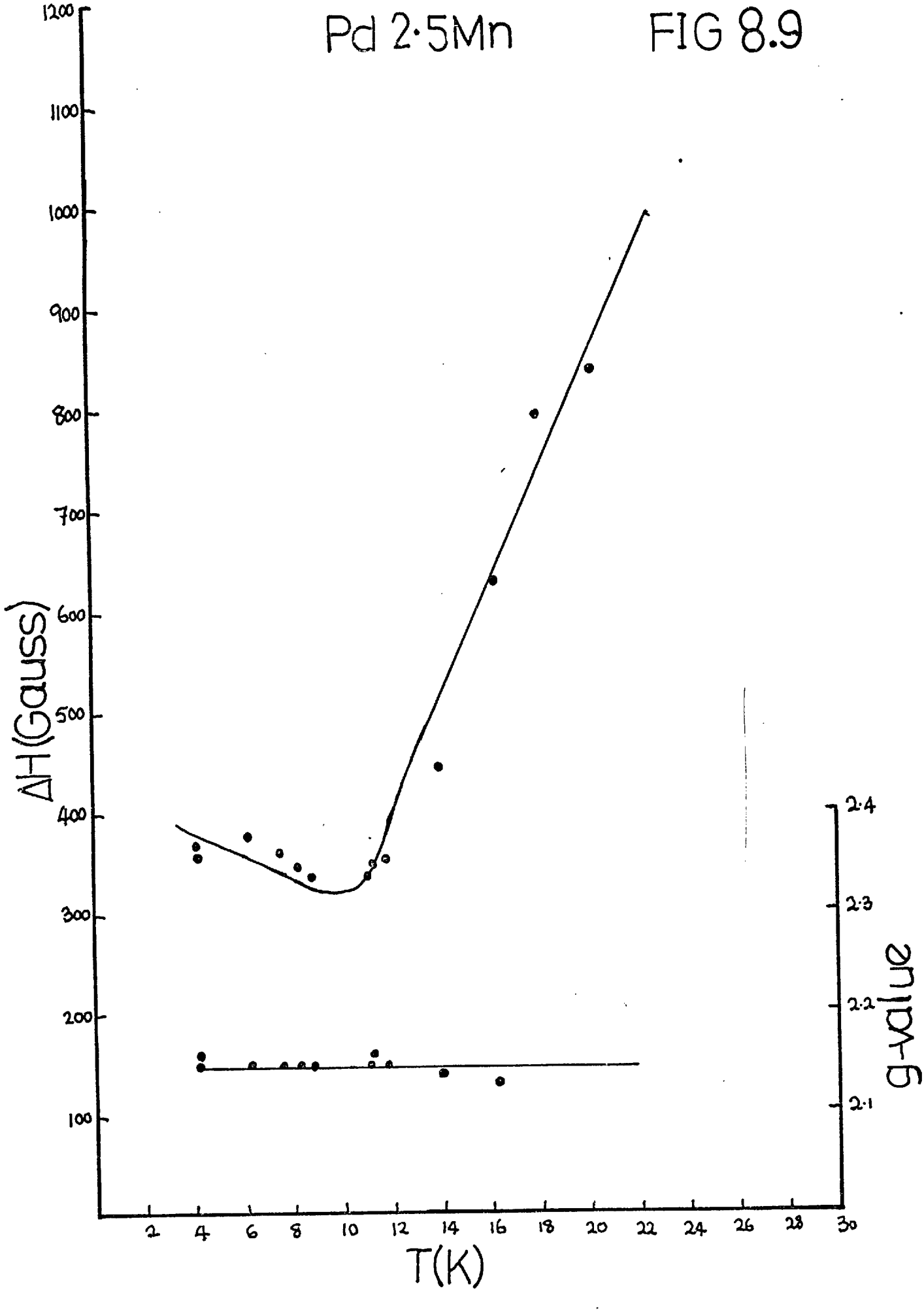
Experiments on the Zn-Mn solid solutions are discussed in the section below on $Zn_{13}Mn$ and $Zn_{10}Mn$ (8.3(1)).


Pd 0·6Mn
FIG 8.6
ΔH(Gauss)
1200
1100
1000
900
800
700
600
500
400
300
200
100
2·4
2·3
2·2
2·1
g-value
2
4
6
8
10
12
14
16
18
20
22
24
26
28
30
T(K)

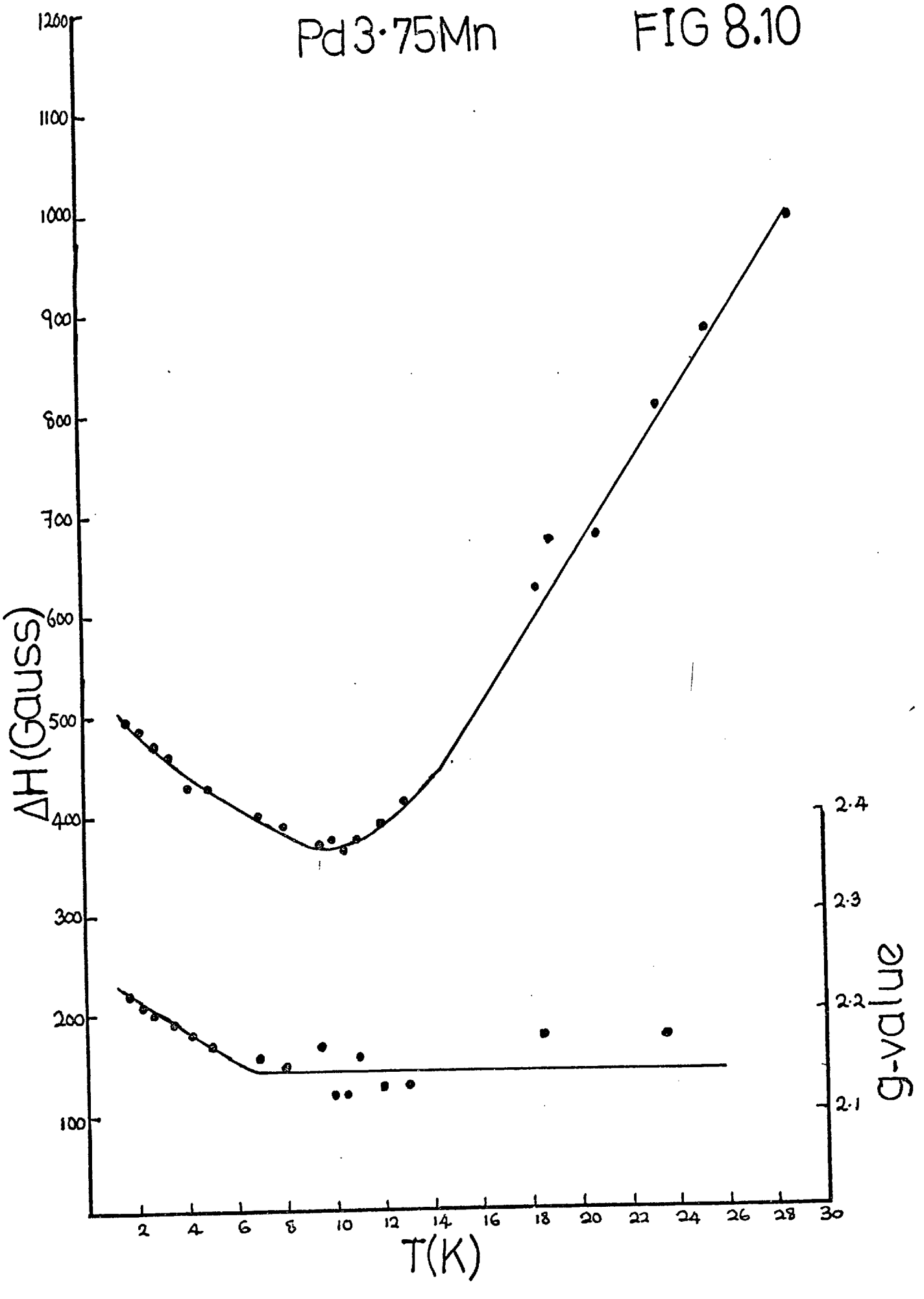

Pd 0·9Mn
FIG 8.7
ΔH (Gauss)
1200
1100
1000
900
800
700
600
500
400
300
200
100
g-value
2·4
2·3
2·2
2·1
2
4
6
8
10
12
14
16
18
20
22
24
26
28
30
T(K)

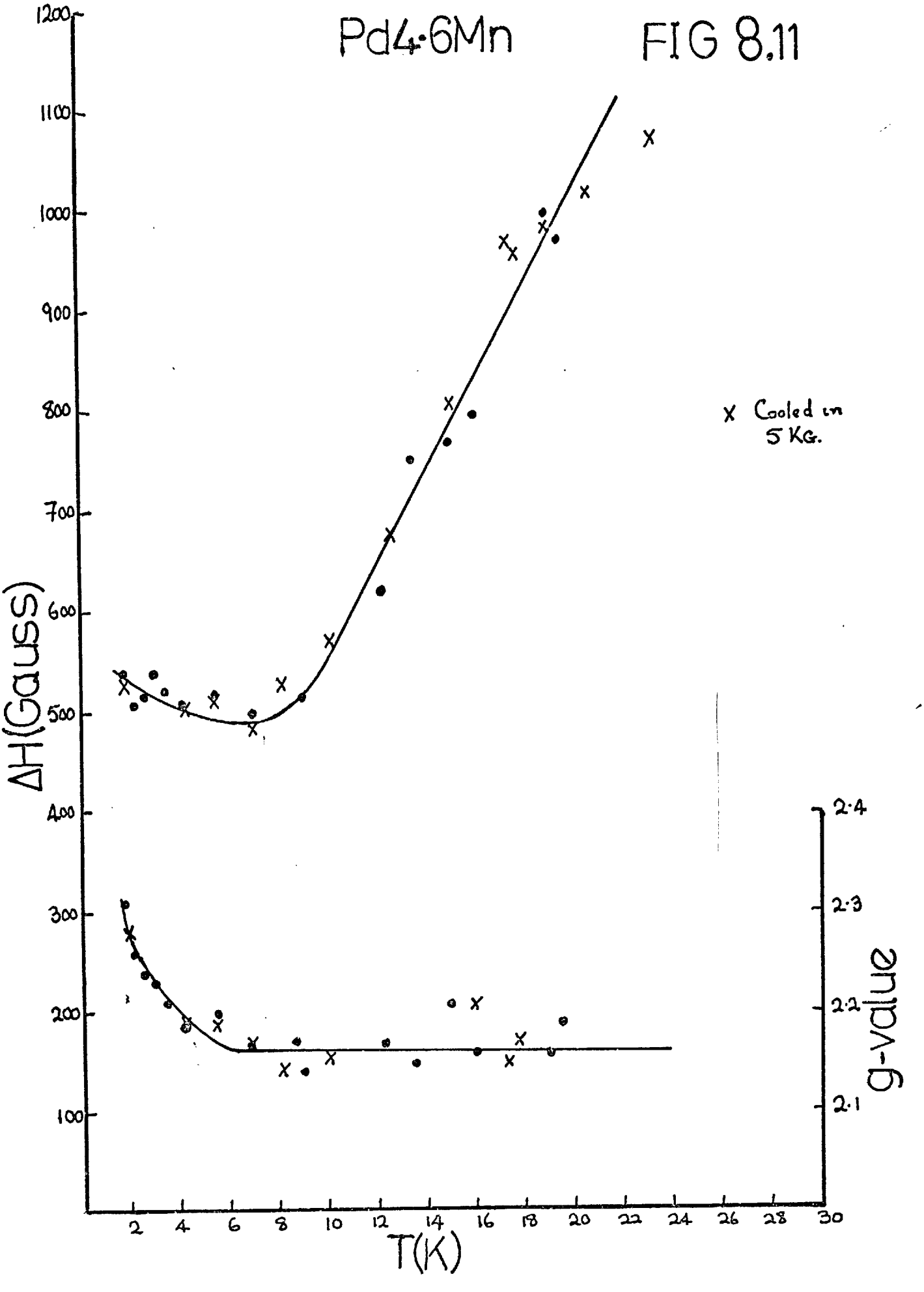

Pd 2·3Mn
FIG 8.8
ΔH (Gauss)
1200
1100
1000
900
800
700
600
500
400
300
200
100
2
4
6
8
10
12
14
16
18
20
22
24
26
28
30
T(K)
2·4
2·3
2·2
2·1
g-value

Pd 2·5Mn FIG 8.9

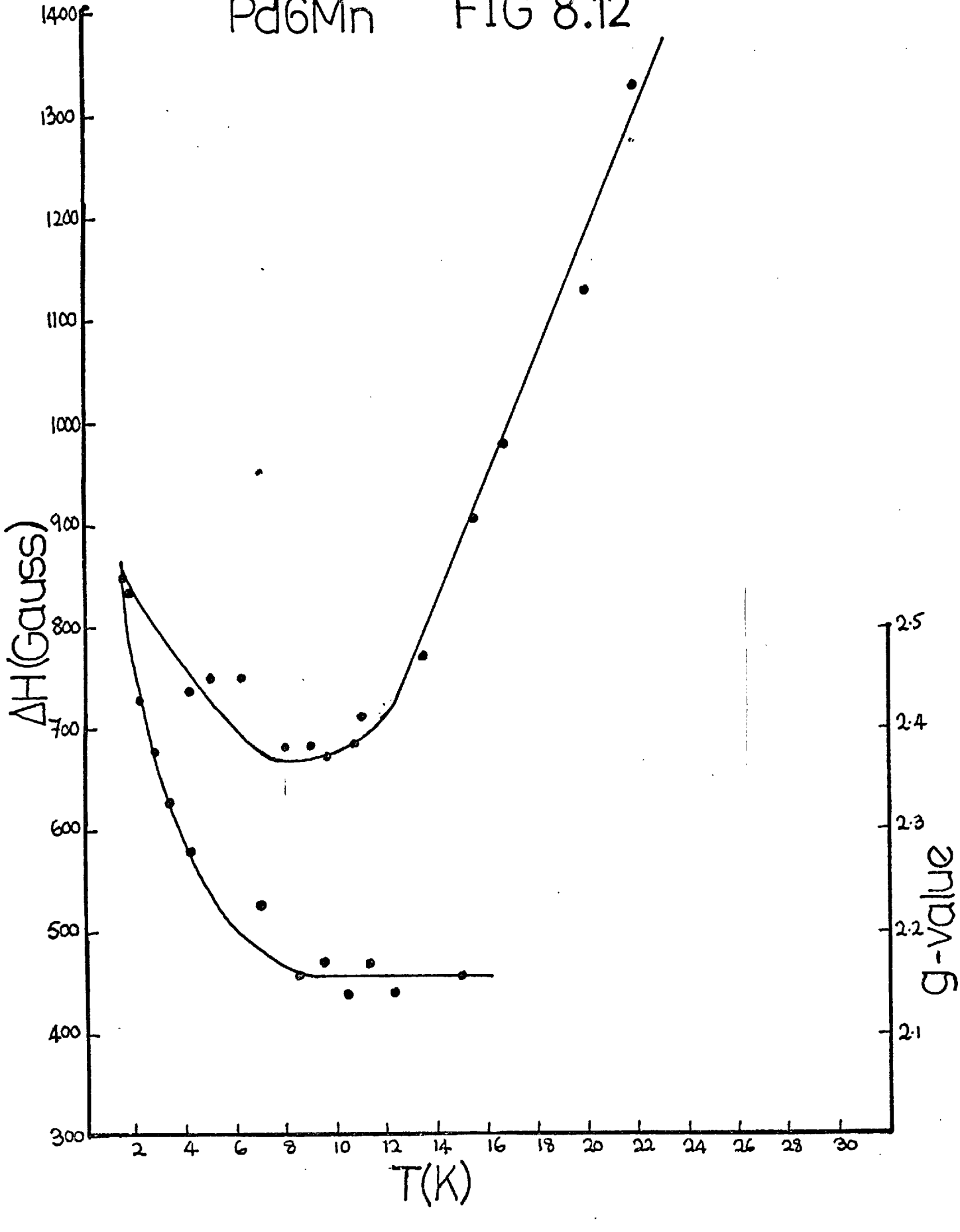


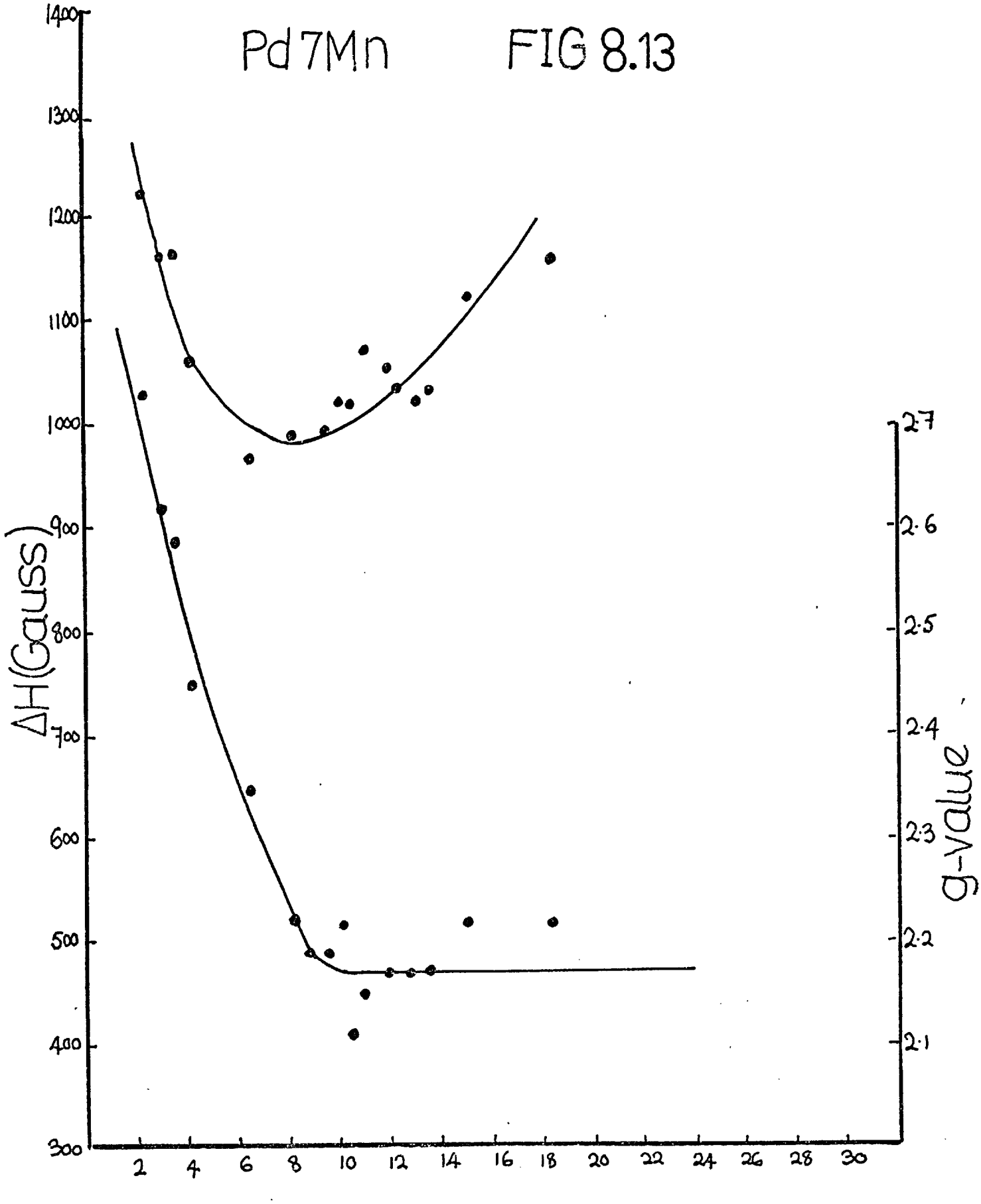
Pd 3·75Mn FIG 8.10




Pd4·6Mn
FIG 8.11
X Cooled in 5 KG.
ΔH(Gauss)
g-value
T(K)
1200
1100
1000
900
800
700
600
500
400
300
200
100
2·4
2·3
2·2
2·1
2
4
6
8
10
12
14
16
18
20
22
24
26
28
30

Pd6Mn FIG 8.12




Pd 7Mn
FIG 8.13
ΔH(Gauss)
g-value
1400
1300
1200
1100
1000
900
800
700
600
500
400
300
2·7
2·6
2·5
2·4
2·3
2·2
2·1
2
4
6
8
10
12
14
16
18
20
22
24
26
28
30

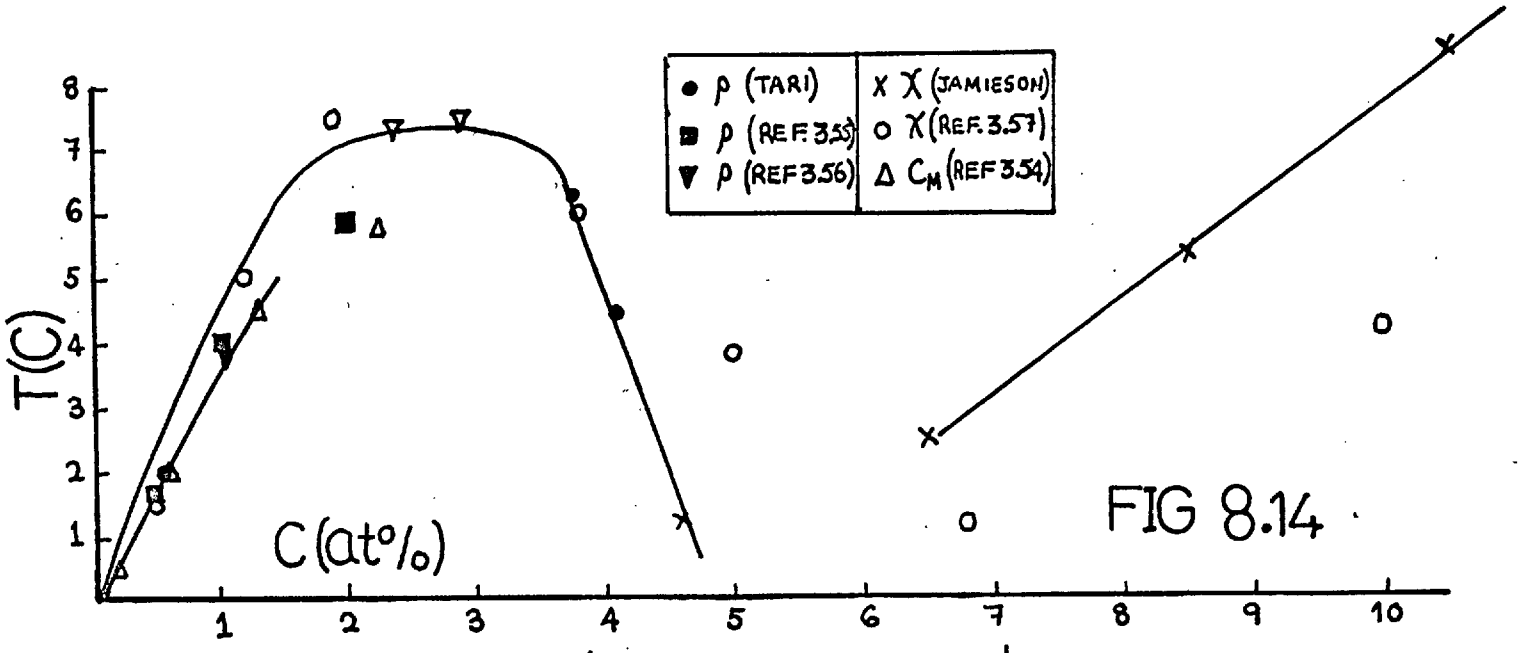


FIG 8.14

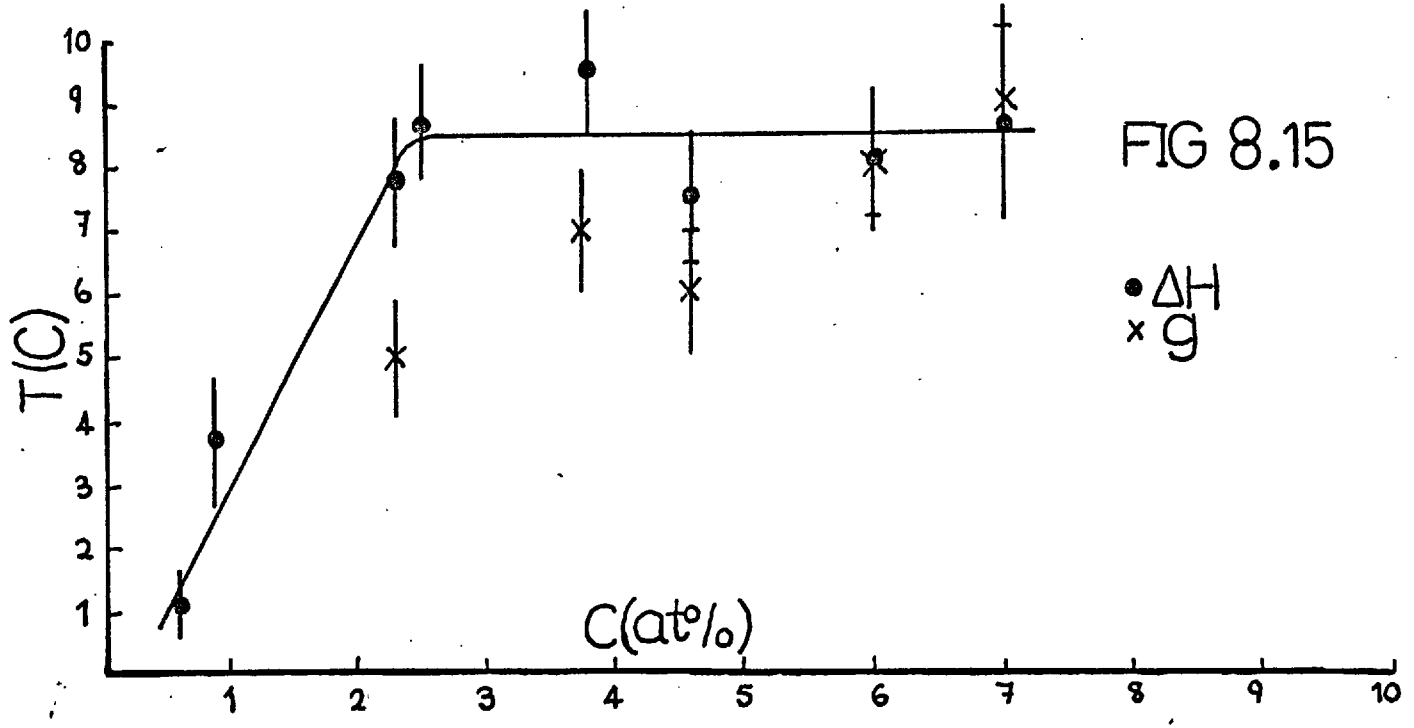


FIG 8.15

● ΔH
× g

FIG 8.16

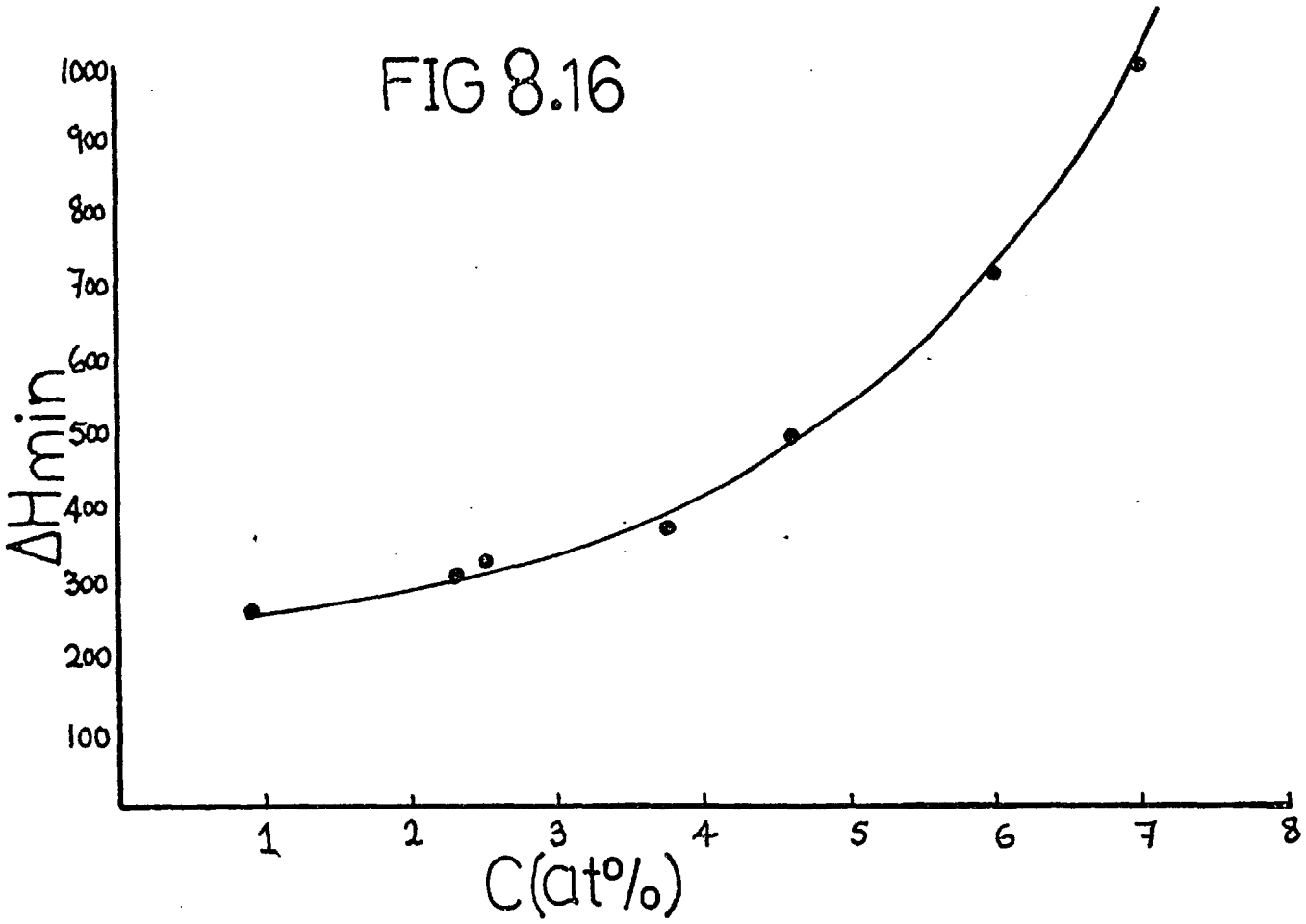
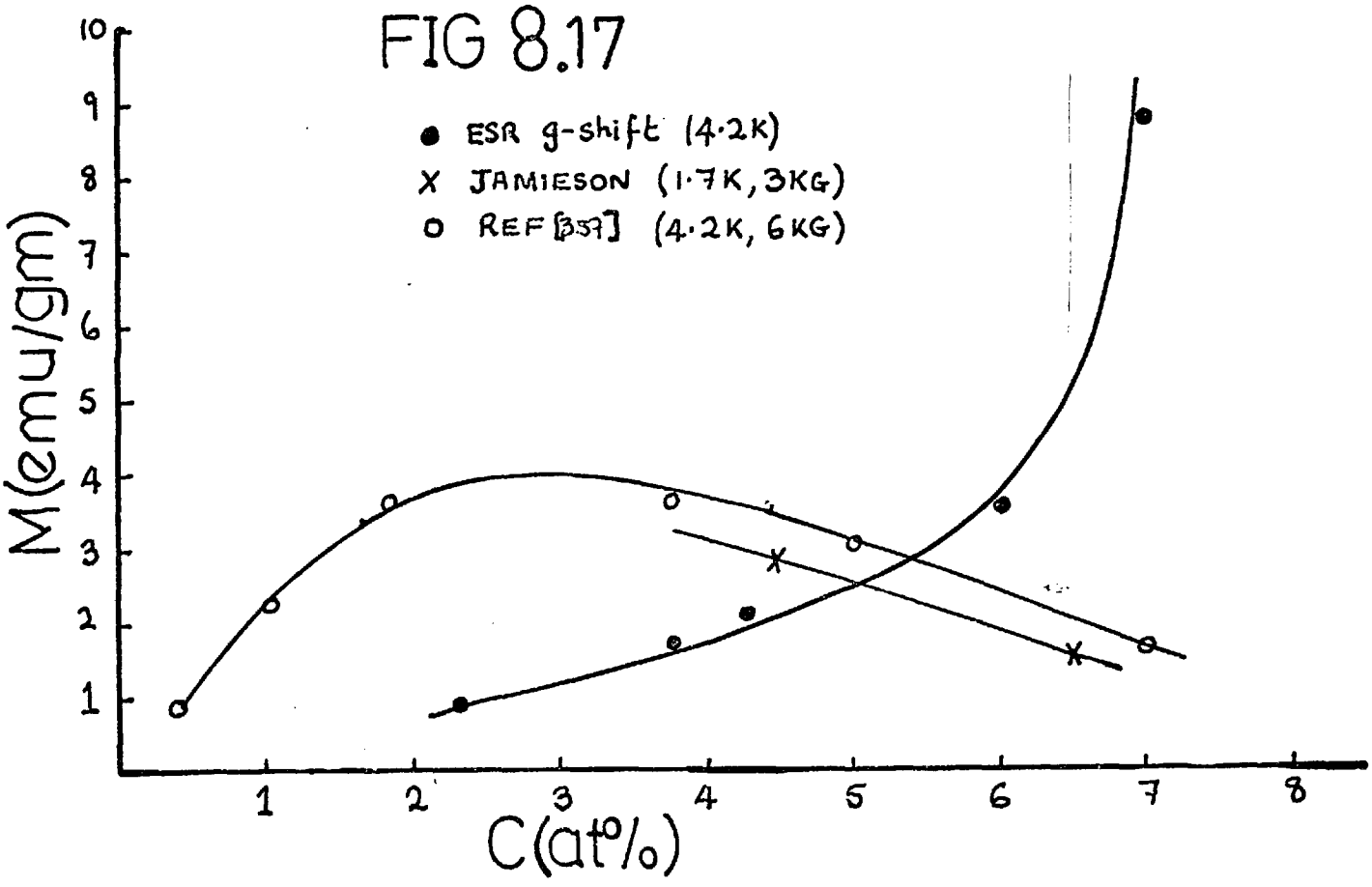


FIG 8.17



8.3 Intermetallic Compounds - Results and Discussion

The original motivation for the present study of the esr behaviour of intermetallic compounds containing s-state ions was to gain more information on the anomalous magnetic behaviour, described in ch. 3, exhibited by the compounds GdB_6, GdB_4, $GdZn_{12}$ and Gd_2Zn_{17}. This original work has led to a more extended study of the characteristic esr behaviour of other compounds containing Gd, Eu^{2+} or Mn in the vicinity of their Neel or Curie temperatures. In addition, the value of the g-shift and the high temperature slope of the linewidth have been compared with the values of the moment deduced from static susceptibility measurements and the sign of the g-shifts, compared with theory.

(a) Ag_3Gd

The esr results for this compound are shown in fig. (8.18). At temperatures above about 60K, a temperature independent g-value of $g = 2.00 \pm 0.02$ is obtained. The large error quoted on this value reflects the large linewidth and the consequent uncertainty in the correction factor discussed in ch. 7. We note that in the Ag 0.2 Gd alloy measured in this work and discussed in ch. 7, a value $g = 1.995 \pm 0.005$ was obtained, in good agreement with the results of Nakamura et al (5.36) and Griffiths and Coles (5.37) and with the value for the compound quoted here. In the model of Coles et al (1.37) for the sign of J we would expect $\Delta g > 0$ for this compound and, whilst the error is such that no definite conclusions can be drawn as to the sign of Δg in this case, the result is not inconsistent with a positive g-shift. The high temperature linewidth shows a slope of $\sim 0.7 G.K^{-1}$ and this agrees well with the proximity of the observed g-value to the Gd free ion value. At about 70K the linewidth shows a minimum and at lower temperatures broadens rapidly; the centre of the esr line also shifts to lower fields.

This behaviour, commencing at about $2T_N$, we associate with the onset of magnetic order. Below the Neel temperature (35K) no signal is observable.

(b) $\underline{GdAl_2}$

Fig. (8.19) shows the esr results on the compound $GdAl_2$. Two samples were, in fact, measured and they gave almost identical results.

In the paramagnetic regime above about 200K, the corrected g-value is 1.989 ± 0.005 and this is in fair agreement with the value obtained by Peter et al (5.6, 5.26) of 1.982 and with the recent work of Hacker et al (5.12) who quoted a room temperature g-value of 1.984. These results appear to confirm a negative g-shift for this compound, which is rather surprising since, as discussed above, the g-shift of Gd in $LaAl_2$ is unequivocally positive; the sign of Δg is, furthermore, in disagreement with the predicitions of the theory of Coles et al. At 300K, demagnetising effects are expected to be negligible (5.26) and above 200K in the present study the g-value is temperature independent. One possible explanation for the negative g-shift may be that the large concentration of Gd in this compound complicates the band structure by conferring to it considerable d-character. Use of a free electron picture gives $E_F \simeq 5.1$ eV for $GdAl_2$, assuming three conduction electrons per lattice site, and leads, using the measured g-shift and equation 4.41, to a value $J = -0.02$ eV.

The linewidth in the paramagnetic regime has a slope of 2.1 $G.K^{-1}$. This is in good agreement with the value of 2.3 $G.K^{-1}$ quoted by Peter et al and is in fairly good agreement with the value predicted by the Korringa relation, 4.54. The absolute value of the linewidth at 295K is 517 ± 25 Gauss, and the value of 445 ± 20 Gauss at 260K is again in excellent agreement with the data of Peter et al who quoted a value of 500 Gauss for the half-width at half-power.

Below about 200K the resonant field begins to shift to lower values and the line broadens. The susceptibility and resistivity measurements, discussed in ch. 3, all quote values for the Curie temperature of $GdAl_2$ between 150K and 180K, with the most careful measurement (3.6) suggesting T_C = 167.8K. The behaviour of the resonant field and linewidth is thus, as in the Pd-Gd alloys discussed above, to be associated with the transition to ferromagnetism. If the magnetisation data of Hacker et al for $GdAl_2$ in 3KGauss are used, a fairly good fit to the experimental points for H_x may be obtained by using a demagnetising factor FM, with $F \sim 2.7$ in this case. These points are shown as solid triangles in fig. (8.19). In comparing the value of 2.7 used here, with the value $\sim \pi$ used to fit the resonant field data for Pd-Gd, it should be borne in mind that the powders for the two samples were produced in entirely different ways, and it is thus not surprising that the factor, F, should be different in the two cases.

Because of the crudeness of the estimated demagnetisation factor, it is clearly impossible to make any meaningful comments about the g-value in the ferromagnetic regime. In order to obtain g-values below 200K, small regular shaped specimens such as discs or plates (with a consequent loss of surface and thus intensity) would have to be fabricated and a careful analysis of the demagnetisation corrections at different orientations made, as in the work of Rodbell and Moore on pure Gd (5.4).

We note that if we identify the temperature at which the linewidth begins to broaden by $T_{\Delta Hmin}$ and the temperature at which the shift in resonant field begins by Tg,

$$\frac{T_{\Delta Hmin}}{T_C} \sim \frac{Tg}{T_C} \sim 1.2$$

(c) GdB_6 and GdB_4

Fig. (8.20) shows the esr data for GdB_6. The g-value remains constant between 70K and 300K at a value of 2.00 ± 0.01 and this value is in excellent agreement with the results of Coles et al (5.15) and Miller and Hacker (5.16). A figure of 334 ± 15 Gauss is obtained for the linewidth at 298K and this is found to broaden to 425 ± 20 Gauss at 77K, again in good agreement with the previously obtained fixed temperature data.

No previous esr data have been published for GdB_4. The g-value (fig. (8.21)) at 300K is 2.10 ± 0.03 and the linewidth broadens from 1143 ± 55 Gauss at room temperature to about 1600 Gauss at 77K. The rather large error bar on the g-value for this compound reflects the fact that the GdB_4 line was both broad and of fairly low amplitdue; lineshape corrections are thus difficult to determine with accuracy. A stress annealed sample of GdB_4 gave precisely the same linewidth and g-value.

The increase in the g-value over the free ion value obtained for GdB_6 is in quite good agreement with the slight increase of the effective moment reported by Fisk (1.6). The g-value of GdB_4 is enhanced by $\sim 5\%$, whilst the effective moment is close to the free ion value.

The Néel temperatures of GdB_6 and GdB_4 are 14K and 42K respectively (1.6) and once again, as in the case of Ag_3Gd, no signal is observed below these temperatures. Above T_N the linewidth broadens with decreasing temperature for both compounds, and in both cases there is also an apparent shift in the resonant frequency. Unlike Ag_3Gd, however, it is impossible to say from the data whether the decrease in H_x constitutes a genuine shift to lower resonant fields on approaching T_N, or whether it merely reflects an incomplete lineshape correction in this region of rapid line broadening.

The most remarkable aspect of the present results is the increase in linewidth which sets in at temperatures of about seven times T_N in the case of GdB_6 and four times T_N for GdB_4. The explanation of this behaviour must be related to the anomalies shown by the compounds in their other properties above T_N. As discussed in ch. 3, GdB_6 (3.31, 3.32) shows deviations from Curie-Weiss behaviour (fig. (3.2)) at about 80 - 100K, its resistivity shows a larger temperature dependence than is expected in this temperature regime, the specific heat shows an anomaly at 30K and $\theta/T_N \sim -4$ whereas $\theta/T_N \sim -1$ for DyB_6. TbB_6 shows similar, but less marked, behaviour. GdB_4 shows deviations from Curie-Weiss behaviour at about 60K and measurements of the resistivity of the heavy rare earth tetraborides made in conjunction with this study by Fisk, are shown in fig. (8.22). The resistivity of GdB_4 clearly shows a similar form to GdB_6 above T_N.

These effects cannot, of course, be attributed to the crystal field, since in Gd compounds the crystal field splitting is expected to be $\sim$ 0.1 - 1K. Measurements by Fisk (1.6) of Gd in YB_6 support this view, showing Curie-Weiss behaviour to 1.5K. Fisk suggested that the free energy of simple long-range order in GdB_6 may be adversely affected by its effects on the conduction electron configuration. With one free electron per unit cell, the first Brillioun zone is half full and Mattis and Donath (2.28) showed that the simple Neel type antiferromagnetism is expected to occur on a free electron model for this electron concentration. When ordering occurs at a temperature $\sim |\theta|$, an energy gap develops and splits each zone in half. The size of the gap is given approximately by $\underline{J}\ (g - 1)\ \underline{J}_z$ (2.32), which is largest for s-state ions and $\sim$ 0.25 eV for GdB_6. These superzone band gaps might significantly modify the conduction electron energy spectrum and the RKKY interaction and prevent the ordering from going to completion. At 14K, it is suggested, the compound orders into an alternative spin structure. Fisk suggests that similar effects may occur in GdB_4.

An alternative explanation might be that the tendency to reduce magnetic entropy by short-range order is much greater than to reduce it by long range order, over the temperature regime in which anomalous behaviour occurs. MnO orders antiferromagnetically at 116K, but neutron scattering still shows the presence of short-range order at room temperature. As discussed in ch. 4, a number of antiferromagnetic insulators, including MnO, show an increase in esr linewidth at temperatures several times T_N and in a number of cases $\frac{\theta}{T_N}$ is correspondingly high.

The linewidths of a number of the insulators discussed in ch. 4 were found to be well described in the short-range order regime by the expression of Kawasaki (4.24), although values of $|\rho|$ ranging from $\frac{1}{2}$ to 6/5 were observed, as against the theoretical value of 5/3. Plots of $\ln (T - T_N)$ v $\ln|(\Delta H - BT)$ for the present data are shown in fig. (8.23b). In the case of GdB_6, a reasonable straight line fit may be made to the limited number of points available between 25K and 78K and $|\rho| \sim 1.4$. The data for GdB_4 likewise gives a reasonable fit between 66K and 122K with $|\rho| \sim 1.6$. It is not clear how significant these results are since, of course, data fitted to a logarithmic relation over only one decade must always be treated with considerable reservation; it is, however, extremely difficult to measure accurate values of the linewidth for $T < T_N + 10$, where the lines are so broad. The temperature also drifts during the course of a sweep.

The behaviour of these compounds above their ordering temperatures will finally only be clearly elucidated by neutron diffraction measurements. The common Gd and B isotopes have very high neutron absorption cross-sections and thus experiments can only be performed on samples of Tb borides prepared from the B^{11} isotope (see ch. 6). It might well be argued that in the Tb compounds, crystal field effects may be important, but the similarity between the magnetic properties of the Tb and Gd borides suggests that the mechanisms causing the bizarre behaviour may be the same. The effect of

crystal fields in the non s-state ions might possibly lead to a suppression of some of the short-range order and this may account for the fact that the observed effects are largest in the s-state ions. Preliminary neutron diffraction experiments show fairly strong magnetic peaks at 4.2K in TbB_6^{11}, and from these it is hoped to elucidate the hitherto unknown magnetic structure of the hexaborides.

No signal was observed from a sample of ErB_4 at 4.2K.

(d) Cu_2Gd, "Cu_4Gd" and Cu_6Gd

The data for the Cu_2Gd compound is shown in fig. (8.24). The g-value in the paramagnetic regime between 60K and 300K is constant at 2.013 ± 0.005 and the positive g-shift is in good agreement with the prediction of the theory of Coles et al, despite the relatively high concentration of Gd (c.f. $GdAl_2$). Using a free electron model and assuming five conduction electrons per formula unit, values of $E_F = 6.5$ eV and $J_{eff} = +0.016$ eV are obtained. The linewidth in the paramagnetic regime has a slope of 2.5 $G.K^{-1}$ compared to a value ~ 6 $G.K^{-1}$ deduced from the Korringa relation. The increase in the g-value over the free ion value ($\sim +1\%$) is rather less than the enhancement of 6% found from susceptibility measurements (3.19).

At low temperatures the esr measurements confirm thatthe compound orders antiferromagnetically. The linewidth shows a minimum at $T_{\Delta Hmin} \sim 65$K and below this temperature the line broadens very rapidly. The lowest temperature at which a resonance is observed is 37 ± 1K, where $\Delta H \sim 2$KGauss. This suggests that the value for T_N quoted by Brun and Felchner (3.20), 41K, may be a little high. The apparent shift in the resonant field could again be due to the incomplete inclusion of the line-shape correction.

Assuming a value of $T_N \sim 40K$, we note that $T_{\Delta Hmin}/T_N \sim 1.6$, which is far less than the values obtained for the borides above. Some short-range order (ch. 2)is, of course, expected and in this case, like Ag_3Gd, its extent is quite unexceptional. This compound is one of the few in which the magnetic structure is known (3.20), but in the absence of comparable data for the compounds which show the anomalous behaviour, there is no possibility at present of correlating the observed extent of the 'pseudo ordering' with magnetic structure.

No magnetic or structural data are available for the compound containing about 20% Gd and labelled "Cu_4Gd" and this provides an opportunity to predict the magnetic behaviour from the esr data. The results are shown in fig (8.25).

Between 40K and 160K, the g-value remains constant at 2.01 ± 0.01, with the expected positive g-shift. The slope of the linewidth at high temperature is 4.5 ± 2.5 $G.K^{-1}$; the large error bar on this value reflects the broad and weak signal obtained at temperatures much above 100K. Substituting the measured g-shift into the Korringa relation suggests a value for the slope ~ 5 $G.K^{-1}$, in good agreement with the value above.

By comparison with the previous compounds, the form of the esr data would suggest that this compound orders antiferromagnetically at $T_N \sim 15K$. The linewidth shows a minimum at a temperature $T_{\Delta Hmin} \sim 50K$ and thus, in this case, $T_{\Delta Hmin}/T_N \sim 3.5$, which is similar to the value found for GdB_4. These esr results suggest that "Cu_4Gd" may also exhibit anomalous magnetic behaviour above T_N, and a sample is at present being prepared for measurements of its resistivity and susceptibility.

The interesting behaviour shown by "Cu_4Gd" led to interest in the magnetic properties of the compounds at the copper rich end of the system. The esr data for the compound Cu_6Gd is shown in fig. (8.26). Again, no other magnetic data are available.

The corrected g-value for the compound is constant above 60K with a g-value of 2.025 $\pm$ 0.010, and on a free electron model we obtain E_F = 6.3 eV and J_{eff} = +0.007 eV. The slope of the high temperature linewidth is $\sim$ 7 $G.K^{-1}$ which is about three times less than the value predicted by the Korringa relation using the measured value of g.

By analogy with the result for the $GdAl_2$ compound, using the value $\frac{T_{\Delta H_{min}}}{T_N} \sim 1.2$ found in that case, Cu_6Gd would appear to order ferromagnetically at T_C = 45 - 50K.

(e) $\underline{GdIn_3}$

The susceptibility measurements on this compound (3.11) suggested that there were no significant deviations from Curie-Weiss behaviour above T_N and neutron diffraction experiments (3.12) confirmed the absence of an appreciable range of short-range order in $TbIn_3$.

Unfortunately, both the samples of $GdIn_3$ gave only low amplitude signals with linewidths at 295K and 77K in excess of 2.5KGauss. These widths were not reduced by stress annealing the samples and no useful data could be obtained.

(f) $\underline{Pd_2Eu \text{ and } PdEu}$

The results of the measurements on the Pd_2Eu compound are shown in fig. (8.27). Between 120K and 300K the corrected g-value is 2.01 $\pm$ 0.01 and the positive g-shift is consistent with the idea that the Pd d-band is full in this compound. The linewidth at room temperature is 430 $\pm$ 20 Gauss and the linewidth has a slope of 0.6 $G.K^{-1}$, which is a factor of four or five less than the value predicted by the unenhanced Korringa relation.

The shift of the resonant frequency to lower fields and the increase in the linewidth below about 100K, closely resembles the behaviour of $GdAl_2$ at somewhat higher temperatures, and it is thus to be concluded that Pd_2Eu is ferromagnetic at low temperatures. If we assume a factor $T_{\Delta H min}/T_N \sim 1.2$, as in $GdAl_2$, a Curie temperature of $\sim$ 80K is obtained which is in excellent agreement with the values of the Curie-Weiss obtained by Wickman et al (3.27) and by Harris and Longworth (3.26).

The PdEu compound gave, below about 100K, a distorted signal which would appear to be attributable to the second phase (probably Pd_2Eu) reported to be present in the sample by Longworth. At higher temperatures, however, a good single resonance was observed with a g-value of 2.007 ± 0.010 and a linewidth at room temperature of 740 ± 35 Gauss. The slope of the linewidth is ~ 0.8 $G.K^{-1}$ which, again, is rather smaller than the value predicted by the simple Korringa relation.

Below 100K, despite the complicating effects of the second phase, there does appear to be a broadening of the original signal and this is not inconsistent with the recent results of the Mössbauer study of Longworth which suggests that the compound becomes ferromagnetic at about 50K.

(g) $\underline{Pd_3Gd, Yb}$

The esr results on the Pd_3Gd compound are shown in fig. (8.28). The corrected g-value is constant from about 15K to 77K and equal to 2.04 ± 0.01. Above 77K the intensity of the signal becomes too weak to ascribe a g-value. The linewidth shows a slope in the paramagnetic regime of 6 $G.K^{-1}$ and at 78K the line is 1450 ± 50 Gauss broad. As in

the Pd-Eu compounds, the positive sign of the g-shift suggests, in agreement with other observations described in ch. 3, that the d-band in this compound is full. The measured g-shift suggests, once again, a larger slope (~ 40 G.K^{-1}) than is observed, but agrees well with the enhancement of the paramagnetic moment reported by Gardner et al (3.23) and Hutchens et al (3.25).

The behaviour of the compound close to the ordering temperature is puzzling. The previous magnetic data suggest strongly that, at low fields, the compound is an antiferromagnet with $T_N = 7.5$K and on the basis of the other work in this thesis on antiferromagnets, we might have expected a shift in resonant frequency and broadening of the line at, (in the absence of deviations from Curie-Weiss behaviour in the inverse susceptibility), about $2T_N$ and no signal below 7.5K. The shift in resonant field and line broadening from about $2T_N$ are observed, but the resonance may be followed to the lowest temperature of 1.8K.

The clue to this behaviour may lie in the fact that Pd_3Gd is in fact a metamagnet; fairly low fields $\sim$ 6 - 7KGauss being required to produce a transition from antiferromagnetic to ferromagnetic order. Very similar behaviour was observed in $EuAl_4$ by Wernick et al (5.9). Here, a signal was reported at 1.8K, about 4K below the Neel point for the compound and, again, the esr measurements were made in a field close to the critical field for a transition from antiferromagnetism to ferromagnetism ($\sim$ 15KGauss).

The esr data obtained in the present experiments showed no anomalies at 7.5K, a single resonance line being observed with no pronounced changes in intensity or shape.

The interesting behaviour of Pd_3Gd and $EuAl_4$ suggests a number of experiments:

(i) An investigation of the behaviour of $EuAl_4$ at X-band. It would be interesting to see whether in a field of 3KGauss ($\sim 1/5\ H_{crit}$) 'normal' antiferromagnetic behaviour was shown in esr.

(ii) A study of other systems which show metamagnetic properties in low fields, such as $GdZn_2$ (3.30) and $EuAl_2$ (3.2, 5.6), with a view to establishing a relationship between the type of esr behaviour close to the ordering temperature and the ratio of measuring field to critical field.

(iii) An investigation of the effects of cooling the samples in fields of various strengths. A sample of Pd_3Gd cooled in 5KGauss showed exactly the same esr behaviour as the zero field cooled sample.

The work of Hutchens et al suggests that the compound Pd_3Yb does not order above 1.8K and thus this intermetallic compound appears to be a good candidate for the possible observation of a non s-state resonance. The measurements on Pd_3Yb have to date, however, been plagued by the problems of metallurgy outlined in ch. 6. Initial work on what was presumed to be the compound, gave what appeared to be a weak resonance which remained almost unchanged between 4.2K and 20K with $g \sim 3$. This is not far from the g-value of Yb in Au reported by Hirst et al (5.63) where $g = 3.30$. To check whether this 'signal' was, in fact, due to solid solution of Yb in Pd, the sample of 10% (nominal) Yb in Pd was investigated and a similar line of much the same intensity was observed. A run on the 'empty' cavity loaded with a Au-Ag specimen showed that the effect was not due to contamination of the cavity.

No conclusions can, at present, be drawn about the origin of this line but further investigation, when samples of good metallurgical quality are available, is clearly warranted.

(h) The Pt-Cd compounds

The g-value of Pt_2Gd (fig. (8.29)) is constant above about 60K at $g = 2.023 \pm 0.005$. This value is in good agreement with the results of Davidov and Shaltiel (5.11) and with the susceptibility measurements of Wallace and Vlasov (3.29), which suggest a paramagnetic moment for the compound about 2% above the free ion value. The present measurement flatly contradicts the results of Vijaraghavan et al (5.10) who observed a large negative g-shift for Pt_2Gd. Substitution of the observed g-shift in the Korringa relation suggests a slope of about 17 $G.K^{-1}$ for the linewidth at high temperatures, which is rather higher than the value of 6 - 7 $G.K^{-1}$ observed.

As discussed in ch. 6, there exists a considerable range of composition over which the Laves phase compounds are formed, and measurements were made on compounds containing 28at% and 25at% Gd, corresponding to stoichiometries "$Pt_{2.57}Gd$" and "Pt_3Gd". The results for the "Pt_3Gd" compound are shown in fig. (8.30) and the principal values of interest summarised in table 8.3. The g-values for all three compounds are very nearly the same but there is an appreciable variation in the values of the linewidth at 77K. The slope of the linewidth, $\frac{d\Delta H}{dT}$, for the "$Pt_{2.57}Gd$" compound, has a greater uncertainty than the others since fewer points were taken at high temperatures.

TABLE 8.3

	T_g	$T_{\Delta H min}$	ΔH_{77}	g	$\frac{d\Delta H}{dT}$
Pt_2Gd (33%)	57 ± 5	70 ± 3	858 ± 45	2.023	6.2 ± 0.5
$Pt_{2.57}Gd$ (28%)	56 ± 5	66 ± 3	710 ± 35	2.028	7.5 ± 1.0
Pt_3Gd (25%)	52 ± 5	58 ± 3	774 ± 40	2.022	6.6 ± 0.5

All three compounds show the behaviour expected for a transition to a ferromagnetic state at low temperatures. By analogy with the $GdAl_2$ compound discussed above, the data would suggest an ordering temperature of ~55K for the Pt_2Gd compound. This is rather higher than the value obtained by Crangle and Ross for Pt_2Gd (3.28) of 37K in zero field, but is closer to the value of 47K obtained by Wallace and Vlasov.

Careful analysis of the data for the three alloys suggests, in fact, that there may be a reduction in the ordering temperature on moving towards the Pt rich end of the phase field. It is difficult to deduce this fact from the data with any certainty, but the temperature at which the linewidth begins to broaden appears to decrease steadily as the concentration of Gd is decreased. The data for the "Pt_3Gd" compound would suggest an ordering temperature of perhaps 45K. The temperature at which the centre of the resonance line begins to shift to lower fields, T_g, does not show such strong concentration dependence, although it may show some, and it is consistently lower than $T_{\Delta H min}$. Values of $T_g < T_{\Delta H min}$ have also been found in the Pd-Gd and Pd-Mn dilute alloy systems and possibly exist in Cu_6Gd and $GdAl_2$. This may be a manifestation of the short-range order above the Curie temperature in these alloys.

In principle (2.1, 2.2., 2.3), it is possible to calculate the expected variation of T_C by computing the lattice sum in the RKKY formula (2.3) and then considering the effect of introducing random voids in the sum, on replacing Gd atoms by Pt atoms. As discussed in some detail in ch. 2, however, this approach seeks to explain quantitatively fairly small changes on the basis of a theory which is far from rigorous. A computation of this sort has therefore not been attempted.

In order to investigate the effects described above by more conventional methods, resistivity and susceptibility specimens of the samples have been prepared.

(i) $\underline{Zn_{12}Gd}$ and $\underline{Zn_{17}Gd_2}$

The Gd_2Zn_{17} compound (fig. (8.31)) gives a constant g-value between about 30K and 300K of 1.995 ± 0.005, which is close to the free ion value and in good agreement with Stewart's (2.4) value for the reduction in the paramagnetic moment from the free ion value ($\sim -0.7\%$). The linewidth above about 100K has a slope of 0.3 $G.K^{-1}$ with $\Delta H = 308 \pm 15$ Gauss at room temperature. The observed value of the slope is consistent with the g-shift through the simple Korringa relation.

$GdZn_{12}$ has $g = 1.980 \pm 0.005$ from 30K to 300K (fig. (8.32)). This unequivocally negative g-shift is surprising since, for a simple metal such as Zn, we might expect a positive g-shift and Stewart (2.4) in fact does obtain an increase of about 6% in the paramagnetic moment over the free ion value from his susceptibility measurements. Application of the Korringa formula to the g-value result would suggest a high temperature slope in the linewidth of about 6 $G.K^{-1}$, but in practice, the line broadens from 190 ± 10 Gauss at 77K to 250 ± 12 Gauss at 295K giving a slope ~ 0.25 $G.K^{-1}$, some twenty-five times smaller. Even if the compound is fairly severely bottlenecked, this does not account (equation 4.49) for a change in sign of Δg, and the discrepancy between

the sign of Δg and Δp remains extremely puzzling.

Both compounds are interesting from the point of view of their magnetic ordering behaviour. Both compounds are antiferromagnetic at low temperatures, both show striking deviations from Curie-Weiss behaviour (fig. (3.1)) and both give values of $\frac{|\theta|}{T_N} \gg 1$. Stewart obtained a value of T_N = 10K for Gd_2Zn_{17} and the lowest temperature at which an esr line could be identified was 11K, where $\Delta H \sim 1400$ Gauss. Above this temperature the line narrows, showing a weak minimum at 90 - 100K; this suggests that ordering effects are observed in the esr linewidth at a temperature of about ten times the nominal ordering temperature. Deviation from Curie-Weiss behaviour becomes apparent at about three times the Néel temperature. The resonant field appears to shift to lower values at 20 - 30K, although the fairly small apparent shift can, again, be accounted for by a very small overestimate of the lineshape correction factor.

$GdZn_{12}$ shows entirely parallel behaviour. Stewart obtained T_N = 16K and no esr signal is observed below about 17K, where the line is $\sim$ 700 Gauss wide. In this case, the line begins to broaden at 70 - 80K (i.e., $\frac{T \Delta H_{min}}{T_N} \sim 5$) compared with a temperature $\sim$50K at which departures from linearity in the inverse susceptibility are observed. It is again possible that the resonant field is shifted to lower values below 30K.

The results described above for the Gd-Zn compounds are very similar to those of the Gd-B compounds and we might expect that the mechanism responsible for the anomalous behaviour above T_N, whether it is the effect of short-range order, the formation of superzone boundaries, or some other mechanism, is the same in both cases. The magnetic structures of the $(R.E)_2Zn_{17}$ and $(R.E)Zn_{12}$ compounds are not known. In fig. (8.23a), $\ln(T - T_N)$ has been plotted against $\ln(\Delta H - BT)$ for the compounds, and

with the reservations expressed for the same plot in the case of the borides, we note that a reasonable straight line fit is obtained between $T_N + 2$ and $T_N + 30$ for $GdZn_{12}$ with $|\rho| = 0.7$ and between $T_N + 5$ and $T_N + 52$ for Gd_2Zn_{17} with $|\rho| = 1.1$.

No signal was observed from a sample of $Zn_{12}Er$ ($T_N = 2.9$, $\theta = 3$) at 4.2K or 77K.

(j) Au_3Mn

Very few intermetallic compounds containing Mn order antiferromagnetically at sufficiently low temperatures for the extent of line broadening above T_N to be observed. Au_3Mn orders at 145K and appears to show deviations from Curie-Weiss behaviour at about 250K. It was thus hoped to compare the esr behaviour of this compound with that of the Gd antiferromagnets.

Both of the samples prepared in this study (ch.6) showed fairly strong superlattice lines in their X-ray diffraction data but, unfortunately, no esr signal was observed between room temperature and 77K in either case.

(k) Pd_2MnSn

This compound was investigated to compare the behaviour of a transition metal ferromagnet with the behaviour of the rare-earth compounds and, also, in the hope that some light might possibly be shed on the behaviour of the $Zn_{13}Mn$ compound discussed below.

In fact, the esr behaviour of Pd_2MnSn (fig. (8.33)) appears to be parallel to that of $GdAl_2$ and the other ferromagnets described above. The line again broadens inhomogenously below 220K and the centre of the line shifts to lower fields at about the same temperature. As in $GdAl_2$:

$$\frac{T_{\Delta H_{min}}}{T_C} \sim \frac{T_g}{T_C} \sim 1.2T_C$$

A constant corrected g-value above 220K of 2.013 ± 0.005 was obtained and this leads to a predicted slope of the linewidth of ~ 7 G.K^{-1}, compared to an observed slope ~ 4.5 G.K^{-1}. It is interesting to note that in this compound, the high temperature linewidth extrapolates unequivocally to a large negative linewidth at T = 0K $\sim$ -800 Gauss. Similar negative intercepts were observed in some Pd-Mn dilute alloys (above) and no explanation can be offered for this result.

(1) $Zn_{13}Mn$ and $Zn_{10}Mn$

The esr results on the Zn-Mn alloys are the most puzzling of all the results in this thesis. They do not appear to fit in with the typical esr behaviour of either ferromagnets or antiferromagnets.

The results of the runs on the ζ-phase, $Zn_{13}Mn$, are shown in fig. (8.34). Sample 1 corresponds to Dunlop's sample 1334 and sample 2 to his sample 135 (2.7). They both show similar behaviour, the esr signal first appearing between 120K and 150K with $g \sim 2$ and shifting monotonically to $g \sim 3$ at liquid helium temperatures. There is a difference in the absolute value of the linewidth of the two samples $\sim 10 - 15\%$, but the general behaviour is the same, with what appears to be a weak maximum at 30 - 40K, which is rather higher than the ordering temperature of 20K obtained by Dunlop from the Arrott plot and peak in the magnetoresistivity.

It might be argued that the form of the temperature dependence of the resonant field is fairly similar to that of a conventional ferromagnet with $T_C \sim 100 - 120$K, but if the value of 1.8 emu per gm obtained by Dunlop is used to calculate the value of the demagnetising field at 4.2K, only about 20% of the observed shift can be accounted for, even assuming a factor $F = 4\pi$. Furthermore, the linewidth does not show the temperature dependence normally associated with ferromagnets (c.f. Pd_2MnSn).

In an attempt to cast more light on the rather bizarre behaviour of this compound, esr runs were performed on solid solutions of Mn in Zn containing 0.1 and 0.4at% Mn. No signals were observed at 4.2K from any of these alloys in either the annealed or unannealed states (see ch.6). This negative result contradicts the previous measurements of Collings et al (5.60) and Miyako (5.61), although the latter result must be treated with some caution since the stated concentrations of Mn (0.5at% and 1.0at%) are above the solubility limit of 0.4at%. This negative result obtained in this work suggests that local environment effects (i.e., the surrounding Zn atoms) may be an important factor in the observation of a resonance in $Zn_{13}Mn$. However, a run on the alloy $Zn_{13}(Fe_{0.95}Mn_{0.05})$ in which Mn atoms have the same local environment of Zn atoms as the $Zn_{13}Mn$, also failed to produce a signal at 77K, 4.2K or 1.7K.

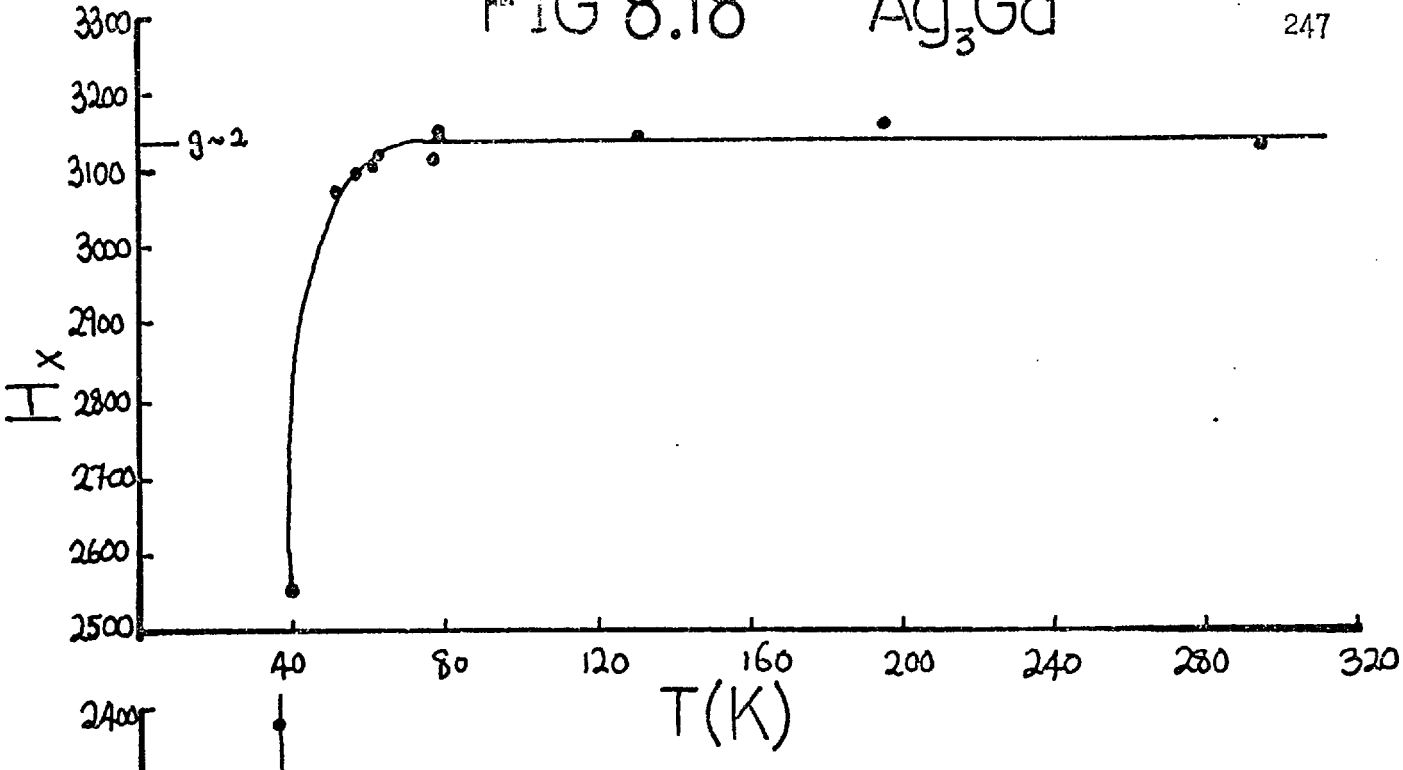
No magnetic data are available on the δ -phase compound "$Zn_{10}Mn$", but it was hoped, again, that its resonance behaviour would provide clues to the $Zn_{13}Mn$ result. It has, in fact, created more problems. The data (fig. (8.35)) for the shift in the resonant field look quantitatively similar to that of the more dilute compound, although the shift is only about half the value obtained in the latter compound. The temperature dependence of the linewidth is however quite different; a minimum being found at 200K with a slope at higher temperatures ~ 4 G.K^{-1} (extrapolating once again to a residual linewidth $\sim$ -600 Gauss at T = 0K). Below the minimum in ΔH, the linewidth increases monotonically from 220 $\pm$ 12 Gauss at 200K to 1000 $\pm$ 50 Gauss at 30K. At lower temperatures the signal is distorted by what appears to be a signal from second phase (perhaps $Zn_{13}Mn$).

The esr data for $Zn_{10}Mn$ shows the broad features expected for a ferromagnet with $T_C \sim 160 - 180$K; however, compared with the data for

Pd_2MnSn, the transition appears far less sharp with a much flatter increase in ΔH and reduction in H_x with decreasing temperature. It will clearly be of interest to measure the other magnetic properties of this alloy and to see if the g-shift at low temperatures can be simply accounted for by the magnetisation in 3KGauss.

The form of the order in these alloys will probably only be resolved when neutron diffraction measurements can be made on single crystals.

FIG 8.18 Ag_3Gd



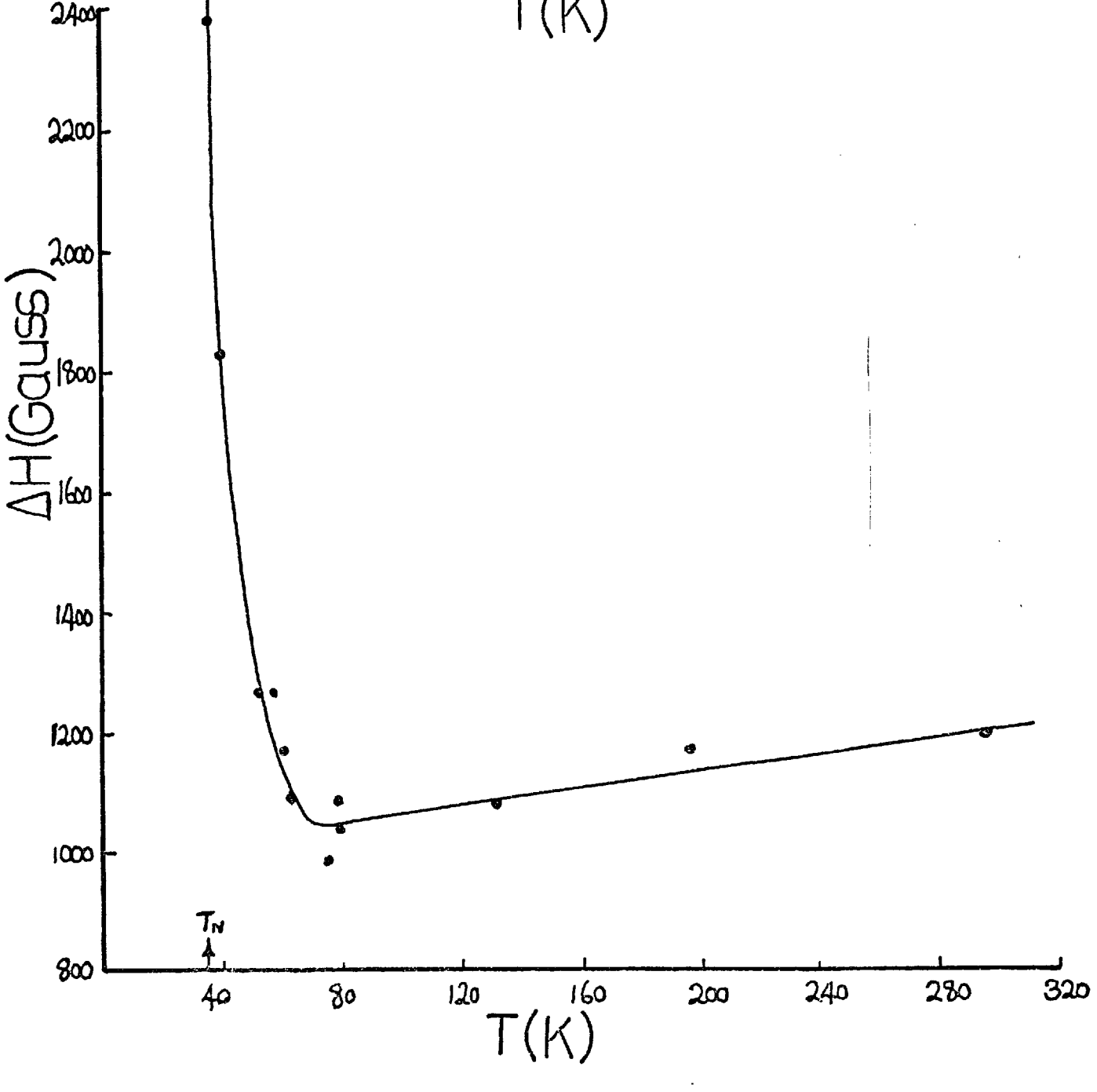
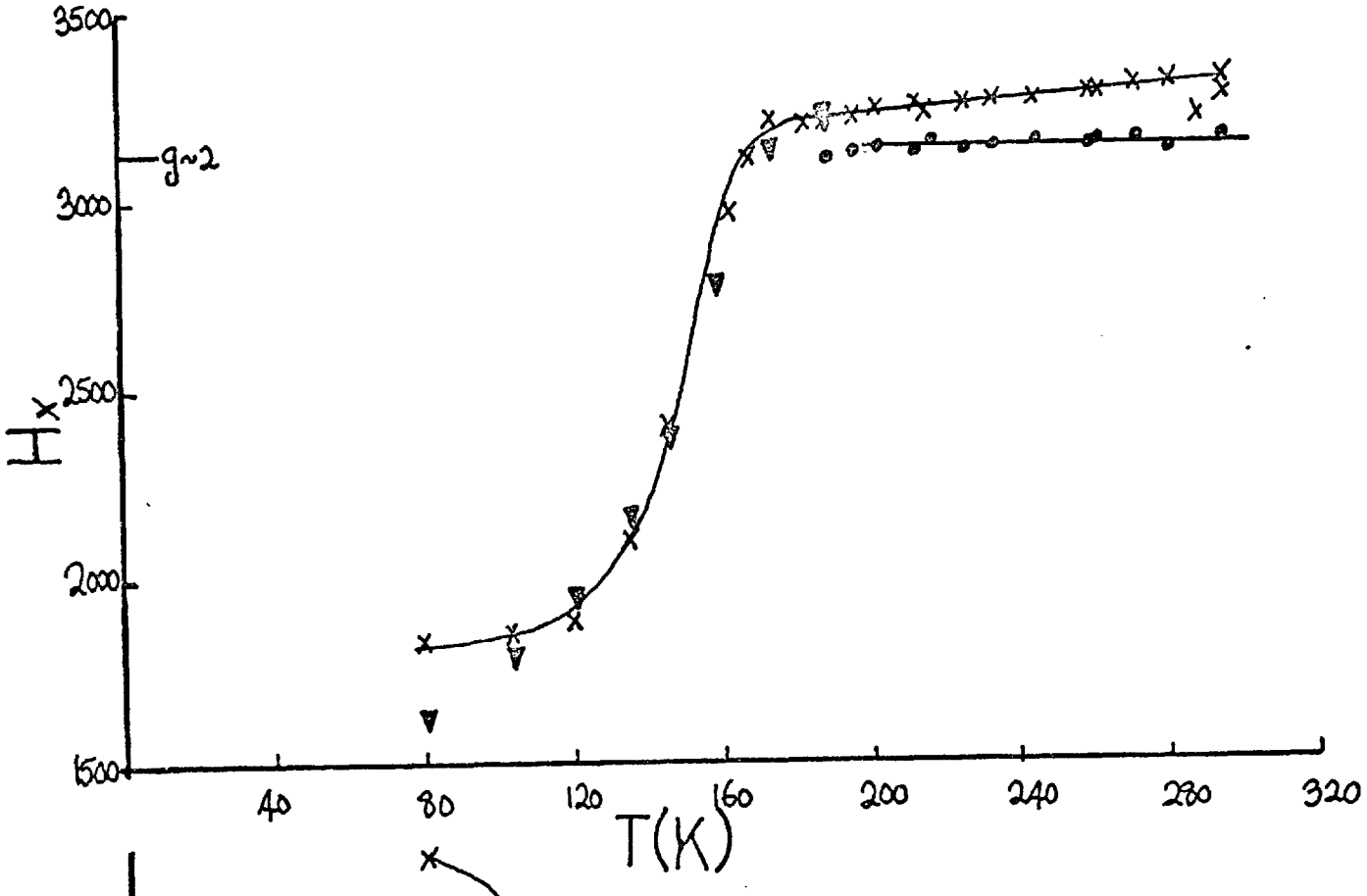
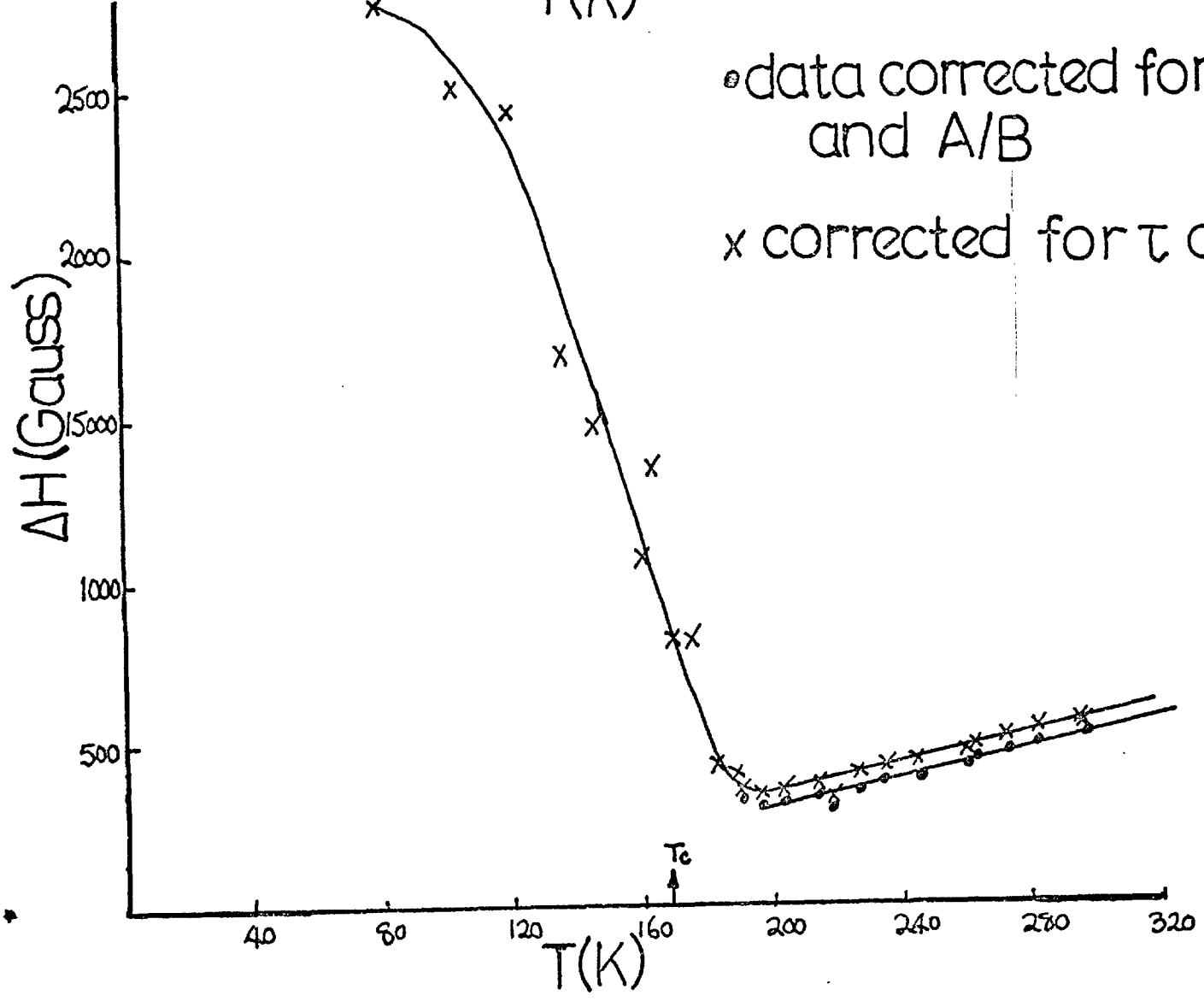


FIG 8.19 $GdAl_2$

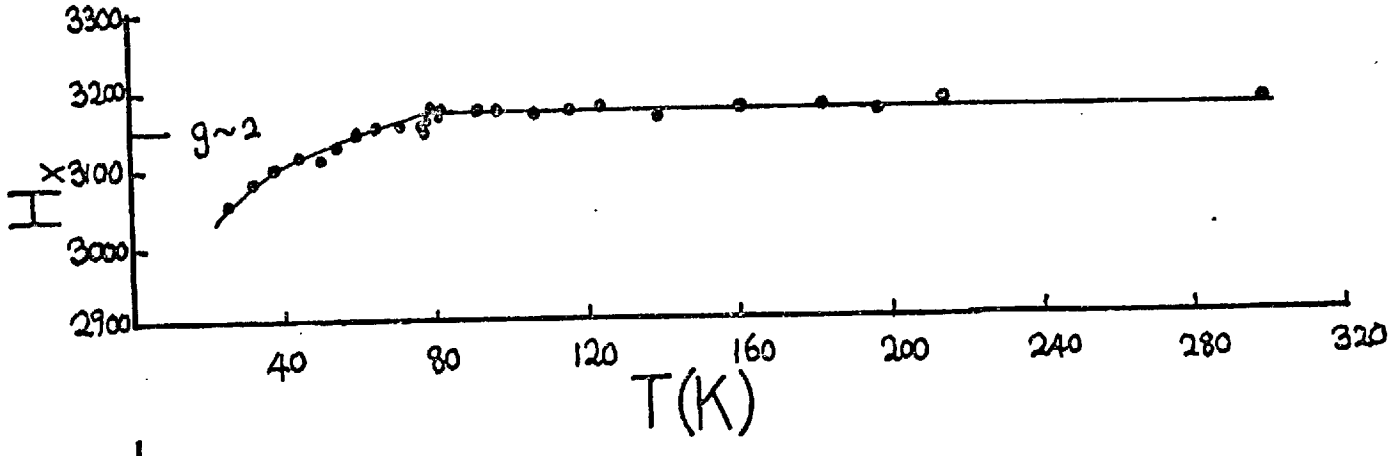




• data corrected for τ and A/B

x corrected for τ only

FIG 8.20 GdB_6


3300
3200
g~2
H x3100
3000
2900
40
80
120
160
200
240
280
320
T(K)

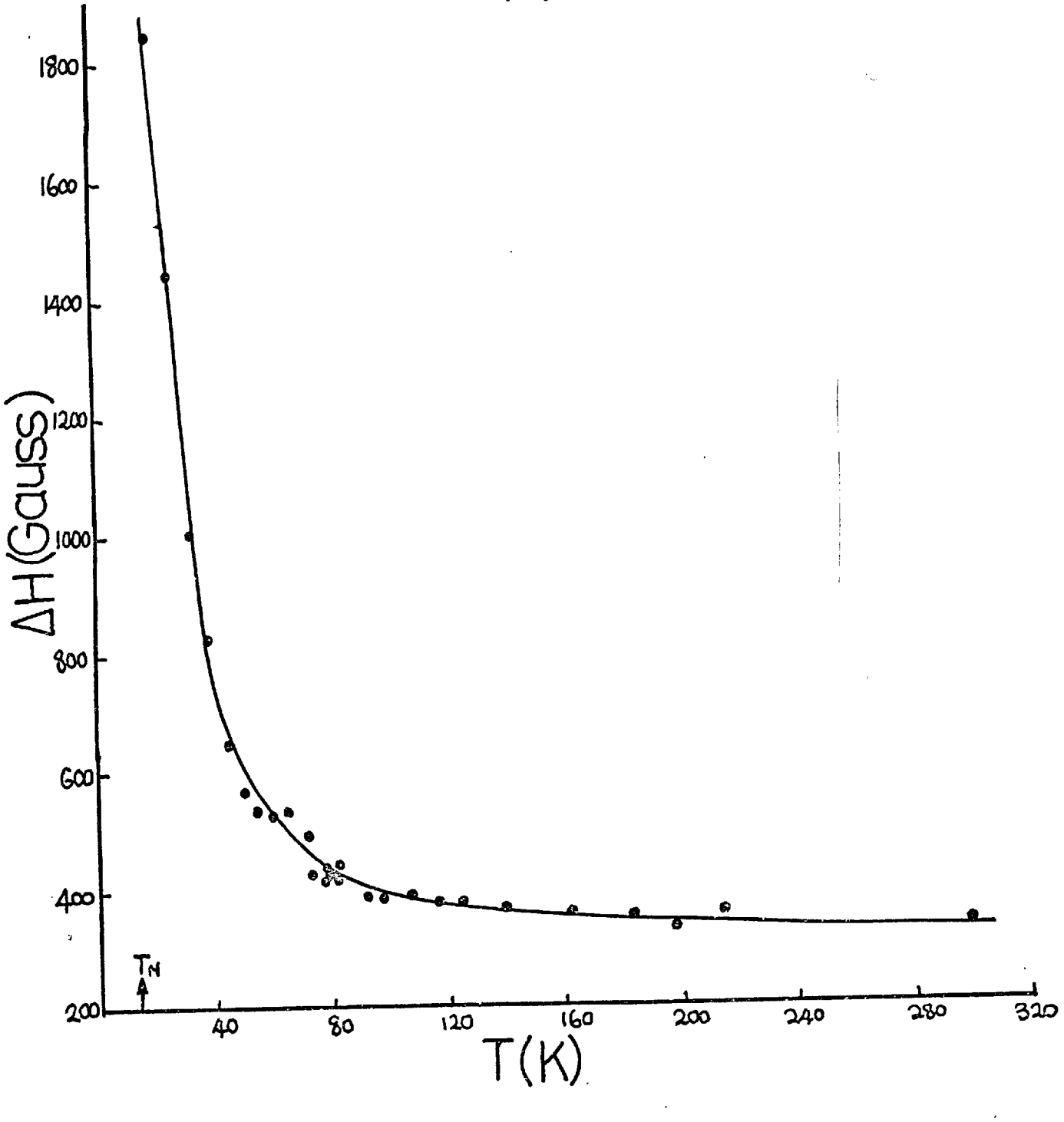
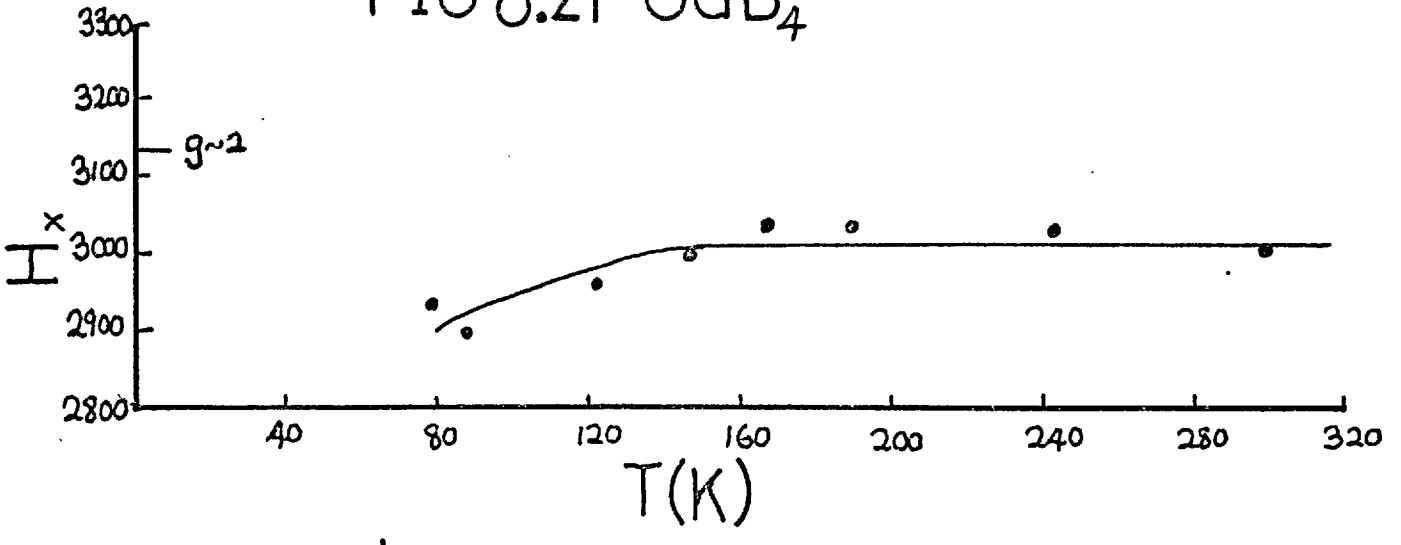

1800
1600
1400
1200
1000
800
600
400
200
ΔH(Gauss)
T_N
40
80
120
160
200
240
280
320
T(K)

FIG 8.21 GdB_4


3300
3200
g~2
3100
H^x
3000
2900
2800
40
80
120
160
200
240
280
320
T(K)

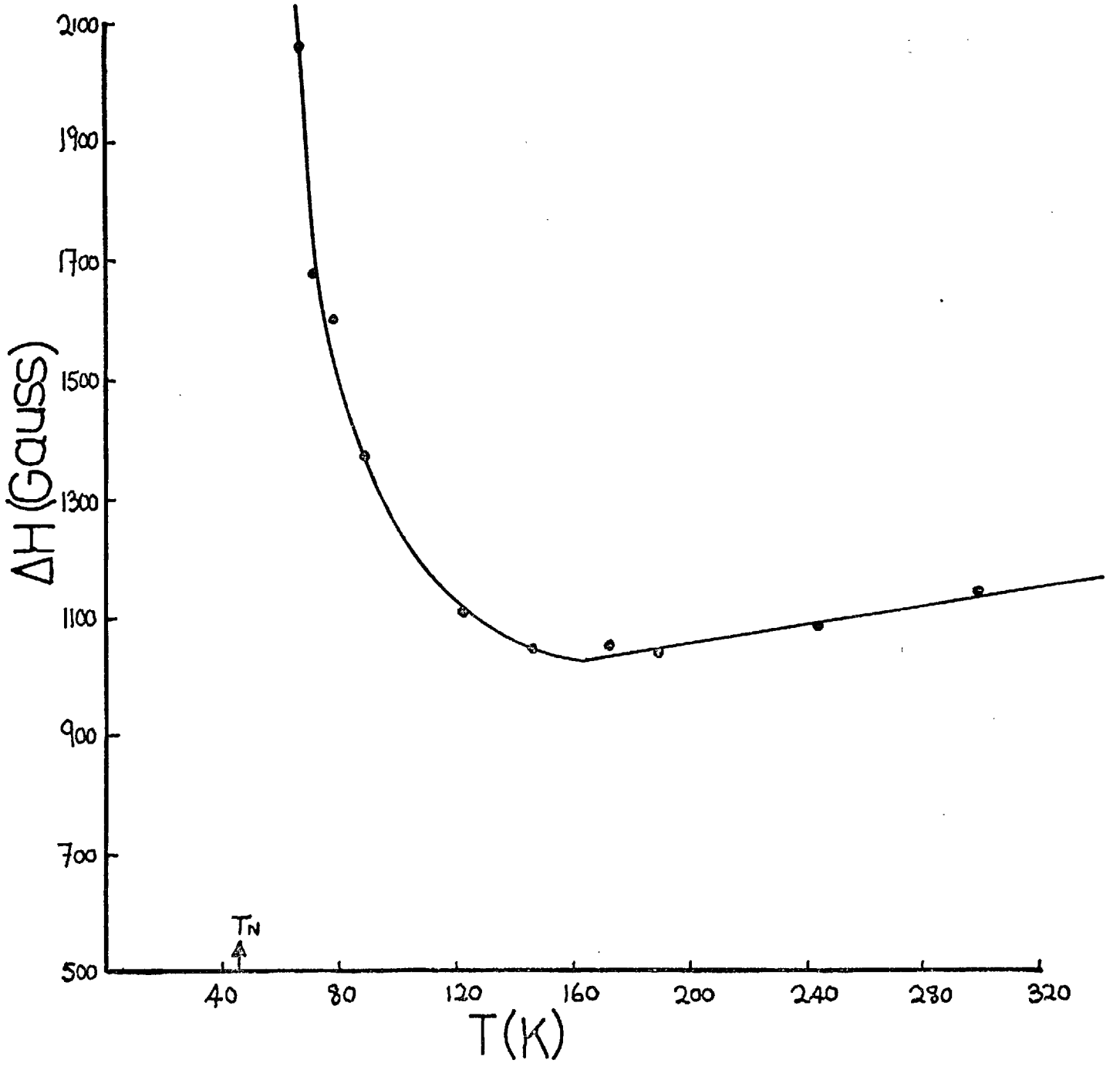

2100
1900
1700
1500
1300
1100
900
700
500
ΔH (Gauss)
T_N
40
80
120
160
200
240
280
320
T(K)

FIG 8.22 After Fisk

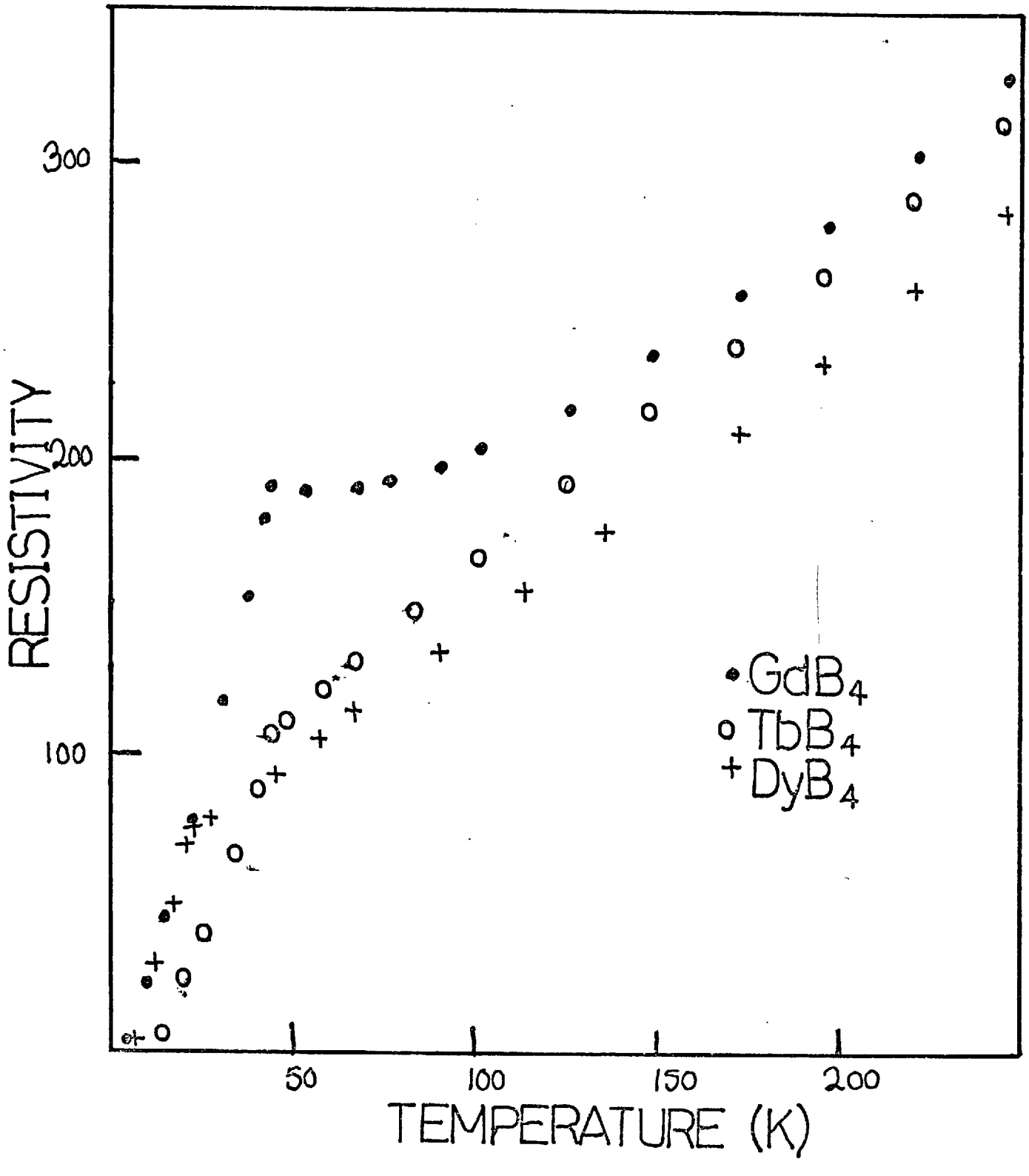


FIG 8.23

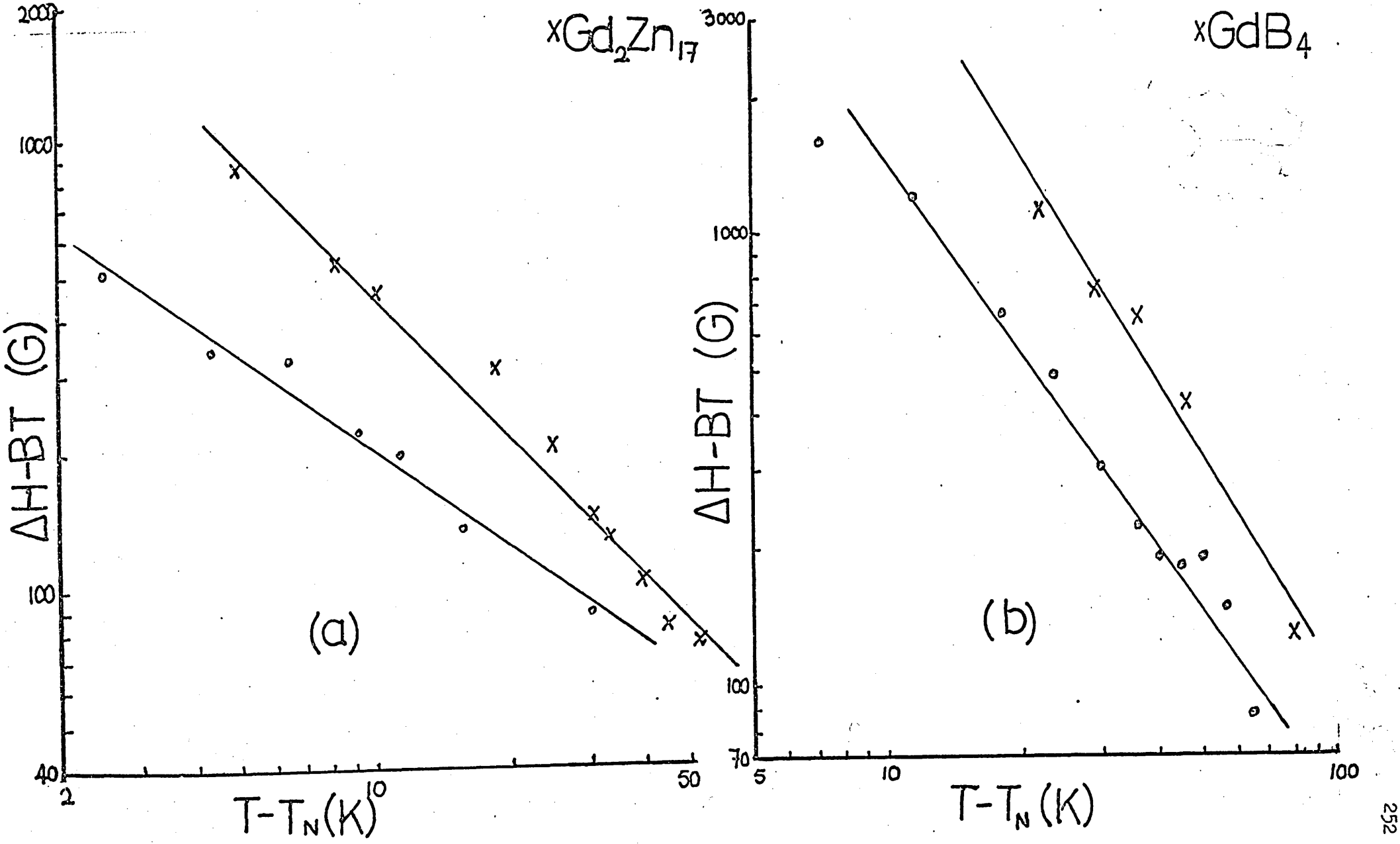
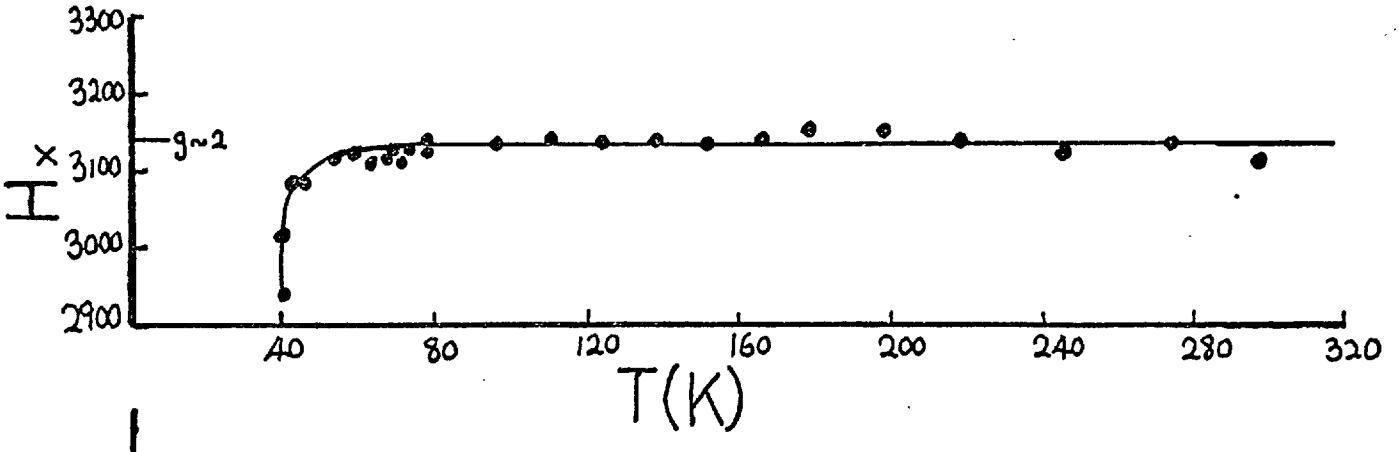

•GdZn12
xGd2Zn17
•GdB6
xGdB4
2000
1000
100
40
ΔH-BT (G)
(a)
2
10
50
T-TN(K)
3000
1000
100
70
ΔH-BT (G)
(b)
5
10
100
T-TN (K)

FIG 8.24 Cu_2Gd



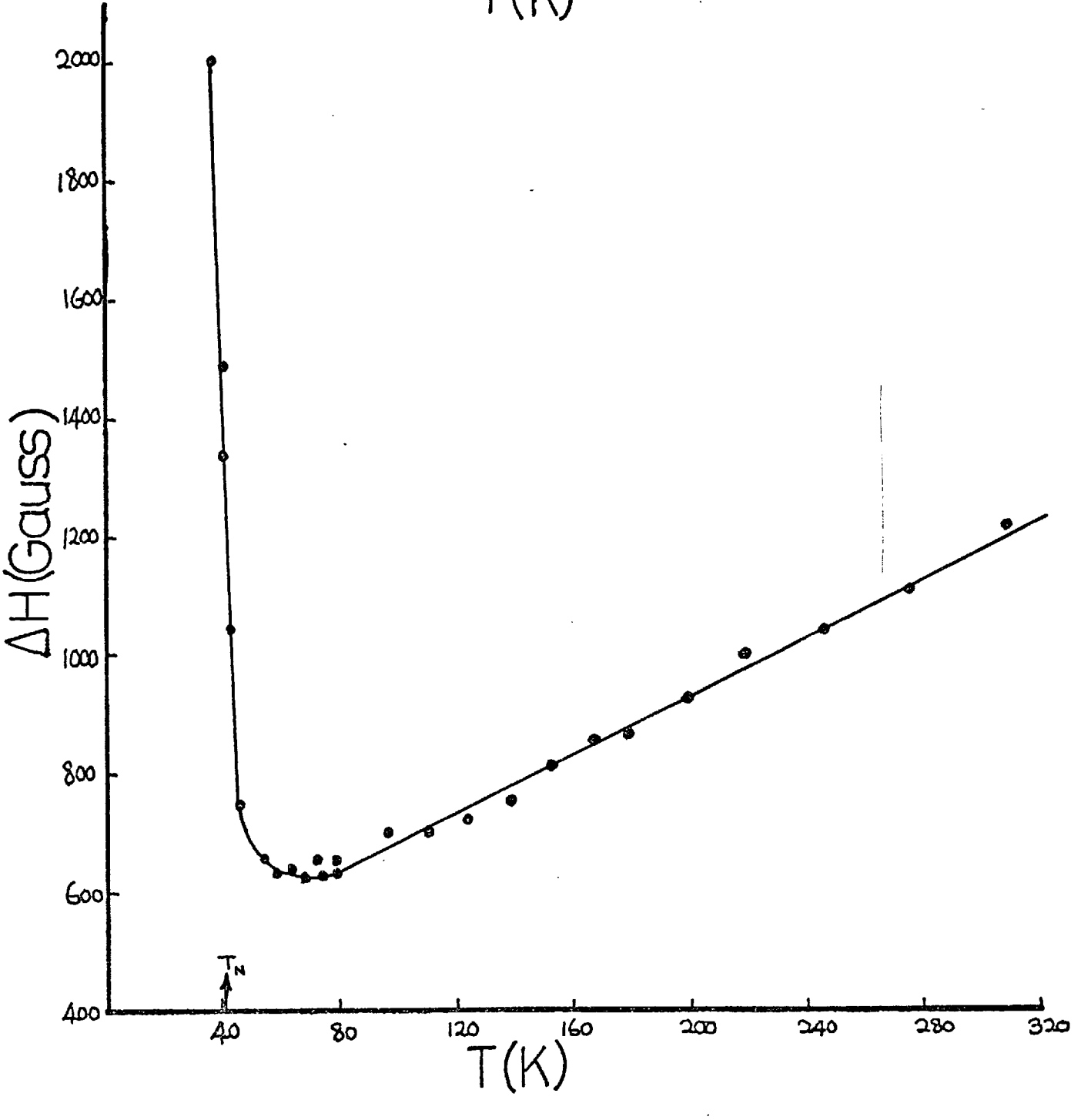
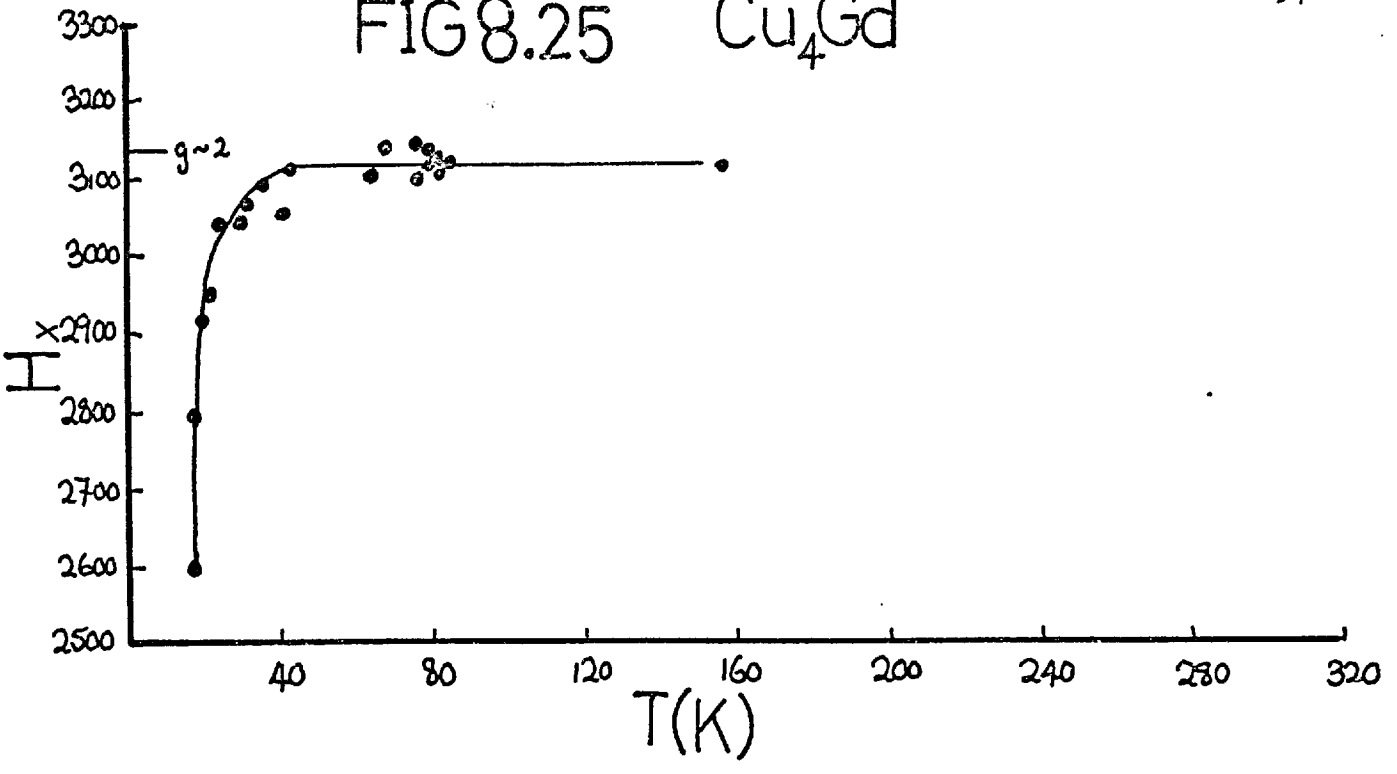
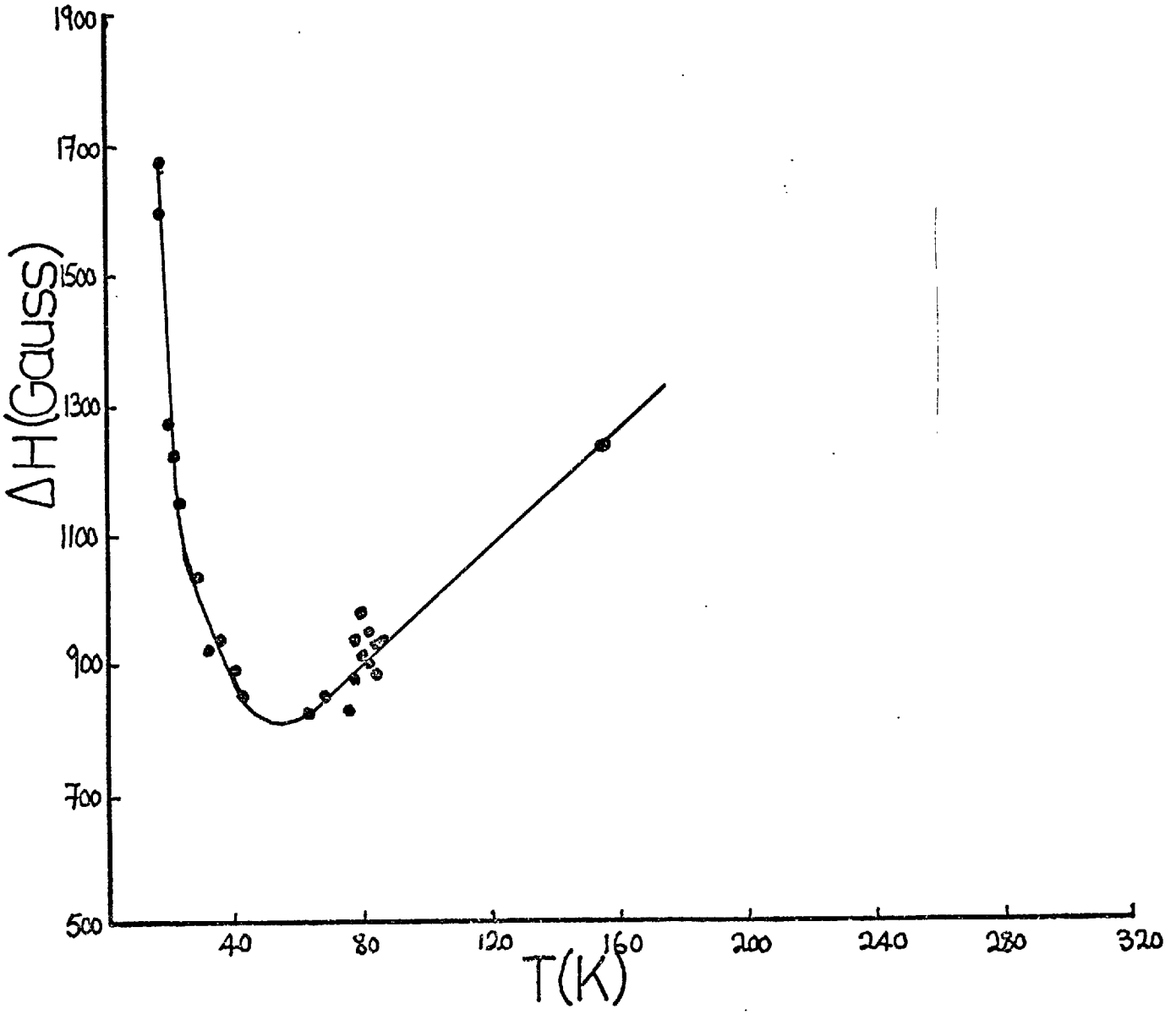


FIG 8.25 "Cu_4Gd"





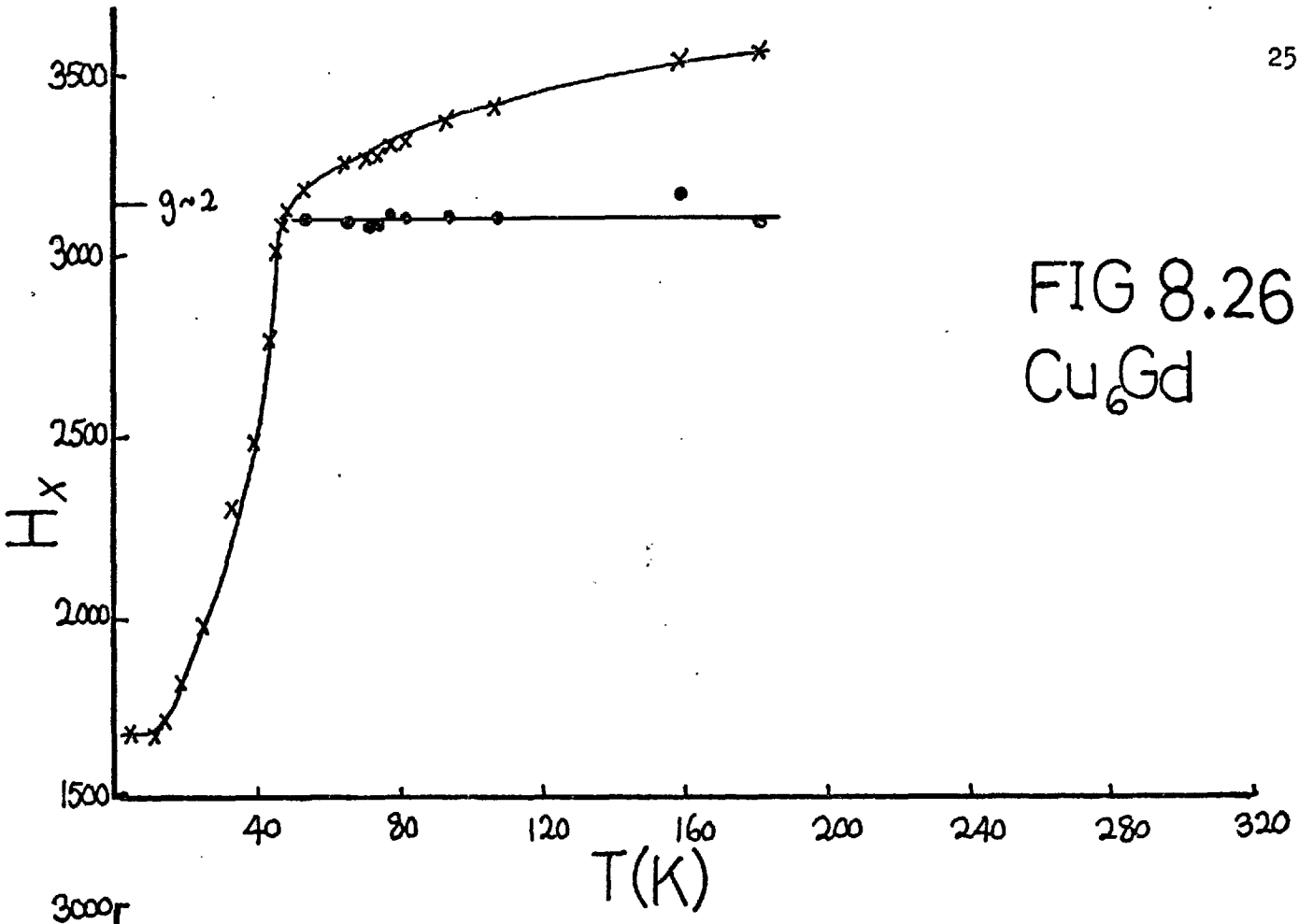
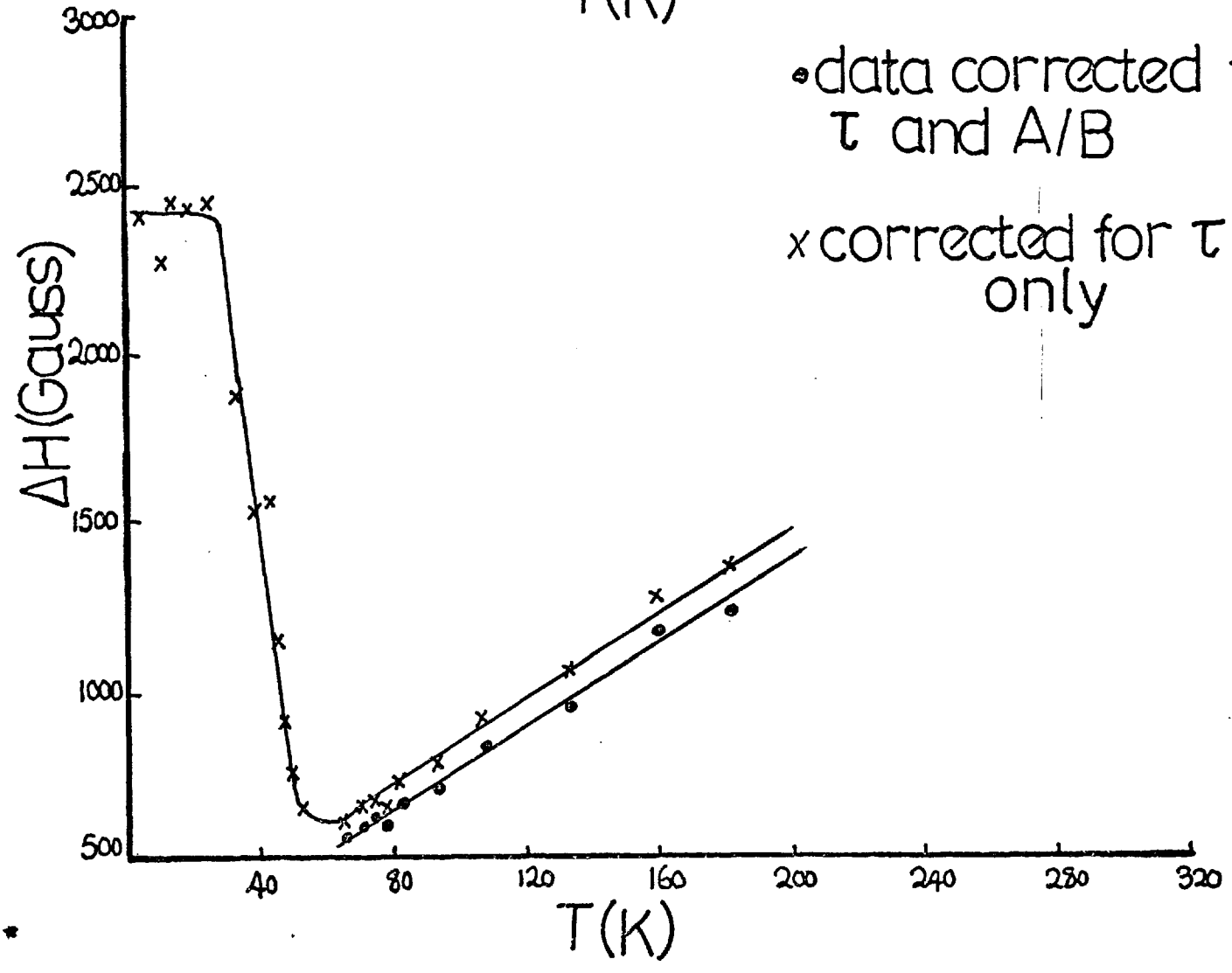
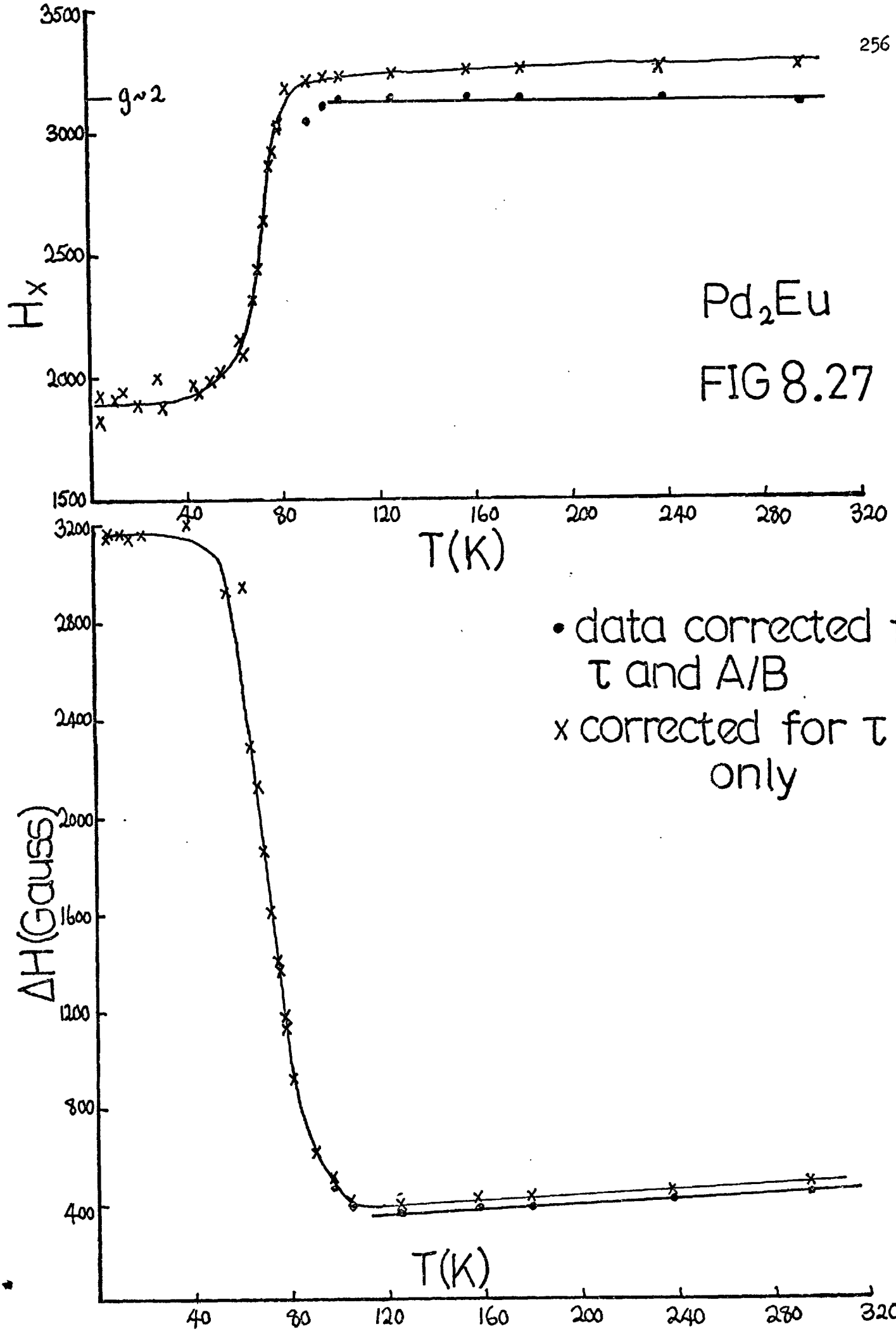


FIG 8.26
Cu_6Gd



• data corrected for τ and A/B

x corrected for τ only



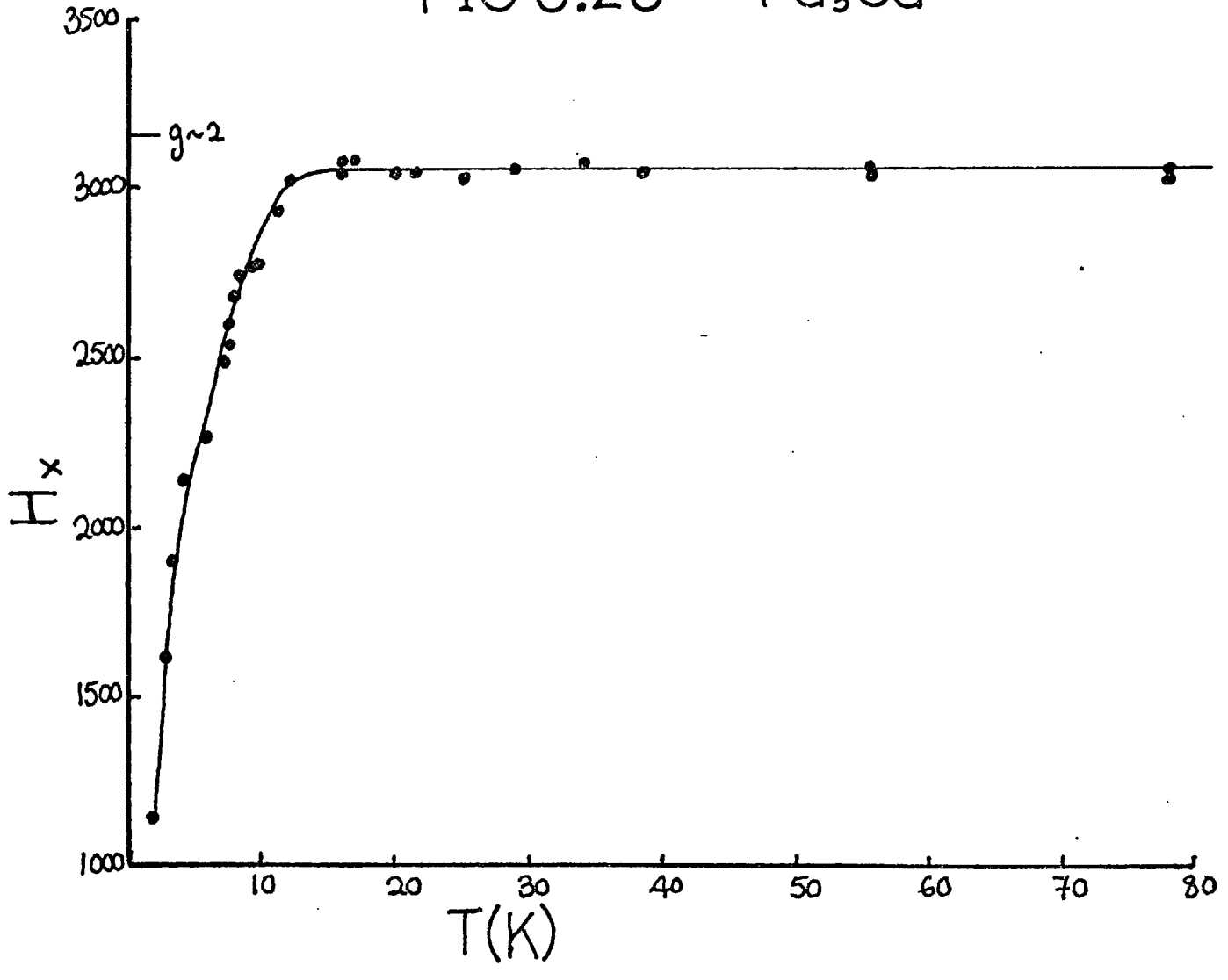
Pd_2Eu

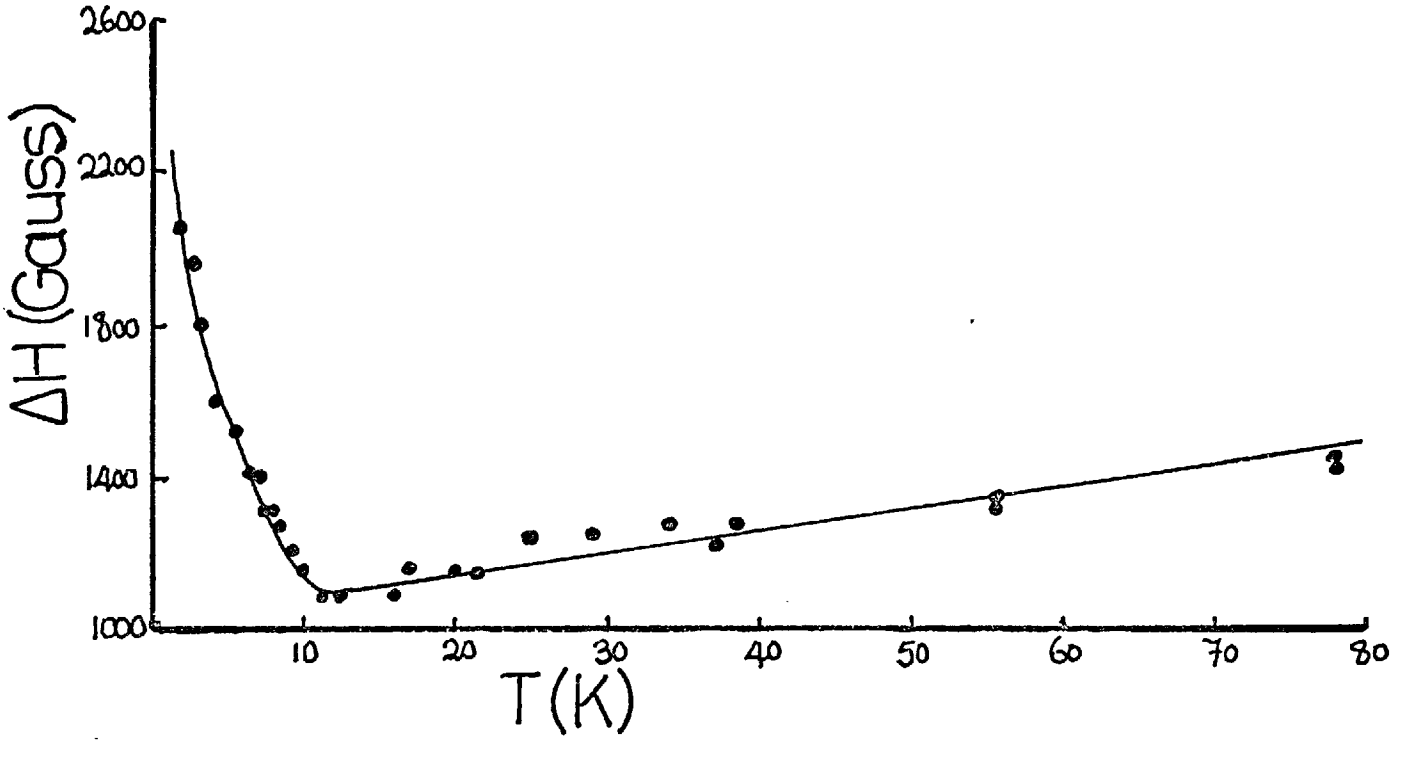
FIG 8.27

• data corrected for τ and A/B

x corrected for τ only

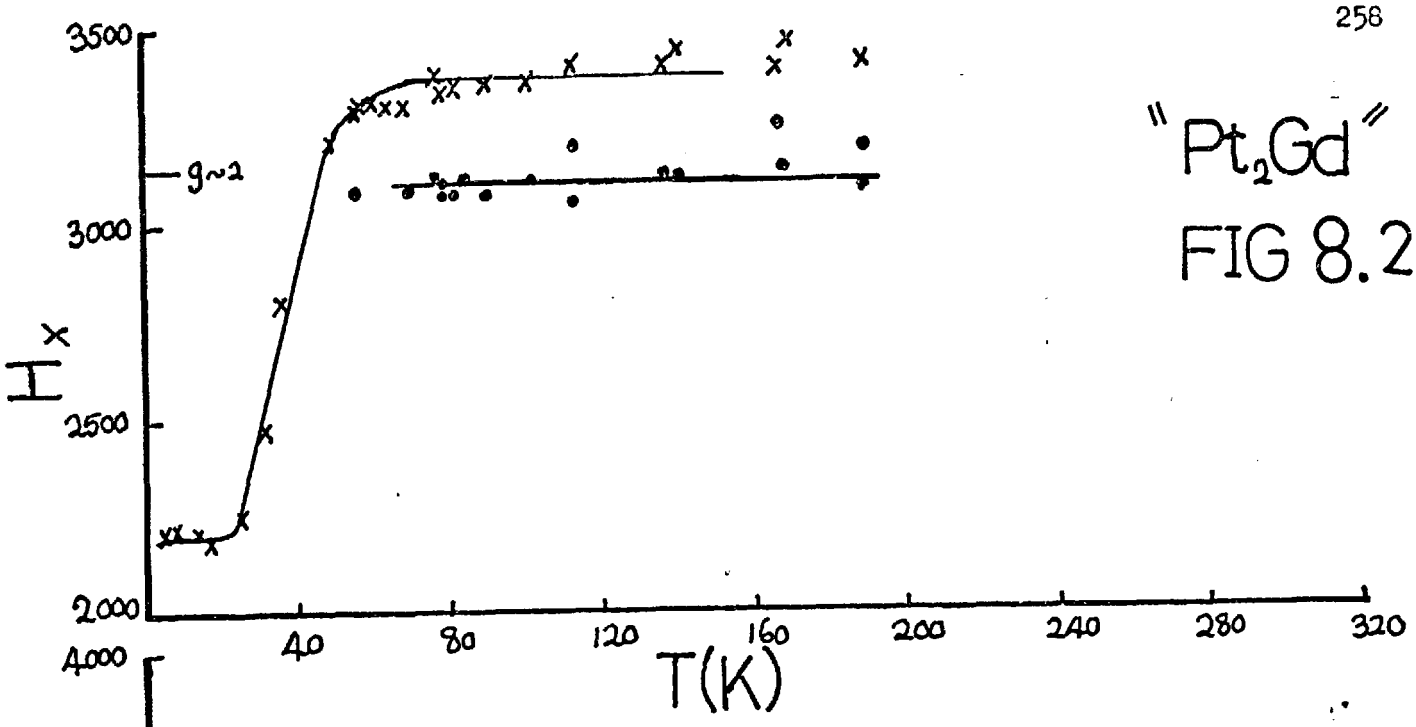
FIG 8.28 Pd_3Gd

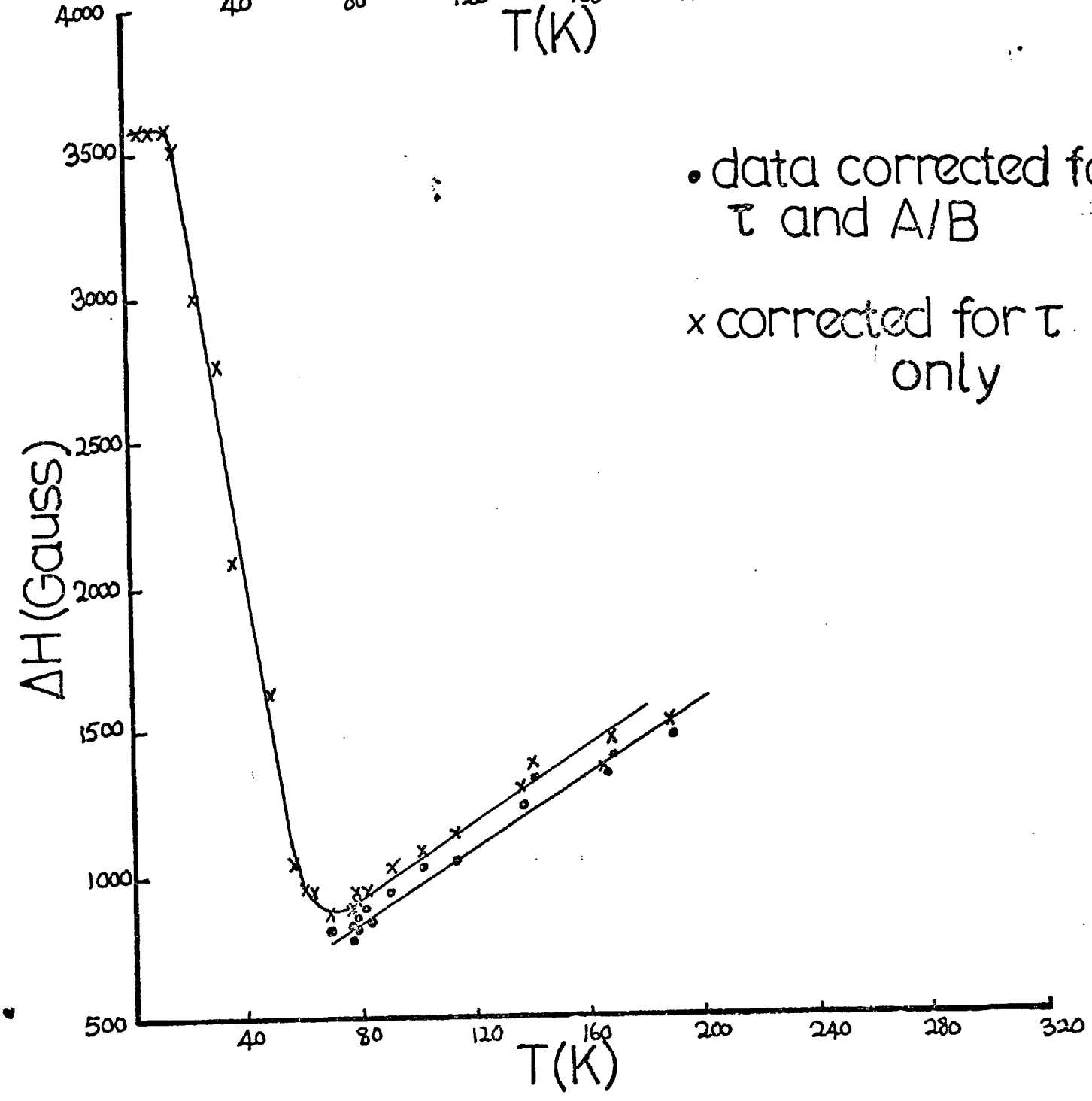




"Pt_2Gd"

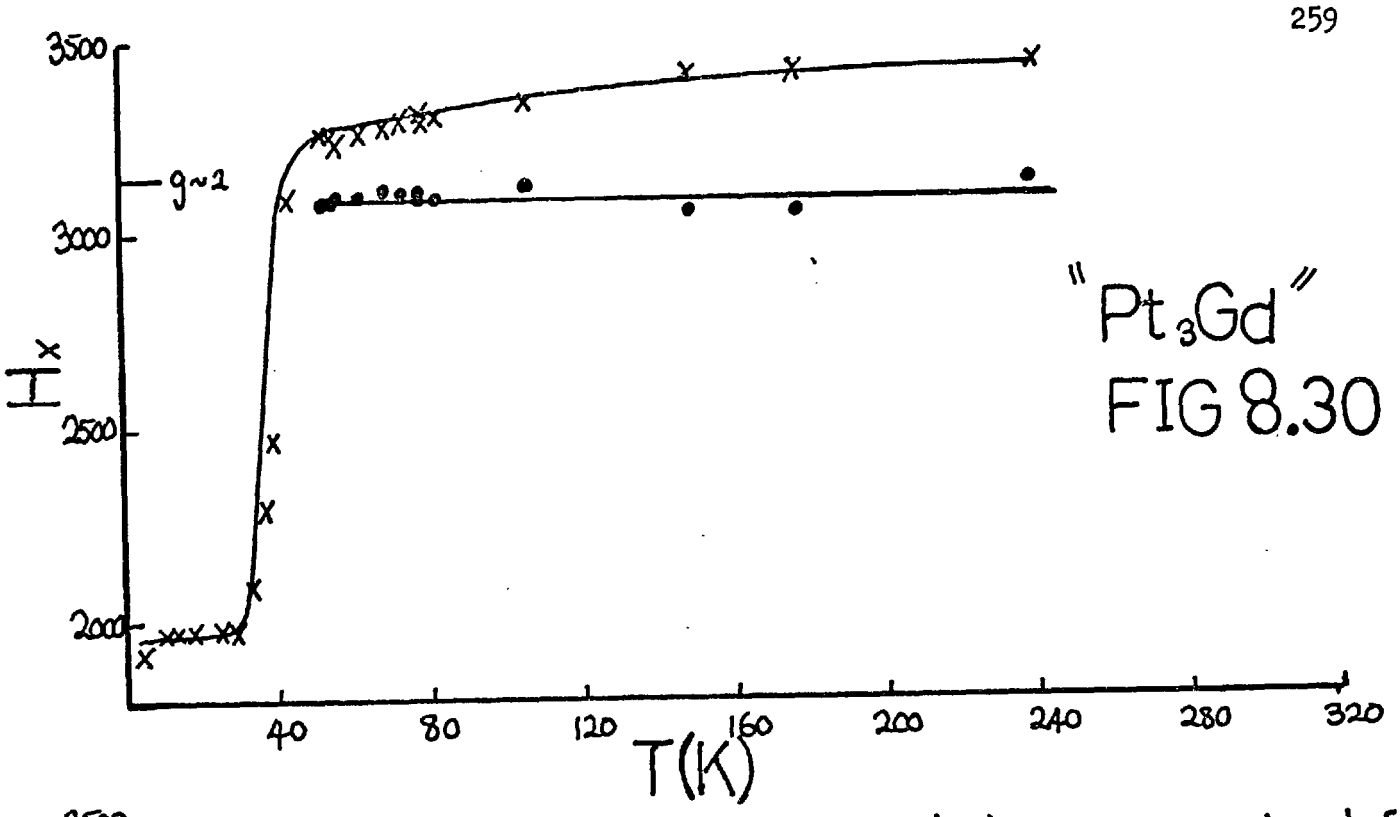
FIG 8.29



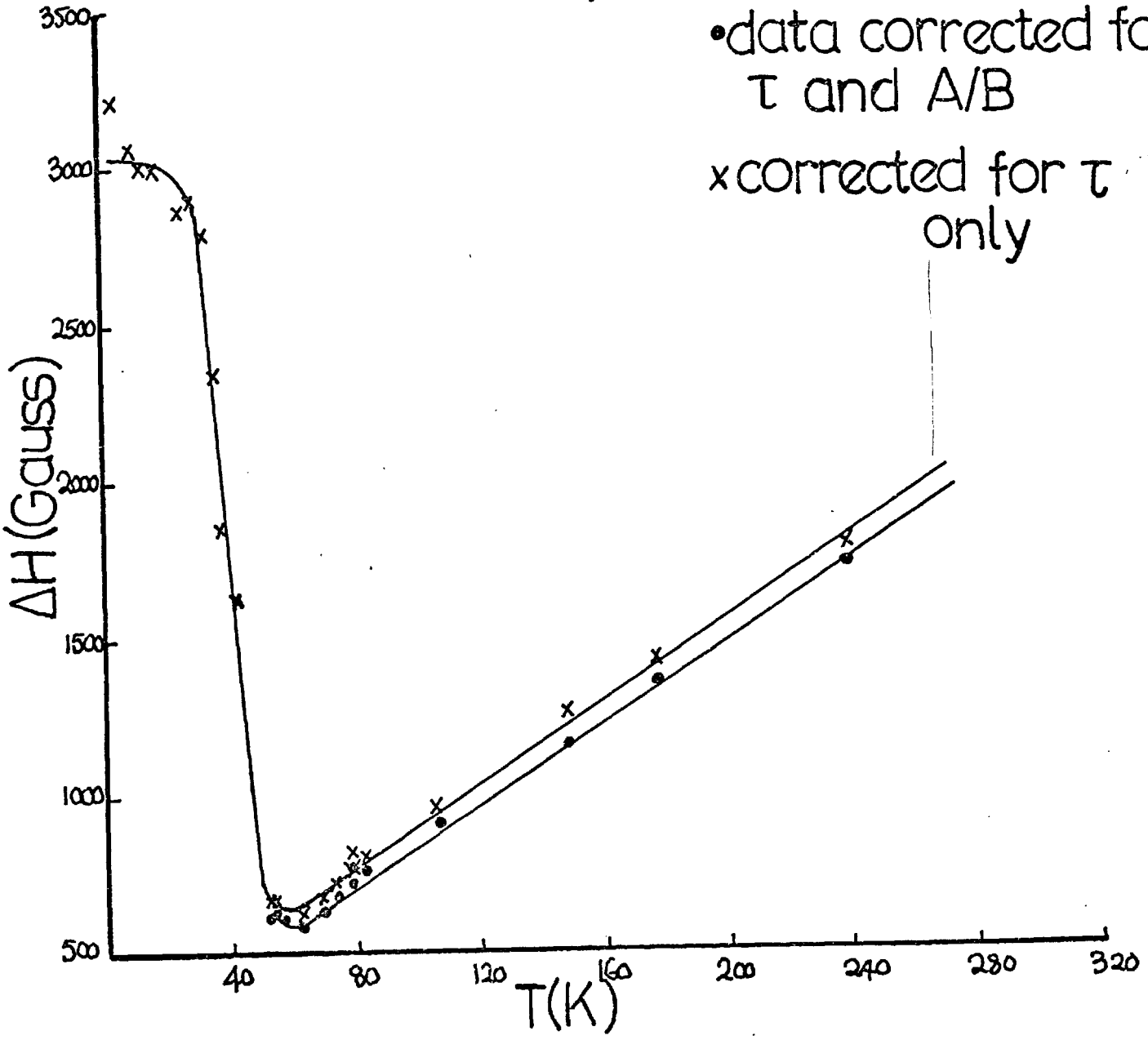


• data corrected for τ and A/B

x corrected for τ only



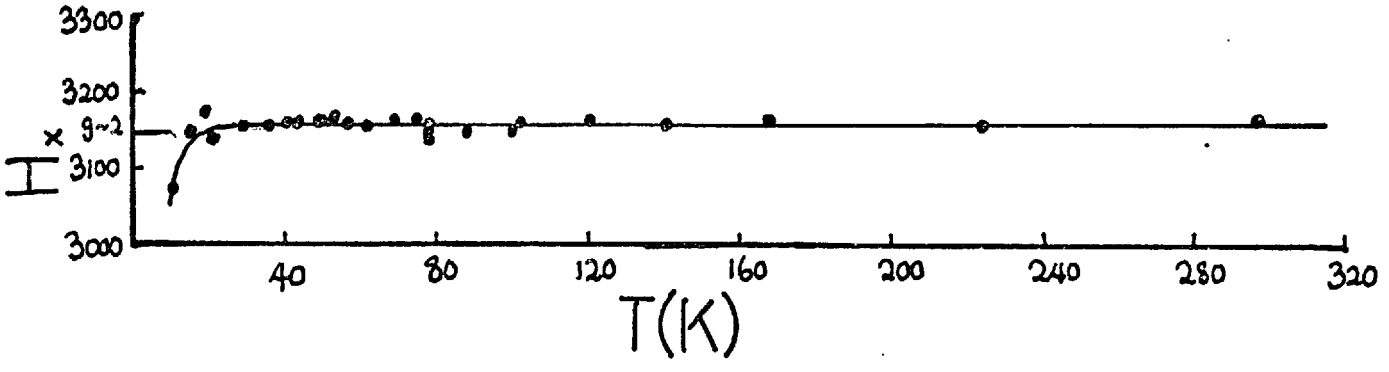
"Pt_3Gd"
FIG 8.30

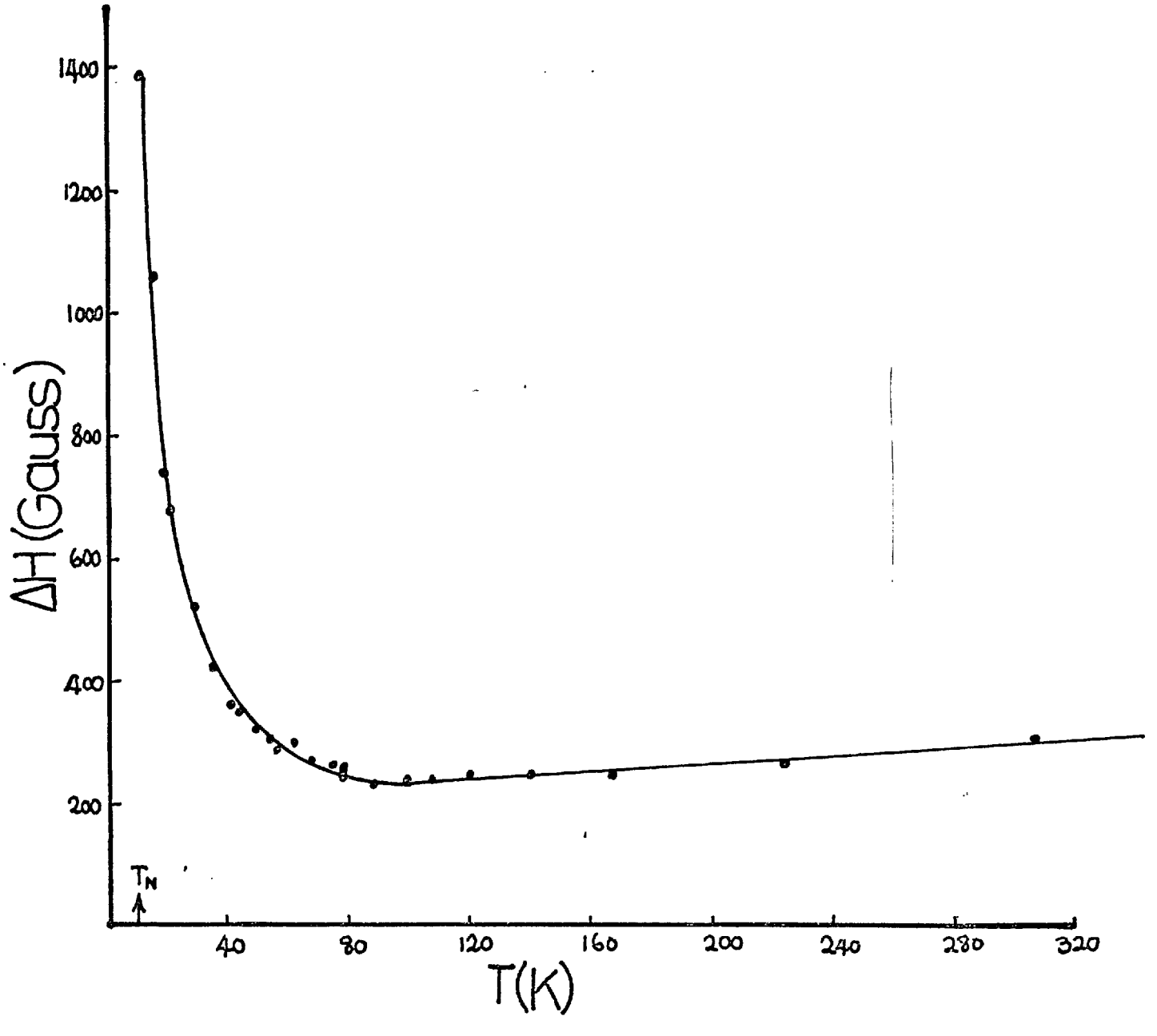


•data corrected for τ and A/B

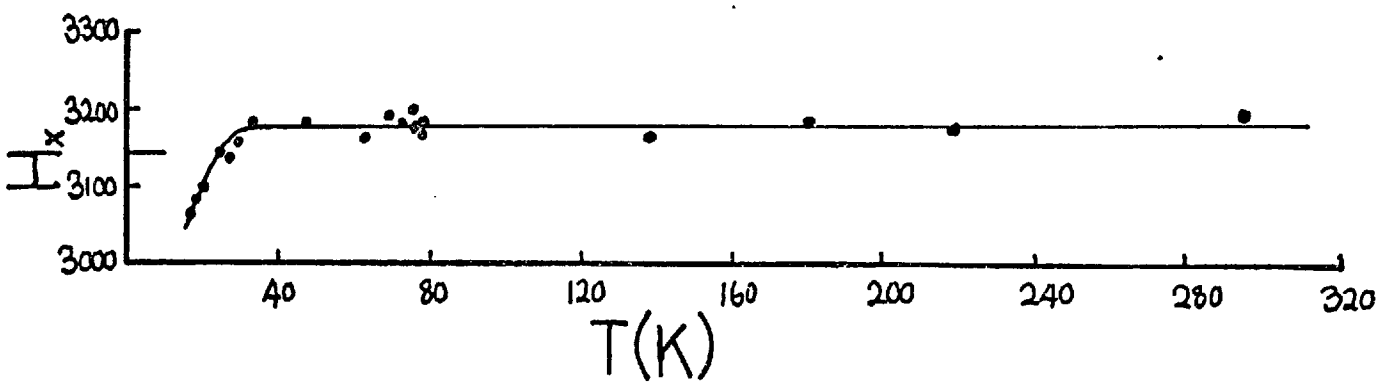
x corrected for τ only

Gd_2Zn_{17} FIG 8.31





$GdZn_{12}$ FIG 8.32



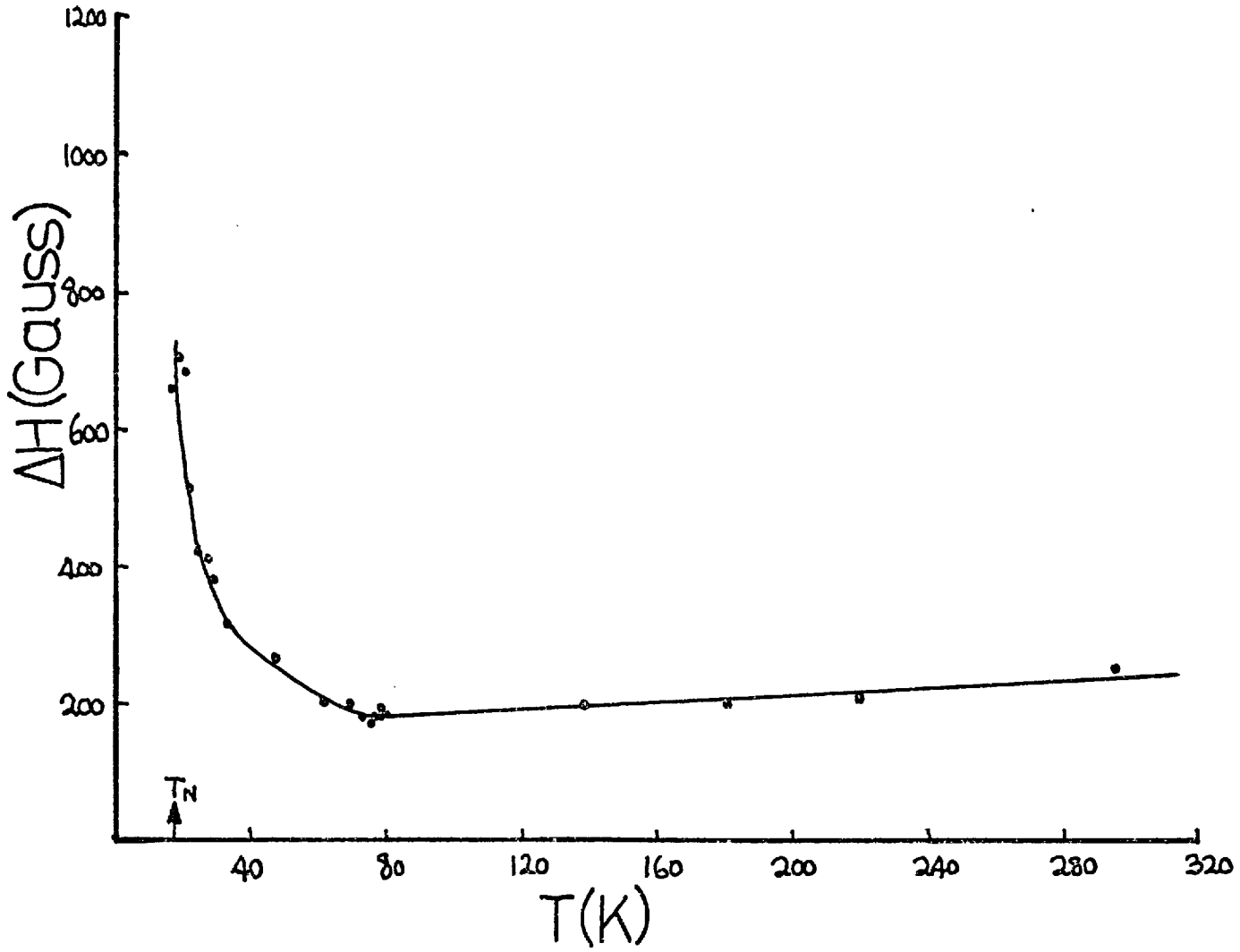
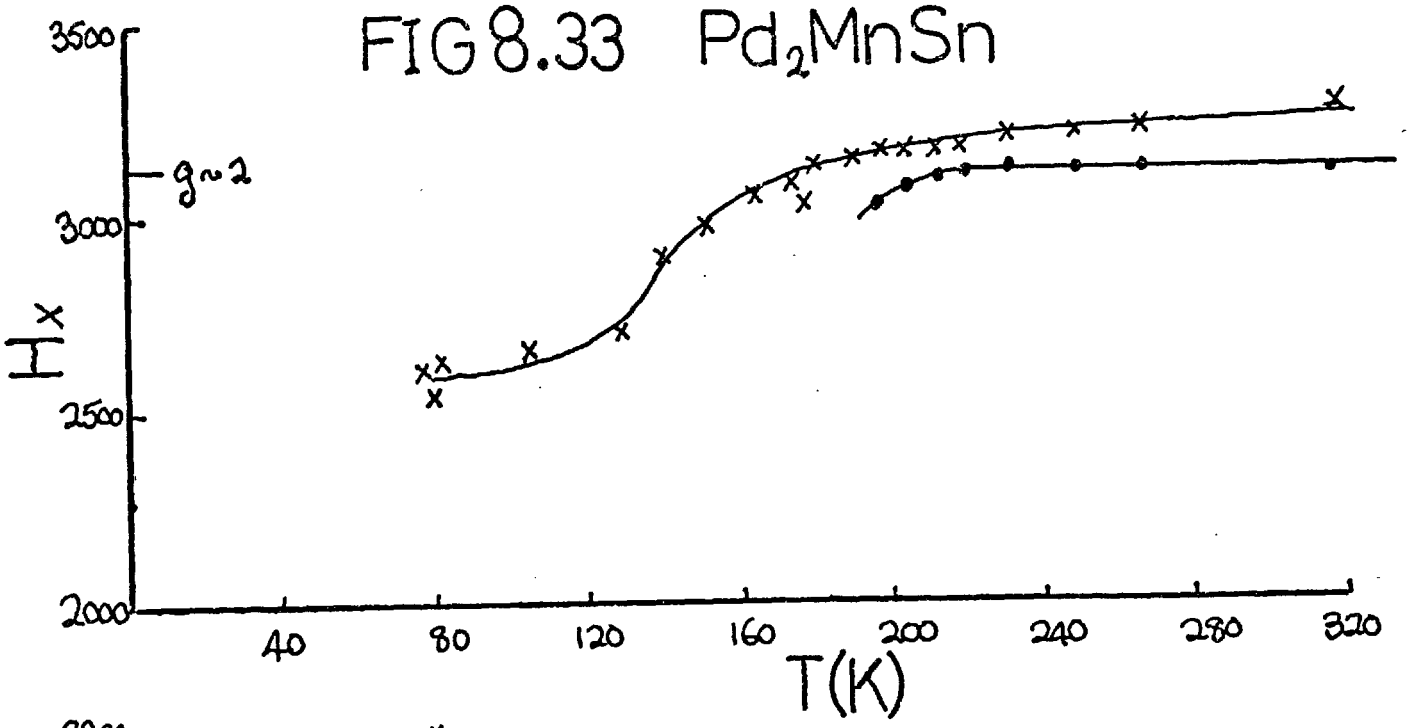


FIG 8.33 Pd_2MnSn



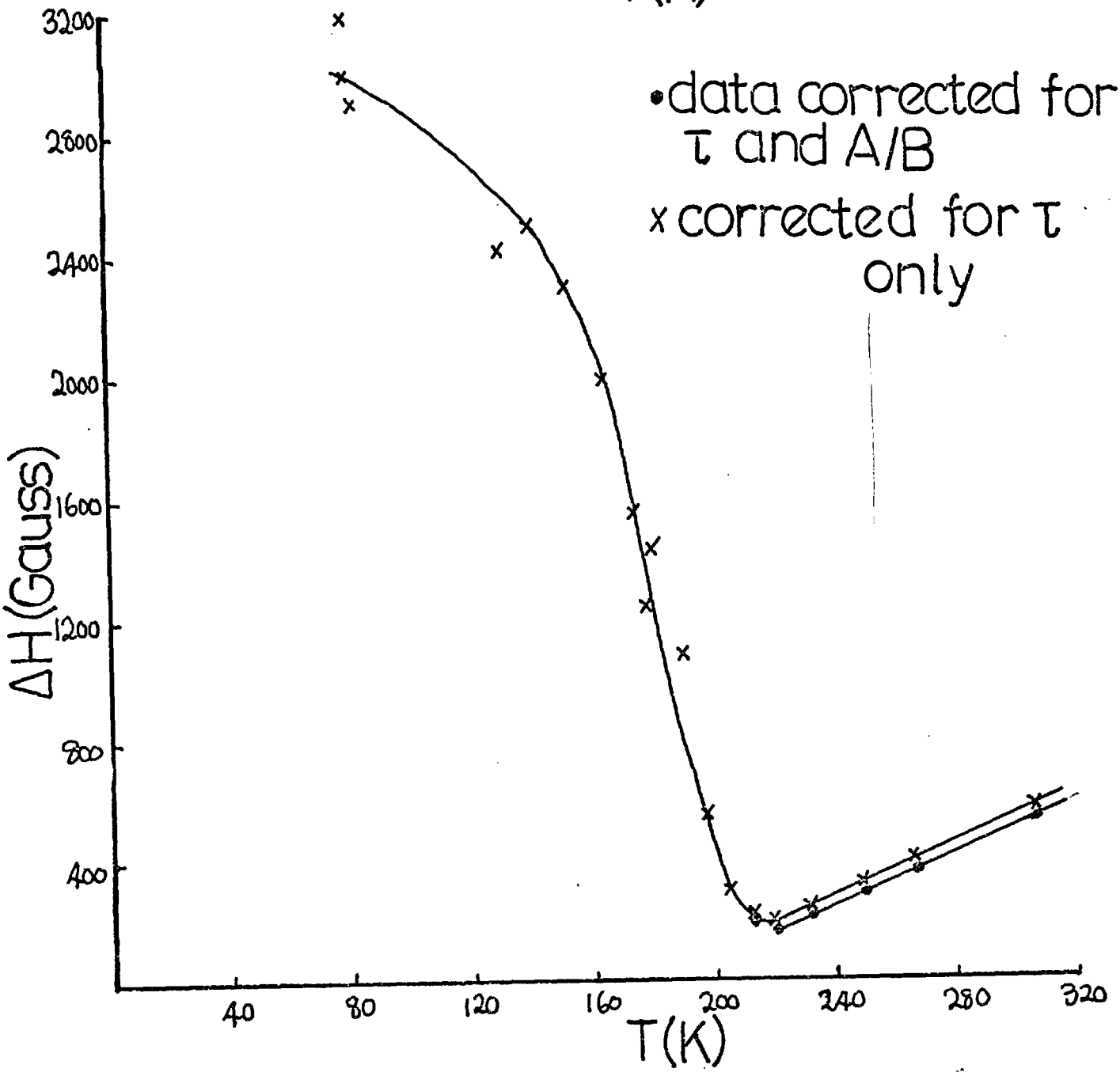
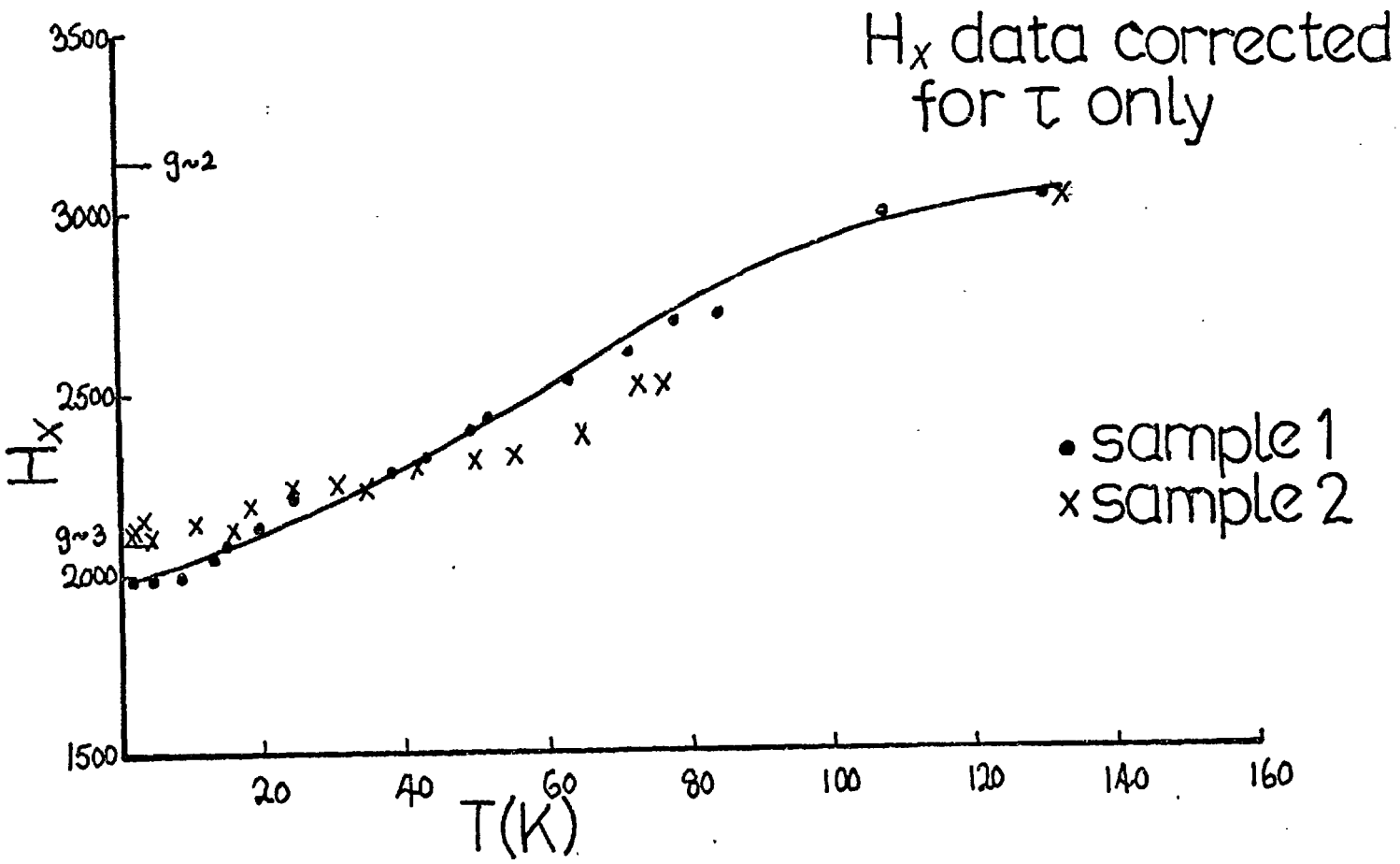


FIG 8.34 $Zn_{13}Mn$ (ζ-phase)



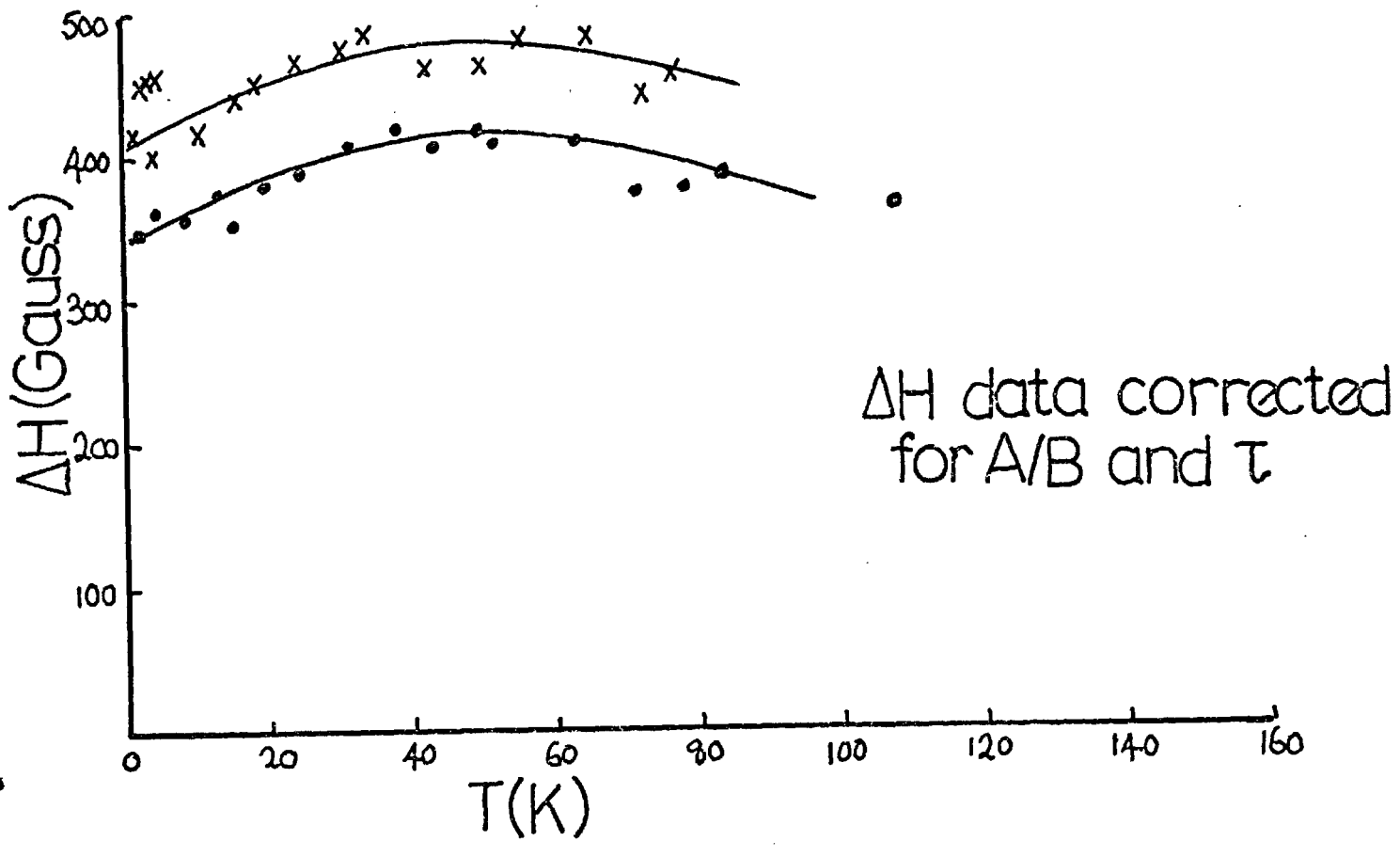
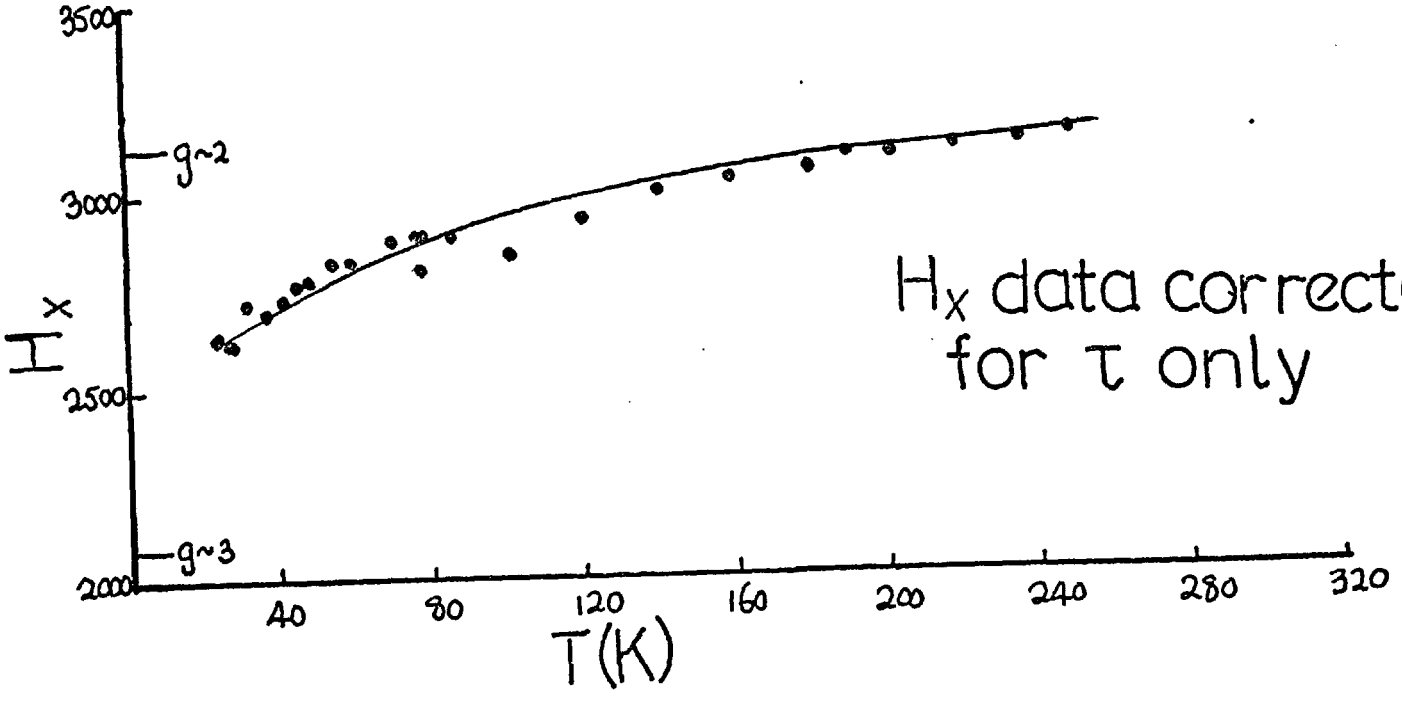
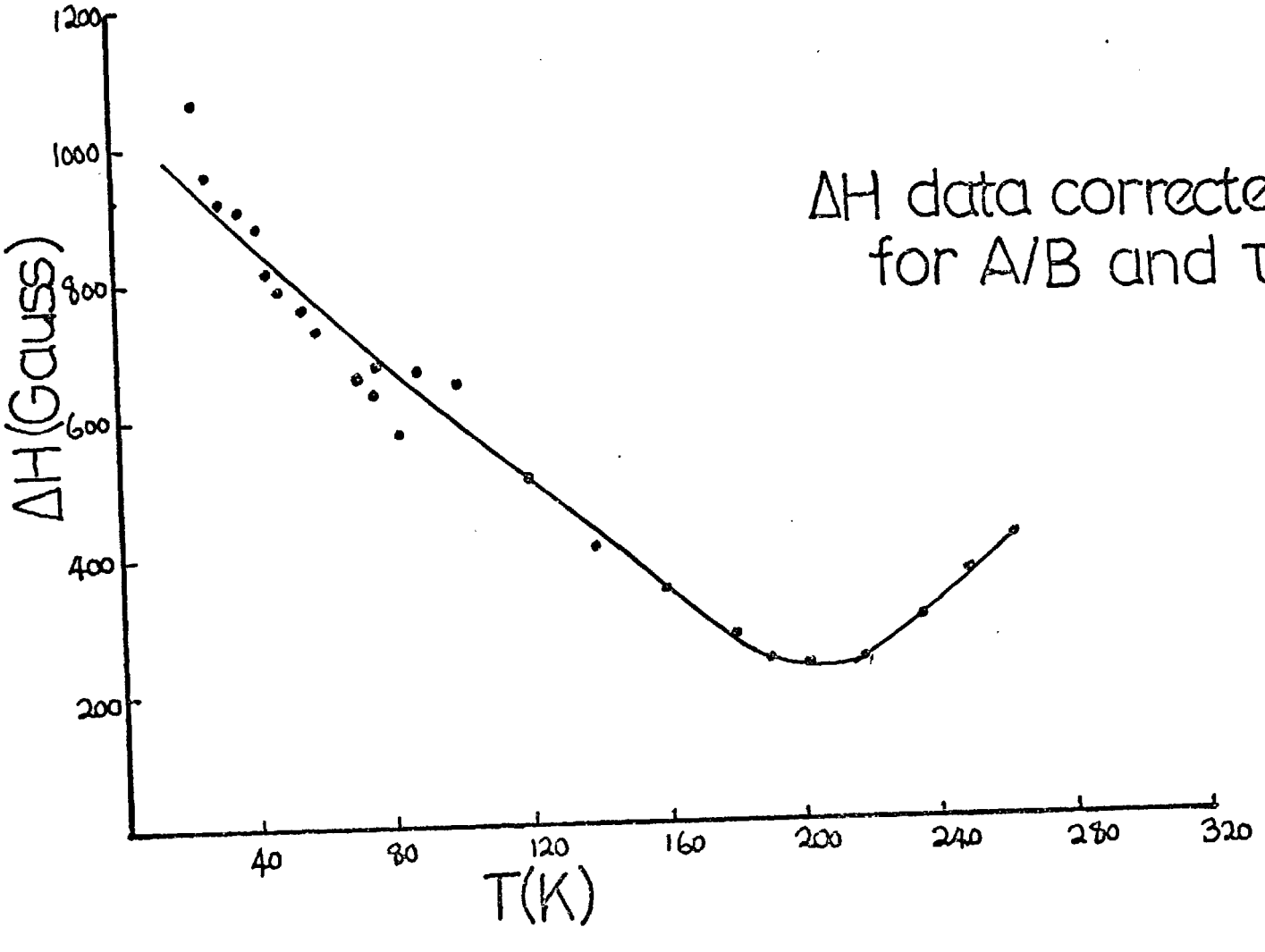


FIG 8.35 $Zn_{10}Mn$ (δ-phase)



H_x data corrected for τ only



ΔH data corrected for A/B and τ

8.4 Intermetallic Compounds - Conclusions

It is clear from 8.3 that the general trends of behaviour in esr associated with different types of magnetic order may be distinguished fairly readily:

1. Compounds which undergo a transition to ferromagnetic order show a shift in resonant field which, very approximately, seems to follow the form of the magnetisation of the sample at the field in which the measurements are made. Furthermore, the linewidth broadens inhomogenously due to the distribution of demagnetising factors for the different particle shapes in the powder. In an ad-hoc way, the temperature at which the compound orders in zero field may be identified with a temperature $\sim 0.8 - 0.9$ times the temperature at which the line begins to broaden and the resonant field to decrease. The compounds $GdAl_2$, $GdPt_2$, $EuPd_2$, Cu_6Gd EuPd and Pd_2MnSn behave in this way.

2. Compounds which order antiferromagnetically do not give an esr signal below T_N. It has been observed that, whereas in some compounds (e.g., Ag_3Gd, Cu_2Gd) the esr linewidth begins to broaden at a temperature less than twice T_N, in other compounds (e.g., GdB_6, GdB_4, $GdZn_{12}$, Gd_2Zn_{17} and "Cu_4Gd") the linewidth begins to broaden at temperatures of up to ten times the Néel temperature. These compounds also appear to show anomalous behaviour above T_N in their inverse susceptibility and resistivity, although the effects in these properties are usually less drastic than in the esr linewidth and are usually observed over a more limited temperature range, frequently $\frac{\theta}{T_N} \gg 1$. The behaviour has been tentatively identified with the presence of an extended regime of short-range order in these compounds, but could possibly be due to the formation of superzone band gaps at a temperature $\sim|\theta|$. Other compounds which may also exhibit this behaviour would appear to be GdAl, GdAg, GdAu, GdCu, $GdZn_2$, $EuAl_2$ and possibly $GdAl_3$ (see ch. 3).

3. The compound Pd_3Gd, whilst showing clear signs of antiferromagnetism in its inverse susceptibility and resistivity, does give an esr signal below T_N. It is suggested that this property may be common to other compounds which are known to be metamagnetic, with a transition to ferromagnetism in critical fields comparable with the field used in the esr experiment. It would be interesting toinvestigate $EuAl_4$, $EuAl_2$ and $GdZn_2$ with a view to examining this suggestion.

4. The esr behaviour of $Zn_{13}Mn$ and $Zn_{10}Mn$ does not fall clearly into any of the above categories. It is possible that $Zn_{10}Mn$ is ferromagnetic but $Zn_{13}Mn$ shows completely anomalous behaviour.

REFERENCES

Chapter 1

1.1 J. H. VAN VLECK, "Theory of Electric and Magnetic Susceptibilities", Oxford University Press, 1932.

1.2 J. O. DIMMOCK, A. J. FREEMAN and R. E. WATSON, Prc. Int. Conf. on Optical Props. of Metals (Amsterdam) 1966.

1.3 T. SUGAWARA, H. NAGASAWA, S. YOSIDA, 11th Int. Conf. on L.T. Physics (St. Andrews), 1969.

1.4 D. GAINON, P. DONZÉ and J. SIERRO, Solid State Comms. 5, 151, 1967.

1.5 J. BOES, A. J. VAN DAM AND J. BIJVOET, Phys. Letts., 28A, 101, 1968.

1.6 Z. FISK, Thesis, University of California, La Jolla, 1969.

1.7 B. T. MATTHIAS, M. PETER, J. H. WILLIAMS, A. M. CLOGSTON, E. CORENZWIT and R. C. SHERWOOD, Phys. Rev. Letts, 5, 542, 1960.

1.8 P. W. ANDERSON, "Many Body Physics" ed. C. DE WIT and R. BALIAN, 1967 Lecture Notes Les Houches Summer School, Gordon and Breach, New York, 1968.

1.9 A. J. HEEGER, Solid State Physics, 23 (Academic Press, New York).

1.10 J. FRIEDEL, Nuovo Cimento, 7, 287, 1958.

1.11 A. BLANDIN and J. FRIEDEL, J. de Physique, 20, 160, 1959.

1.12 P. W. ANDERSON, Phys. Rev. 124, 41, 1961.

1.13 K. YOSIDA, A. OKIJI and S. CHIKAZUMI, Prog. Theor. Phys., 33, 559, 1965.

1.14 A. P. KLEIN and A. J. HEEGER, Phys. Rev. 144, 458, 1966.

1.15 P. A. WOLFF, Phys. Rev., 124, 1030, 1961.

1.16 A. M. CLOGSTON, Phys. Rev., 125, 439, 1962.

1.17 N. RIVIER, Thesis, University of Cambridge, 1968.

1.18 J. R. SCHRIEFFER and D. C. MATTIS, Phys. Rev., 140, 1412, 1965.

1.19 N. RIVIER, M. SUNJIC and M. J. ZUCKERMAN, Phys. Letts., 28a, 492, 1969.

1.20 A. D. CAPLIN and C. RIZZUTTO, Phys. Rev. Letts., 21,746, 1968.

1.21 J. KASUYA, Prg. Theor. Phys., 16, 45, 1956

1.22 T. A. KAPLAN and D. H. LYONS, Phys. Rev., 129, 2072, 1963.

1.23 P. G. DE GENNES, Comptes Rendues, 247, 1836, 1958.

1.24 S. H. LIU, Phys. Rev., 121, 451, 1961.

1.25 C. ZENER, Phys. Rev., 81, 440, 1951.

1.26 K. YOSIDA, Phys. Rev., 106, 893, 1957.

1.27 M. A. RUDERMANN and C. KITTEL, Phys. Rev., 96, 99, 1954.

1.28 P. A. WOL F, Phys. Rev., 120, 814, 1960.

1.29 R. E. WATSON and A. J. FREEMAN, Phys. Rev., 152, 566, 1966.

1.30 A. W. OVERHAUSER, JAP, 34, 1019, 1963.

1.31 P. G. DE GENNES, J. de Physique, 23, 510, 1962.

1.32 R. E. WATSON and A. J. FREEMAN, Phys. Rev. 178, 725, 1969.

1.33 B. GIOVANNINI, M. PETER and J. R. SCHRIEFFER, Phys. Rev. Letts., 12, 736, 1964.

1.34 J. R. SCHRIEFFER and P. A. WOLFF, Phys. Rev., 194, 491, 1966.

1.35 J. KONDO, Prog. Theor. Phys., 32, 37, 1964.

1.36 R. E. WATSON, S. KOIDE, M. PETER and A. J. FREEMAN, Phys. Rev. 139 , A167, 1965.

1.37 B. R. COLES, D. GRIFFITHS, R. J. LOWIN R. H. TAYLOR, J. Phys. (C), 3, L121, 1970.

1.38 C. G. SHULL and Y. YAMADA, J. Phys. Soc. Japan, 17, Suppl. B III, 1, 1962.

1.39 H. A. MOOK and C. G. SHULL, JAP, 37, 1034, 1966

1.40 R. MOON, Phys. Rev., 136, A195, 1964.

1.41 W. C. PHILLIPS, Phys. Rev., 138, A1649, 1965.

1.42 I. A. CAMPBELL, J. Phys. F. Metal Physics, 2, L47, 1972.

1.43 M. PETER, J. DUPRAZ and H. COTTET, Helv. Acta Phys., 40, 301, 1967.

1.44 W. C. KOEHLER and E. O. WOLLAN, Phys. Rev., 92, 1380, 1953.

1.45 A. A. ABRIKOSOV and L. P. GORKOV, JETP, 12, 1243, 1961

1.46 K. N. R. TAYLOR, Adv. in Physics, 20, 551, 1971.

1.47 M. B. MAPLE and Z. FISK, Proc. 11th Int. Conf. L.T. Physics (Edinburgh) 1968.

1.48 J. R. COOPER, Thesis, Univ. of London, 1969.

1.49 M. B. MAPLE, Phys. Letts., 26A, 513, 1968, and Thesis, Univ. of California, La Jolla, 1969.

1.50 W. C. THOBURN, S. LEGVOLD and F. H. SPEDDING, Phys. Rev., 110, 1298, 1958.

1.51 R. M. BOZORTH and R. J. GAMBINO, Phys. Rev. 147, 487, 1966.

1.52 D. WOHLLEBEN, Phys. Rev. Letts. 21, 1343, 1968.

1.53 G. J. VAN DEN BERG, Low Temp. Phys. L.T.9 (Part B) (Plenum Press) 1965.

1.54 T. SUGAWARA, J. Phys. Soc, Japan, 20, 2252, 1965.

1.55 J. KONDO, Solid State Physics, 23 (Academic Press, New York).

1.56 Y. NAGAOKA, Phys. Rev., 138, A1112, 1965.

1.57 N. RIVIER and M. J. ZUCKERMAN, Phys. Rev. Letts., 21, 904, 1968.

1.58 M. S. FULLENBAUM and D. S. FALK, Phys. Rev., 157, 452, 1967.

Chapter 2

2.1 K. H. J. BUSCHOW, J. F. FAST, A. M. VAN DIEPEN and H. W. DE WIJN, Phys. Stat. Sol., 24, 715, 1967.

2.2 A. M. VAN DIEPEN, H. W. DE WIJN and K. H. J. BUSCHOW, Phys. Stat. Sol., 29, 189, 1968.

2.3 H. W. DE WIJN, K. H. J. BUSCHOW, A. M. VAN DIEPEN, Phys. Stat Sol., 30, 759, 1968.

2.4 A. M. STEWART, Thesis, Univ. of London, 1971 and to be published.

2.5 D. K. DEBRAY, W. E. WALLACE and E. RYBA, J. Less Common Metals, 22, 19, 1970.

2.6 B. CAROLI, Thesis, Univ. of Paris 1966 and J. Phys. Chem. Sol., 28, 1427, 1967.

2.7 J. B. DUHLOP, Thesis, Univ. of London, 1972.

2.8 S. ALEXANDER and P. W. ANDERSON, Phys. Rev., 133, 6A, 1964.

2.9 T. MORIYA, Prog. Theor. Phys., 33, 157, 1965.

2.10 V. JACCARINO and L. R. WALKER, Phys. Rev. Letts., 15, 258, 1965.

2.11 D. J. KIM, Phys. Rev., 1, 3724, 1970.

2.12 P. A. BECK, Met. Trans., 2, 2015, 1971.

2.13 W. MARSHALL, Phys. Rev., 118, 1519, 1960.

2.14 J. E. ZIMMERMAN and F. H. HOARE, J. Phys. Chem. Solids, 17, 52, 1960.

2.15 M. W. KLEIN and R. BROUT, Phys. Rev., 132, 2412, 1963.

2.16 M. W. KLEIN, Phys. Rev., 136, A1156, 1964.

2.17 M. W. KLEIN, Phys. Rev. Letts., 11, 409, 1963.

2.18 S. H. LIU, Phys. Rev., 157, 411, 1967.

2.19 W. MARSHALL, T. E. CRANSHAW, C. E. JOHNSON and M. S. RIDOUT, Rev. Mod. Phys., 36, 399, 1964.

2.20 U. GONSER, R. W. GRANT, C. J. MEECHAN, A. H. MUIR JR., and H. WIEDERSUCH, JAP, 36, 2124, 1965.

2.21 J. S. SMART, "Effective Field Theories of Magnetism", Saunders, 1966.

2.22 C. DOLB in "Magnetism", ed. G. T. RADO and H. SUHL, Academic Press Vol. 2A, 1964.

2.23 C. DOLB and A. R. MIEDEMA in "Prog. in Low Temp. Phys." ed. C. J. GONSER, North Holland, 4, 1964.

2.24 D. H. MARTIN, "Magnetism in Solids", Iliffe, 1967.

2.25 W. C. KOEHLER, JAP, 36, 2078, 1965.

2.26 R. J. ELLIOTT in "Magnetism" ed. G. T. RADO and H. SUHL, Academic Press, Vol. 2A, 1964.

2.27 K. YOSIDA in "Prog. in Law Temp. Phys." ed. C. J. GORTER, North Holland, 4, 1964.

2.28 D. MATTIS and W. E. DONATH, Phys. Rev., 128, 1618, 1962.

2.29 A. J. FEDRO and T. ARAI, Phys. Rev., 170, 583, 1968.

2.30 J. C. SLATER, Phys. Rev., 82, 538, 1951.

2.31 B. R. COLES, Adv. in Physics, 7, 40, 1958.

2.32 R. J. ELLIOTT and F. A. WEDGWOOD, Proc. Phys. Soc., 84, 63, 1964.

Chapter 3

3.1 H. J. WILLIAMS, J. H. WERNICK, R. C. SHERWOOD, E. A. NESBITT, J. Phys. Soc. Japan, 17 BI, 91, 1962.

3.2 K. H. MADER and W. E. WALLACE, J. Chem. Phys., 49, 1521, 1968.

3.3 N. MERESON, C. OLSEN and G. ARNOLD, JAP, 37, 4575, 1966.

3.4 J. A. MYDOSH, M. P. KAWATRA, J. I. BUDNICK, Phys. Letts., 24A, 421, 1967.

3.5 H. J. VAN DAAL and K. H. J. BUSCHOW, Sol. State Comms., 7, 217, 1969.

3.6 C. DEENADAS, A. W. THOMPSON, R. S. CRAIG and W. E. WALLACE, J. Phys. Chem. Solids, 32, 1853, 1971.

3.7 F. KISSELL and W. E. WALLACE, J. Less Common Metals, 11, 417, 1966.

3.8 B. BARBARA, C. BECLE, R. LEMAIRE, R. PAUTHENET, JAP, 39, 1084, 1968.

3.9 C. BECLE, R. LEMAIRE, R. PAUTHENET, Comptes Rendues (B), 266, 994, 1968; C. BECLE and R. LEMAIRE, Phys. Letts., 27A, 541, 1968; C. BECLE, R. LEMAIRE, E. PARTHE, Sol. State Comms. 6, 115, 1968.

3.10 K. H. J. BUSCHOW and J. F. FAST, Z. Für Phys. Chem., 50, 1, 1966.

3.11 K. H. J. BUSCHOW, H. W. DE WIJN and A. M. VAN DIEPEN, J. Chem. Phys., 50, 137, 1969.

3.12 G. MERESON and N. ARNOLD, J. Chem. Phys., 51, 1495, 1969 ibid 53, 2818, 1970.

3.13 R. E. WALLINE and W. E. WALLACE, J. Chem. Phys., 42, 604, 1965.

3.14 A. M. VAN DIEPEN, Phys. Stat. Sol., 30, 759, 1968.

3.15 J. PIERRE, "Les Elements des Terres Rares" II CNRS, 55, 1970.

3.16 C. CHAO, JAP, 37, 2018, 1966.

3.17 J. PIERRE and R. PAUTHERT, Comptes Rendues (B), 260, 2739, 1965.

3.18 J. W. CABLE, W. C. KOEHLER, E. O. WOLLAN, Phys. Rev., 136 (A), 240, 1964.

3.19 R. C. SHERWOOD, J. H. WILLIAMS, J. H. WERNICK, JAP, 35, 1049, 1964

3.20 T. O. BRUN, G. P, FELCHNER and J. S. KOUVEL, to be published.

3.21 G. WILLIAMS, Thesis, Univ. of London, 1969.

3.22 K. H. J. BUSCHOW, A. M. VAN DIEPEN, H. W. DE WIJN, Proc. 8th Conf. on Rare-Earths (Reno), 53, 1970.

3.23 W. GARDNER, J. PENFOLD, T. F. SMITH, I. R. HARRIS, J. Phys. (F) 2, 133, 1972.

3.24 E. BUCHER, K. ANDRES and A. S. COOPER, to be published.

3.25 R. D. HUTCHENS, V. U. S. RAO, J. E. GREEDAN, W. E. WALLACE and R. S. CRAIG, JAP, 42, 1293, 1971.

3.26 I. R. HARRIS and G. LONGWORTH, J. Less Common Metals, 23, 281, 1971.

3.27 H. H. WICKMAN, J. H. WERNICK, R. C. SHERWOOD, F. C. WAGNER, J. Phys. Chem. Solids, 29, 181, 1968.

3.28 J. CRANGLE and J. W. ROSS, Proc. Int. Conf. Mag. (Nottingham), 240, 1964.

3.29 W. E. WALLACE and Y. G. VLASOV, Inorganic Chem. 6, 2216, 1967.

3.30 D. K. DEBRAY, W. E. WALLACE and E. RYBA, J. Less Common Metals, 22, 19, 1970.

3.31 B. R. COLES and D. GRIFFITHS, Proc. Phys. Soc., 77, 213, 1961.

3.32 B. R. COLES, T. COLB, J. LALBE AND H. LAURENCE, Proc. Phys. Soc., 79, 84, 1962.

3.33 E. F. WESTRUM JR., Prog. in Science and Techn. of Rare Earths, Vol. 3 (Oxford, Pergamon) p.459.

3.34 Z. FISK, Phys. Letts., 34A, 261, 1971.

3.35 A. J. P. MEYER, Comptes Rendues, 244, 2028, 1957.

3.36 I. S. JACOBS, J. S. KOUVEL and P. E. LAWRENCE, J. Phys. Soc. Japan BI, 17, 157, 1962.

3.37 P. J. WEBSTER and R. S. TEBBLE, Phil. Mag. 16, 347, 1967, ibid JAP 39, 471, 1968.

3.38 P. J. WEBSTER, Contemp. Phys., 10, 559, 1969.

3.39 Y. NAKAGAWA, S. SAKAI and T. HORI, J. Phys. Soc.Japan, 17, BI, 168, 1962.

3.40 J. CRANGLE, Phys. Rev. Letts., 13, 569, 1964.

3.41 M. P. SARACHIK and D. J. SHALTIEL, JAP, 38, 1155, 1967.

3.42 C. W. CHEN, L. R. EDWARDS and S. LEGVOLD, Phys. Stat. Solid., 26, 611, 1968.

3.43 P. W. BELLARBY and J. CRANGLE, J. Phys. (c) Suppl. 3, 362, 1970.

3.44 R. P. GUERTIN and S. FONER, JAP, 41, 917, 1970.

3.45 J. CRANGLE, Phil. Mag. 5, 335, 1960, and J. CRANGLE and W. R. SCOTT, JAP, 36, 921, 1965.

3.46 J. W. CABLE, E. O. WOLLAN and W. C. KOEHLER, JAP, 34, 1189, 1963.

3.47 G. G. LOW, Proc. Int. Conf. Mag. (Nottingham), 133, 1964 and G. G. LOW and T. M. HOLDEN, Proc. Phys. Soc., 89, 119, 1966.

3.48 B. W. VEAL and J. A. RAYNE, Phys. Rev. 135, A442, 1964.

3.49 B. R. COLES, J. H. WASZINK and J. LORAM, Proc. Int. Conf. Mag. (Nottingham), 165, 1964.

3.50 G. WILLIAMS and J. LORAM, J. Phys. Chem. Sol., 30, 1827, 1969.

3.51 D. M. S. BAGGULEY, W. A. CROSSLEY and J. LIDSEGANG, Proc. Phys. Soc., 90, 1047, 1967.

3.52 G. CHOUTEAU and R. TOURNIER, Proc. 7th Int. Conf. Mag., 1970 (Grenoble) J. de Phys., 32, C1 - 1002, 1971.

3.53 R. M. BOZORTH, P. A. WOLFF, D. D. DAVIS, V. B. COMPTON and J. H. WERNICK, Phys. Rev., 122, 1157, 1961.

3.54 B. M. BOERSTEL, Thesis, Univ. of Leiden, 1970 and references therein.

3.55
(a) G. WILLIAMS, J. Phys. Chem. Sol., 31, 529, 1970, and
(b) G. WILLIAMS and J. LORAM, Solid State Comms., 7, 1261, 1969.

3.56 M. P. SARACHIK and D. SHALTIEL, JAP, 38, 1155, 1967.

3.57 J. RAULT and J. P. BURGER, Comptes Rendues (B), 269, 1085, 1969.

3.58 W. M. STAR, S. FONER and E. J. McNIFF JR., Phys. Letts. 39A, 189, 1972

3.59 J. S. KOUVEL, J. Phys. Chem. Solids, 21, 57, 1961.

3.60 R. J. BORG, R. BOOTH and C. E. VIOLET, Phys. Rev. Letts, 11, 464, 1963.

3.61 O. S. LUTES and J. L. SCHMIDT, Phys. Rev., 125, 433, 1962.

3.62 V. CARBELLA, J. A. MYDOSH and J. I. BUDNICK, JAP, 42, 1689, 1971.

3.63 J. A. MYDOSH, M. P. KAWATRA, J. I. BUDNICK, T. A. KITCHEN and R. J. BORG, Proc. 11th Int. Conf. Low Temp. Phys. (St. Andrews) 1324, 1968.

3.64 E. W. COLLINGS, F. T. HEDGCOCK AND Y. MUTO, Phys. Rev., 134, A1521, 1964, and E. W. COLLINGS, F. T. HEDGCOCK and W. B. MUIR, Proc. 8th Int. Conf. Low Temp. Phys. (London) 253, 1962.

3.65 D. L. MARTIN, Phys. Rev. 167, 640, 1968, ibid 186, 642, 1969.

3.66 A. MURANI and B. R. COLES, J. Phys. C, 2, S159, 1970 and to be published.

3.67 A. TARI and B. R. COLES, J. Phys. (F) 1, L59, 1971.

3.68 P. LEDERER and D. L. MILLS, Phys. Rev., 165, 837, 1968.

3.69 A. I. SCHINDLER and M. J. RICE, Phys. Rev. 164, 759, 1967 and A. I. SCHINDLER and D. R. COLES, JAP, 39, 956, 1968.

3.70 D. K. FINNEMORE, L. J. WILLIAMS, F. H. SPEDDING and D. C. HOPKINS, Phys. Rev., 176, 712, 1968 ibid Phys. Rev. Letts. 15, 891, 1965.

3.71 F. A. MÜLLER, R. GERSDORF, L. W. ROELAND, Phys. Letts., 31a, 424, 1970.

3.72 J. J. VUILLEMIN and M. PRIESTLY, Phys. Rev. Lett. 14, 307, 1965.

Chapter 4

4.1 E. BLOCH, Phys. Rev. 70, 460, 1946.

4.2 C. P. SLICHTER, "Principles of Magnetic Resonance", Harper and Row, 1964.

4.3 G. E. PAKE, "Paramagnetic Resonance", Benjamin, 1962.

4.4 G. WILLIAMS and L. HIRST, Phys. Rev., 185, 407, 1969.

4.5 A. P. MURANI, J. Phys. C., Metal Physics Suppl. No. 2, S153, 1970.

4.6 W. LOW, "Paramagnetic Resonance Solids", Academic Press, 1960.

4.7 C. KITTEL and A. H. MITCHELL, Phys. Rev., 101, 1611, 1956.

4.8 H. HASEGAWA, Prog. Theor. Phys. 21, 483, 1951.

4.9 A. OVERHAUSER, Phys. Rev., 89, 689, 1953.

4.10 J. KORRINGA, Physica, 16, 601, 1950.

4.11 R. ORBACH, Proc. Colloque Ampere XVI, 1970 (Bucharest, Rumania)

4.12 T. MORIYA, J. Phys. Soc. Japan, 18, 516, 1965.

4.13 A. NARATH in "Hyperfine Interactions", ed. A. J. FREEMAN and R. B. FRANKEL (Academic Press, New York) 1967, p.344.

4.14 J. DUPRZ, B. GIOVANNINI, R. ORBACH, J. D. RILEY, N. RIVIER and J. ZITKOVA, "Magnetic Resonance", Plenum Press, 1970.

4.15 H. J. SPENCER and S. DONIACH, Phys. Rev. Letts., 18, 994, 1967.

4.16 S. E. BARNES, J. DUPRAZ and R. ORBACH, JAP, 42, 1659, 1971.

4.17 J. H. VAN VLECK, Phys. Rev. 74, 1169, 1948.

4.18 C. KITTEL and E. ABRAHAMS, Phys. Rev. 90, 238, 1951.

4.19 P. W. ANDERSON and P. R. WEISS, Rev. Mod. Phys., 25, 269, 1953.

4.20 C. KITTEL, Phys. Rev. 71, 270, 1947, ibid 73, 155, 1948.

4.21 T. NAGAMIYA, Prog. Theor. Phys., 6, 342, 1951; C. KITTEL, Phys. Rev., 82, 565, 1951; F. KEFFER and C. KITTEL, Phys. Rev. 85, 329, 1952.

4.22 H. MORI and K. KAWASAKI, Prog. Theor. Phys., 28, 971, 1962.

4.23 H. MORI, Prog. Theor. Phys. 30, 478, 1963 ibid 30, 576, 1963.

4.24 K. KAWASAKI, Prog. Theor. Phys., 39, 285, 1968.

4.25 L. R. MAXWELL and T. R. McGUIRE, Rev. Mod. Phys., 25, 279, 1953.

4.26 N. J. ZIMMERMAN, F. P. VAN DER MARK and J. VAN DEN HANDEL, Physica, 46, 204, 1970.

4.27 M. S. SEEHRA and T. G. CASTNER, Sol. State Comms., 8, 787, 1970.

4.28 J. W. BATTLES, JAP, 42, 1286, 1971.

4.29 M. B. SALAMON, Phys. Rev., 155, 2, 1967.

Chapter 5

5.1 A. F. KIP, Rev. Mod. Phys. 25, 229, 1953.

5.2 Y. CHIBA and A. NAKAMURA, J. Phys. Soc. Japan, 29, 792, 1970.

5.3 J. POPPLEWELL and R. S. TEBBLE, JAP, 34, 1343, 1963.

5.4 D. S. RODBELL and T. W. MOORE, Proc. Int. Conf. on Magnetism (Nottingham) 428, 1964.

5.5 M. PETER and B. T. MATTHIAS, Phys. Rev. Letts., 4, 449, 1960.

5.6 V. JACCARINO, B. T. MATTHIAS, M. PETER, H. SUHL and J. H. WERNICK, Phys. Rev. Letts, 5, 252, 1960.

5.7 M. PETER, JAP, 32, 3388, 1961.

5.8 D. SHALTIEL, J. H. WERNICK. H. J. WILLIAMS and M. PETER, Phys. Rev., 135, 1346, 1964.

5.9 J. H. WERNICK, H. J. WILLIAMS and A. C. GOSSARD, J. Phys. Chem. Solids, 28, 271, 1967.

5.10 R. VIJAYARAGHAVAN, SATISH K. MALIK, V. UDAYA SHANKAR RAO, Phys. Rev. Letts. 20, 106, 1968 ibid JAP, 39, 1086, 1968.

5.11 D. DAVIDOV and D. SHALTIEL, Phys. Rev., 169, 329, 1968.

5.12 H. HACKER, R. GUPTA and M. L. SHEPPARD, Phys. Stat. Sol., 9, 601, 1972.

5.13 K. OKUDA and M. DATE, J. Phys. Soc. Japan, 25, 1732, 1968.

5.14 E. BURZO and I. URSU, Sol. State Comms., 9, 2289, 1971.

5.15 B. R. COLES, T. COLE, J. LAIBE and N. LAURANCE, Proc. Phys. Soc., 79, 84, 1962.

5.16 D. E. MILLER and H.HACKER JR., Sol. State Comms., 9, 881, 1971.

5.17 D. SHALTIEL, J. H. WERNICK and V. JACCARINO, JAP 35 (2), 978, 1964.

5.18 D. SHALTIEL, A. C. GOSSARD, J. H. WERNICK, Phys. Rev., 137, 1027, 1965.

5.19 H. COTTET, P. DONZE, J. DUPRAZ, B. GIOVANNINI, M. PETER, Z. ANGEW, Phys. 24, 249, 1968 and Helv. Acta Phys. 40, 357, 1967.

5.20 D. DAVIDOV, H. LOTEM and D. SHALTIEL, 28A, 672, 1969.

5.21 D. DAVIDOV and D. SHALTIEL, Phys. Rev. Letts., 21, 1752, 1968.

5.22 D. DAVIDOV, G. DOUBLON and D. SHALTIEL, Phys. Rev. 3B, 3651, 1971.

5.23 W. SCHÄFER, H. K. SCHMIDT, B. ELSCHNER and K. H. J. BUSCHOW, Phys. Letts., 33A, 23, 1970.

5.24 R. J. LOWIN, Thesis, Univ. of London, 1970.

5.25 R. DAVIDOV, H. LOTEM. D. SHALTIEL, M. WEGER, J. H. WERNICK, Phys. Rev. 2, 184, 1969.

5.26
(a) M. PETER, D. SHALTIEL, J. H. WERNICK, J. H. WILLIAMS, J. B. MOCK and R. C. SHERWOOD, Phys. Rev. 126, 1395, 1962.
(b) D. W. BUDWORTH, F. E. HOARE and J. PRESTON, Proc. Roy. Soc. (London), A.257, 250, 1960.

5.27 M. PETER, D. SHALTIEL, J. H. WERNICK, H. J. WILLIAMS, J. B. MOCK and R. C. SHERWOOD, Phys. Rev. Letts., 9, 50, 1962.

5.28 D. SHALTIEL, JAP, 34, 1190, 1963.

5.29 A. M. HARRIS, J. POPPLEWELL and R. S. TEBBLE, Proc. Phys. Soc, 85, 513, 1965.

5.30 H. COTTET, Thesis, Univ. of Geneva 1971.

5.31 H. COTTET and M. PETER, Sol. State Comms., 8, 1601, 1970.

5.32 H. C. PRADDAUDE and H. GÄRTNER, Phys. Letts., 34(a), 217, 1971.

5.33 D. SHALTIEL, R. A. DEVINE, J. M. MONET, J. ORTELLI, P. DONZE and M. PETER, to be published.

5.34 A. M. HARRIS, J. POPPLEWELL and R. S. TEBBLE, Proc. Phys. Soc., 85, 513, 1965.

5.35 M. B. SALAMON, Phys. Rev. Letts., 26, 704, 1971.

5.36 A. NAKAMURA, Y. NISHIHARA and N. KINOSHITA, Proc. Int. Conf. L. T. Physics (Kyoto), 1970.

5.37 D. GRIFFITHS and B. R. COLES, Phys. Rev. Letts., 16, 1093, 1966

5.38 S. EHARA, Can. J. Phys., 49, 352, 1971.

5.39 G. WILLIAMS, J. Phys (F), 2, L6, 1972.

5.40 L. J. TAO. D. DAVIDOV, R. ORBACH, D. SHALTIEL and C. R. BURR, Phys. Rev. Letts., 26, 1438, 1971.

5.41 C. R. BURR and R. ORBACH, Phys. Rev. Letts, 19, 1133, 1967.

5.42 E. P. CHOCK, R. CHUI, D. DAVIDOV, R. ORBACH, D. SHALTIEL and L. J. TAO, Phys. Rev. Letts., 27, 582, 1971.

5.43 D. DAVIDOV, R. ORBACH, C. RETTORI, D. SHALTIEL and L. J. TAO, Phys. Rev., 5B, 1711, 1972.

5.44 W. SCHÄFER, H. K. SCHMIDT and S. HÜFNER, Phys. Letts., 28A, 4, 1968.

5.45 J. OWEN, M. E. BROWNE, V. ARP and A. F. KIP, J. Phys. Chem. Solids, 2, 85, 1957.

5.46 J. OWEN, M. E. BROWNE, W. D. KNIGHT and C. KITTEL, Phys. Rev. 102, 1501, 1956.

5.47 D. SHALTIEL and J. H. WERNICK, Phys. Rev., 136, A245, 1964.

5.48 S. GESCHWIND, G. E. DEVLIN and J. H. WERNICK, JAP, 37, 1221, 1966.

5.49 D. GRIFFITHS, Proc. Phys. Soc., 90, 707, 1967.

5.50 A. C. GOSSARD, A. J. HEEGER and J. H. WERNICK, Bull. Am. Phys. Soc. 12, 1031, 1967, ibid JAP, 38, 1251, 1967.

5.51 K. OKUDA and M. DATE, J. Phys. Soc. Japan, 22, 1512, 1967 ibid 27, 839, 1969.

5.52 J. A. McELROY and A. J. HEEGER, Phys. Rev. Letts. 20, 1481, 1968.

5.53 A. NAKAMURA and N. KINOSHITA, J. Phys. Soc. Japan, 22, 335, 1967 ibid 23, 449, 1967.

5.54 A. C. GOSSARD, T. Y. KOMETANI and J. H. WERNICK, JAP, 39, 849, 1968.

5.55 Y. MIKADO, T. WATANABE and M. WATANABE, Phys. Rev. 182, 495, 1969.

5.56 R. R. ELLISTON, Phys. Stat. Solid., 9A, 111, 1970.

5.57 Y. ODA and K. ASAYAMA, J. Phys. Soc. Japan, 25, 1510, 1968, ibid 29, 4, 1970.

5.58 H. NAGASHIMA and H. ABE, Report of ISSP (A), No. 489, Oct. 1971.

5.59 E. W. COLLINGS and F. T. HEDGCOCK, Phys. Rev., 126, 1654, 1962.

5.60 E. W. COLLINGS, F. T. HEDGCOCK and W. B. MUIR, Proc. 8th Conf. Low Temp. Physics (London) 253, 1962.

5.61 Y. MIYAKO, Proc. 12th Int. Conf. Low Temp. Physics (Kyoto), 363, 1970.

5.62 M. B. SALAMON and F. J. FEIGL, J. Phys. Chem. Sol. 29, 1443, 1968.

5.63 L. L. HIRST, G. WILLIAMS, D. GRIFFITHS and B. R. COLES, JAP, 39, 844, 1968.

5.64 R. CHUI, R. ORBACH and B. I. GEHMAN, Phys. Rev. B2, 2298, 1970.

5.65 L. J. TAO, D. DAVIDOV, R. ORBACH, E. P. CHOCK, Phys. Rev., B4, S, 1971.

5.66 E. P. CHOCK, D. DAVIDOV, R. ORBACH, C. RETTORI, L. J. TAO, Phys. Rev. 5B, 2735, 1972.

5.67 D. DAVIDOV, R. ORBACH, L. J. TAO and E. P. CHOCK, Phys. Letts., 34A, 379, 1971.

5.68 D. DAVIDOV, R. ORBACH, C. RETTORI, D. SHALTIEL, L. J. TAO and B. RICKS, Phys. Letts, 35A, 339, 1971.

5.69 D. DAVIDOV, R. ORBACH, C. RETTORI, L. J. TAO and E. P. CHOCK, Phys. Rev. Letts., 28, 490, 1972.

5.70 D. DAVIDOV, R. ORBACH, C. RETTORI, D. SHALTIEL and L. J. TAO, Sol. State Comms. 10, 451, 1971.

5.71 D. COWAN, Phys. Rev. Letts., 18, 770, 1967.

5.72 S. SCHULTZ, M. R. SHANABARGER and P. M. PLATZMAN, 19, 749, 1967.

5.73 P. MONOD and S. SCHULTZ, Phys. Rev. 173, 645, 1968.

Chapter 6

6.1 For Example, HUME ROTHERY and RAYNOR "The Structure of Metals and Alloys", Institute of Metals, 1962.

6.2 F. LAVES, Naturwissenschaften, 27, 65, 1939.

6.3 A. E. DWIGHT, Trans. Am. Soc. Metals, 53, 479, 1961.

6.4 F. LAVES and H. WITTE, Metallwirtschaft 14, 645, 1936, ibid 15, 840, 1936.

6.5 H. KLEE and H. WITTE, Z. Phys. Chem., 202, 352, 1954.

6.6 J. H. WERNICK, "Intermetallic Compound" ed. WESTBROOK, Wiley, 197, 1967

6.7 H. E. N. STONE, J. Phys. E., 4, 1058, 1971.

6.8 S. STEEB, D. GODEL and C. LOHR, J. Less Common Metals, 15, 137, 1968.

6.9 K. A. GSCHNEIDER JR., O. D. McMASTERS, D. G. ALEXANDER and R. F. VENTEICHER, Met. Trans., 1, 1961, 1970.

6.10 O. D. McMASTERS, G. BRUZZONE, A. PALENZONA and K. A. GSCHNEIDER JR., J. Less Common Metals, 25, 135, 1971.

6.11 K. H. J. BUSCHOW and J. H. N. VAN VUCHT, Phillips Research Rep., 22, 233, 1967.

6.12 K. H. J. BUSCHOW, J. Less Common Metals, 8. 209, 1965.

6.13 O. J. C. RUNNALS and R. R. BOUCHER, J. Less Common Metals, 13, 431, 1967.

6.14 "The Constitution of Binary Alloys, 2nd Supplement, SCHUNK, McGraw Hill, 1969.

6.15 D. WATANABE, J. Phys. Soc. Japan, 13, 535, 1958.

6.16 D. P. MORRIS and J. L. HUGHES, Acta Cryst., 17, 209, 1964.

6.17 D. P. MORRIS, J. L. HUGHES and G. DAVIES, Phil. Mag., 8, 1977, 1963.

6.18 H. C. LONGUET-HIGGINS and M. de V. ROBERTS, Proc. Roy. Soc. (London) A224, 336, 1954.

6.19 A. ZALKIN and D. H. TEMPLETON, Acta Cryst., 6, 269, 1953.

6.20 W. N. LIPSCOMB and D. BRITTON, J. Chem. Phys., 33, 275, 1960.

6.21 A. C. LARSON and D. T. CROMER, Acta Cryst, 14, 73, 1961.

6.22 K. A. GSCHNEIDER JR., "The Rare Earths", Wiley, 159, 1961.

6.23 K. H. J. BUSCHOW, Phillips Res. Rep., 25, 227, 1970.

6.24 J. L. MORIARTY and N. C. BAENZIGER cited by LUNDIN in "The Rare Earths" (unpublished data), ed. F. H. SPEDDING and A. H. DAANE, Wiley, 1961, ibid Acta Cryst., 14, 946, 1961.

6.25 K. H. J. BUSCHOW, A. S. VAN DER GOOT and J. BIRKHAN, J. Less Common Metals, 20, 309, 1970.

6.27 D. T. CROMER, A. LARSON and R. B. ROOF, Acta Cryst., 13, 1913, 1960.

6.28 "The Constitution of Binary Alloys", HANSEN, McGraw Hill, 1958.

6.29 I. R. HARRIS and G. V. RAYNOR, J. Less Common Metals, 9, 7, 1965.

6.30 I. R. HARRIS and G. V. RAYNOR, J. Less Common Metals, 9, 263, 1965.

6.31 I. R. HARRIS, J. Less Common Metals, 14, 459, 1968

6.32 A. IANDELLI and A. PALENZONA, J. Less Common Metals, 12, 333, 1967.

6.33 I. R. HARRIS and M. NORMAN, J. Less Common Metals, 22, 127, 1970.

Chapter 7

7.1 R. ROSENBAUM, Rev. Sci. Inst., 39, 890, 1968.

7.2 R. BERMAN, "Int. Adv. in Cryogenics", Plenum Press, 1965.

73. D. GRIFFITHS, J. Sci. Inst. 2(2), 1124, 1962.

7.4 G. FEHER, Bell. Syst. Techn. J., 36, 449, 1957.

7.5 H. C. TORREY and C. A. WHITMER etc. "Crystal Rectifiers", Rad. Lab. Series, McGraw-Hill, 15, 1947.

7.6 T. H. WILMSHURST, "ESR Spectrometers", Hilger, 1967.

7.7 J. P. GORDON, Rev. Sci. Inst., 32, 658, 1961.

7.8 F. DYSON, Phys. Rev., 98, 349, 1955.

7.9 G. FEHER and A. F. KIP, Phys. Rev., 98, 337, 1955.

APPENDIX 1

Search for a Cerium Resonance

The Ce^{3+} ion has a configuration $6S_2 4f_1$ and application of Hund's rule leads to a value J = 5/2. This manifold is split by a cubic or octahedral crystal field into a Γ_7 doublet and a Γ_8 quartet, and the tables of Lea et al (A.1) suggest that for a crystal field of octahedral symmetry, the Γ_7 state is lowest with g = 1.45, whilst for a cubic crystal field the quartet is the ground state.

White et al (A.2) from static susceptibility measurements on $CeAl_2$ deduced that in this compound the Γ_7 doublet is the ground state and this contention is supported by the specific heat measurements of Hill and Da Silva (A.3). Lowin (5.24) searched for an esr signal at helium temperatures in both $CeAl_2$ and $LaAl_2$ with 0.9% of the La atoms replaced by Ce, but was unable to detect a resonance. This is not surprising, since although the Γ_7 doublet may be lowest in these alloys, the appearance of a well-defined Kondo anomaly in the resistivity (A.4) would suggest that the exchange integral between the 4f moment and the conduction electrons is large. From his neutron diffraction data on $CeAl_2$, Rainford (A.5) estimates a spin-lattice relaxation time $\sim 4 \times 10^{-13}$ secs. at T = 0K, which is equivalent to a linewidth $\sim 10^5$ Gauss.

In this work, the possibility of observing a Ce resonance in a number of other compounds and solid solutions has been explored. The lattice parameter of YAl_2 is $\sim 3.5\%$ smaller than that of $LaAl_2$ and thus we might expect that the Ce ion in this case will be under greater pressure. The 4f level will thus be squeezed closer to the Fermi level, mixing with the conduction electrons will increase and there will be a tendency towards an even broader line than in the $LaAl_2$ - Ce case. Indeed, no resonance line was observed at 1.7K from an YAl_2 alloy containing 3% Ce.

Murani (A.6) has recently shown that in Au-Ce alloys, there is no detectable Kondo effect in the resistivity and the nuclear orientation study of Flouquet (A.7) suggests that in these alloys the Γ_7 state is lowest. Unfortunately, no signal was observed at 1.6K from the alloy prepared by Murani, diluted to 300 ppm Ce.

Although no clear experimental evidence exists to suggest that the Γ_7 state is lowest, an attempt was made to observe resonance in the alloys:

1. $CeIn_3$
2. $LaIn_3$ - 3at% Ce

and 3. Rh 0.1at% Ce

but again without success.

It is clearly of interest to continue searching for a resonance from the Ce^{3+} ion in any compounds or solid solutions in which the Γ_7 state is known to be lowest and where the value of the local moment - conduction electron exchange is small. It would be interesting to use single crystals of materials containing Ce, in the hope of observing resonance from a Γ_8 quartet ground state as observed in AuDy by Davidov et al (5.69). Extension of the present measurements to the He_3 range would also increase the probability of observing a Ce resonance and the Au-Ce alloy would be an ideal candidate for such an investigation.

REFERENCES

A.1 K. R. LEA, M. J. M. LEASK and W. P. WOLF, J. Phys. Chem. Solids, 23, 1381, 1962

A.2 R. M. WHITE, H. J. WILLIAMS, J. H. WERNICK and R. C. SHERWOOD, Phys. Rev. 131, 1039, 1963.

A.3 R. W. HILL and J. M. MACHADO DA SILVA, Phys. Letts., A30, 13, 1969.

A.4 H. J. VAN DAAL and K. H. J. BUSCHOW, Phys. Stat. Sol. (a) 3, 853, 1970.

A.5 B. RAINFORD, Thesis, Univ. of Oxford, 1969.

A.6 A. P. MURANI, to be published.

A.7 J. FLOUQUET, Phys. Rev. Letts., 27, 515, 1971.

APPENDIX 2

Summary of Magnetic and Crystallographic Data on Intermetallic Compounds

TABLE A.1 Ionic properties of the rare-earths of importance to their magnetic behaviour.

Ion	No. of 4f electrons	Ground state	S	L	J	g	$g\sqrt{J(J+1)}$	$(g-1)^2J(J+1)$	gJ
La^{3+}	0	$^1S_0$	0	0	0	0	0	0	0
Ce^{3+}	1	$^2F_{5/2}$	0.5	3	2.5	0.86	2.54	0.17	2.14
Pr^{3+}	2	$^3H_4$	1	5	4	0.8	3.58	0.80	3.20
Nd^{3+}	3	$^4I_{9/2}$	1.5	6	4.5	0.73	3.62	1.84	3.28
Pm^{3+}	4	$^5I_4$	2	6	4	0.6	2.68	3.2	2.40
Sm^{3+}	5	$^6H_{5/2}$	2.5	5	2.5	0.286	0.84	4.54	0.72
$Eu^{3+}Sm^{2+}$	6	$^7F_0$	3	3	0	0	0.0	0	0
$Gd^{3+}Eu^{2+}$	7	$^8S_{7/2}$	3.5	0	3.5	2	7.94	15.75	7
Tb^{3+}	8	$^7F_6$	3	3	6	1.5	9.72	10.5	9
Dy^{3+}	9	$^6H_{15/2}$	2.5	5	7.5	1.33	10.63	7.08	10
Ho^{3+}	10	$^5I_8$	2	6	8	1.25	10.6	4.5	10
Er^{3+}	11	$^4I_{15/2}$	1.5	6	7.5	1.2	9.59	2.55	9
Tm^{3+}	12	$^3H_6$	1	5	6	1.17	7.57	1.17	7
Yb^{3+}	13	$^2F_{7/2}$	0.5	3	3.5	1.14	4.54	0.32	4
$Lu^{3+}Yb^{2+}$	14	$^1S_0$	0	0	0	0	0	0	0

Comp'd	Structure System	Structure Type	a	b	c	P_{eff}	θ	μ	T_C	T_N
TABLE A.2 RAl System										
LaAl	Ortho	CeAl	5.809	7.734	9.531					
CeAl	Ortho	CeAl	5.670	7.680	9.270	2.34	4			9
PrAl	Ortho	ErAl	5.745	5.964	11.771	3.58	11			20
NdAl	Ortho	ErAl	5.729	5.940	11.728	3.53	-4			29
SmAl	Ortho	ErAl	5.678	5.899	11.622					
GdAl	Ortho	ErAl	5.656	5.888	11.527	8.52	85			42
TbAl	Ortho	ErAl	5.621	5.834	11.370	10.1	24			72
DyAl	Ortho	ErAl	5.604	5.822	11.369	11.1	17			20
HoAl	Ortho	ErAl	5.621	5.801	11.339	11.3	17	7.1	26	
ErAl	Ortho	ErAl	5.570	5.801	11.272	10.1	28			13
TmAl						7.7	-2			10
YAl	Ortho	CrB	3.884	4.385	11.522					
ErAl type		Pnma		-						
Structure unknown										
TABLE A.3 RAl_2 System										
$LaAl_2$	Cubic	$MgCu_2$	8.131							
$CeAl_2$	Cubic	$MgCu_2$	8.047					2.5		2
$PrAl_2$	Cubic	$MgCu_2$	8.015						33	
$NdAl_2$	Cubic	$MgCu_2$	7.987			3.1	61	2.5	66	
$SmAl_2$	Cubic	$MgCu_2$	7.926						123	
$EuAl_2$	Cubic	$MgCu_2$	8.110			7.88	0			15
$GdAl_2$	Cubic	$MgCu_2$	7.887			7.92	180	7.0	170	
$TbAl_2$	Cubic	$MgCu_2$	7.850			9.82	108	8.1	114	
$DyAl_2$	Cubic	$MgCu_2$	7.821			9.7	68	9.1	58	
$HoAl_2$	Cubic	$MgCu_2$	7.802					7.86	27	
$ErAl_2$	Cubic	$MgCu_2$	7.780			9.56	16	7.6	14	
$TmAl_2$	Cubic	$MgCu_2$	7.760					4.69	8	

$MgCu_2$ type Fd3m z = 8

(0, 0, 0); (0, $\frac{1}{2}$, $\frac{1}{2}$); ($\frac{1}{2}$, 0, $\frac{1}{2}$); ($\frac{1}{2}$, $\frac{1}{2}$, 0) plus

8 Mg (0, 0, 0), ($\frac{1}{4}$, $\frac{1}{4}$, $\frac{1}{4}$)

16 Cu ($\frac{5}{8}$, $\frac{5}{8}$, $\frac{5}{8}$); ($\frac{5}{8}$, $\frac{7}{8}$, $\frac{7}{8}$); ($\frac{7}{8}$, $\frac{5}{8}$, $\frac{7}{8}$); ($\frac{7}{8}$, $\frac{7}{8}$, $\frac{5}{8}$)

Comp'd	Structure System	Type	a	b	c	P_{eff}	θ	μ	T_C	T_N
TABLE A.4 RAl_3 System										
$LaAl_3$	Hex	Ni_3Sn	6.662		4.609					
$CeAl_3$	Hex	Ni_3Sn	6.545		4.609	2.63	-46			
$PrAl_3$	Hex	Ni_3Sn	6.504		4.604	3.74	-14			
$NdAl_3$	Hex	Ni_3Sn	6.472		4.606	4.11	+5			
$SmAl_3$	Hex	Ni_3Sn	6.380		4.597					
$GdAl_3$	Hex	Ni_3Sn	6.320		4.592	8.29	-89			17
$TbAl_3$	Hex	$BaPb_3$	6.175		21.180	10.0	-64			21
$DyAl_3$	Rhomb (Hex-index)	$HoAl_3$	6.080		35.940	10.85	-51			23
$HoAl_3$	Rhomb (Hex-index)	$HoAl_3$	6.052		35.930	10.89	-26			9
$ErAl_3$	Cubic	Cu_3Au	4.215			9.87	+6	6.2	21	
$TmAl_3$	Cubic	Cu_3Au	4.200			7.88	-19			
$YbAl_3$	Cubic	Cu_3Au	4.202			4.62	-300			
$LuAl_3$										
YAl_3	Hex-	Ni_3Sn	6.28		4.58					
	Rhomb (Hex-index)	$BaPb_3$	6.194		21.138					

Ni_3Sn type $P6_3/mmc$ $z = 2$

2 Sn (1/3, 2/3, $\frac{1}{4}$); (2/3, 1/3, $\frac{3}{4}$)

6 Ni (x, 2x, $\frac{1}{4}$); ($2\bar{x}$, $\bar{x}$, $\frac{1}{4}$); (x, $\bar{x}$, $\frac{1}{4}$) (2x, x, $\frac{3}{4}$); ($\bar{x}$, x, $\frac{3}{4}$)

TABLE A.5

$EuAl_4$	Tetra-gonal	$BaAl_4$	4.398		11.170	8.02				6

$BaAl_4$ type I_4/mmm $z = 2$

(0, 0, 0); ($\frac{1}{2}$, $\frac{1}{2}$, $\frac{1}{2}$) plus

2 Ba (0, 0, 0)

4 Al (1) (0, $\frac{1}{2}$, $\frac{1}{4}$); ($\frac{1}{2}$, 0, $\frac{1}{4}$)
(2) (0, 0, z); (0, 0, $\bar{z}$) $z = 0.38$

Comp'd	Structure System	Type	a	b	c	P_{eff}	θ	μ	T_C	T_N
TABLE A.6 RIn_3 System										
$LaIn_3$	Cubic	$AuCu_3$								
$CeIn_3$	Cubic	$AuCu_3$	4.688			2.70	-62	2.70		10
						2.54	-46			
$PrIn_3$	Cubic	$AuCu_3$	4.671			3.58	-10			
$NdIn_3$	Cubic	$AuCu_3$	4.653			3.62	-17			7
$SmIn_3$	Cubic	$AuCu_3$	4.627							
$GdIn_3$	Cubic	$AuCu_3$	4.607			8.20	-85			45
$TbIn_3$	Cubic	$AuCu_2$	4.588			10.05	-62			36
$DyIn_3$	Cubic	$AuCu_3$	4.579			10.78	-35			23
$HoIn_3$	Cubic	$AuCu_3$	4.573			10.65	-18			11
$ErIn_3$	Cubic	$AuCu_3$	4.564			9.75	-10			6
$TmIn_3$	Cubic	$AuCu_3$	4.548			7.6	-6			
$YbIn_3$	Cubic	$AuCu_3$	4.611							
$LuIn_3$	Cubic	$AuCu_3$	4.544							
YIn_3	Cubic	$AuCu_3$	4.592							
$AuCu_3$ type			Pm3m		z = 1					
Au (0, 0,0)										
3 Cu ($\frac{1}{2}$, $\frac{1}{2}$, 0); ($\frac{1}{2}$, 0, $\frac{1}{2}$); (0, $\frac{1}{2}$, $\frac{1}{2}$)										
TABLE A.7 RCu System										
CeCu	Ortho	FeB	7.30	4.30	6.36					
SmCu	Cubic	CsCl	3.528							
GdCu	Cubic	CsCl	3.502			8.6	-70			140
TbCu	Cubic	CsCl	3.480			9.7	-22			117
DyCu	Cubic	CsCl	3.461			10.7	-26			64
HoCu	Cubic	CsCl	3.445			10.6	-18			28
ErCu	Cubic	CsCl	3.432			9.6	-12			15
TmCu	Cubic	CsCl	3.414			7.5	-5			9.5
LuCu	Cubic	CsCl	3.390							
YCu	Cubic	CsCl	3.477							
CsCl type			Pm3m		z = 1					
Cs (0, 0, 0)										
Cl ($\frac{1}{2}$, $\frac{1}{2}$, $\frac{1}{2}$)										

Comp'd	Structure System	Structure Type	a	b	c	P_{eff}	θ	μ	T_C	T_N
TABLE A.8 RAg System										
LaAg	Cubic	CsCl	3.768							
CeAg	Cubic	CsCl	3.739			2.51	-20	0.95		
PrAg	Cubic	CsCl	3.739			3.44	2	1.55	14	
NdAg	Cubic	CsCl	3.715			3.53	-3			22
SmAg	Cubic	CsCl	3.673							
GdAg	Cubic	CsCl	3.648			8.2	-70			150
TbAg	Cubic	CsCl	3.625			10.15	-36			106
DyAg	Cubic	CsCl	3.608			10.45	-23			63
HoAg	Cubic	CsCl	3.592			10.3	-17			33
ErAg	Cubic	CsCl	3.574			9.2	-9.5			21
TmAg	Cubic	CsCl	3.562			7.15	-7			9.5
LuAg	Cubic	CsCl	3.541							
YAg	Cubic	CsCl	3.617							
Structure as RCu System										
TABLE A.9 RAu System										
PrAu	Cubic	CsCl	3.68							
NdAu	Cubic	CsCl	3.659							
SmAu	Cubic	CsCl	3.621							
GdAu	Cubic	CsCl	3.601			7.92	29			31
	Ortho	CrB	4.522	10.826	4.734					
TbAu	Cubic	CsCl	3.576			9.54	23			40
DyAu	Cubic	CsCl	3.555			10.22	7			14
HoAu	Cubic	CsCl	3.541			10.50	0			10
ErAu	Cubic	CsCl	3.527			9.42	-4			13-19
TmAu	Cubic	CsCl	3.516			7.32	-5			8-19
LaAu	Cubic	CsCl	3.497							
YAu	Cubic	CsCl	3.559							
Structure as RCu System										

Comp'd	Structure System	Structure Type	a	b	c	P_{eff}	θ	μ	T_C	T_N
TABLE A.10 RCu_2 System										
$LaCu_2$	Hex	AlB_2	4.348		3.818					
$CeCu_2$	Ortho	$CeCu_2$	4.435	7.057	7.475			0.8		
$PrCu_2$	Ortho	$CeCu_2$	4.400	7.024	7.435	3.51		2.3		
$NdCu_2$	Ortho	$CeCu_2$	4.387	7.000	7.420	3.56		1.9		
$SmCu_2$	Ortho	$CeCu_2$	4.360	6.925	7.375			0.1		
$EuCu_2$	Ortho	$CeCu_2$	4.434	7.250	7.553	7.4		5.8		
$GdCu_2$	Ortho	$CeCu_2$	4.320	6.858	7.330	8.4		6.0		41
$TbCu_2$	Ortho	$CeCu_2$	4.310	6.825	7.320	9.8		7.4		54
$DyCu_2$	Ortho	$CeCu_2$	4.300	6.792	7.300	10.75		8.7		24
$HoCu_2$	Ortho	$CeCu_2$	4.280	6.759	7.290	10.5		9.2		9
$ErCu_2$	Ortho	$CeCu_2$	4.275	6.726	7.265	9.35		5.6		11
$TmCu_2$	Ortho	$CeCu_2$	4.266	6.695	7.247	7.49		4.2		
$YbCu_2$	Ortho	$CeCu_2$	4.286	6.894	7.382					
$LuCu_2$	Ortho	$CeCu_2$	4.245	6.627	7.220					
YCu_2	Ortho	$CeCu_2$	4.305	6.800	7.315					

$CeCu_2$ type Imma z = 4

(0, 0, 0); $(\frac{1}{2}, \frac{1}{2}, \frac{1}{2})$ plus

4 Ce $\pm$ $(0, \frac{1}{4}, x)$, x = 0.54

8 Cu $\pm$ (0, y, z); $\pm$ $(0, \frac{1}{2} + y, \bar{z})$, y = 0.05, z = 0.16

TABLE A.11 RAg_3 System					
$LaAg_3$	Hex	$PuAg_3$	12.848		9.487
$CeAg_3$	Hex	$PuAg_3$	12.753		9.401
$PrAg_3$	Hex	$PuAg_3$	12.719		9.401
$NdAg_3$	Hex	$PuAg_3$	12.726		9.389
$SmAg_3$	Hex	$PuAg_3$	12.619		9.280
$GdAg_3$	Hex	$PuAg_3$	12.613		9.226
$TbAg_3$	Hex	$PuAg_3$	12.628		9.272
$DyAg_3$	Hex	$PuAg_3$	12.644		9.270
$HoAg_3$	Hex	$PuAg_3$	12.554		9.210
$ErAg_3$	Hex	$PuAg_3$	12.463		9.155
$TmAg_3$	Hex	$PuAg_3$	12.553		9.203
YAg_3	Hex	$PuAg_3$	12.526		9.190

Structure unknown

Comp'd	Structure System	Structure Type	a	b	c	P_{eff}	θ	μ	T_C	T_N

TABLE A.12 RCu_5 System

$GdCu_5$	Cubic	$AuBe_5$	7.06							
$TbCu_5$	Cubic	$AuBe_5$	7.041			9.6	2			15
$DyCu_5$	Cubic	$AuBe_5$	7.027			10.9	2	6.5		7
$HoCu_5$	Cubic	$AuBe_5$	7.016			10.8	0	7.6	?	
$ErCu_5$	Cubic	$AuBe_5$	7.003			9.7	0	7.3	?	
$TmCu_5$	Cubic	$AuBe_5$	6.991			7.4	0	4.9	?	

$AuBe_5$ type F43m z = 4

(0, 0, 0); $(0, \frac{1}{2}, \frac{1}{2})$; $(\frac{1}{2}, 0, \frac{1}{2})$; $(\frac{1}{2}, \frac{1}{2}, 0)$ plus

4 Au (0, 0, 0)

4 Be $\begin{matrix}(1)\ (\frac{1}{4}, \frac{1}{4}, \frac{1}{4}) \\ (2)\ (x, x, x)\end{matrix}$; $(x, \bar{x}, \bar{x})$; $(\bar{x}, x, \bar{x})$; $(\bar{x}, \bar{x}, x)$, $x = \frac{5}{8}$

TABLE A.13 RCu_6 System

$CeCu_6$	Ortho	$CeCu_6$	8.108	5.102	10.160
$PrCu_6$	Ortho	$CeCu_6$	8.101	5.081	10.140
$NdCu_6$	Ortho	$CeCu_6$	8.092	5.062	10.105
$SmCu_6$	Ortho	$CeCu_6$	8.060	5.034	10.049
$GdCu_6$	Ortho	$CeCu_6$	8.040	5.009	9.995
YCu_6	Ortho	$CeCu_6$	8.115	5.078	10.122

$CeCu_6$ type Pnma z = 4

4 Ce $\pm$ (m, $\frac{1}{4}$, n); $\pm$ $(\frac{1}{2} - m, \frac{3}{4}, \frac{1}{2} + n)$ m = 0.2604 $\pm$ 1 n = 0.4353 $\pm$ 1

4 Cu $\pm$ (p, $\frac{1}{4}$, q); $\pm$ $(\frac{1}{2} - p, \frac{3}{4}, \frac{1}{2} + q)$ p = 0.1470 $\pm$ 3 q = 0.1419 $\pm$ 3

4 Cu $\pm$ (r, $\frac{1}{4}$, s); $\pm$ $(\frac{1}{2} - r, \frac{3}{4}, \frac{1}{2} + s)$ r = 0.3172 $\pm$ 3 s = 0.7448 $\pm$ 3

4 Cu $\pm$ (t, $\frac{1}{4}$, u); $\pm$ $(\frac{1}{2} - t, \frac{3}{4}, \frac{1}{2} + u)$ t = 0.0617 $\pm$ 3 u = 0.9021 $\pm$ 3

4 Cu $\pm$ (v, $\frac{1}{4}$, w); $\pm$ $(\frac{1}{2} - v, \frac{3}{4}, \frac{1}{2} + w)$ v = 0.4020 $\pm$ 3 w = 0.9845 $\pm$ 3

8 Cu $\pm$ (x, y, z); $\pm$ $(\frac{1}{2} + x, \frac{1}{2} - y, \frac{1}{2} - z)$; $\pm$ $(\bar{x}, \frac{1}{2} + y, \bar{z})$; $\pm$ $(\frac{1}{2} - x, \bar{y}, \frac{1}{2} + z)$

x = 0.4356 $\pm$ 2 y = 0.0046 $\pm$ 4 z = 0.1904 $\pm$ 2

TABLE A.14

$EuPd_2$	Cubic	$MgCu_2$	7.8	80

Structure as RAl_2

Comp'd	Structure System	Structure Type	a	b	c	P_{eff}	θ	μ	T_C	T_N
TABLE A.15 RPd_3 System										
$LaPd_3$	Cubic	$AuCu_3$	4.235							
$CePd_3$	Cubic	$AuCu_3$	4.136							
$PrPd_3$	Cubic	$AuCu_3$	4.138							
$NdPd_3$	Cubic	$AuCu_3$	4.130			3.4	-7			
$SmPd_3$	Cubic	$AuCu_3$	4.105			3.4	1			
$EuPd_3$	Cubic	$AuCu_3$	4.095							
$GdPd_3$	Cubic	$AuCu_3$	4.090			8.6	19	5.4		7.5
$TbPd_3$	Cubic	$AuCu_3$	4.077							2.0
$DyPd_3$	Cubic	$AuCu_3$	4.068			10.1	2	5.2		
$HoPd_3$	Cubic	$AuCu_3$	4.064							
$ErPd_3$	Cubic	$AuCu_3$	4.056							
$TmPd_3$	Cubic	$AuCu_3$	4.040							
$YbPd_3$	Cubic	$AuCu_3$	4.040							
$LuPd_3$	Cubic	$AuCu_3$	4.022							
YPd_3	Cubic	$AuCu_3$	4.074							
Structure as RIn_3										
TABLE A.16 RPt_2 System										
$LaPt_2$	Cubic	$MgCu_2$	7.774							
$CePt_2$	Cubic	$MgCu_2$	7.723							
$PrPt_2$	Cubic	$MgCu_2$	7.709			3.43	0	1.67	13.5	
$NdPt_2$	Cubic	$MgCu_2$	7.694			3.60	0	2.11	10	
$SmPt_2$	Cubic	$MgCu_2$	7.662							
$EuPt_2$	Cubic	$MgCu_2$	7.731			7.9			105	
$GdPt_2$	Cubic	$MgCu_2$	7.637			8.10	32	6.77	50	
$TbPt_2$	Cubic	$MgCu_2$	7.613			9.61	17	7.08	26	
$DyPt_2$	Cubic	$MgCu_2$	7.597			10.58	7	7.34	25	
$HoPt_2$	Cubic	$MgCu_2$	7.586			10.60	2	8.88	19	
$ErPt_2$	Cubic	$MgCu_2$	7.570			9.50	1	7.48	15	
YPt_2	Cubic	$MgCu_2$	7.590							
Structure as RAl_2										

Comp'd	Structure System	Type	a	b	c	P_{eff}	θ	μ	T_C	T_N
TABLE A.17 RZn_2 System										
$LaZn_2$	Ortho	$CeCu_2$	4.689	7.638	7.593					
$CeZn_2$	Ortho	$CeCu_2$	4.461	7.539	7.501	2.25	24			7
$PrZn_2$	Ortho	$CeCu_2$	4.619	7.474	7.533	3.56	14			
$NdZn_2$	Ortho	$CeCu_2$	4.599	7.409	7.566	3.40	28	1.82	24	
$SmZn_2$	Ortho	$CeCu_2$	4.552	7.299	7.590					45
$EuZn_2$	Ortho	$CeCu_2$	4.728	7.650	7.655		45			23
										20
$GdZn_2$	Ortho	$CeCu_2$	4.513	7.214	7.606	8.48	70			68
$TbZn_2$	Ortho	$CeCu_2$	4.492	7.142	7.595	9.62	58			55
										25
$DyZn_2$	Ortho	$CeCu_2$	4.477	7.090	7.600					
$HoZn_2$	Ortho	$CeCu_2$	4.460	7.042	7.612	9.71	26			12
$ErZn_2$	Ortho	$CeCu_2$	4.48	6.984	7.610					
$TmZn_2$	Ortho	$CeCu_2$	4.433	6.944	7.604					
$YbZn_2$	Ortho	$CeCu_2$	4.573	7.325	7.569					
$LuZn_2$	Ortho	$CeCu_2$	4.416	6.866	7.600					
Structure as RCu_2										
TABLE A.18 RZn_{12} System										
$SmZn_{12}$	Tetra-gonal	$ThMn_{12}$	8.927		5.215	0.7	-36			16
$GdZn_{12}$	"	$ThMn_{12}$	8.898		5.210	8.4	-58			16
$TbZn_{12}$	"	$ThMn_{12}$	8.884		5.200	10.1	-38			14
$DyZn_{12}$	"	$ThMn_{12}$	8.877		5.198					
$HoZn_{12}$	"	$ThMn_{12}$	8.868		5.195					
$ErZn_{12}$	"	$ThMn_{12}$	8.863		5.193	9.7	3			2.9
$TmZn_{12}$	"	$ThMn_{12}$	8.852		5.190					
$LuZn_{12}$	"	$ThMn_{12}$	8.848		5.186					

$ThMn_{12}$ type 4/mmm z = 2

(0, 0, 0); $(\frac{1}{2}, \frac{1}{2}, \frac{1}{2})$ plus

2 Th (0, 0, 0)

8 Mn (1) $(\frac{1}{4}, \frac{1}{4}, z)$; $(\frac{3}{4}, \frac{3}{4}, \frac{1}{4})$; $(\frac{1}{4}, \frac{3}{4}, \frac{1}{4})$; $(\frac{3}{4}, \frac{1}{4}, \frac{1}{4})$
(2) $(x, 0, 0)$; $(\bar{x}, 0, 0)$; $(0, x, 0)$; $(0, \bar{x}, 0)$ x = 0.36
(3) $(z, \frac{1}{2}, 0)$; $(\bar{x}, \frac{1}{2}, 0)$; $(\frac{1}{2}, x, 0)$; $(\frac{1}{2}, \bar{x}, 0)$ x = 0.28

Comp'd	Structure System	Type	a	b	c	P_{eff}	θ	μ	T_C	T_N

TABLE A.19 R_2Zn_{17} System

Gd_2Zn_{17}	Rhomb	Th_2Ni_{17}	8.994		13.169	7.84	-53			10
Tb_2Zn_{17}	Rhomb	"	8.977		13.161	9.84	-17			28
Dy_2Zn_{17}	Rhomb	"	8.967		13.139	11.01				
Ho_2Zn_{17}	Rhomb	"	8.956		13.133	10.08				
Er_2Zn_{17}	Rhomb	"	8.942		13.118	9.63				
Tm_2Zn_{17}	Rhomb	"	8.937		13.110	7.64				

Th_2Ni_{17} R3m z = 2

6 Ni (1) $(\frac{1}{2}, 0, 0)$; $(0, \frac{1}{2}, 0)$; $(\frac{1}{2}, \frac{1}{2}, 0)$; $(\frac{1}{2}, \frac{1}{2}, 0)$; $(\frac{1}{2}, \frac{1}{2}, \frac{1}{2})$; $(\frac{1}{2}, 0, \frac{1}{2})$; $(0, \frac{1}{2}, \frac{1}{2})$

12 Ni (2) $\pm (x, 0, \frac{1}{4})$; $\pm (0, x, \frac{1}{4})$; $\pm (x, x, \frac{1}{4})$; $\pm (\bar{x}, 0, \frac{1}{4})$; $\pm (0, \bar{x}, \frac{1}{4})$; $\pm (\bar{x}, \bar{x}, \frac{1}{4})$ x = 1/3

12 Ni (3) $\pm (x, 2x, 0)$; $\pm (\bar{x}, x, 0)$; $\pm (2x, x, 0)$; $\pm (x, 2x, \frac{1}{2})$; $\pm (\bar{x}, \bar{x}, \frac{1}{2})$; $\pm (x, 2x, \frac{1}{2})$ x = 1/6

4 Ni (4) $\pm (\frac{1}{3}, 2/3, z)$; $\pm (1/3, 2, \frac{1}{2} - z)$ z = 0.11

2 Th (1) $\pm (0, 0, \frac{1}{4})$

2 Th (2) $\pm (1/3, 2/3, \frac{3}{4})$

TABLE A.20 RB_6 System

LaB_6	Cubic	CaB_6	4.154							
CeB_6	Cubic	CaB_6	4.139			2.49	-76			3
PrB_6	Cubic	CaB_6	4.130			3.59	-68			7
NdB_6	Cubic	CaB_6	4.125			3.54	-42			8.6
EuB_6	Cubic	CaB_6	4.178			8.7	9			
GdB_6	Cubic	CaB_6	4.111			8.01	-55			14
TbB_6	Cubic	CaB_6	4.102			9.43	-35			23
DyB_6	Cubic	CaB_6	4.098			10.63	-21			21
HoB_6	Cubic	CaB_6	4.097							6

CaB_6 type Pm3m z = 1

Ca (0, 0,)

6B $(x, \frac{1}{2}, \frac{1}{2})$; $(\frac{1}{2}, x, \frac{1}{2})$; $(\frac{1}{2}, \frac{1}{2}, x)$; $(\bar{x}, \frac{1}{2}, \frac{1}{2})$; $(\frac{1}{2}, x, \frac{1}{2})$; $(\frac{1}{2}, \frac{1}{2}, \bar{x})$ x = 0.207

Comp'd	Structure System	Type	a	b	c	P_{eff}	θ	μ	T_C	T_N

TABLE A.21 RB_4 System

GdB_4	Tetragonal	UB_4	7.144			7.92	-60			42
TbB_4	"	UB_4	7.118			9.72	-36			43
DyB_4	"	UB_4	7.101			10.6	-21			22
HoB_4	"	UB_4	7.075			10.6	-15			8
ErB_4	"	UB_4	7.071			9.6	-20			17.3
TmB_4	"	UB_4								12.8

UB_4 type P4/mbm z = 4

4U $\pm$ (u, $\frac{1}{2}$ + u, 0); $\pm$ ($\frac{1}{2}$ - u, u, 0) u = 0.31

4B (1) $\pm$ (0, 0, v); $\pm$ ($\frac{1}{2}$, $\frac{1}{2}$, v), v = 0.214

(2) $\pm$ (w, $\frac{1}{2}$ + w, $\frac{1}{2}$); $\pm$ ($\frac{1}{2}$ - w, w, $\frac{1}{2}$), w = 0.086

8B (3) $\pm$ (x, y, $\frac{1}{2}$); $\pm$ ($\frac{1}{2}$ + x, $\frac{1}{2}$ - y, $\frac{1}{2}$); $\pm$ ($\bar{y}$, x, $\frac{1}{2}$); $\pm$ ($\frac{1}{2}$ + y, $\frac{1}{2}$ + x, $\frac{1}{2}$)

x = 0.174 y = 0.042

TABLE A.22 Pd_2MnX System

Pd_2MnSn	Cubic	Heusler	6.380			4.23			189	
Pd_2MnIn	Cubic	Heusler	6.373			4.3				142
Pd_2MnSb	Cubic	Heusler	6.424			4.40			247	

Heusler ($AlCu_2Mn$) type Fm3m z = 4

4 Pd (1) (0, 0, 0); (0, $\frac{1}{2}$, $\frac{1}{2}$); ($\frac{1}{2}$, 0, $\frac{1}{2}$); ($\frac{1}{2}$, $\frac{1}{2}$, 0)

4 Pd (2) ($\frac{1}{2}$, $\frac{1}{2}$, $\frac{1}{2}$); ($\frac{1}{2}$, 0, 0); (0, $\frac{1}{2}$, 0); (0, 0, $\frac{1}{2}$)

4 Mn ($\frac{1}{4}$, $\frac{1}{4}$, $\frac{1}{4}$); ($\frac{1}{4}$, $\frac{3}{4}$, $\frac{3}{4}$); ($\frac{3}{4}$, $\frac{1}{4}$, $\frac{3}{4}$); ($\frac{3}{4}$, $\frac{3}{4}$, $\frac{1}{4}$)

4 Sn ($\frac{3}{4}$, $\frac{3}{4}$, $\frac{3}{4}$); ($\frac{3}{4}$, $\frac{1}{4}$, $\frac{1}{4}$); ($\frac{1}{4}$, $\frac{3}{4}$, $\frac{1}{4}$); ($\frac{1}{4}$, $\frac{1}{4}$, $\frac{1}{4}$);

TABLE A.23 $Zn_{13}M$ System

$CoZn_{13}$	Monoclinic		13.31	7.54	4.99					
$FeZn_{13}$	"		13.42	7.61	5.06					
$MnZn_{13}$	"		13.48	7.66	5.13	1.8		36		

ζ - $CoZn_{13}$ C2/m z = 2

* For an approximate structure see P.J. Brown, Acta Cryst., 15, 608, 1962 and ref (2.7)

Much of the magnetic data in these tables has been taken from Appendix II of "Intermetallic Rare-Earth Compounds" by K. N. R. Taylor (1.46). The structural data has been collected from "A Handbook of Lattice Spacings and Structures of Metals and Alloys", Vol. 2, by W. B. Pearson, Pergamon, 1967, and from references quoted in ch. 6.

APPENDIX 3

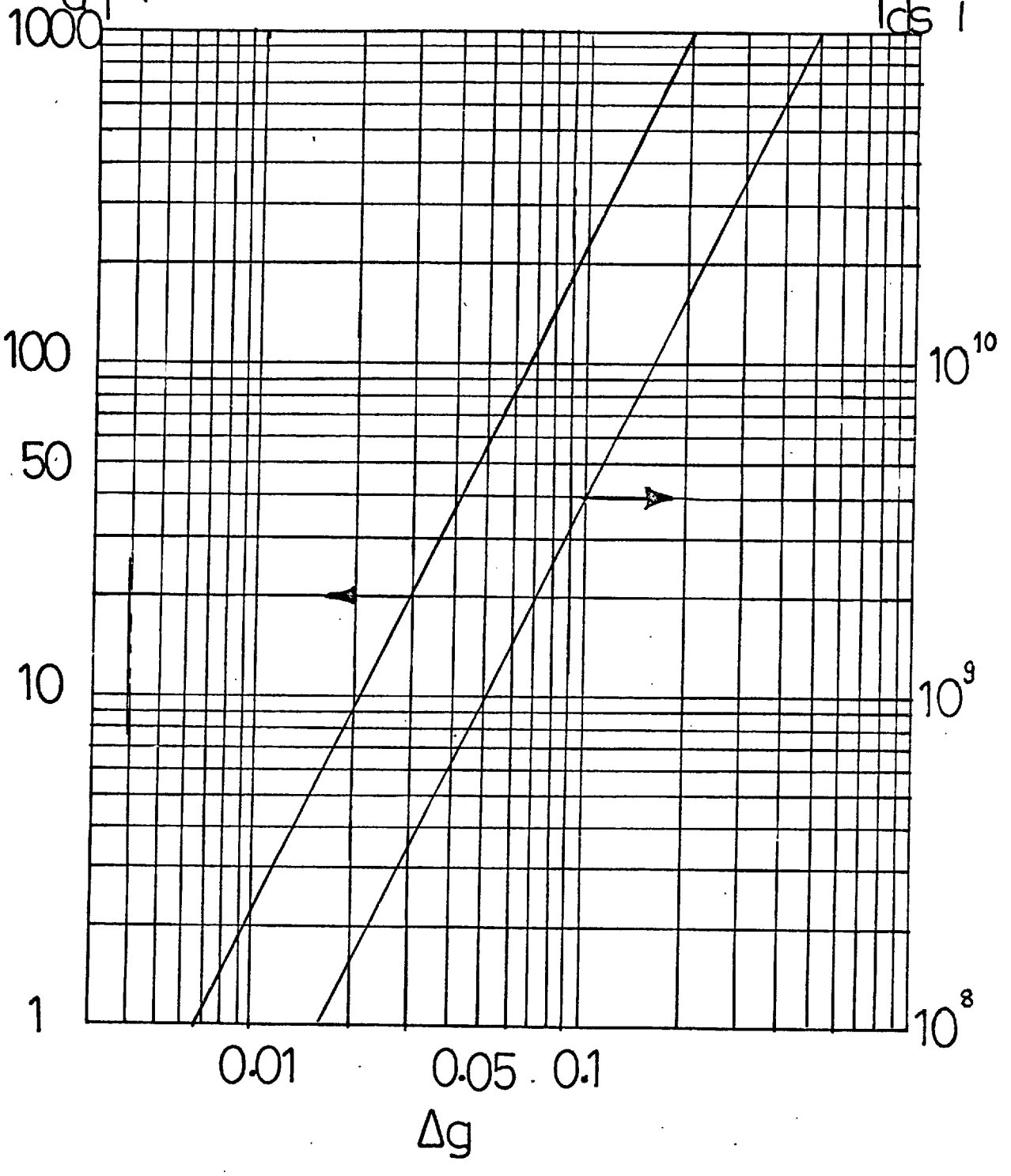


FIG A.3a KORRINGA RELATION

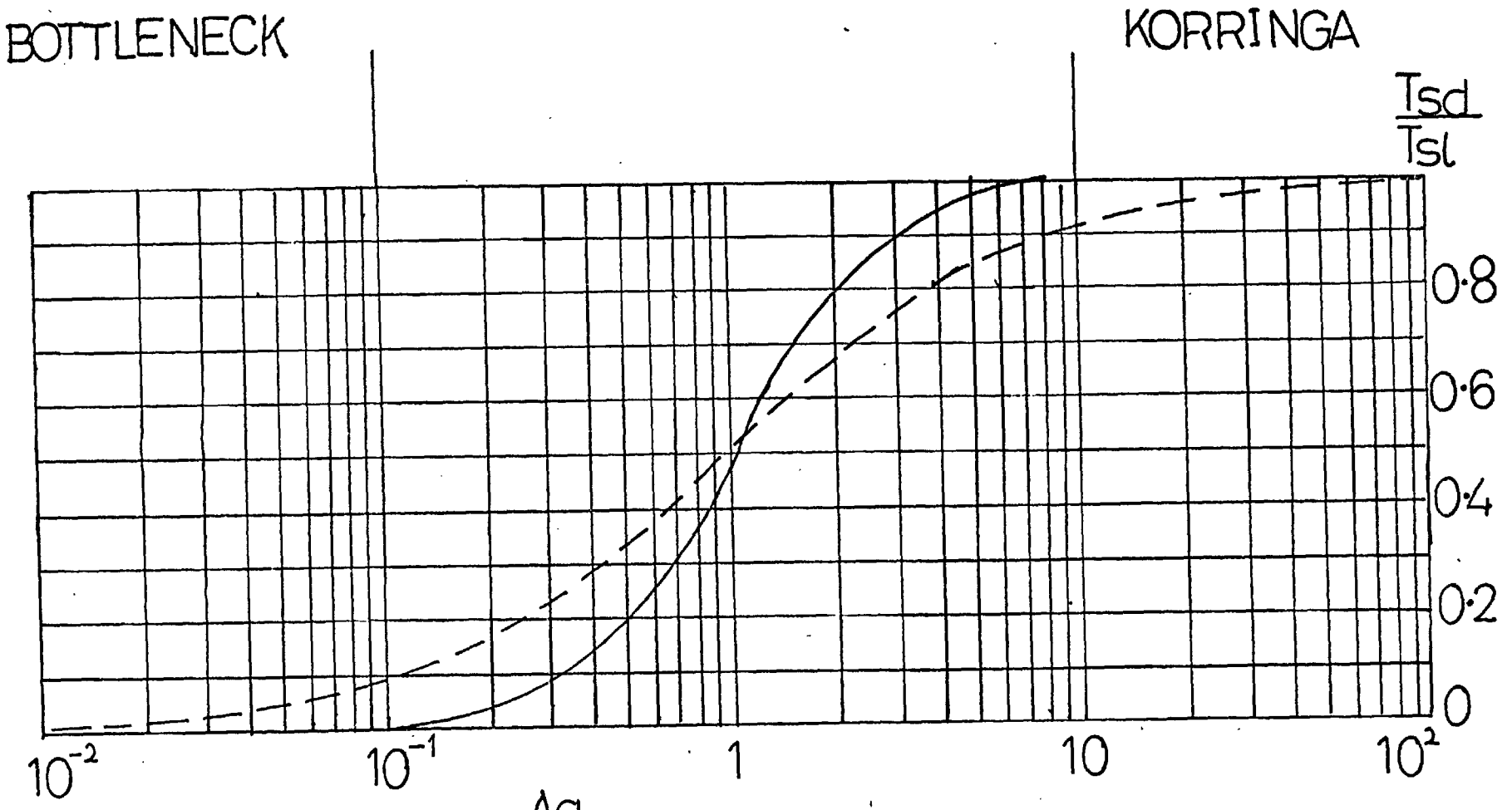


FIG A.3b
After Ref 5.30

APPENDIX 4

ESR OF IONS IN METALS

Classification by Magnetic Impurity and Host Matrix

(papers published prior to April 1972)

5.	IMPURITY	HOST	YEAR		REF.
-	Ce	Au	72	This Work	(-ve)
5.24	"	$LaAl_2$	70	Lowin	(-ve)
-	"	$LaIn_3$	72	This Work	(-ve)
5.24	"	RAl_2	70	Lowin	(-ve)
-	"	RIn_3	72	This Work	(-ve)
-	"	Rh	72	This Work	(-ve)
-	"	YAl_2	72	This Work	(-ve)
5.37	Dy	Ag	66	Griffiths, Coles	(-ve)
5.67	"	Ag	71	Davidov et al	
5.69	"	Au	72	Davidov et al	
5.43	"	Th	72	Davidov et al	
5.37	Er	Ag	66	Griffiths, Coles	
5.63	"	Ag	68	Hirst et al	
5.24	"	Ag	70	Lowin	
5.64	"	Ag	70	Chui et al	
5.65	"	Au	71	Tao et al	
5.66	"	Au	72	Chock et al	
5.68	"	Cu	71	Davidov et al	
5.41	"	Mg	67	Burr, Orbach	

5.	IMPURITY	HOST	YEAR	REF	
5.70	Er	Pd	72	Davidov et al	
5.68	"	Pt	71	Davidov et al	
5.70	"	Pt	72	Davidov et al	
5.68	"	Th	71	Davidov et al	
5.43	"	Th	72	Davidov et al	
5.68	"	Rh	72	Davidov et al	
-	"	RB_4	72	This Work	(-ve)
-	"	RZn_{12}	72	This Work	(-ve)
5.5	Eu	Eu	60	Peter, Matthias	
5.6	"	RAl_2	60	Jaccarino et al	
5.5	"	RIr_2	60	Peter, Matthias	(-ve)
5.7	"	RAl_2	61	Peter	
5.7	"	RMg_2	61	Peter	
5.9	"	RAl_4	67	Wernick et al	
5.41	"	Mg	67	Burr, Orbach	
5.44	"	Yb	68	Schäfer et al	
-	"	Pd_2R	72	This Work	
-	"	PdR	72	This Work	
5.59	Fe	Al	62	Collings, Hedgcock	(-ve)
5.59	"	Mg	62	Collings, Hedgcock	(-ve)
5.62	"	Cr	68	Salamon, Feigl	(doubtful)
5.26a	Gd	Ag	62	Peter et al	
5.37	"	Ag	66	Griffiths, Coles	
5.36	"	Ag	70	Nakamura et al	
-	"	Ag	72	This Work	

5.	IMPURITY	HOST	YEAR	REF.
5.26a	Gd	Au	62	Peter et al (-ve)
5.42	"	Au	71	Chock et al
5.1	"	Gd	53	Kip
5.4	"	Gd	64	Rodbell, Moore
5.2	"	Gd	70	Chiba, Nakamura
5.26a	"	Ir	62	Peter et al (-ve)
5.34	"	La	66	Harris et al
5.30	"	La	71	Cottet
-	"	La	72	This Work
5.29	"	Lu	65	Harris et al
5.34	"	Lu	66	Harris et al
5.47	"	Mg	67	Burr, Orbach
5.40	"	Mg	71	Tao et al
5.38	"	Mg	71	Ehara
5.26a	"	Pd	62	Peter et al
5.8	"	Pd	64	Shaltiel et al
5.31	"	Pd	70	Cottet, Peter
-	"	Pd	70	Coles et al and This Work
5.32	"	Pd	71	Praddaude, Gärtner
5.30	"	Pd	71	Cottet
5.33	"	Pd	72	Shaltiel et al
-	"	Pd	72	This Work
5.26a	"	Pt	62	Peter et al (-ve)
5.30	"	Pt	71	Cottet
5.34	"	Sc	66	Harris et al
5.30	"	Sc	71	Cottet
5.35	"	Sc	71	Salamon
5.43	"	Th	72	Davidov et al
5.3	"	Y	63	Popplewell, Tebble

5.	IMPURITY	HOST	YEAR	REF
5.29	Gd	Y	65	Harris et al
5.34	"	Y	66	Harris et al
5.30	"	Y	71	Cottet
5.26a	"	Ag-Pd	63	Peter et al
5.31	"	Ag-Pd	71	Cottet, Peter
5.30	"	Ag-Pd	71	Cottet
5.31	"	Cr-Pd	71	Cottet, Peter
5.30	"	Cr-Pd	71	Cottet
5.28	"	H-Pd	63	Shaltiel
5.19	"	Ni-Rh	68	Cottet et al
5.31	"	Ni-Pd	71	Cottet, Peter
5.30	"	Ni-Pd	71	Cottet
-	"	Ni-Pd	72	This Work
5.30	"	Pt-Pd	71	Cottet
5.31	"	Pd-Rh	71	Cottet, Peter
5.30	"	Pd-Rh	71	Cottet
5.26a	"	Pd-Rh	62	Peter et al
-	"	RAg_3	72	This Work
5.6	"	RAl_2	60	Jaccarino et al
5.8	"	RAl_2	64	Shaltiel et al
5.8	"	RAl_2	64	Shaltiel et al ($LaAl_2$ - Gd)
5.11	"	RAl_2	68	Davidov, Shaltiel
5.23	"	RAl_2	70	Schäfer et al (YAl_2-Gd)
5.24	"	RAl_2	71	Lowin ($LaAl_2$-Gd)
-	"	RAl_2	70	Coles et al ($LaAl_2$-Gd)
5.12	"	RAl_2	72	Hacker et al
-	"	RAl_2	72	This Work
5.15	"	RB_6	62	Coles et al
5.16	"	RB_6	71	Miller, Hacker

5.	IMPURITY	HOST	YEAR	REF.
-	Gd	TB_6	71	Fisk et al (This Work)
-	"	RB_4	71	Fisk et al (This Work)
-	"	RCu_6	72	This Work
5.26a	"	RCu_5	62	Shaltiel et al($Y/LaCu_5$-Ni)
-	"	RCu_4	72	This Work
-	"	RCu_2	72	This Work
-	"	RIn_2	72	This Work
5.5	"	RIr_2	60	Peter, Matthias
5.8	"	RIr_2	64	Shaltiel et al ($LaIr_2$-Gd)
5.11	"	RIr_2	68	Davidov, Shaltiel
5.11	"	RMn_2	68	Davidov, Shaltiel
5.8	"	RNi_5	64	Shaltiel et al ($NiCu_5$/Y, La)
5.11	"	RNi_5	68	Davidov, Shaltiel ($LaNi_5$Gd)
5.14	"	RNi_5	71	Burzo, Ursu
5.8	"	RPt_2	64	Shaltiel et al ($LaPt_2$-Gd)
5.10	"	RPt_2	68	Vijayarhaghavan et al
5.10	"	RPt_2	68	Vijayarhaghavan et al
5.11	"	RPt_2	68	Davidov, Shaltiel
-	"	$RPt_{2/3}$	72	This Work
5.8	"	RPt_5	64	Shaltiel et al ($LaPt_5$-Gd)
-	"	RPd_3	72	This Work
5.8	"	RRh_2	64	Shaltiel et al ($LaRh_2$-Gd)
5.11	"	RRh_2	68	Davidov, Shaltiel
5.8	"	RRu_2	64	Shaltiel et al (Sc, Y, Ce, La-Gd)
5.18	"	RRu_2	65	Shaltiel et al ($LaRu_2$-Th-Gd)
5.19	"	RRu_2	68	Cottet et al ($LaRu_2$-Gd)
5.20	"	RRu_2	69	Davidov et al ($LaRu_2$-Gd)
5.8	"	UNi_5	64	Shaltiel et al
5.8	"	UPd_3	64	Shaltiel et al

5.	IMPURITY	HOST	YEAR	REF.
5.25	Gd	$UThPd_3$	69	Davidov et al
5.8	"	$ThRu_2$	64	Shaltiel et al
5.17	"	$ZrRu_2$	64	Shaltiel et al
5.22	"	$ZrZn_2$	71	Davidov et al
-	"	RZn_{12}	72	This Work
-	"	R_2Zn_{17}	72	This Work
5.37	Ho	Ag	66	Griffiths, Coles (-ve)
5.24	"	$LaAl_2$	71	Lowin (-ve)
5.45	Mn	Ag	57	Owen et al
5.47	"	Ag	64	Shaltiel, Wernick
5.50	"	Ag	67	Gossard et al
5.56	"	Ag	70	Elliston
5.59	"	Al	62	Collings, Hedgcock (-ve)
5.8	"	Au	64	Shaltiel, Wernick
5.46	"	Cu	56	Owen et al
5.45	"	Cu	57	Owen et al
5.48	"	Cu	66	Geschwind et al
5.50	"	Cu	67	Gossard et al
5.49	"	Cu	67	Griffiths
5.53	"	Cu	67	Nakamura, Kinoshita
5.51	"	Cu	67	Okuda, Date
5.57	"	Cu	68	Oda, Asayama
5.52	"	Cu	68	McElroy, Heeger
5.53	"	Cu	69	Nakamura, Kinoshita
5.57	"	Cu	70	Oda, Asayama
5.58	"	Cu	71	Nagashima, Abe
5.30	"	Cu	71	Cottet
5.45	"	Mg	57	Owen et al

5.	IMPURITY	HOST	YEAR	REF.	
5.59	Mn	Mg	62	Collings, Hedgcock	
5.47	"	Pd	64	Shaltiel, Wernick	
5.30	"	Pd	71	Cottet	
-	"	Pd	72	This Work	
5.60	"	Zn	62	Collings et al	
5.61	"	Zn	70	Miyako	
-	"	Zn	72	This Work	(-ve)
-	"	$Zn_{13}T$	70	Caplin et al and This Work	
-	"	$Zn_{10}T$	72	This Work	
-	"	$Zn_{13}Fe$	72	This Work	
5.24	Tm	$LaAl_2$	71	Lowin	
5.63	Yb	Au	68	Hirst et al	
5.24	"	Au	71	Lowin	
5.65	"	Au	71	Tao et al	
5.66	"	Au	72	Chock et al	
5.73	Cr	Cu	68	Monod, Schultz	TESR
5.72	Mn	Cu	67	Schultz et al	
5.72	Mn	Ag	67	Schultz et al	
5.71	Mn	Cu	67	Cowan	

APPENDIX 5

FIG A.5a

Correction Factor For ΔH

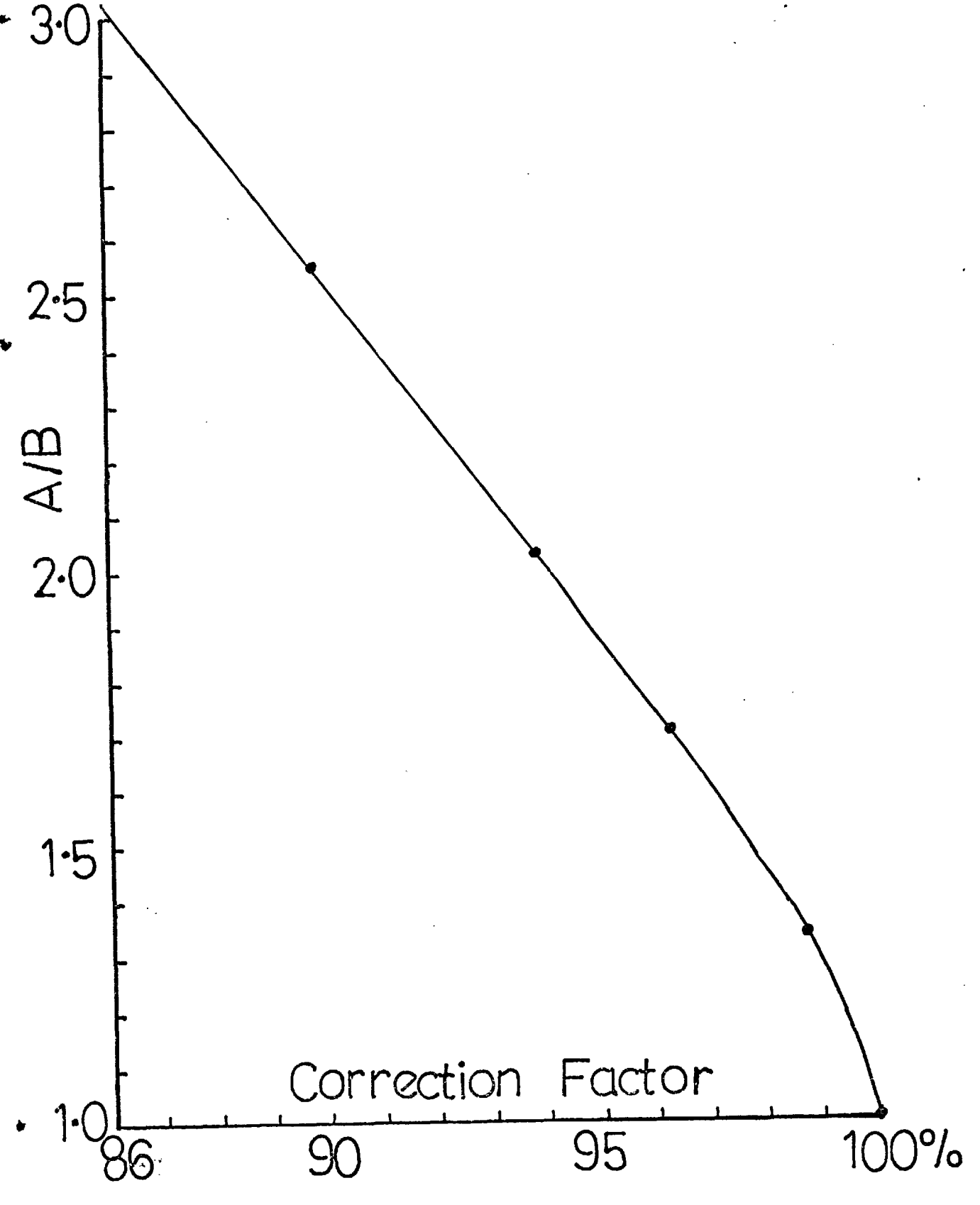
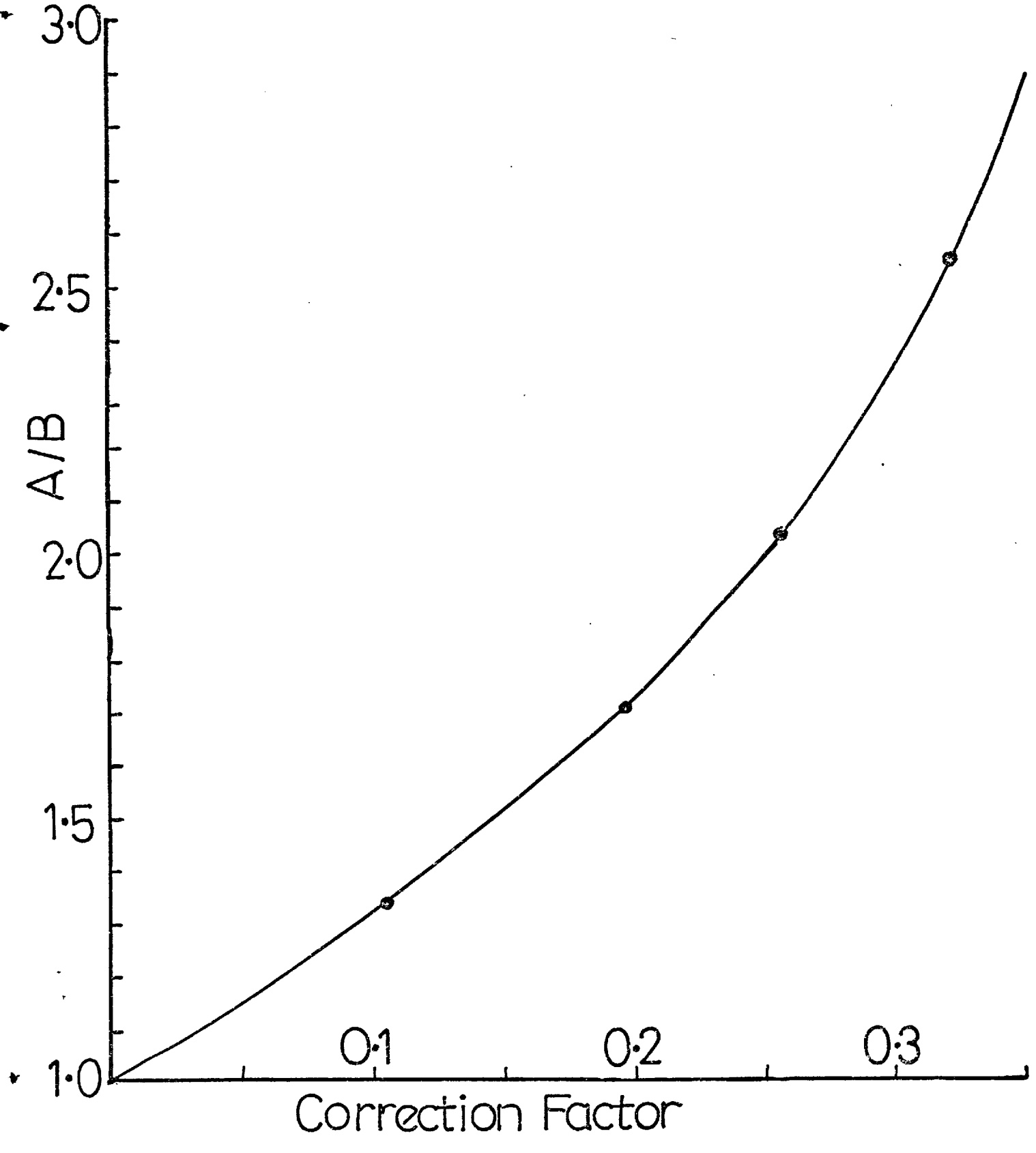


FIG A.5b

Correction Factor For H_x



g shifts of Gd in dilute alloys

Abstract. Electron paramagnetic resonance data for 0·45% Gd in $LaAl_2$ are reported. Δg is found to be $+0{\cdot}027$, and the linewidth $102 \pm 15 + (45 \pm 5)T$ Oe where T is the absolute temperature. The negative g shift for Gd in Pd is ascribed to a negative d–s interband effective exchange in Pd and a positive 4f-conduction electron exchange.

It is now well known that the effective exchange interaction (J_{eff}) between the local moment on a solute atom and the conduction electrons of the host metal contains contributions of both signs, the positive one from true exchange and the negative one from the mixing of local state and conduction electron states. (The latter, J_{mix}, was first suggested by Anderson and Clogston (1961), de Gennes (1962) and Kondo (1962) and is discussed in detail by Watson *et al.* (1965). It has also been recognized that this is a one-atom analogue of the inter*band* mixing which in pure transition metals leads to an antiparallel polarization of the conduction electrons directly visible in the neutron scattering (Shull and Yamada 1962) and Mössbauer effect in pure iron, although complicated in the latter by core polarization effects). The role of this negative contribution is clearly seen in dilute alloys of 3d elements in simple hosts, especially in the prominent resistance minima which require for their explanation (Kondo 1964) a negative effective interaction, and where strong mixing and fairly broad virtual states are to be expected. The exact manner in which J_{eff} manifests itself in a particular property is, however, variable; and it has been emphasized, especially by Peter *et al.* (1967), that many properties involve averages, sometimes complicated ones, of the wave-vector dependence $J_{eff}(q)$, although the direct g shift of the epr of the solute atom depends only on the value for $q = 0$. The observation, therefore, of well defined negative g shifts for Gd in such hosts as Pd, $LaRu_2$, $LaNi_5$ (for references, see the review by Peter *et al.* 1967) seems to imply the dominance of 4f-conduction electron mixing or virtual mixing effects.

On *a priori* grounds, however, such a dominance would scarcely be expected for Gd atoms in simple hosts, since the $4f^7$ configuration for this atom is extremely stable, and the energy denominators in the usual perturbation theory treatments of J_{mix} will be very large ($\simeq 10$ eV). We present here evidence, supplementing that already available, that for some simple hosts, Δg and J_{eff} have the positive sign to be expected from the dominance of true exchange, and a suggestion for the origin of the negative Δg observed in the above-mentioned hosts that does not involve large 4f-conduction electron mixing.

We have studied the epr of a homogeneous single-phase sample of the Laves phase intermetallic compound $LaAl_2$ in which 0·45 at. % of the La has been replaced by Gd.† The techniques were those described previously (Griffiths and Coles 1966) except that the brittleness of the material made it possible to prepare powder specimens by grinding and unnecessary to give them subsequent anneals. In contrast to previous reports of zero g shift in somewhat more concentrated alloys (Shaltiel *et al.* 1964) we find $\Delta g = +0{\cdot}027 \pm 0{\cdot}01$ and a linewidth ΔH at 4·2 K of 292 ± 5 Oe varying at lower temperatures, down to 1·8 K, as $a + bT$, where a is 102 ± 15 Oe and b is 45 ± 5 Oe K^{-1}.

In the simplest treatments of the g shift due to χ_e, the conduction electron susceptibility (Yosida 1965), one obtains $\Delta g = J_{eff} N(E)_F$ where $N(E)_F$ is the density of states at the Fermi surface, and this remains valid more generally if $\chi_e/2\mu_B^2$ is substituted for $N(E)_F$ where μ_B is the Bohr magneton. The measured susceptibility (corrected for core diamagnetism) of $LaAl_2$ is 150×10^{-6} e.m.u. $mole^{-1}$ (Maple 1969), and this leads to a J value of about $+0{\cdot}017$ eV. The temperature dependence of the linewidth is in good agreement with the Korringa (1950) relationship, $g\mu_B \Delta H / 2\pi kT = (\Delta g)^2$, which predicts a g shift of 0·031;

† We are grateful to Dr M. B. Maple of University of California, La Jolla and Dr J. R. Cooper for the provision and metallurgical evaluation of this alloy.

and this seems to imply (Peter *et al.* 1967) that exchange enhancement does not play an important part in χ_e for $LaAl_2$. For other $LaAl_2$–Gd alloys Maple and Fisk (private communication) have detected no resistance minimum and an enhanced effective moment per Gd atom; these observations support a positive sign for J_{cff}.

For Gd in Pd, however, the g shift first observed by Peter *et al.* (1962) is large ($\simeq 0{\cdot}12$ for $Pd_{97}Gd_3$) and unambiguously negative. (Since this amount of Gd, like comparable amounts of Lu, (Shaltiel *et al.* 1964) will significantly reduce the d-band susceptibility of the host palladium, for more dilute alloys one expects even larger shifts; and such increases, on dilution, have been observed by Cottet (to be published) and (to $g = 1{\cdot}79$ at 0·25 % Gd) by two of the present authors (Griffiths and Taylor, to be published).) In the light of previous remarks, however, the sign remains puzzling, even if the mixing postulated is with the d-band of palladium, as suggested by Shaltiel *et al.* (1964). We suggest that this difficulty can be overcome if it is accepted that d–s hybridization leads in palladium as in iron to a polarization of the s-band antiparallel to the magnetization of the d band, so that a large d-band susceptibility combined with a *true, positive* exchange between the s electrons and the $4f^7$ shell of the Gd atoms produces the negative g shift observed. A similar argument could hold for $LaRu_2$–Gd and for $GdNi_5$ (note that Δg for $GdCu_5$ is positive). When present in large concentrations in stoichiometric compounds with nontransition elements (e.g. $GdAl_2$) and in pure gadolinium metal the band structure may be complicated by the d-like character conferred by the Gd atoms themselves: this factor and the large magnetizations of such materials make the interpretation to be given to their g shifts very uncertain.

Helpful discussions with Dr H. Cottet, Dr Z. Fisk and Mr A. M. Stewart are gratefully acknowledged.

Department of Physics,
Imperial College,
London, SW7.

B. R. Coles
D. Griffiths
R. J. Lowin
R. H. Taylor
4th May 1970

Anderson, P. W., and Clogston, A. M., 1961, *Bull. Am. Phys. Soc.*, **6**, 124.
de Gennes, P. G., 1962, *J. Phys. Radium*, **23**, 510–21.
Griffiths, D., and Coles, B. R., 1966, *Phys. Rev. Lett.*, **16**, 1093–5.
Kondo, J., 1962, *Prog. theor. Phys.*, **28**, 846–56.
—— 1964, *Prog. theor. Phys.*, **32**, 37–49.
Korringa, J., 1950, *Physica*, **16**, 601–10.
Maple, M. B., 1969, *PhD Thesis*, University of California, San Diego.
Peter, M., *et al.*, 1962, *Phys. Rev.*, **126**, 1395–1402.
Peter, M., Dupraz, J., and Cottet, H., 1967, *Helv. Phys. Acta*, 40, 301–20.
Shaltiel, D., Wernick, J. H., and Jaccarino, V., 1964, *J. appl. Phys.*, 35, 978–80.
Shaltiel, D., Wernick, J. H., Williams, H. J., and Peter, M., 1964, *Phys. Rev.*, **135A**, 1346–62.
Shull, C. G., and Yamada, Y., 1962, *J. Phys. Soc. Japan*, **17**, Suppl. BIII, 1.
Watson, R. E., Koide, S., Peter, M., and Freeman, A. J., 1965, *Phys. Rev.*, **139A**, 167–78.
Yosida, K., 1957, *Phys. Rev.*, **106**, 893–8.

SUSCEPTIBILITY AND RESISTIVITY OF ζ-PHASE ZINC-TRANSITION METAL COMPOUNDS

A. D. CAPLIN, J. B. DUNLOP and R. H. TAYLOR
Physics Department, Imperial College, London S. W. 7. England

Résumé. — Les phases ζ des composés $Zn_{13}Mn$, $Zn_{13}Fe$ et $Zn_{13}Co$ sont bien ordonnées. La distance entre les ions de transition est ~ 5 Å. L'ion Mn porte un moment magnétique alors que les ions Fe et Co n'en portent pas comme dans les solutions correspondantes dans Zn. En dessous de 20 °K, $Zn_{13}Mn$ s'ordonne et est faiblement ferromagnétique. On observe un fort signal en R. P. E. et le facteur g passe de la valeur 2,0 à 200 °K à la valeur 3,0 en dessous de 4° K. A basse température la résistivité de $Zn_{13}Fe$ et $Zn_{13}Co$ varie considérablement avec la température, indiquant un phénomène de diffusion des électrons.

Abstract. — The ζ-phase compounds $Zn_{13}Mn$, $Zn_{13}Fe$ and $Zn_{13}Co$ are crystallographically well-ordered with ~ 5 Å between transitional ions. Mn carries a moment but Fe and Co do not, just as in the corresponding dilute solid solutions in Zn. Below 20 °K $Zn_{13}Mn$ orders and is weakly ferromagnetic ; a strong e.p.r. signal is observable and the g-factor increases from 2.0 at 200 °K to 3.0 below 4 °K. There is strong temperature-dependence of the resistivities of $Zn_{13}Fe$ and $Zn_{13}Co$ at low temperatures, indicative of electron-electron scattering.

The dilute transitional impurity dissolved in a free-electron-like solvent, and the pure transition metal itself, represent two limiting cases in the theory of magnetism. An intermediate situation which, by combining the localized nature of the former problem with the periodicity of the latter, should prove amenable to understanding, is provided by the ordered ζ-phase compounds $Zn_{13}X$, where X can be Mn, Fe or Co. Brown [1] has shown that in these materials the transition ions are well-separated (~ 5 Å) and each is surrounded by a slightly distorted sphere of zinc atoms.

The high temperature susceptibility of ζ-Mn fits a Curie-Weiss law (Fig. 1) with $p_{eff} = 1.82\ \mu_B$, $\theta = 36$ °K and $\chi_0 = 0.53 \times 10^{-6}$ emu/g. It orders ferromagnetically at about 20 °K (deduced from a plot of H/M versus M^2 [2]) with a saturation moment of only 0.3 μ_B per Mn ion (Fig. 2). Our e. p. r. experiments (at X-band on powder samples) show a strong signal below 200 °K, with $g = 2.0$ down to 150 °K, and an increasing positive g-shift at lower temperatures (Fig. 3) ; no correction for demagnetizing fields has been made, for at most it would account for 20 % of the observed shift. The susceptibilities of ζ-Fe and ζ-Co are small and almost temperature-independent (Fig. 1) ; the ζ-Fe samples show considerable variability, but are distinctly more paramagnetic than ζ-Co, whose susceptibility is about equal to that of pure Zn (− 0.1 × 10^{-6} emu/g).

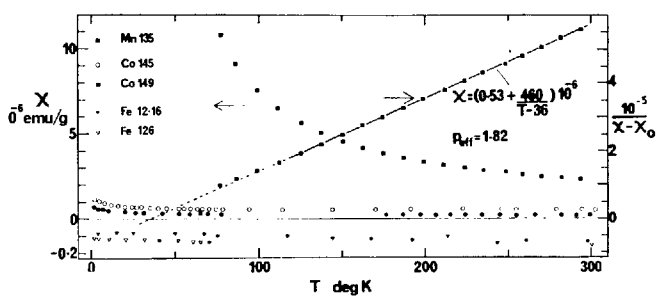


Fig. 1. — Magnetic susceptibilities of the ζ-phase Mn, Fe and Co compounds ; note the ten-fold scale expansion below the axis for ζ-Co. The Curie-Weiss plot for the ζ-Mn data is a best fit to the points above 150 °K.

Erratum : The symbols for Co alloys and the symbols for Fe alloys have been inadvertently interchanged in the figure.

The room temperature resistivities of these compounds are high : about 90, 30 and 20 μΩcm for ζ-Mn, ζ-Fe and ζ-Co respectively, but our samples had quite good resistance ratios, generally between 10 and 30. Their resistivities are strongly temperature-dependent at low temperatures (Fig. 4) ; that of ζ-Mn is very exactly proportional to $T^{3/2}$, but with some additional term near the magnetic transition. The temperature dependence of ζ-Fe and ζ-Co is between T^2 and T^3. The magnetoresistance of ζ-Mn is large and negative, and peaks at a temperature close to that of the magnetic transition (Fig. 2).

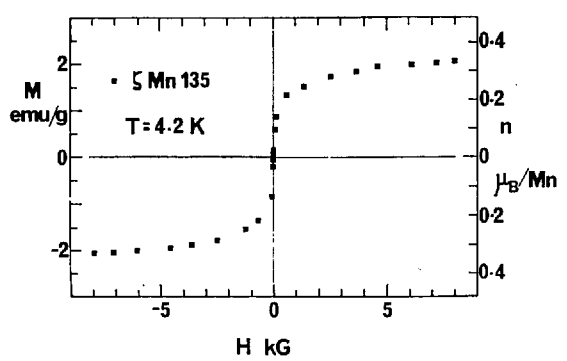


Fig. 2. — Magnetization curve of a ζ-Mn sample at 4.2 °K.

Our contention that in the compound the magnetic state of each ion is determined by the local environment is supported by the close correlation of magnetic properties with the corresponding dilute solution in zinc : in solution Mn, Fe and Co are respectively magnetic, on the borderline, and nonmagnetic [3] ; even the irreproducibility of ζ-Fe is mirrored by the sensitivity of the dilute solution to sample treatment [4]. It therefore seems reasonable to think of the transition ion in the compound as forming a virtual bound

state (v. b. s.), with the implication that s-d hybridization, and not d-d overlap, is the important interaction. The increased paramagnetism of ζ-Fe with respect to ζ-Co, which corresponds to an additional density of states of ~ 10 states/eV per Fe, may be attributable to exchange enchancement of the v. b. s. as the magnetic regime is approached. The extraordinarily large *g*-shift and small saturation moment of ζ-Mn are more difficult to understand.

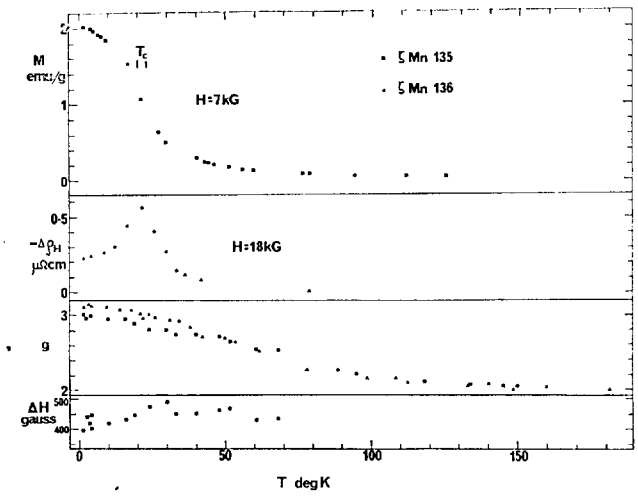


FIG. 3. — Magnetization, magnetoresistance, e.p.r. *g*-value and e.p.r. line width of the ζ-Mn compound as a function of temperature. The indicated transition temperature T_c is that determined from an Arrott plot [2].

If these materials were not ordered the resistivity would be large at all temperatures, about 110, 105 and 50 μΩcm respectively [5] ; at $T = 0$ the resistivity of a perfectly ordered sample vanishes because, to think in virtual bound state terms, the strong scattering at each transitional ion is repeated from unit cell to unit cell and is therefore non-dissipative. The $T^{3/2}$ behaviour of ζ-Mn no doubt represents scattering by spin excitations ; the temperature-dependence of the resistivity of ζ-Fe and ζ-Co is too large and too slow to be a phonon term, and it is more likely that it corresponds to the onset of incoherent scattering : at finite temperatures the occupancy of the v. b. s. fluctuates, consequently the scattering phase shift is no longer quite the same in every unit cell, and a finite resistivity appears. This description is essentially equivalent to that of electron-electron scattering in a pure

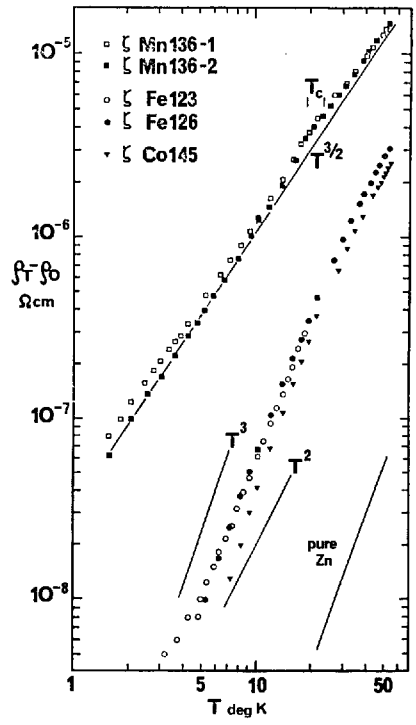


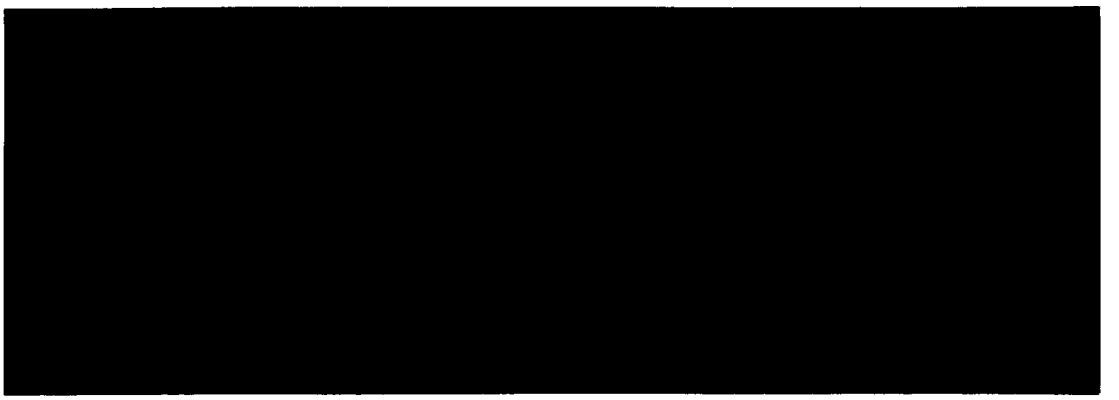
FIG. 4. — Temperature-dependent part of the resistivity for the ζ-phase Mn, Fe and Co compounds. The resistivity of pure Zn is also shown for purposes of comparison.

transition metal, but in a situation in which it would be inappropriate to speak of a d *band*.

We would like to thank Dr H. E. N. Stone for his invaluable metallurgical advice and assistance. This work has been performed during the tenure of S. R. C. studentships by two of us (J. B. D. and R. H. T.), and with S. R. C. financial support.

References

[1] BROWN (P. J.), *Acta Cryst.*, 1962, **15**, 608.
[2] ARROTT (A.), *Phys. Rev.*, 1957, **108**, 1394.
[3] VAN DEN BERG (G. J.), *Low Temp. Phys.* - LT9 (Part B), 1965, 955. Plenum Press.
[4] CAPLIN (A. D.), *Physics Letters*, 1967, **26**, 46.
[5] BOATO (G.), BUGO (M.) and RIZZUTO (C.), *Nuovo Cimento*, 1966, **45**, 226.



Reprinted from **The Journal of Physics** series

Letters to the Editor

The Institute of Physics London and Bristol

J. Phys. C: Solid St. Phys., 1971, Vol 4. L292–L295. Printed in Great Britain.

Anomalous magnetic behaviour of gadolinium borides

Z.FISK†, R.H.TAYLOR and B.R.COLES
Physics Department,
Imperial College,
Prince Consort Road,
London SW7 2BZ, U.K.
6th August 1971

Abstract. GdB_6 and GdB_4 have Néel temperatures (T_N) much lower than those expected from a comparison with the Tb and Dy compounds. Magnetic susceptibility, electrical resistivity and esr measurements reveal anomalies in the vicinity of the expected T_N. We suggest that a significant amount of short range order sets in between here and the observed T_N.

Both the paramagnetic Curie–Weiss temperatures, Θ, and the magnetic ordering temperatures of metallic, heavy rare earth compounds are in many cases approximately proportional to the de Gennes' factor $G = (g - 1)^2 J (J + 1)$, where g is the Lande g factor and J the total momentum of the f electron configuration. We see from table 1 that $\Theta \propto (g - 1)^2 J (J + 1)$ for both the hexa- and tetraborides of Gd, Tb, and Dy, while T_N is not. The ratio Θ/T_N is determined by the particular type of spin ordering in the antiferromagnetic state, and we ask why DyB_6 and DyB_4 can order in a spin arrangement such that $\Theta/T_N = -1$ while GdB_6 and GdB_4 cannot? One expects ordering at the highest possible temperature.

Table 1. Data on rare earth hexa- and tetraborides

Boride	f configuration	T_N† (K)	u_{eff} Calc	(u_B) Exp	Θ† (K)	G
GdB_6	f^7	17·5, 14‡	7·94	8·01	−55	15·75
TbB_6	f^8	23	9·72	9·43	−35	10·5
DyB_6	f^9	21	10·6	10·63	−21	7·08
GdB_4	f^7	42	7·94	7.92	−60	15·75
TbB_4	f^8	43	9·72	9·72	−36	10·5
DyB_4	f^9	22	10·6	10·35	−21	7·08

†T_N for hexaborides from Matthias *et al.* (1968); Θ for hexaborides from Paderno *et al.* (1967). Tetraboride data from this study; Θ for tetraborides agree reasonably with data of Paderno and Pokrzywnicki (1967).
‡Value from Coles *et al.* (1962); also found in this study.

The trivalent rare earths form metallic hexaborides which theory (Longuet-Higgins and Roberts 1954) and experiment (Johnson and Daane 1963) show to have one conduction electron per rare earth atom. We might expect the RKKY interaction to be responsible for the magnetic interactions in the rare earth hexaborides, and experiments on the rate of depression of the superconducting transition temperature of isostructural YB_6 by rare earth impurities (Fisk *et al.* 1969) show that the f electron–conduction electron interaction is strong enough to account for the observed values of Θ. A simple free electron model calculation shows that the RKKY interaction will be antiferromagnetic between nearest neighbours in the hexaborides.

†Now at The James Franck Institute, University of Chicago, 5640 Ellis Ave, Chicago, Illinois 60637, USA.

The measurements of Coles *et al.* (1962) of the temperature dependence of the magnetic susceptibility and the electrical resistivity of GdB_6 show deviations from Curie–Weiss behaviour and a larger temperature dependence of the electrical resistivity than expected, both effects already noticeable at about 70 K, far above the sharp kinks in those properties at 15 K normally associated with T_N. Furthermore the measurement of Westrum (1968) of the specific heat of GdB_6 has, in addition to a λ anomaly at 16 K, what appears to be a Schottky anomaly at 30 K. No explanation has been advanced to explain this latter; crystal field splitting of the Gd f^7 configuration being expected to be much too small to account for it. We note that measurements we have performed on the susceptibility of Gd impurities in YB_6 show Curie–Weiss behaviour to 1·5 K in agreement with the above expectation.

The results of our esr measurements on GdB_6 are shown in figures 1 and 2. We observe that the linewidth (ΔH) begins to show considerable temperature dependence in the same regions where the anomalies in the magnetic susceptibility and electrical resistivity are observed. The g value also shows slight temperature dependence, but in this temperature range the lineshape correction factor is large.

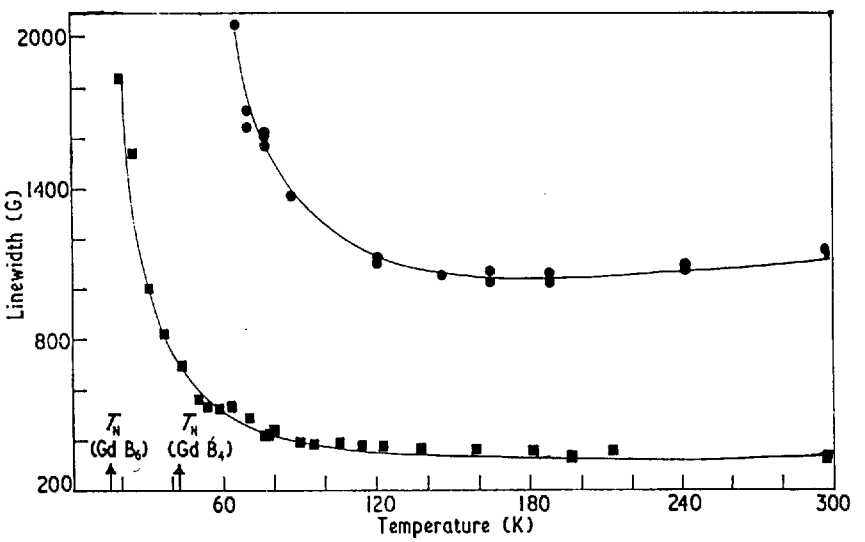


Figure 1. Temperature dependence of the esr linewidth (ΔH) of GdB_6 (■) and GdB_4 (●). Correction has been made for lineshape.

The situation for the heavy rare earth tetraborides is similar. In this case, $\Theta \propto G$ and $\Theta/T_N \simeq -1$ for TbB_4 and DyB_4 but not for GdB_4. Figure 3 gives our data for the electrical resistivity of these borides. We see that GdB_4 behaves anomalously in the vicinity of 70 K. Measurements we have made of the magnetic susceptibility of GdB_4 show deviations from Curie–Weiss behaviour around 60 K and that at T_N the susceptibility is 0·93 of the value expected by extrapolation from above this temperature. Our esr data for GdB_4 is plotted in figures 1 and 2, and again the linewidth shows considerable temperature dependence in this region.

Susceptibility data for RE-Al compounds and for dilute intermetallic RE-Zn compounds (Stewart 1970) seem to manifest a similar tendency.

We suggest that these anomalies can be explained if the tendency to reduce magnetic entropy by short range order is much greater than that to reduce it by long range order in

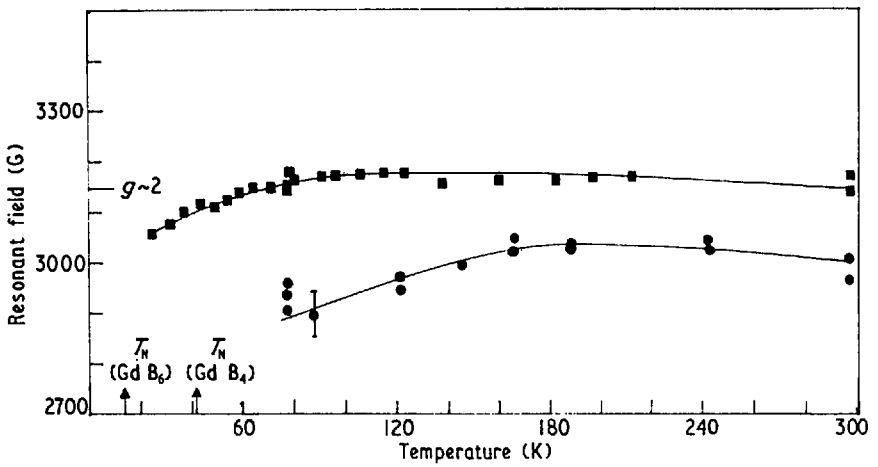


Figure 2. Temperature dependence of the esr resonant frequency of GdB_6 (■) and GdB_4(●). Correction has been made for the lineshape and finite sweep speed but not for the demagnetizing factor. For GdB_6: g value at 300 K = 2·00 ± 0·01, at 77 K = 2·00 ± 0·01. For GdB_4: g value at 300 K = 2·10 ± 0·03.

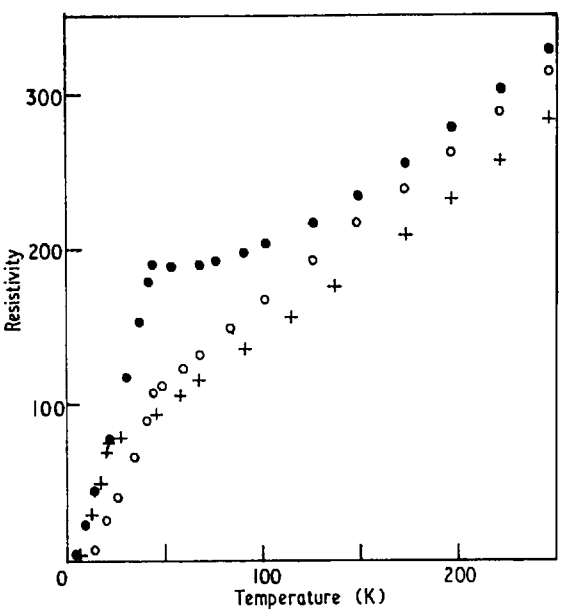


Figure 3. Temperature dependence of the electrical resistivity of GdB_4(●), TbB_4 (○) and DyB_4(+). The absolute value of the resistivity was not determined. The data are normalized by the slope at 250 K and the residual term has been substracted.

these gadolinium compounds. It is well known that in some nonmetallic compounds (eg MnO) the crystallographic features, in conjunction with orbital occupation and super-exchange interaction mechanisms, cause an anomalously small reduction in internal energy for the long range ordered state. This results in an extended temperature regime (approximately between T_N and $|\Theta|$) where the free energy favours only short range ordering. This order is easily visible in neutron scattering at room temperature in MnO although T_N is 116 K (Θ is -610 K).

Conceivably, the free energy of simple antiferromagnetic long range order in GdB_6 is adversely affected by its effects on the conduction electron configuration. For its simple cubic rare earth metal lattice with one conduction electron per Gd atom the simplest Néel type ordering (NaCl type magnetic unit cell, $\Theta/T_N \sim -1$) is expected (Mattis and Donath 1962) to occur for ordering by the RKKY type interaction *via* free electrons. The consequent splitting of the conduction electron Brillouin zone might significantly modify both the conduction electron energy spectrum and the RKKY interaction; if the new zone gaps were large enough we would have a semiconductor and no normal RKKY interaction. These gaps would be largest for the rare earth element with largest spin. We speculate that the long range ordering that finally occurs below 14 K in GdB_6 is to some alternative spin structure.

The situation is more complicated for the tetraborides. The crystal structure is tetragonal with four formula units per unit cell. It is thought that in this case also there is one conduction electron per rare earth atom (Lipscomb and Britton 1960). An argument similar to that used for GdB_6 applied to GdB_4 could explain the anomalies observed. The tetraborides TbB_4 and DyB_4 order with $\Theta/T_N \sim -1$. The parallel between the compounds which one sees in the table suggests that similar explanations may account for GdB_4 and GdB_6.

We thank R. Harris, B. T. Matthias and A. M. Stewart for many useful discussions and UKAEA (Harwell) for financial support of the programme of which this work forms a part; one of us (RHT) held an SRC studentship during the course of this work.

Note added in proof. Recent studies of the esr linewidth of MnO above T_N (BATTLES, J. W., 1971, *J. appl. Phys.*, **42**, 1286,) show the excess broadening we would expect from the above observations; well above T_N it is probably only a matter of nomenclature whether one speaks of short range order or long-lived critical spin fluctuations.

COLES, B. R., COLE, T., LAMBE, J., and LAURENCE, N., 1962, *Proc. Phys. Soc.*, **79**, 84
FISK, Z., MATTHIAS, B. T., and CORENZWIT, E., 1969, *Proc. nat. Acad. Sci. USA*, **64**, 115.
JOHNSON, R. W., and DAANE, A. H., 1963, *J. chem. Phys.*, **38**, 425.
LIPSCOMB, W. N., and BRITTON, D., 1960, *J. chem. Phys.*, **33**, 275.
LONGUET-HIGGINS, H. C., and ROBERTS, M. DEV., 1954, *Proc. R. Soc.* A, **224**, 336.
MATTHIAS, B. T., *et al.*, 1968, *Science*, **159**, 530.
MATTIS, D., and DONATH, W. E., 1962, *Phys. Rev.*, **128**, 1618.
PADERNO, YU. B., and POKRZYWNICKI, S., 1967, *Phys. Stat. Solidi*, **24**, K11.
PADERNO, YU. B., POKRZYWNICKI, S., and STALINSKI, B., 1967, *Phys. Stat. Solidi*, **24**, K73.
STEWART, A. M., 1970, *PhD thesis*, University of London.
WESTRUM, JR., E. F., 1968, *Progress in the Science and Technology of the Rare Earths*, Vol. 3, (Oxford: Pergamon) p. 459.